ARTIFICIAL ANTIGEN PRESENTING CELLS

FOR CANCER IMMUNOTHERAPY

by

Karlo Perica

A dissertation submitted to Johns Hopkins University in conformity with the requirements for the degree of Doctor of Philosophy

Baltimore, Maryland

October 2014

Abstract

Artificial Antigen Presenting Cells (aAPC) are synthetic platforms for T cell activation, made by coupling T cell activating proteins to cell-sized, spherical particles. While this size and shape are chosen to mimic endogenous APC and simplify manufacture, respectively, platforms based on alternative geometries and sizes could have significant advantages. I thus set out to develop nanoscale aAPC and ellipsoid aAPC, and to understand the relevant nanoscale structures governing T cell activation that may impact on APC design.

For example, T cells regulate binding sensitivity through nanoscale changes in lateral membrane organization, which may affect nano- but not micro-aAPC binding and function. Cells activated by a high dose of peptide lost ability to bind CD8-dependent but not CD8-independent MHC-peptide, a phenomenon attributed to loss of nanoscale co-localization between CD8 and TCR.

I next developed aAPC based on biocompatible iron-dextran paramagnetic particles 50-100 nm in diameter induced antigen-specific T cell proliferation in vitro and enhanced tumor rejection in a subcutaneous mouse melanoma model. Nano-aAPC bound 2-fold more TCR on activated cells with highly clustered TCR compared to naive cells with less clustered TCR, leading to weaker stimulation of naive cells. To enhance naive T cell activation, a magnetic field was used to drive aggregation of paramagnetic nano-aAPC, resulting in a doubling of the size of TCR clusters and increased T cell expansion in vitro and after adoptive transfer in vivo.

We coupled magnet-enhanced T cell activation to a magnetic column pre-enrichment strategy using nano-aAPC. Since nano-aAPC are functionalized with MHC-peptide that

can bind and activate TCR, iron-oxide cores to capture bound cells in a magnetic column, and co-stimulatory anti-CD28, they can enrich and expand cognate cells. Magnetic enrichment 1000-fold expansion in one week with the frequency of antigen-specific cells increasing from <0.1% in naive precursors to 10-20% after just one stimulation. Enrichment also significantly enhanced proliferation in lymphopenic hosts after adoptive transfer by reducing competition for proliferative cytokines. Enrichment and expansion with nano-aAPC is a streamlined approach to generating tumor-specific T cells from naive precursors with minimal culture.

Finally, I developed "stretched," ellipsoid micro-aAPC that increased T cell proliferation 2-5 fold compared to equivalent doses of spherical aAPC. Ellipsoid aAPC made larger contact surfaces with T cells, better recapitulating endogenous interactions.

Thesis Committee

Jonathan P. Schneck, M.D. Ph.D. *(primary advisor, reader)*

Professor, Department of Pathology,

Johns Hopkins University School of Medicine

Jordan J. Green, Ph.D.

Assistant Professor, Department of Biomedical Engineering

Johns Hopkins University School of Medicine

Hai-Quan Mao, Ph.D. *(reader)*

Associate Professor, Department of Materials Science and Engineering,

Johns Hopkins University School of Medicine

Michael Edidin, Ph.D.

Professor, Department of Biology,

Johns Hopkins University

TABLE OF CONTENTS

TABLE OF FIGURES

1 State of the Art

1.1 Mechanisms of T Cell Activation

T cells face a seemingly insurmountable challenge: from a sea of irrelevant self-antigens, they must find and respond to a small number of pathogenic or dangerous antigens. However, peptide antigens from both self proteins and from pathogens are presented in the context of a Major Histocompatability Complex (MHC) protein, meaning that only a small portion of the peptide-MHC ligand they recognize makes the difference between target and distraction. And the consequences of a mistake, an inappropriate response to self-antigen, is horror autotoxicus, as Paul Ehrlich described violent and destructive autoimmunity.

As a result of this daunting task, a complex machinery has developed around the T cell receptor, assisting in and modulating the recognition of cognate (specific) antigen. Like the B cell receptor, the T cell receptor relies on accessory proteins to initiate downstream signaling. Unlike the BCR, however, all TCR interactions with cognate ligand take place during cell-cell interactions. The TCR is no antibody: its binding, signaling, and spatial organization only make sense within the context of a membrane.

In this chapter, I will briefly review biophysical aspects of TCR signaling, with a particular emphasis on TCR behavior within the membrane. I will further focus the discussion on spatial organization, the patterns of receptor clustering and distribution that can modulate T cell responses.

1.1.1 TCR-MHC Recognition: What Makes a 'Cognate' Antigen?

A key property of the T cell is specificity: T cells will only activate and respond to one or a small number of peptides presented in the context of specific MHC alleles. This MHC-peptide

combination (pMHC) is the cognate antigen for a given T cell receptor, and underlies the ability of T cells to differentiate between healthy and pathologic tissue. Despite being absolutely critical to understanding T cell function, the question of why certain TCR-pMHC binding events can trigger T cell activation, whereas a vast majority cannot, is still poorly understood. In other words: what makes a certain MHC-peptide cognate for a certain TCR?

This question can be addressed in two ways. The first approach is biophysical: viewing T cell activation as a "black-box," can certain kinetic or equilibrium binding parameters predict successful TCR-MHC interactions? The second is mechanistic: how does a TCR transduce a binding event into a signal within the cell? Does the signal involve a comformational change in the protein, a mechanical stimulus, or a change in protein aggregation or clustering? These two approaches are complementary, and an understanding of each is required to appreciate the specificity of the TCR. A review of each approach follows.

1.1.1.1 Biophysical Models of TCR Binding

Even prior to a complete mechanistic understanding of T cell activation, biophysical approaches can shed significant light on TCR triggering by MHC. Such approaches begin by measuring kinetic and equilibrium binding parameters and attempting to identify which parameters are critical in determining antigen specificity.

TCR-pMHC binding parameters have traditionally been measured by two techniques. The first is Surface Plasmon Resonance (SPR), in which soluble ligands flows across a receptor fixed to a gold substrate. A binding event leads to the SPR effect, allowing the on rates, off rates, and overall avidity of binding to be measured. The second approach involves soluble, fluorescently tagged MHC constructs such as dimers and tetramers, whose association to and disassociation from T cells can be monitored by flow cytometry or microscopy [1–3].

Both approaches have yielded the same conclusion: TCR avidity for cognate MHC is surprisingly weak, in the micromolar range, compared to nanomolar avidity for antibodies and their ligands. As will be discussed further, it is important to remember that in both approaches either pMHC, TCR, or both are removed from the context of an APC or T cell membrane, significantly altering binding behavior.

Despite the somewhat artificial basis of these measurements, a large literature exists attempting to correlate biophysical parameters of TCR-pMHC binding with T cell response. The overall approach broadly follows three steps: 1) TCR-pMHC binding parameters are measured for a panel of TCR and antigens; 2) these antigens are classified as cognate agonists or non-cognate antagonists based on their ability to induce a functional response in T cells, such as downstream signaling, cytokine production, or proliferation; 3) binding parameters and T cell responses are plotted against each other to identify the parameter that best predicts response.

The results of these studies have been frequently contradictory, and data have supported several models. Avidity models propose that the equilibrium disassociation constant is the critical parameter for activation[2,4–6], since equilibrium parameters determine the total number of TCR engaged during prolonged APC/T cell contact. In contrast, kinetic models propose that association or disassociation rates are the critical determinant[7–10].

Kinetic models can be further subdivided into the nonexclusive categories serial triggering and kinetic proofreading. In the serial triggering model[11–13], disassociation rates cannot exceed a certain value, because a given pMHC must rapidly make serial contacts with multiple TCR to generate sufficient signal. In contrast, kinetic proofreading [7,14–16] suggests that disassociation rate cannot drop below a certain value because many sequential events are required for signaling

complex assembly, an idea supported mechanistically by the underlying complexity of the downstream T cell signaling complex. More recently, a "confinement time model" was proposed in which a rapid association rate could compensate for a rapid disassociation rate[16,17] by increasing rapid re-binding events.

A number of explanations have been proposed for these conflicting results, including variations in the functional outcome measured, insufficiently broad panels of TCR-pMHC measurements, or correlation between parameters complicating attempts to differentiate them. More generally, these discrepancies have led researchers "back to the drawing board," and motivated productive attempts to make more accurate and physiological measurements of TCR-MHC interactions. For example, binding parameters measured *in situ* using advanced imaging techniques show large increases in both association (100-fold) and disassociation (4-12 fold), ultimately resulting in increasing affinity[18].

Other approaches have focused on measuring two rather than three-dimensional binding parameters. During T cell/APC interactions, receptors are confined to the two-dimensional axis of cell-cell contact, whereas measurements using soluble MHC involve a third degree of freedom during binding. Two dimensional measurements may be made by assessing interactions of TCR with an MHC-coated bead[19,20], and may lead to more accurate description of TCR-pMHC binding. 2D affinity analysis has resulted in the identification of a wider range of T cells reactive with given ligands covering a broad range of affinities [21,22].

Despite this progress, no single biophysical explanation exists for TCR specificity. It is becoming clear that measurements derived *in vitro* under artificial binding conditions are only the first step toward understanding why certain pMHC trigger activation and others do not.

Moving forward, it is important to remember that TCR recognize MHC in the context of a cell-cell interaction, and that the actions and mechanisms of antigen recognition cannot be completely separated from the membrane.

1.1.1.2 Possible Mechanisms of TCR Signal Transduction

With the identification of the TCR protein in late 1982 and early 1983 by the Allison[23], Reinherz[24], and Kappler/Marrack[25] groups, and the subsequent cloning of the TCRβ chain by Hedrick and Davis in 1984[26], it became clear that TCR itself did not contain an extensive intracellular domain, and possessed no obvious mechanism for transmitting a binding event into a signal within the cell. Subsequent work shifted attention to the CD3 accessory protein, which was closely associated with TCR and contained Immunoreceptor Tyrosine-Based Activation Motifs (ITAMs) that were phosphorylated during T cell activation[27]. Thus, a mechanism was required to transduce an extracellular binding event between TCR and pMHC into an intracellular phosphorylation of ITAM residues on CD3.

By analogy to other receptor systems, a change in protein conformation was proposed to mediate this outside-inside signaling. Flexibility observed after TCR-pMHC binding occurs primarily in the antigen-binding CDR3 portion of the TCR protein, suggesting that external TCR surface can adjust to "fit" its cognate ligand[28]. Furthermore, structural studies have shown that a conformational change occurs in the AB-loop of TCRα, which is near the CD3ε binding site[29]. Finally, it is known that after MHC binding, a C-terminal proline –rich sequence is exposed on CD3ε[30]. However, this motif appears to be involved in regulating TCR/CD3 expression, not downstream signaling[31].

Thus, a complete picture of how MHC alters TCR and/or CD3 conformation, and whether this process is required for T cell activation, has not been described. Despite the growing body of

solved pMHC/TCR crystal structures, a ternary pMHC/TCR/CD3 crystal structure does not yet exist due to the immense technical challenges involved. Furthermore, conformational models have struggled to explain how a common conformational signal is transduced despite the wide variety of TCR sequences and structures, with different TCR clones yielding different structural features[28].

A common structural mechanism that is an alternative to conformational change involves the transmission of mechanical forces after MHC binding. This theory was advanced in part because the CD3γε heterodimer was found to be rigid rather than conformationally responsive[32]. Although several variants of the proposed model exist, a common theme includes a pulling action on TCR creating a "piston-like" movement of rigid CD3 that exposes activating ITAM residues.

During T cell activation, fluctuations of the APC membrane can generate a pico- to fentonewton force on the T cell membrane[33]. These forces can also be triggered by a timed series of active pushing and pulling processes by the T cell[34]. Mechanical forces in this range induced by micromanipulation of TCR by pMHC or clonotypic antibodies can trigger downstream signaling responses in T cells [35,36], and mechanical signals between T cells and APC enhanced by shear flow triggered stronger T cell stimulation *in vitro*[37]. Thus, mechanical triggering is a compelling mechanism of activation. However, no studies to date have firmly defined a necessary role for mechanical force generation during T cell signaling, and it remains to be seen

Thus, both conformational and mechanical models of triggering are intriguing but have not yet yielded conclusive evidence as the primary mechanism of TCR triggering. Other mechanisms

have been explored in parallel, including the influence of rearrangements in spatial organization of membrane receptors

1.1.2 Spatial Organization During T cell Activation

The idea that spatial organization of the TCR and accessory signaling proteins plays a critical role in T cell activation gained support with the discovery of the immune synapse[38], a micro-scale cell-cell interaction structure formed by T cells and APC. During immune synapse formation, adhesion molecules such as LFA-1 migrate to the periphery of the T cell contact site, the peripheral Supramolecular Adhesion Cluster (pSMAC), whereas TCR, CD3, and a host of signaling proteins are found in the cSMAC. However, the discovery of the synapse was soon followed by studies that showed that synapse formation, which occurs minutes after T cell-APC contact, was preceded by strong TCR signaling, and was thus not the long-sought after mechanism of T cell activation[39]. Thus, today the immune synapse is appreciated as a structure that is a consequence of sustained T cell-APC interactions, and modulates T cell response, but is not absolutely required for TCR triggering.

Regardless, the search was on for other structures and changes in the lateral organization of TCR that could explain the early activation events involved in T cell activation. This search was aided by several technical innovations, chief among them the use of model lipid bilayers coupled to Total Internal Reflection Microscopy (TIRF). Model bilayers provide a large, flat contact surface which can be functionalized with pMHC and adhesion ligands at the appropriate density[40], and TIRF provides a high-resolution, low-background image of the T cell-APC contact interface[41].

These studies revealed that TCR clusters, 100's of nm in diameter and containing 10's to 100's of TCR, were formed soon after contact with cognate MHC (reviewed in [42]). These clusters are enriched for signaling molecules such as Lck, Zap-70, Lat, and SLP76, suggesting they are

directly involved in T cell signaling. Microcluster formation precedes but is closely associated with synapse formation, as both involve a cortical F-actin flow that leads to inward migration of TCR.

By what mechanism could spatial rearrangements during T cell activation lead to phosphorylation of downstream signaling proteins? A common element in spatial models is kinase concentration and phosphatase exclusion – phosphorylating proteins are concentrated in the region that contains their substrate, whereas dephosphorylating proteins are excluded, tipping the local balance towards phosphorylation and signaling. Consistent with this hypothesis, it was recently shown that close apposition between the T cell and APC membrane drove exclusion of proteins such as CD45, whereas the binding energy between TCR and pMHC was sufficient to keep these proteins within the contact area[43]. This mechanism was shown to be sufficient for T cell signaling in a reconstituted system. Furthermore, new high-resolution imaging techniques have shown nanoscale co-localization of TCR and downstream signaling proteins, which is enhanced after cognate pMHC binding[44].

1.1.2.1 Persistent Changes in TCR Organization Before and After T Cell Activation

Spatial heterogeneity in membrane organization and TCR clustering can be detected even in the absence of activation by cognate antigen. Using immunoprecipitation and immunoblotting techniques, Fernandez-Miguel et al. demonstrated that the αβ T cell receptor can exist as a multivalent structure on naive T cells, composed of at least two TCR and a higher order CD3 stoichiometry[45]. While immunoprecipitation is highly dependent on technical considerations such the detergent used during membrane lysis, disassociation with a milder reagent showed a similar effect[46]. TCR likely exist in several distinct monovalent and multivalent forms at

baseline, prior to antigen engagement[47]. During T cell activation, these TCR islands concatenate to form the large microclusters that are observed by TIRF imaging[44].

Following activation, TCR undergo a state-dependent, persistent increase in the extent of TCR clustering. Binding assays using dimeric MHC-Ig fusion proteins demonstrated that T cells activated four days previously showed enhanced binding of low concentrations of MHC, with a high degree of cooperativity[1,48]. Since this effect was not observed with monovalent MHC, the authors predicted a higher degree of clustering led to enhanced binding of MHC dimers. Persistent TCR clusters on activated cells was directly visualized using electron[49] and k-Space Image Correlation microscopy[50], with a distinct increase in clustering noted compared to naive cells.

In general, receptor clustering prior to ligand engagement can be a mechanism of enhanced binding and increased sensitivity. For example, clustering of chemo-receptors on *E coli.* significantly lowers the threshold and enhances the dynamic range of chemotactic responses[51]. Preliminary evidence suggests that such clustering may be partially responsible for the high degree of T cell sensitivity to antigen; for example, only multivalent but not monovalent TCR/CD3 complexes were phosphorylated after stimulation with a low dose of antigen[46,52]. Enhanced clustering may also partially explain the increased sensitivity of previously activated T cells to antigen, acting in concert with changes in downstream signaling[53]. However, the mechanisms of persistent TCR clustering and how they relate to clustering observed during ligand engagement are still not understood.

1.1.3 The Role of the Accessory Protein CD8 in Binding and Signaling

While the TCR/CD3 complex is the primary molecule involve in T cell signaling, many accessory proteins influence binding and signaling. For example, two distinct classes of T cells

can be characterized by expression of either CD8 or CD4 co-receptor proteins in addition to TCR/CD3. These two sub-types, termed killer and helper T cells respectively, are functionally distinct and arise from positive selection by either MHC Class I ligands in the case of CD8, or MHC Class II ligands in the case of CD4, during thymic development.

Co-receptors have two complementary but controversial roles during T cell activation (reviewed in [54]). It is known that both CD4 and CD8 have binding sites on their respective MHC ligands, and crystal structures have been described for the ternary pMHC-TCR-CD8/4 complex. However, the precise contribution of co-receptor binding to pMHC has been a matter of some debate. Co-receptors are cytoplasmically associated with the src-family tyrosine kinases Lck and Fyn, which are involved in early T cell signal transduction. The binding of co-receptor to MHC spatially localizes these kinases with the CD3 ITAMs they phosphorylate, which enhances but is not required for T cell activation[55].

Secondly, co-receptor binding may stabilize binding between TCR with pMHC, but the contribution of this role may be context-dependent. Experiments have shown that the presence of CD4 does not significantly contribute to TCR-pMHC binding [18]. The affinity of CD8 for MHC Class I is weak, at approximately 50 μM in the mouse and 150 μM in the human[54], 10-100 fold weaker than between TCR and MHC. Affinity is similarly low when measured using 2D techniques [56]. A role for CD8 is further marginalized by evidence that pMHC binds TCR prior to engaging CD8 [57]. This has led some authors to argue that the co-receptor does not make a significant contribution by binding MHC, except insofar as it co-localizes Lck[58].

Despite this, significant evidence exists that at least some TCR are dependent on the presence of CD8 to bind cognate soluble MHC[59,60], whereas others are “CD8-independent” [61,62].

Micropippette assays have revealed that despite being of low affinity and binding MHC in a second phase after TCR, the cumulative effect of CD8-MHC interactions can still be significant[20]. CD8 stabilization may thus be beneficial only for particularly weak pMHC ligands[63], and its presence can enhance T cell binding and activation in such cases[64]. Furthermore, a role for CD8 binding to MHC can vary with the activation state and may be lost as a mechanism of T cell suppression or activation [65–67]. Thus, in evaluating the binding contribution of CD8, it is important to consider both the affinity of TCR for MHC as well as the particular state of the relevant T cell.

1.1.4 References

1. Fahmy TM, Bieler JG, Schneck JP. Probing T cell membrane organization using dimeric MHC-Ig complexes. *Journal of Immunological Methods*. 268(1), 93–106 (2002).
2. Holmberg K, Mariathasan S, Ohteki T, Pamela O, Gascoigne NRJ. TCR Binding Kinetics Measured with MHC Class I Tetramers Reveal a Positive Selecting Peptide with Relatively High Affinity for TCR. *Journal of Immunology*. 171, 2427–2434 (2003).
3. Davis MM, Altman JD, Newell EW. Interrogating the repertoire: broadening the scope of peptide-MHC multimer analysis. *Nature reviews. Immunology*. 11(8), 551–8 (2011).
4. Boulter JM, Schmitz N, Sewell AK, Godkin AJ, Bachmann MF, Gallimore AM. Potent T cell agonism mediated by a very rapid TCR/pMHC interaction. *European Journal of Immunology*. 37(3), 798–806 (2007).
5. Mcmahan RH, Mcwilliams JA, Jordan KR, Dow SW, Wilson DB, Slansky JE. Relating TCR-peptide-MHC affinity to immunogenicity for the design of tumor vaccines. 116(9), 2543–2551 (2006).
6. Tian S, Maile R, Collins EJ, Frelinger JA. Affinity , Not Dissociation Rate 1. *PRism*. (2010).
7. Carreño LJ, Bueno SM, Bull P, Nathenson SG, Kalergis AM. The half-life of the T-cell receptor/peptide-major histocompatibility complex interaction can modulate T-cell activation in response to bacterial challenge. *Immunology*. 121(2), 227–37 (2007).
8. Qi S, Krogsgaard M, Davis M, AK. Molecular flexibility can influence the stimulatory ability of receptor–ligand interactions at cell–cell junctions. *Proceedings of the*. 103(12), 4416–21 (2006).
9. Kalergis AM, Boucheron N, Doucey M, *et al.* Efficient T cell activation requires an optimal dwell-time of interaction between the TCR and the pMHC complex. 2(3), 229–234 (2001).

10. Krogsgaard M, Prado N, Adams EJ, *et al.* Evidence that structural rearrangements and/or flexibility during TCR binding can contribute to T cell activation. *Molecular cell*. 12(6), 1367–78 (2003).

11. Valitutti S, Muller S, Cella M, Padovan E, Lanzavecchia A. Serial triggering of many T-cell receptors by a few peptide–MHC complexes. *Nature*. (1995).

12. Dushek O, Coombs D. Analysis of serial engagement and peptide-MHC transport in T cell receptor microclusters. *Biophysical Journal*. 94(9), 3447–60 (2008).

13. Wofsy C, Coombs D, Goldstein B. Calculations show substantial serial engagement of T cell receptors. *Biophysical Journal*. 80(2), 606–12 (2001).

14. Mckeithan TW. Kinetic proofreading in T-cell receptor signal transduction. *Proc. Natl. Acad. Sci. USA*. 92, 5042 (1995).

15. Rabinowitz JD, Beeson C, Lyons DS, Davis MM, McConnell HM. Kinetic discrimination in T-cell activation. *Proceedings of the National Academy of Sciences of the United States of America*. 93(4), 1401 (1996).

16. Aleksic M, Dushek O, Zhang H, *et al.* Dependence of T cell antigen recognition on T cell receptor-peptide MHC confinement time. *Immunity*. 32(2), 163–74 (2010).

17. Dushek O, Das R, Coombs D. A role for rebinding in rapid and reliable T cell responses to antigen. *PLoS computational biology*. 5(11), e1000578 (2009).

18. Huppa JB, Axmann M, Mörtelmaier M a, *et al.* TCR-peptide-MHC interactions in situ show accelerated kinetics and increased affinity. *Nature*. 463(7283), 963–7 (2010).

19. Jiang N, Huang J, Edwards L, Liu B. Two-stage cooperative T cell receptor-peptide major histocompatibility complex-CD8 trimolecular interactions amplify antigen discrimination. *Immunity*. 34(1), 13–23 (2011).

20. Huang J, Zarnitsyna VI, Liu B, *et al.* The kinetics of two-dimensional TCR and pMHC interactions determine T-cell responsiveness. *Nature*. 464(7290), 932–6 (2010).

21. Sabatino JJ, Huang J, Zhu C, Evavold BD. High prevalence of low affinity peptide-MHC II tetramer-negative effectors during polyclonal CD4+ T cell responses. *The Journal of experimental medicine*. 208(1), 81–90 (2011).

22. Zhu C, Jiang N, Huang J, Zarnitsyna VI, Evavold BD. Insights from in situ analysis of TCR-pMHC recognition: response of an interaction network. *Immunological reviews*. 251(1), 49–64 (2013).

23. Allison JP, Mcintyre BW, Bloch D. Tumor-specific antigen of murine T-lymphoma defined with monoclonal antibody. *Journal of Immunology*. 129, 2293–2300 (1982).

24. Meuer BYSC, Fitzgerald KA, Hussey RE, Hodgdon JC, Schlossman SF, Reinherz EL. Clonotypic Structures Involved in Antigen-Specific Human T Cell Function. *Journal of Experimental Medicine*. 157(February), 705–719 (1983).

25. Haskins K, Kubo R, White J, Pigeon M, Kappler J, Marrack P. Major Histocompatability Complex-Restricted Antigen Receptor on T Cells. *Journal of Experimental Medicine*. 157(April), 1149–1169 (1983).

26. Hedrick SM, Cohen DI, Nielsen EA, Davis MM. Isolation of cDNA clones encoding T cell-specific membrane-associated proteins. *Nature*. 308, 149–153 (1984).

27. Guy CS, Vignali DAA. Organization of proximal signal initiation at the TCR:CD3 Complex. *Immunological Reviews*. 232(1), 7–21 (2009).

28. Rudolph MG, Stanfield RL, Wilson I a. How TCRs bind MHCs, peptides, and coreceptors. *Annual review of immunology*. 24, 419–66 (2006).

29. Kjer-nielsen L, Clements CS, Purcell AW, *et al.* A Structural Basis for the Selection of Dominant. 18, 53–64 (2003).

30. Gil D, Schamel WWA, Sa F, Alarco B. Recruitment of Nck by CD3 ♪ Reveals a Ligand- Induced Conformational Change Essential for T Cell Receptor Signaling and Synapse Formation. 109, 901–912 (2002).

31. Mingueneau M, Sansoni A, Grégoire C, *et al.* The proline-rich sequence of CD3epsilon controls T cell antigen receptor expression on and signaling potency in preselection CD4+CD8+ thymocytes. *Nature immunology*. 9(5), 522–32 (2008).

32. Sun ZJ, Kim KS, Wagner G, Reinherz EL. Mechanisms Contributing to T Cell Receptor Signaling and Assembly Revealed by the Solution Structure of an Ectodomain Fragment of the CD3 ♪♪ Heterodimer. 105, 913–923 (2001).

33. Henry N, Hivroz C. Early T-cell activation biophysics. *HFSP journal*. 3(6), 401–11 (2009).

34. Husson J, Chemin K, Bohineust A, Hivroz C, Henry N. Force generation upon T cell receptor engagement. *PloS one*. 6(5), e19680 (2011).

35. Li Y-C, Chen B-M, Wu P-C, *et al.* Cutting Edge: mechanical forces acting on T cells immobilized via the TCR complex can trigger TCR signaling. *Journal of Immunology*. 184(11), 5959–63 (2010).

36. Kim ST, Takeuchi K, Sun Z-YJ, *et al.* The alphabeta T cell receptor is an anisotropic mechanosensor. *The Journal of biological chemistry*. 284(45), 31028–37 (2009).

37. Lim TS, Mortellaro A, Lim CT, Hämmerling GJ, Ricciardi-castagnoli P. Mechanical Interactions between Dendritic Cells and T Cells Correlate with T Cell Responsiveness. (2012).

38. Monks CRF, Freiberg BA, Kupfer H, Sciaky N, Kupfer A. Three-dimensional segregation of supramolecular activation clusters in T cells. *Nature*. 395(6697), 82–86 (1998).

39. Lee K-H, Holdorf AD, Dustin ML, Chan AC, Allen PM, Shaw AS. T cell receptor signaling precedes immunological synapse formation. *Science*. 295(5559), 1539–42 (2002).

40. Simons K, Vaz WLC. Model systems, lipid rafts, and cell membranes. *Annual review of biophysics and biomolecular structure*. 33, 269–95 (2004).

41. Groves JT, Parthasarathy R, Forstner MB. Fluorescence imaging of membrane dynamics. *Annual review of biomedical engineering*. 10, 311–38 (2008).

42. Dustin ML, Groves JT. Receptor signaling clusters in the immune synapse. *Annual review of biophysics*. 41, 543–56 (2012).

43. James JR, Vale RD. Biophysical mechanism of T-cell receptor triggering in a reconstituted system. *Nature*. 487(7405), 64–9 (2012).

44. Lillemeier BF, Mörtelmaier M a, Forstner MB, Huppa JB, Groves JT, Davis MM. TCR and Lat are expressed on separate protein islands on T cell membranes and concatenate during activation. *Nature Immunology*. 11(1), 90–6 (2010).

45. Fernández-Miguel G, Alarcón B. Multivalent structure of an αβT cell receptor. *Proceedings of the*. 96(February), 1547–1552 (1999).

46. Schamel WW a, Arechaga I, Risueño RM, *et al.* Coexistence of multivalent and monovalent TCRs explains high sensitivity and wide range of response. *The Journal of experimental medicine*. 202(4), 493–503 (2005).

47. Alarcón B, Swamy M, van Santen HM, Schamel WW a. T-cell antigen-receptor stoichiometry: pre-clustering for sensitivity. *EMBO reports*. 7(5), 490–5 (2006).

48. Fahmy TM, Bieler JG, Edidin M, Schneck JP. Increased TCR avidity after T cell activation: a mechanism for sensing low-density antigen. *Immunity*. 14(2), 135–43 (2001).

49. Kumar R, Ferez M, Swamy M, *et al.* Increased Sensitivity of Antigen-Experienced T Cells through the Enrichment of Oligomeric T Cell Receptor Complexes. *Immunity*. 35(3), 375–87 (2011).

50. Boyle S, Kolin DL, Bieler JG, Schneck JP, Wiseman PW, Edidin M. Quantum Dot Fluorescence Characterizes the Nanoscale Organization of T Cell Receptors for Antigen. *Biophysical Journal*. 101(11), L57–L59 (2011).

51. Bray D, Levin MD, Morton-Firth CJ. Receptor clustering as a cellular mechanism to control sensitivity. *Nature*. 393(6680), 85–88 (1998).

52. Schamel WW a. The stoichiometry of the T cell antigen receptor and its implications for the signal transduction mechanism. *Signal Transduction*. 7(4), 311–319 (2007).

53. Adachi K, Davis MM. T-cell receptor ligation induces distinct signaling pathways in naïve vs . antigen-experienced T cells. *Proceedings of the National Academy of Sciences*. (2010).

54. Li Y, Yin Y, Mariuzza R a. Structural and biophysical insights into the role of CD4 and CD8 in T cell activation. *Frontiers in immunology*. 4(July), 206 (2013).

55. Arcaro A, Grégoire C, Bakker TR, *et al.* CD8beta endows CD8 with efficient coreceptor function by coupling T cell receptor/CD3 to raft-associated CD8/p56(lck) complexes. *The Journal of experimental medicine*. 194(10), 1485–95 (2001).

56. Huang J, Edwards LJ, Evavold BD, Zhu C. Kinetics of MHC-CD8 interaction at the T cell membrane. *Journal of Immunology*. 179(11), 7653–62 (2007).

57. Yachi PP, Ampudia J, Gascoigne NRJ, Zal T. Non-stimulatory peptides contribute to antigen induced CD8-TCR interaction at the immunological synapse. *Nature Immunology*. 6(8), 785–792 (2006).

58. Artyomov MN, Lis M, Devadas S, Davis MM, Chakraborty AK. CD4 and CD8 binding to MHC molecules primarily acts to enhance Lck delivery. *PNAS*. (2010).

59. Daniels M a, Jameson SC. Critical role for CD8 in T cell receptor binding and activation by peptide/major histocompatibility complex multimers. *The Journal of experimental medicine*. 191(2), 335–46 (2000).

60. Gakamsky DM, Luescher IF, Pramanik A, *et al.* CD8 kinetically promotes ligand binding to the T-cell antigen receptor. *Biophysical Journal*. 89(3), 2121–33 (2005).

61. Choi EM-L, Chen J-L, Wooldridge L, *et al.* High avidity antigen-specific CTL identified by CD8-independent tetramer staining. *Journal of immunology (Baltimore, Md. : 1950)*. 171(10), 5116–23 (2003).

62. Cho BK, Lian KC, Lee P, *et al.* Differences in antigen recognition and cytolytic activity of CD8(+) and CD8(-) T cells that express the same antigen-specific receptor. *Proceedings of the National Academy of Sciences of the United States of America*. 98(4), 1723–7 (2001).

63. Kerry SE, Buslepp J, Cramer L a, *et al.* Interplay between TCR affinity and necessity of coreceptor ligation: high-affinity peptide-MHC/TCR interaction overcomes lack of CD8 engagement. *Journal of Immunology*. 171(9), 4493–503 (2003).

64. Stone JD, Aggen DH, Chervin AS, *et al.* Opposite effects of endogenous peptide-MHC class I on T cell activity in the presence and absence of CD8. *Journal of Immunology*. 186(9), 5193–200 (2011).

65. Kao C, Daniels MA, Jameson SC. Loss of CD8 and TCR binding to Class I MHC ligands following T cell activation. *International Immunology*. 17(12), 1607–17 (2005).

66. Demotte N, Stroobant V, Courtoy PJ, *et al.* Restoring the association of the T cell receptor with CD8 reverses anergy in human tumor-infiltrating lymphocytes. *Immunity*. 28(3), 414–24 (2008).

67. Cawthon AG, Alexander-Miller M a. Optimal colocalization of TCR and CD8 as a novel mechanism for the control of functional avidity. *Journal of Immunology*. 169(7), 3492–8 (2002).

1.2 Artificial Antigen Presenting Cells

Artificial Antigen Presenting Cells (aAPC) are bioengineered platforms for T cell stimulation. Like endogenous APC, aAPC deliver a series of receptor and cytokine-mediated activating signals that trigger T cell signaling and activation. In turn, activated T cells mediate a therapeutic effect that takes advantage of three critical properties of adaptive immunotherapy: 1) T cell responses are specific, targeting specific antigens on diseased tissue while sparing the healthy host; 2) T cells responses are robust, undergoing up to 1,000-fold clonal expansion after activation; and 3) T cell responses have memory, maintaining therapeutic effect for many years after initial treatment.

Thus, there is tremendous interest in developing flexible, reliable, and economical techniques for inducing T cell immunity. As we will discuss, aAPC possess a number of advantages over competing techniques in achieving these goals.

aAPC have been built upon a wide variety of biocompatible platforms, including cell lines, liposomes, and biodegradable polymer particles, and coupled to a wide variety of proteins that deliver T cell activating signals. Building an optimal aAPC requires carefully selecting the platform and proteins that will lead to optimal T cell effector function *in vivo* and *in vitro*. In this chapter, I will review the basic principles of aAPC design, and review previous experience with platforms developed with various components. First, we will motivate the need for aAPC by comparing aAPC-based T cell stimulation techniques to comparable technologies.

1.2.1 When and Why to Use APC

aAPC are one of only several strategies for *in vitro* or *in vivo* T cell activation. *In vitro*, T cells can be expanded with culture and stimulation techniques that rely autologous APC, soluble

activating proteins and autologous feeder cells, or peptide-pulsed APC lines. *In vivo,* vaccination with DNA, peptide and adjuvant, or whole-cell vaccines can lead to antigen processing by host APC and direct T cell priming. While each of these approaches can be effective and is in therapeutic development, aAPC have several advantages that must be considered when choosing a T cell activation strategy.

APC Dysfunction and Immune Suppression

In vivo vaccination approaches for T cell expansion depend upon a functional APC compartment that can process antigen, recognize danger signals, and prime active immunity. APC dysfunction in several pathological states, and particularly cancer, motivates a desire to replace or supplement the endogenous APC compartment with fully functional aAPC.

The peripheral blood of cervical carcinoma patients shows decreased numbers of CD11c+ and CD123+ DCs, correlated with increased levels of immunosuppressive cytokines IL-6 and TGF-β in serum[1]. Similarly, blood DCs from breast cancer patients undergo spontaneous apoptosis[2]. What DC remain are poorly functional, with DCs from lymph nodes and peripheral blood of cancer patients showing low stimulatory capacity *ex vivo*[3], and despite being associated with a mature phenotype, decreased production of immunostimulatory cytokines such as IL-12[4].

Within the tumor microenvironment, APC can go beyond simple dysfunction toward active immune suppression. Tumor-associated DCs upregulate a variety of genes associated with immunosuppression (IDO, ARG, TGF-β, and PD-L1) and tolerize T cells by a FOXO3-depndent mechanism [5,6]. Macrophages are polarized toward related wound-healing (M2) or immunosuppressive phenotypes characterized by fibrosis and TGF-β production, respectively, rather than effective T cell priming and support[7]. Myeloid compartment differentiation is re-

directed towards production of myeloid-derived suppressor cells (MDSC), which inhibit T cell function through a variety of overlapping mechanisms [8,9]. Thus, even if antigen is delivered to host APC by a vaccine platform, it may not lead to T cell activation, which may be a factor in poor results to vaccine based approaches for cancer immunotherapy[10].

Cost-And-Ease of Manufacture

Biologic therapies that rely on *in vitro* culture of T cells with autologus APC or feeder cells are expensive and labor intensive processes. For cellular therapies for cancer, methods for expanding peripheral blood lymphocytes or tumor infiltrating lymphocytes are themselves a complex biologic that must be repeatedly assessed for safety and reliability, adding to complexity and expense. By way of example, an adoptive immunotherapy for cancer, sipuleucel-T (Provenge®), was recently approved by the FDA for treating prostate cancer and costs $93,000 per course of treatment[11]. The complicated culture process must be performed individually for each new patient, and the high price may limit its long term benefit. In contrast, aAPC can be produced for many patients in bulk and designed from easily manufactured, biocompatible platforms, creating an off-the-shelf reagent that has significantly reduced cost compared to cellular biologics.

Choosing the Right Signals

In designing an aAPC, the engineer must select the T cell stimulatory molecules that will be coupled to the platform and influence T cell development. This presents an opportunity to precisely control the signals received by T cells in a way that is not possible when relying on endogenous APC, which deliver innumerable, interacting, incompletely understood signals to a given cell. Since T cell behavior and effector phenotype are modulated at least in part by signals

received during initial activation, this could lead to the expansion of high quality T cells which are optimally designed for a specific application.

What describes an "optimal" T cell? The characteristics required for effective therapy will obviously vary with pathological state, but can be broadly described in general. Optimal T cells have high functional avidity, meaning they mediate effector response in response to low doses of antigen[12,13]. They may have high binding avidity, meaning that the interaction between TCR and MHC, in contrast to many anti-cancer responses which are modulated by central tolerance to self antigen and are of low avidity [14]. They are polyfunctional, meaning that they can produce a large number of effector cytokines, a trait associated with control of chronic viral infections[15,16]. They are not exhausted and maintain proliferative capacity[17,18], as indicated by telomere length [19–21] and surface phenotype (high CD45RO, CCR7, IL-7R, CD27; low KLGR-1, PD-1, CTLA-4, TIM-3, LAG-3) [22].

The precise signals required to tune T cell quality in general, and particularly in the context of aAPC, are unknown. However, aAPC are a reductionist system, thus represent both a platform from which to study basic aspects of T cell stimulation and a mechanism for implementing that knowledge therpeutically. For example, virus-specific T cells generated by aAPC were more polyfunctional than those generated by autologous monocyte derived dendritic cells[23], which may be due the dose and density of antigen delivered **[Yen Paper]**. The lessons garnered from such studies may then be adapted to tune T cell development and craft an optimal response.

1.2.2 Designing an aAPC: The Signal 1/2/3 Paradigm

A general paradigm for the design of aAPC has been to mimic T cell activation by endogenous APC, and to select T cell activating signals that lead to optimal stimulation. As discussed in Chapter 1.1, and briefly described here, T cells require a series of carefully orchestrated

activation signals to trigger activation. In the healthy host, these are provided by endogenous APC such as macrophages, B cells, and dendritic cells. In aAPC design, these same signals are generated by coupling proteins expressed by these cells to an aAPC platform that trigger responses from receptors on the T cell membrane.

Signal 1

The first signal, Signal 1, is mediated by the interaction of TCR on the T cell with peptide presented on MHC peptide on the APC. Class I MHC preferentially interacts with T cell receptors are specific for one or several MHC-peptide combinations, and thus Signal 1 determines specificity of the T cell response for a given epitope. MHC-binding to TCR triggers activation of the TCR-associated CD3 signaling complex through as-of-yet poorly understood mechanisms[24,25]. In aAPC design, Signal 1 can be provided by either MHC-peptide binding to TCR, or by engaging the CD3 complex directly with an anti-CD3 antibody.

Soluble MHC proteins can be produced recombinantly and loaded with appropriate peptide for a variety of antigens of interest. Although Class I MHC have been more widely used and generated for a larger number of alleles, Class II MHC for stimulating CD4 T cell responses are also available. The aAPC engineer must select a combination of MHC allele and peptide presented by that allele that induces a T cell response against the antigen of interest; in humans, HLA-A201 has been most frequently studied, based on its high frequency in the United States. In mice, K^b and D^b alleles, as well as L^d, are frequently used based on their presence in the common laboratory strains C57BL6/J and Balb/c, respectively. Following stimulation, the yield and frequency of antigen-specific cells can be monitored using soluble, multimeric MHC reagents.

Alternatively, Signal 1 can be provided by an antibody against the CD3 signaling complex. A variety of activating CD3 antibodies are available, including the OTK31 clone in humans and 145-2C11 in mice, but the mechanism by which antibody binding triggers downstream T cell activation is not yet understood. Importantly, activation via CD3 triggers non-specific expansion of *all* T cells, including regulatory T cells and cells reactive against irrelevant antigens; over time, this can result in preferential expansion of irrelevant cells and reduced activity against the target. Thus, for most applications, a source of T cells enriched for activity against the antigens of interest is required. In cancer immunotherapy, tumor infiltrating lymphocytes can provide such a source of anti-tumor activity[26], or antigen-specific cells can be purified from Peripheral Blood Mononuclear Cells or other polyclonal sources by HLA-tetramer-based enrichment[27]. Unfortunately, anti-CD3/anti-CD28 beads have shown the ability to expand and sustain CD4 [28]but not CD8 T cell cultures [29,30] without additional feeder cell support, making them an appropriate choice only when CD4 cells are required, or the additional cost and labor associated with culturing autologous feeder cells can be tolerated.

Signal 2

Signal 2, the co-stimulatory signal, is a series of interactions between receptors on the APC and T cell surface that provide both activating and inhibitory signals. The prototypical interaction, between B7.1 on the APC and CD28 on the T cell surface, leads to optimal T cell expansion. If Signal 1 is engaged in the absence of Signal 2 *in vitro*, CD4+ T cells enter a state of *anergy*, in which T cell proliferation and effector function after re-stimulation are limited[31]. Ineffective Signal 2 stimulation can also lead to the development of suppressive, regulatory T cells, and the balance between anergy and regulatory development is an area of active study.

A wide variety of activating Signal 2 interactions exist, including the B7 family co-receptors B7.1 and B7.2,and their cognate APC ligand CD28; and the TNF family co-receptors OX-40, CD70, 4-1BB, which interact with OX40L, CD27, and 4-1BBL on the APC, respectively. Co-stimulatory signals can also be inhibitory to T cell expansion and effector function, such as the interaction of B7.1 and CTLA-4 or PD-1 with PD-L1 (B7.H1) or PD-L2[32].

In aAPC design, Signal 2 can be provided by coupling one of the aforementioned APC receptors to the surface of an aAPC platform. In practice, activating antibodies against co-stimulatory T cell receptors, such as the anti-mouse CD28 antibody 37.51, have been shown to be an effective replacement for more expensive recombinant APC proteins[33]. While the downstream signaling mechanisms of each co-stimulatory receptor vary, engagement by certain "activating" antibody clones appears to be a commonly effective mechanism for triggering co-stimulatory receptor activation.

Minimally, the addition of anti-CD28 antibody is required to design effective aAPC that induce robust T cell proliferation [34,35] and maintain the full complement of T cell effector functions[35,36]. Under certain conditions of extremely strong Signal 1 activation, robust expansion can be observed with Signal 1 alone[37], but the precise phenotypic characteristics of such T cells and their effectiveness in immunotherapy have not been described. On the other hand, many platforms instead rely on multiple co-stimulatory signals delivered simultaneously[38].

The precise signals delivered by each Signal 2 are likely to differ, and thus the choice of Signal 2 protein may be an important parameter in optimal aAPC design. For example, 4-1BBL may be more effective than anti-CD28 as an activating signal for CD8 T cell expansion[39,40], or even

synergize with simultaneously presented CD28[41]. The role of inhibitory signals has been explored to a lesser extent; the addition of a PD-L1 to aAPC does not appear to decrease T cell proliferation[42], but may have a role in shaping the subsequent response.

Signal 3

Signal 3 is a catch-all term for a variety of soluble signals released by APC that influence T cell activation and development. These include lymphotrophic cytokines such as IL-2, IL-7, and IL-15; inflammatory signals such as TNF-α; and cytokines which modulate T cell development such as TGF-β, IL-12, IL-4, and IL-5. The precise effect of each of these signals is beyond the scope of this review, but the cytokine milieu released by APC before and during T cell activation is a critical determinant of T cell development after activation [43–45].

During *in vitro* T cell stimulation by aAPC, the addition of exogenous IL-2 is required for robust T cell expansion[46–48]. Alternatively, proliferation can be supported by a variety of common gamma chain cytokines, such as IL-7, IL-15, and IL-21, which may have the further benefit of maintaining T cell replicative potential and inducing memory formation compared to IL-2 [49,50]. These cytokines have been added to aAPC-stimulated cultures to generate cells more amenable to tumor immunotherapy[51]. IL-12 and Type 1 interferons added to culture can support proliferation at low to intermediate antigen doses, and the development of full effector function at any antigen dose [52–54].

There may be a further benefit to delivery of Signal 3 directly from aAPC, which could increase local cytokine concentration at the T cell-aAPC interface, spatially co-localize all 3 T cell stimulatory signals, and deliver cytokines to the appropriate site after *in vivo* administration. Thus far, application of Signal 3 in aAPC design has been limited by the capabilities of aAPC

platforms. While membrane proteins can be coupled to the surface of latex or iron-dextran microspheres, most platforms cannot mediate the controlled release of soluble T cell ligands. However, recent developments in design of aAPC based on biodegradable polymers, which can release encapsulated proteins in a spatially localized manner during hydrolytic degradation, have shown that IL-2 delivery from aAPC can significantly enhance T cell proliferation *in vitro*[55–57]. This "paracrine" delivery was ten-fold more effective in inducing T cell expansion than the same overall dose of IL-2 in the culture media[56]

1.2.3 Selecting a Platform

aAPC are constructed by coupling T cell activating proteins described in the previous section to a suitable, biocompatible platform. While soluble MHC can induce some T cell activation[58–60], fixing such MHC-antigen or anti-CD3 to a physical substrate, such as a latex bead, liposome, or microplate surface, significantly enhances the strength of T cell stimulation[59,61–65] through mechanisms that may involve mechanical signals delivered by solid substrates [66–68] or aggregation of TCR by physically constrained MHC [25,69]. The aAPC platform also spatially localizes multiple T cell activating signals, increasing the likelihood that a T cell will be exposed to both MHC and co-stimulatory signals simultaneously[70]. Finally, fixation to a nano- or microscale construct significantly alters antigen trafficking, internalization, degradation, and clearance[71] properties *in vivo*, which is discussed in greater detail below.

Cell-based

Initial aAPC design focused on creating APC-like cells without the need to culture autologous APC from each patient. These "cell-based" aAPC are thus based on readily cultured cell lines[72,73], particularly the K562 human erythromyeloid line[38,39,74–80] and the murine NIH/3T3 fibroblast line[81–83]. Importantly, K562 does not naturally express any T cell

activating proteins such as MHC or co-stimulatory proteins, allowing the investigator to select the precise signals delivered to T cells. These proteins of interest must then be stably expressed in the relevant line, for example by lentiviral gene transfer [80]. However, K562 cells do naturally express ICAM-1 and LFA-3, required to form an immune synapse, as well as negative co-stimulatory proteins PD-L1, PD-L2, and B7-H3.

Unlike the synthetic bead-based platforms reviewed below, cell-based aAPC maintain features of a cell that may be relevant to T cell activation, such as antigen processing machinery and a fluid lipid membrane. The ability to process protein and present antigenic peptides on transfected MHC reduces the need to identify antigenic eptiopes *a priori*. Cell lines cannot of course be safely administered *in vivo* as a T cell vaccine, and are thus limited to *in vitro* applications.

Liposomes

Among the earliest cell-free platforms used for T cell activation were lipsomes, spherical vesicles with an aqueous interior generated by self-assembly of ampiphilic phospholipids and cholesterol. Liposomes have been used extensively as carriers [84] for water soluble drugs trapped in their aqueous core, and are sufficiently biocompatible to be administered *in vivo*. Liposome-based aAPC can be generated by detergent disruption of membranes from cells that express or are transduced to express the relevant T cell-activating signals[85,86], or by directly by mixing purified membrane proteins with ampiphilic lipids and surfactants at known ratios[63,64,87–90]. Exosomes derived from dendritic cells, which like liposomes are lipidbilayer structures that express MHC and other T cell activating proteins, have thus far been weakly immunogenic[91] but are being examined as an aAPC platform.

Like cells, liposomes have fluid lipid exteriors which allow the free movement of protein. Unlike cells, liposomes can be generated in sizes ranging from <100 nm to several microns in diameter; the importance of aAPC size as a design parameter will be reviewed below. Furthermore, liposomes can be used to deliver soluble Signal 3 molecules trapped within their core.

Latex Beads

Latex (polystyrene) beads were one of the first synthetic bead-based platforms used in aAPC design. They have been instrumental as a reductionist system for studying basic aspects of T cell biology[29,47,92–95], as well as translational platform for adoptive immunotherapy [96–99]. Latex-based aAPC are synthesized by chemically coupling soluble proteins to a functionalized polystyrene surface, or indirectly by attaching biotin-labeled T cell activating proteins to avidin-coated particles.

Polystyrene-based microparticle systems have predominantly used to expand T cells *in vitro*, as they have present serious biocompatibility concerns if co-infused with T cells or administered directly *in vivo*. Intravenously administered rigid particles greater than 3-5 μm in diameter lodge in small capillary beds, particularly in the lung[100–102], which could cause capillary infarction. This has motivated the development of particles which can be removed from or degrade during culture, as will be described in further sections.

MHC presented on rigid bead-based platforms, or fixed on a cell surface by gluteraldehyde [37], may provide a stronger stimulatory signal than MHC presented on a cell membrane, and substrate rigidity [66–68] is known to be a critical parameter for T cell activation. Alternatively, a hybrid lipid-latex particle can be synthesized by coating a silica or polystyrene microsphere

with plasma membrane vesicles[61,103–105], which combines the potential advantages of both a rigid substrate and a fluid membrane.

Magnetic Particles

Iron-oxide core, dextran coated nano- and microparticles have been extensively used for cell isolation and purification, with paramagnetic particles binding ligand-labeled cells of interest and trapping them in a magnetic field[106,107]. Although iron-dextran nanoparticles display excellent biocompatibility when co-infused with labeled cells [108–110], iron-dexran microparticles can lodge in capillary beds like their polystyrene counterparts. Unlike polystyrene particles, however, paramagnetic iron-dextran microparticles can be removed from T cell culture using a magnetic field, or degrade into iron and dextran metabolites after *in vivo* injection, providing a considerable advantage in biocompatibility. Furthermore, removal of paramagnetic beads and their co-stimulatory signals may actually enhanced T cell proliferation under certain circumstances[46].

Iron-dextran micropraticles have been thus been extensively characterized as aAPC [34,111–115]. They have been studied both as platforms for translational application of tumor antigens[34,114], and as a tool for the study of basic aspects of T cell antigen recogntition and development[23,116–118]. CD3/CD28 coupled iron-dextran are commercially available as CD4 expansion platforms[119], have been used to support regulatory T cell expansion in a number of settings [78,120]. Their availability as clinical-grade reagants that can be removed prior to infusion makes them a popular choice for non-specific T cell expansion in a trial setting[121,122].

Biodegradable Polymer

Like liposomes, microspheres assembled from biodegradable polymers were initially developed as vehicles for drug delivery[123,124]. Microparticles can be synthesized in a variety of sizes (100's of nms to 10 micrometers in diameter) from a variety of polymers, such as poly (lactic acid) (PLL), poly (glycolic acid) (PGA), and their co-polymer, poly (lactic-co-glycolic acid). Over several hours to weeks, depending on their formulation, biodegradable polymer particles are hydrolyzed to non-toxic end products, releasing drugs encapsulated within them.

Due to their excellent biocompatibility and degradation properties, biodegradable polymer particles are an excellent choice for aAPC platforms that will be administered *in vivo*[125]. Importantly, they can be designed to release soluble cytokine signals as they degrade, and are the most promising platforms for integrating these signals into aAPC design[126,127].

1.2.4 Choosing a Therapeutic Approach

The selection of T cell activating proteins and aAPC platform should be made in concert with the development of a therapeutic approach. There are two basic approaches to using aAPC: they can be used to generate T cell responses in vitro that are then adoptively transferred into the patient, or directly administered *in vivo* as a T cell vaccine. Both approaches have advantages and disadvantages, which will be reviewed below.

Adoptive Immunotherapy

Antigen-specific T cells generated *in vitro* and adoptively transferred into a patient can mediate profound immunotherapeutic effects. For example, adoptive transfer of large numbers tumor infiltrating lymphocytes (TILs) generated from melanoma cultures can mediate complete and durable regression of even large and metastatic tumors[26]. Adoptive transfer of CMV-specific lymphocytes has been studied as a means of limiting immunosuppression post-transplant[33,128], and regulatory T cells have been transferred to control autoimmune

disease[129] and Graft-vs.-Host disease[78]. A critical step thus involves generating a large number of antigen-specific T cells *in vitro*, which can be performed using aAPC (reviewed in[130]).

Adoptive immunotherapy possess several key advantages over direct *in vivo* injection and vaccination. By stimulating T cells in a constrained *in vitro* culture environment, the investigator can ignore otherwise challenging issues of aAPC biodistribution, clearance, and trafficking. Furthermore, adoptive immunotherapy at least temporarily separates the patient and their accompanying pathology from the therapeutic cells, allowing each to be conditioned and treated separately. For example, high intensity lymphodepletion with chemotherapy or radiation prior to adoptive transfer significantly enhances immunotherapy for metastatic melanoma [131–133] by at least two mechanisms[26,134]: depleting the immunosuppressive regulatory cells that inhibit productive anti-tumor responses, and it creating "space" in the lymphoid compartment that decreases competition for lymphotrophic cytokines and improves retention of transferred cells. This approach is made possible by the physical separation of the patient and their *ex vivo* cultured cells, which would otherwise be depleted as well. On the other hand, *in vitro* T cell culture is costly and labor-intensive compared to direct administration, and can be described as designing a "new drug" for each patient.

The most direct method of generating antigen-specific T cells involves expanding polyclonal populations of CD8 or CD4-sorted lymphocytes, splenocytes, or PBMC with aAPC bearing the MHC-peptide of interest. This is a particularly useful approach if antigens specific to the cellular targets involved in disease have been described, and robust T cell responses can be generated against these antigens in most patients. The amount and frequency of antigen-specific cells that can be generated is highly dependent on aAPC platform, antigen choice, and culture conditions.

CD8+ T cells can be expected to expand approximately 10-50 fold after one week[40], and up to several hundred fold over 2-4 weeks[75,112]. The resulting antigen specificity of the culture depends on the precursor frequency of the cells of interest: naive CD8 precursor frequencies are estimated to be on the order of 10-800 per 10 million [135], but responses against common pathogens such as flu exist at considerably higher frequencies [116]. Thus, representative frequencies at one week can be as high as 5% after one week o stimulation[73] for tumor antigen, or up to 20% for CMV[136]. This increases significantly with repeated stimulation, . These numbers compare favorably with the numbers of T cells required for adoptive immunotherapy. For example, approximately 10^6 antigen specific T cells are required for the durable regression of established subcutaneous melanoma in mice[137], and approximately 10^{10} are transferred for cancer immunotherapy during clinical trials[138], numbers which can be reliably generated by aAPC stimulation for many relevant antigens.

Alternatively, one can simultaneously generate T cell populations against multiple antigens of interest with aAPC platforms conjugated to anti-CD3. This approach is particularly relevant if the investigator has access to a pool of T cells that already has the required activity; for example, T cells with activity against melanoma can be cultured from Tumor Infiltrating Lymphocytes. Unfortunately, TILs cannot be expanded from all melanoma patients, nor in most other cancers[139]. Furthermore, depending on the starting T cell population, CD3-based stimulation may preferentially expand T cells with irrelevant specificities, decreasing the antigen-specificity of the resulting culture[77].

To avoid this problem, or if a source of antigen-specific cells is unavailable, T cells against the antigens of interest can first be sorted with MHC multimers, then expanded polyclonally with

anti-CD3 aAPC [27,140–143]. This allows the generation of T cell populations from readily accessible compartments such as peripheral blood.

Direct Vaccination

Direct injection of aAPC as a T cell vaccine is simpler and cheaper than adoptive immunotherapy. However, several key challenges arise when designing an effective direct injection strategy. Chief among these are particle clearance and the trafficking properties of the selected aAPC platform.

To activate T cells, aAPC must co-localize with T cells after administration, and must not be cleared prior to encountering these cells. The *in vivo* delivery and biodistribution of bead-based therapeutics is determined by particle size, shape, and surface charges, as well as interaction with host proteins [102,144,145]. Particle size can be a critical determinant; for example, microscale particles have limited lymphatic drainage from their injection site when injected subcutaneously [146]. Furthermore, particles greater than 3-5 μm in diameter can embolize to small capillary beds in the lung when administered intravenously [100–102], and are preferentially cleared by and targeted to certain phagocytic subsets [147,148]. The trafficking and distribution properties of *in vivo* administered aAPC remains a critical and understudied aspect of aAPC design. Thus, it is not yet known what route of administration is most effective at priming T cell responses, or what percentage of administered aAPC make contact with relevant T cells prior to degradation and clearance.

Despite this, several successful direct vaccination studies have been published using aAPC. The earliest reports involve 5 μm diameter silica microbeads injected intraperitoneally in tumor-bearing mice[61]. Importantly, no antigen-specific responses or tumor activity could be detected

unless a cell-based tumor vaccine was co-administered along with aAPC, suggesting aAPC could only boost existing responses. Alternatively, such aAPC could synergize with administration of cyclophosphamide to reject established P815 mastocytoma and two fibrosarcoma models, although beads alone once again demonstrated minimal activity[103]. This platform was subsequently assessed in a Phase I trial of patients with disseminated melanoma[104], with 8/15 patients developing antigen-specific cytolytic T cells, but only one partial tumor response.

Other cell-free aAPC systems have been shown to be effective without additional modulation. Iron-dextran microparticles injected intravenously [34] can mediate regression of both subcutaneous melanoma and interavenous lung metastases. Similarly, latex particles administered both intravenously and subcutaneously generated robust antigen-specific T cell responses, and subcutaneously administered microparticles mediated B16 melanoma rejection [96]. Still, the paucity of published reports demonstrating the effectiveness of *in vivo* administration of aAPC suggests much remains to be discovered before this therapeutic approach is optimized.

1.2.5 Advanced Considerations in aAPC Design

The selection of T cell stimulating proteins and a therapeutic strategy are the minimal requirements for aAPC design. Advances in particle synthesis, however, are allowing greater control over aAPC design that may further improve T cell responses. These advances have developed in parallel with a better understanding of T cell activation by endogenous APC, and allow the investigator to both mimic and improve upon T cell-APC interactions. These "advanced" considerations are reviewed below:

MHC Valency

The recognition of cognate MHC by TCR takes place in the context of a cell-cell interaction, with close apposition of membranes [24] constraining TCR-MHC binding kinetics to a two-dimensional plane [149]. Soluble MHC monomers, separated from their natural context in the APC membrane, have surprisingly low, micromolar avidity for cognate TCR . This has prompted the development of multimeric MHC constructs such as dimers and tetramers, which enhance overall binding avidity [150–152]. Studies with multivalent MHC suggest that multivalent but not monovalent MHC fixed to a rigid surface can trigger T cell stimulation[153].

By analogy, while monomeric MHC coupled to aAPC microspheres can trigger T cell activation[61,94], multivalent MHC may induce stronger responses[62,112]. However, no comprehensive examination of multivalency has been performed. Furthermore, multivalent MHC constructs can have other biophysical disadvantages: commonly used MHC tetramers have been coupled aAPC [96,98,154], but their rigid tetrahedral geometry orients a fraction of MHC molecules toward the particle surface and away from the interacting T cell.

Antigen Density

A similar effect to MHC multivalency at a slightly larger scale may be mediated by MHC density. Antigen density on APC membranes is known to affect subsequent T cell response [155–158]. This principle may also apply to aAPC design, although antigen presented on aAPC is usually supraphysiologically dense compared to the small numbers (as few as 1-10)[159,160] of cognate MHC-peptides that trigger T cell activation.

A density threshold of monomeric MHC is critical for T cell activation, and the addition of more beads at a lower density is not sufficient to overcome this effect[29,62]. However, the density of MHC may control the avidity if the resulting cultured T cells, with higher avidity resulting from

a lower MHC density [161]. Thus, if high avidity T cell responses are required, investigators must titrate density to achieve T cell proliferation without sacrificing T cell quality.

TCR and MHC Clustering

The spatial organization of surface receptors plays a critical role in T cell binding to MHC and subsequent activation, with TCR organized in microclusters both prior to[162,163] and during T cell activation[164,165]. This is mirrored by clustering of MHC on the APC surface[166]. Receptor clustering is thought to enhance the sensitivity and dynamic range of binding and signaling events by encouraging cooperative binding of multivalent ligands and spatial co-localization of signaling proteins[162,163,167].

There may thus be benefits to manufacturing aAPC with clustered protein signals. One study used αCD3, αCD28, and αLFA-1 monoclonal antibodies, pre-clustered on liposomes using neutravidin rafts, to efficiently activate MART-1 CD8 T cells[63], although the precise role of clustering in enhancing T cell responses could not be clearly defined. In a separate liposome-based study, CD4 stimulation was significantly stronger from aAPC presenting clustered compared to unclustered MHC[168]. Further study will require synthesis of platforms other than liposomes with spatially controlled receptor patterning [169].

Particle Size, Contact Area, and Synapse Formation

Studies on synthetic bead-based aAPC have largely focused on development of cell-sized, micro-scale aAPC in order to better mimic T cells interaction with Antigen Presenting Cells. This choice is theoretically reinforced by microscale T cell-APC interactions observed during activation. For example, the immune synapse is a pattern of surface receptor reorganization several microns in diameter, with centrally located TCR and peripherally located adhesion

molecules. The synapse, while not absolutely required for activation, does modulate antigen search and recognition [170]. A related process, asymmetric cell division, is hypothesized to regulate memory development by providing a microscale geometrical cue that induces polarity during cell division [171].

While synthetic surfaces coupled to T cell stimulatory signal are a common platform for studying synapse formation[172], the ability of cell- or bead-based aAPC to induce synapse or ACD formation is not well-described. However, studies have suggested that a broad contact surface between T cells and aAPC is required, with only beads larger than 2 microns in diameter able to induce T cell proliferation [94,126]. Steenblock et al.[57] demonstrated that polymer-based nanoparticles were much less efficient than microbeads in inducing short-term functional responses, with no reported proliferation.

If nanoscale aAPC were able to induce T cell activation, there would be significant advantages to using these smaller particles. Unlike microparticles, nanoparticles of approximately 50-100 nm diameter can be taken up by lymphatics and transported to the lymph nodes [84,146] thus gaining access to a larger pool of T cells. In addition, nanoscale delivery vehicles preferentially accumulate in tumors through enhanced permeability retention due to poorly formed tumor vasculature[173,174]. By delivering an immunostimulatory signal *in situ,* aAPC in the tumor microenvironment may address one of the most prominent hurdles in cancer immunotherapy, the immunosuppressive tumor microenvironment [175].

On the other hand, there are significant biophysical hurdles that must be addressed in designing a nanoscale aAPC system. For example, nanoparticles might be sensitive to enhanced TCR clustering, which is itself nanoscale, in a way that larger particles are not. In addition, there is a

high degree of local curvature on a nanoparticle compared to microparticle surface, which limits the interaction of neighboring ligands with the cell membrane. Furthermore, while Asymmetric Cell Division immune synapse formation are not absolutely required for T cell activation[176], it is not clear whether nanoscale interactions can recapitulate these microscale structures. Preliminary evidence suggests that 60-90 nm liposomes can induce a 'capping' of TCR on the T cell surface that approximates the immune synapse[88], but many questions remain unanswered, including whether fluid lipid membranes are required on the aAPC for synapse formation, whether the lack of accessory interactions such as LFA-1/ICAM influences synapse formation by aAPC, and the ultimate downstream consequences of T cell activation without strong synapse formation on T cell function.

Particle Shape

Similarly to particle size, particle shape may affects both the interaction between T cells and aAPC, as well as the *in vivo* trafficking of aAPC after injection. Unlike particle size, however, existing design considerations have not been guided by a desire to recapitulate endogenous APC-T cell interactions.

Most synthetic APC platforms are spherical, a shape which is easily synthesized using standard chemical synthesis procedures such as double-emulsion of PLGA[123]. However, non-spherical geometries are critical components of T cell-APC interactions. While spheres minimize surface area for a given diameter, T cell-APC interactions involve the formation of a large, stable contact area where a high density of MHC is presented to a closely apposed T cell membrane[170]. Even prior to T Cell stimulation, activated Dendritic Cells increase surface area for antigen presentation by forming their namesake dendrites, large folded ruffles of APC membrane

optimized for T Cell interactions in the lymph node[177]. Thus, there may be a benefit to increasing the potential area for T cell contact on the aAPC surface by designing aAPC with non-spherical geometries, such as ellipsoids. Alternatively, platforms with enhanced surface areas such as carbon nanotubes may be relevant systems for studying the influence of surface area on T-cell-aAPC interactions.

Particle geometry also influences uptake by the Reticuloendothelial System, with ellipsoid particles with a long characteristic axis displaying showing reduced phagocytosis[178–181]. Interestingly, receptor-mediated internalization of antibody coated non-spherical particles was significantly enhanced, suggesting the interaction of geometry and uptake may be pathway dependent[182]. In either case, it is important to remember that *in vitro* uptake studies may not recapitulate *in vivo* behavior, adsorption of serum proteins such as complement significantly alter trafficking and clearance characteristics of *in vivo* administered micro- and nanoparticles.

1.2.6 References

1. Ye F, Yu Y, Hu Y, Lu W, Xie X. Alterations of dendritic cell subsets in the peripheral circulation of patients with cervical carcinoma. *Journal of experimental & clinical cancer research : CR*. 29, 78 (2010).
2. Pinzon-Charry A, Maxwell T, McGuckin M a, Schmidt C, Furnival C, López JA. Spontaneous apoptosis of blood dendritic cells in patients with breast cancer. *Breast cancer research : BCR*. 8(1), R5 (2006).
3. Satthaporn S, Robins A, Vassanasiri W, *et al.* Dendritic cells are dysfunctional in patients with operable breast cancer. *Cancer immunology, immunotherapy : CII*. 53(6), 510–8 (2004).
4. Della Bella S, Gennaro M, Vaccari M, *et al.* Altered maturation of peripheral blood dendritic cells in patients with breast cancer. *British journal of cancer*. 89(8), 1463–72 (2003).
5. Hurwitz A a, Watkins SK. Immune suppression in the tumor microenvironment: a role for dendritic cell-mediated tolerization of T cells. *Cancer Immunology and Immunotherapy*. 61(2), 289–93 (2012).
6. Ma Y, Shurin G V, Gutkin DW, Shurin MR. Tumor associated regulatory dendritic cells. *Seminars in cancer biology*. 22(4), 298–306 (2012).

7. Mosser DM, Edwards JP. Exploring the full spectrum of macrophage activation. *Nature reviews. Immunology*. 8(12), 958–69 (2008).

8. Nagaraj S, Schrum AG, Cho H-I, Celis E, Gabrilovich DI. Mechanism of T cell tolerance induced by myeloid-derived suppressor cells. *Journal of Immunology*. 184(6), 3106–16 (2010).

9. Gabrilovich DI, Nagaraj S. Myeloid-derived suppressor cells as regulators of the immune system. *Nature reviews. Immunology*. 9(3), 162–74 (2009).

10. Klebanoff CA, Restifo NP. Therapeutic cancer vaccines : are we there yet ? *Immunological Reviews*. 239, 27–44 (2011).

11. Paller CJ, Antonarakis ES. Sipuleucel-T for the treatment of metastatic prostate cancer. *Human Vaccines and Immunotherapeutics*. 8(4), 509–519 (2012).

12. JT S, Alexander-Miller M, Berzofsky J, Belyakov I. Molecular mechanisms and biological significance of CTL Avidity. *Current HIV Research*. 1, 287–294 (2003).

13. Kroger CJ, Alexander-Miller M a. Dose-dependent modulation of CD8 and functional avidity as a result of peptide encounter. *Immunology*. 122(2), 167–78 (2007).

14. Pardoll D. Does the immune system see tumors as foreign or self? *Annual review of immunology*. 21(Table 1), 807–39 (2003).

15. Almeida JR, Price DA, Papagno L, *et al.* Superior control of HIV-1 replication by CD8+ T cells is reflected by their avidity, polyfunctionality, and clonal turnover. *The Journal of experimental medicine*. 204(10), 2473–85 (2007).

16. Seder R a, Darrah PA, Roederer M. T-cell quality in memory and protection: implications for vaccine design. *Nature reviews. Immunology*. 8(4), 247–58 (2008).

17. Hinrichs CS, Borman Z a, Cassard L, *et al.* Adoptively transferred effector cells derived from naive rather than central memory CD8+ T cells mediate superior antitumor immunity. *Proceedings of the National Academy of Sciences of the United States of America*. 106(41), 17469–74 (2009).

18. Gattinoni L, Klebanoff C a, Restifo NP. Paths to stemness: building the ultimate antitumour T cell. *Nature reviews. Cancer*. 12(10), 671–84 (2012).

19. Zhou J, Shen X, Huang J, Hodes RJ, Rosenberg S a, Robbins PF. Telomere length of transferred lymphocytes correlates with in vivo persistence and tumor regression in melanoma patients receiving cell transfer therapy. *Journal of immunology (Baltimore, Md. : 1950)*. 175(10), 7046–52 (2005).

20. Hodes RJ, Hathcock KS, Weng N. Telomeres in T and B cells. *Nature reviews. Immunology*. 2(9), 699–706 (2002).

21. Tran KQ, Zhou J, Durflinger KH, *et al.* Minimally cultured tumor-infiltrating lymphocytes display optimal characteristics for adoptive cell therapy. *Journal of immunotherapy (Hagerstown, Md. : 1997)*. 31(8), 742–51 (2008).

22. Wherry EJ. T cell exhaustion. *Nature Immunology*. 131(6), 492–499 (2011).

23. Ndhlovu ZM, Oelke M, Schneck JP, Griffin DE. Dynamic regulation of functionally distinct virus-specific T cells. *Proceedings of the National Academy of Sciences of the United States of America*. 107(8), 1–6 (2010).

24. James JR, Vale RD. Biophysical mechanism of T-cell receptor triggering in a reconstituted system. *Nature*. 487(7405), 64–9 (2012).

25. Smith-Garvin JE, Koretzky G a, Jordan MS. T cell activation. *Annual review of immunology*. 27, 591–619 (2009).

26. Restifo NP, Dudley ME, Rosenberg S a. Adoptive immunotherapy for cancer: harnessing the T cell response. *Nature reviews. Immunology*. 12(4), 269–81 (2012).

27. Labarrière N, Gervois N, Bonnin A, Bouquié R, Jotereau F, Lang F. PBMC are as good a source of tumor-reactive T lymphocytes as TIL after selection by Melan-A/A2 multimer immunomagnetic sorting. *Cancer immunology, immunotherapy : CII*. 57(2), 185–95 (2008).

28. Levine BL, Bernstein WB, Connors M, *et al.* Effects of CD28 costimulation on long-term proliferation of CD4+ T cells in the absence of exogenous feeder cells. *Journal of Immunology*. 159(12), 5921–30 (1997).

29. Deeths M, Mescher M. B7-1-dependent co-stimulation results in qualitatively and quantitatively different responses by CD4+ and CD8+ T cells. *European journal of immunology*. , 598–608 (1997).

30. Laux I, Khoshnan a, Tindell C, *et al.* Response differences between human CD4(+) and CD8(+) T-cells during CD28 costimulation: implications for immune cell-based therapies and studies related to the expansion of double-positive T-cells during aging. *Clinical immunology (Orlando, Fla.)*. 96(3), 187–97 (2000).

31. Fathman CG, Lineberry NB. Molecular mechanisms of CD4+ T-cell anergy. *Nature reviews. Immunology*. 7(8), 599–609 (2007).

32. Zou W, Chen L. Inhibitory B7-family molecules in the tumour microenvironment. *Nature reviews. Immunology*. 8(6), 467–77 (2008).

33. Riddell SR, Greenberg PD. The use of anti-CD3 and anti-CD28 monoclonal antibodies to clone and expand human antigen-specific T cells. *Journal of immunological methods*. 128(2), 189–201 (1990).

34. Ugel S, Zoso A, De Santo C, *et al.* In vivo administration of artificial antigen-presenting cells activates low-avidity T cells for treatment of cancer. *Cancer Research*. 69(24), 9376–84 (2009).

35. Hombach A, Sent D, Schneider C, Heuser C. Receptors CD28 Costimulation Is Required for Interleukin 2 Secretion and Receptor-mediated T-Cell Proliferation but Does Not Affect Receptor-mediated Target Cell. *Cancer Research*. 61, 1976=1982 (2001).

36. Mescher MF, Popescu FE, Gerner M, Hammerbeck CD, Curtsinger JM. Activation-induced non-responsiveness (anergy) limits CD8 T cell responses to tumors. *Seminars in cancer biology*. 17(4), 299–308 (2007).

37. Luxembourg a T, Brunmark A, Kong Y, *et al.* Requirements for stimulating naive CD8+ T cells via signal 1 alone. *Journal of immunology (Baltimore, Md. : 1950)*. 161(10), 5226–35 (1998).

38. Butler MO, Lee J-S, Ansén S, *et al.* Long-lived antitumor CD8+ lymphocytes for adoptive therapy generated using an artificial antigen-presenting cell. *Clinical cancer research : an official journal of the American Association for Cancer Research*. 13(6), 1857–67 (2007).

39. Sluijter BJR, van den Hout MFCM, Stam a GM, *et al.* 4-1BB-mediated expansion affords superior detection of in vivo primed effector memory CD8+ T cells from melanoma sentinel lymph nodes. *Clinical immunology (Orlando, Fla.)*. 137(2), 221–33 (2010).

40. Zhang H, Snyder KM, Suhoski MM, *et al.* 4-1BB is superior to CD28 costimulation for generating CD8+ cytotoxic lymphocytes for adoptive immunotherapy. *Journal of immunology (Baltimore, Md. : 1950)*. 179(7), 4910–8 (2007).

41. Rudolf D, Silberzahn T, Walter S, *et al.* Potent costimulation of human CD8 T cells by anti-4-1BB and anti-CD28 on synthetic artificial antigen presenting cells. *Cancer immunology, immunotherapy : CII*. 57(2), 175–83 (2008).

42. Fuertes Marraco S a, Baumgaertner P, Legat A, Rufer N, Speiser DE. A stepwise protocol to coat aAPC beads prevents out-competition of anti-CD3 mAb and consequent experimental artefacts. *Journal of immunological methods*. 385(1-2), 90–5 (2012).

43. Zhu J, Yamane H, Paul WE. Differentiation of effector CD4 T cell populations (*). *Annual review of immunology*. 28, 445–89 (2010).

44. Richer MJ, Nolz JC, Harty JT. Pathogen-Specific Inflammatory Milieux Tune the Antigen Sensitivity of CD8+ T Cells by Enhancing T Cell Receptor Signaling. *Immunity*. , 1–13 (2012).

45. Surh CD, Sprent J. Homeostasis of naive and memory T cells. *Immunity*. 29(6), 848–62 (2008).

46. Garlie N, LeFever A. T cells coactivated with immobilized anti-CD3 and anti-CD28 as potential immunotherapy for cancer. ... *of Immunotherapy*. 22(4), 336–345 (1999).

47. Curtsinger JM, Schmidt CS, Mondino A, *et al.* Inflammatory Cytokines Provide a Third Signal for Activation of Naive CD4 + and CD8 + T Cells. *Journal of Immunology*. 162, 3256–3262 (1999).

48. Mescher MF, Curtsinger JM, Agarwal P, *et al.* Signals required for programming effector and memory development by CD8+ T cells. *Immunological Reviews*. 211, 81–92 (2006).

49. Yang S, Ji Y, Gattinoni L, *et al.* Modulating the differentiation status of ex vivo-cultured anti-tumor T cells using cytokine cocktails. *Cancer immunology, immunotherapy : CII*. 62(4), 727–36 (2013).

50. Hinrichs CS, Spolski R, Paulos CM, *et al.* IL-2 and IL-21 confer opposing differentiation programs to CD8+ T cells for adoptive immunotherapy. *Blood*. 111(11), 5326–33 (2008).

51. Butler MO, Friedlander P, Milstein MI, *et al.* Establishment of antitumor memory in humans using in vitro-educated CD8+ T cells. *Science translational medicine*. 3(80), 80ra34 (2011).

52. Curtsinger JM, Lins DC, Mescher MF. Signal 3 determines tolerance versus full activation of naive CD8 T cells: dissociating proliferation and development of effector function. *The Journal of experimental medicine*. 197(9), 1141–51 (2003).

53. Curtsinger J, Valenzuela J. Cutting edge: type I IFNs provide a third signal to CD8 T cells to stimulate clonal expansion and differentiation. *The Journal of ….* , 8–13 (2005).

54. Curtsinger J, Lins D. Signal 3 tolerant CD8 T cells degranulate in response to antigen but lack granzyme B to mediate cytolysis. *The Journal of ….* 175, 4392–4399 (2005).

55. Han H, Peng J-R, Chen P-C, *et al.* A novel system of artificial antigen-presenting cells efficiently stimulates Flu peptide-specific cytotoxic T cells in vitro. *Biochemical and biophysical research communications*. 411(3), 530–5 (2011).

56. Steenblock ER, Fadel T, Labowsky M, Pober JS, Fahmy TM. An artificial antigen-presenting cell with paracrine delivery of IL-2 impacts the magnitude and direction of the T cell response. *The Journal of biological chemistry*. 286(40), 34883–92 (2011).

57. Steenblock ER, Fahmy TM. A comprehensive platform for ex vivo T-cell expansion based on biodegradable polymeric artificial antigen-presenting cells. *Molecular therapy : the journal of the American Society of Gene Therapy*. 16(4), 765–72 (2008).

58. Ge Q, Stone JD, Thompson MT, *et al.* Soluble peptide-MHC monomers cause activation of CD8+ T cells through transfer of the peptide to T cell MHC molecules. *Proceedings of the National Academy of Sciences of the United States of America*. 99(21), 13729–34 (2002).

59. Li Y, Kurlander RJ. Comparison of anti-CD3 and anti-CD28-coated beads with soluble anti-CD3 for expanding human T cells: differing impact on CD8 T cell phenotype and responsiveness to restimulation. *Journal of translational medicine*. 8(1), 104 (2010).

60. Maile R, Wang B, Schooler W, Meyer a, Collins EJ, Frelinger J a. Antigen-specific modulation of an immune response by in vivo administration of soluble MHC class I tetramers. *Journal of Immunology*. 167(7), 3708–14 (2001).

61. Rogers J, Mescher MF. Augmentation of in vivo cytotoxic T lymphocyte activity and reduction of tumor growth by large multivalent immunogen. *Journal of Immunology*. 149(1), 269–76 (1992).

62. Motta I, Lone YC, Kourilsky P. In vitro induction of naive cytotoxic T lymphocytes with complexes of peptide and recombinant MHC class I molecules coated onto beads: role of TCR/ligand density. *European journal of immunology*. 28(11), 3685–95 (1998).

63. Zappasodi R, Di Nicola M, Carlo-Stella C, *et al.* The effect of artificial antigen-presenting cells with preclustered anti-CD28/-CD3/-LFA-1 monoclonal antibodies on the induction of ex vivo expansion of functional human antitumor T cells. *Haematologica*. 93(10), 1523–34 (2008).

64. Herrmann S, Mescher M. The requirements for antigen multivalency in class I antigen recognition and triggering of primed precursor cytolytic T lymphocytes. *The Journal of Immunology*. , 2816–2825 (1986).

65. Lamers C. Optimization of culture conditions for activation and large-scale expansion of human T lymphocytes for bispecific antibody-directed cellular immunotherapy. *... journal of cancer*. 979, 973–979 (1992).

66. Li Y-C, Chen B-M, Wu P-C, *et al.* Cutting Edge: mechanical forces acting on T cells immobilized via the TCR complex can trigger TCR signaling. *Journal of Immunology*. 184(11), 5959–63 (2010).

67. Husson J, Chemin K, Bohineust A, Hivroz C, Henry N. Force generation upon T cell receptor engagement. *PloS one*. 6(5), e19680 (2011).

68. O'Connor RS, Hao X, Shen K, *et al.* Substrate rigidity regulates human T cell activation and proliferation. *Journal of immunology (Baltimore, Md. : 1950)*. 189(3), 1330–9 (2012).

69. Minguet S, Swamy M, Alarcón B, Luescher IF, Schamel WW a. Full activation of the T cell receptor requires both clustering and conformational changes at CD3. *Immunity*. 26(1), 43–54 (2007).

70. Balmert S, Little S. Biomimetic Delivery with Micro-and Nanoparticles. *Advanced Materials*. (2012).

71. Aggarwal P, Hall JB, McLeland CB, Dobrovolskaia M a, McNeil SE. Nanoparticle interaction with plasma proteins as it relates to particle biodistribution, biocompatibility and therapeutic efficacy. *Advanced drug delivery reviews*. 61(6), 428–37 (2009).

72. Kondo S, Demachi-Okamura A, Hirosawa T, *et al.* An HLA-modified ovarian cancer cell line induced CTL responses specific to an epitope derived from claudin-1 presented by HLA-A*24:02 molecules. *Human immunology*. 74(9), 1103–10 (2013).

73. Sasawatari S, Tadaki T, Isogai M, Takahara M, Nieda M, Kakimi K. Efficient priming and expansion of antigen-specific CD8+ T cells by a novel cell-based artificial APC. *Immunology and cell biology*. 84(6), 512–21 (2006).

74. Gong W, Ji M, Cao Z, *et al.* Establishment and characterization of a cell based artificial antigen-presenting cell for expansion and activation of CD8+ T cells ex vivo. *Cellular & molecular immunology*. 5(1), 47–53 (2008).

75. Ye Q, Loisiou M, Levine BL, *et al.* Engineered artificial antigen presenting cells facilitate direct and efficient expansion of tumor infiltrating lymphocytes. *Journal of translational medicine*. 9(1), 131 (2011).

76. Friedman KM, Devillier LE, Feldman S a, Rosenberg S a, Dudley ME. Augmented lymphocyte expansion from solid tumors with engineered cells for costimulatory enhancement. *Journal of immunotherapy (Hagerstown, Md. : 1997)*. 34(9), 651–61 (2011).

77. Maus M V, Thomas AK, Leonard DGB, *et al.* Ex vivo expansion of polyclonal and antigen-specific cytotoxic T lymphocytes by artificial APCs expressing ligands for the T-cell receptor, CD28 and 4-1BB. *Nature biotechnology*. 20(2), 143–8 (2002).

78. Hippen KL, Merkel SC, Schirm DK, *et al.* Massive ex vivo expansion of human natural regulatory T cells (T(regs)) with minimal loss of in vivo functional activity. *Science translational medicine*. 3(83), 83ra41 (2011).

79. Singh H, Figliola MJ, Dawson MJ, *et al.* Manufacture of Clinical-Grade CD19-Specific T Cells Stably Expressing Chimeric Antigen Receptor Using Sleeping Beauty System and Artificial Antigen Presenting Cells. *PloS one*. 8(5), e64138 (2013).

80. Suhoski MM, Golovina TN, Aqui N a, *et al.* Engineering artificial antigen-presenting cells to express a diverse array of co-stimulatory molecules. *Molecular therapy : the journal of the American Society of Gene Therapy*. 15(5), 981–8 (2007).

81. Dupont J, Latouche J-B, Ma C, Sadelain M. Artificial antigen-presenting cells transduced with telomerase efficiently expand epitope-specific, human leukocyte antigen-restricted cytotoxic T cells. *Cancer research*. 65(12), 5417–27 (2005).

82. Latouche JB, Sadelain M. Induction of human cytotoxic T lymphocytes by artificial antigen-presenting cells. *Nature biotechnology*. 18(4), 405–9 (2000).

83. Papanicolaou G a, Latouche J-B, Tan C, *et al.* Rapid expansion of cytomegalovirus-specific cytotoxic T lymphocytes by artificial antigen-presenting cells expressing a single HLA allele. *Blood*. 102(7), 2498–505 (2003).

84. Cai S, Yang Q, Bagby TR, Forrest ML. Lymphatic drug delivery using engineered liposomes and solid lipid nanoparticles. *Advanced drug delivery reviews*. 63(10-11), 901–08 (2011).

85. Herrmann SH, Mescher MF. Lymphocyte recognition of H-2 antigen in liposomes. *Journal of supramolecular structure and cellular biochemistry*. 16(2), 121–31 (1981).

86. Engelhard VH, Strominger JL, Mescher M, Burakoff S. Induction of secondary cytotoxic T lymphocytes by purified HLA-A and HLA-B antigens reconstituted into phospholipid vesicles. *Proceedings of the National Academy of Sciences of the United States of America*. 75(11), 5688–91 (1978).

87. Herrmann SH, Weinberger O, Burakoff J, Mescher MF. Analysis of the Two-Signal Requirement for Precursor Cytolytic T Lymphocyte Activation. *The Journal of Immunology*. 128(5), 1968–1974 (1982).

88. Prakken B, Wauben M, Genini D, *et al.* Artificial antigen-presenting cells as a tool to exploit the immune “synapse”. *Nature medicine*. 6(12), 1406–10 (2000).

89. Haveman LM, Bierings M, Klein MR, *et al.* Selection of perforin expressing CD4+ adenovirus-specific T-cells with artificial antigen presenting cells. *Clinical immunology (Orlando, Fla.)*. 146(3), 228–39 (2013).

90. De La Peña H, Madrigal J a, Rusakiewicz S, *et al.* Artificial exosomes as tools for basic and clinical immunology. *Journal of immunological methods*. 344(2), 121–32 (2009).

91. Viaud S, Théry C, Ploix S, *et al.* Dendritic cell-derived exosomes for cancer immunotherapy: what's next? *Cancer research*. 70(4), 1281–5 (2010).

92. Curtsinger JM, Lins DC, Mescher MF. CD8 + Memory T Cells (CD44 high , Ly-6C +) Are More Sensitive than Naive Cells (CD44 low , Ly-6C -) to TCR/CD8 Signaling in Response to Antigen. *The Journal of Immunology*. 160, 3236–3243 (1998).

93. Curtsinger J, Deeths MJ, Pease P, Mescher MF. Artificial cell surface constructs for studying receptor-ligand contributions to lymphocyte activation. *Journal of immunological methods*. 209(1), 47–57 (1997).

94. Mescher MF. Surface contact requirements for activation of cytotoxic T lymphocytes. *Journal of Immunology*. 149(7), 2402–5 (1992).

95. Tham EL, Jensen PL, Mescher MF. Activation of antigen-specific T cells by artificial cell constructs having immobilized multimeric peptide-class I complexes and recombinant B7-Fc proteins. *Journal of immunological methods*. 249(1-2), 111–9 (2001).

96. Shen C, Cheng K, Miao S, *et al.* Latex bead-based artificial antigen-presenting cells induce tumor-specific CTL responses in the native T-cell repertoires and inhibit tumor growth. *Immunology letters*. 150(1-2), 1–11 (2013).

97. Lu X, Jiang X, Liu R, Zhao H, Liang Z. Adoptive transfer of pTRP2-specific CTLs expanding by bead-based artificial antigen-presenting cells mediates anti-melanoma response. *Cancer letters*. 271(1), 129–39 (2008).

98. Jiang X, Lu X, Liu R, Zhang F, Zhao H. HLA Tetramer Based Artificial Antigen-Presenting Cells Efficiently Stimulate CTLs Specific for Malignant Glioma. *Clinical cancer research : an official journal of the American Association for Cancer Research*. 13(24), 7329–34 (2007).

99. Xiaobing J, Xiaoling L, Ruen L, Fangcheng Z, Hongyang Z. Induction of cytotoxic T-lymphocytes specific for malignant glioma by HLA dimer-based artificial antigen-presenting cells. *Cancer biotherapy & radiopharmaceuticals*. 22(6), 826–35 (2007).

100. Slack JD, Kanke M, Simmons GUYH, Delucasx PP. Acute Hemodynamic Effects and Blood Pool Kinetics of Polystyrene Microspheres following Intravenous Administration. , 660–664 (1980).

101. Kutscher HL, Chao P, Deshmukh M, *et al.* Threshold size for optimal passive pulmonary targeting and retention of rigid microparticles in rats. *Journal of controlled release : official journal of the Controlled Release Society*. 143(1), 31–7 (2010).

102. Decuzzi P, Godin B, Tanaka T, *et al.* Size and shape effects in the biodistribution of intravascularly injected particles. *Journal of controlled release : official journal of the Controlled Release Society*. 141(3), 320–7 (2010).

103. Mescher MF, Rogers JD. Immunotherapy of established murine tumors with large multivalent immunogen and cyclophosphamide. *Journal of Immunotherapy*. 19(2), 102 (1996).

104. Mitchell MS. Phase I Trial of Large Multivalent Immunogen Derived from Melanoma Lysates in Patients with Disseminated Melanoma. *Clinical Cancer Research*. 10(1), 76–83 (2004).

105. Goldberg J, Shrikant P, Mescher MF. In vivo augmentation of tumor-specific CTL responses by class I/peptide antigen complexes on microspheres (large multivalent immunogen). *The Journal of Immunology*. 170(1), 228 (2003).

106. Grützkau A, Radbruch A. Small but mighty: how the MACS-technology based on nanosized superparamagnetic particles has helped to analyze the immune system within the last 20 years. *Cytometry. Part A : the journal of the International Society for Analytical Cytology*. 77(7), 643–7 (2010).

107. Zborowski M, Chalmers JJ. Rare cell separation and analysis by magnetic sorting. *Analytical chemistry*. 83(21), 8050–6 (2011).

108. Kunzmann A, Andersson B, Thurnherr T, Krug H, Scheynius A, Fadeel B. Toxicology of engineered nanomaterials: Focus on biocompatibility, biodistribution and biodegradation. *Biochimica et biophysica acta*. 1810(3), 361–373 (2010).

109. Dobrovolskaia M a, McNeil SE. Immunological properties of engineered nanomaterials. *Nature nanotechnology*. 2(8), 469–78 (2007).

110. Nune SK, Gunda P, Majeti BK, Thallapally PK, Forrest ML. Advances in lymphatic imaging and drug delivery. *Advanced drug delivery reviews*. (2011).

111. Oelke M, Schneck JP. HLA-Ig-based artificial antigen-presenting cells: setting the terms of engagement. *Clinical immunology (Orlando, Fla.)*. 110(3), 243–51 (2004).

112. Oelke M, Maus M V, Didiano D, June CH, Mackensen A, Schneck JP. Ex vivo induction and expansion of antigen-specific cytotoxic T cells by HLA-Ig-coated artificial antigen-presenting cells. *Nature medicine*. 9(5), 619–24 (2003).

113. Oelke M, Schneck JP. Overview of a HLA-Ig based “Lego-like system” for T cell monitoring, modulation and expansion. *Immunologic Research*. 47, 248–56 (2010).

114. Durai M, Krueger C, Ye Z, *et al.* In vivo functional efficacy of tumor-specific T cells expanded using HLA-Ig based artificial antigen presenting cells (aAPC). *Cancer immunology, immunotherapy : CII*. 58(2), 209–20 (2009).

115. Chiu Y-L, Schneck JP, Oelke M. HLA-Ig based artificial antigen presenting cells for efficient ex vivo expansion of human CTL. *Journal of visualized experiments : JoVE*. (50), 1–5 (2011).

116. Lee JB, Oelke M, Ramachandra L, Canaday DH, Schneck JP. Decline of influenza-specific CD8+ T cell repertoire in healthy geriatric donors. *Immunity & ageing : I & A*. 8(1), 6 (2011).

117. Pène J, Rahmoun M, Temmerman S, Yssel H. Use of anti-CD3/CD28 mAb coupled magnetic beads permitting subsequent phenotypic analysis of activated human T cells by indirect immunofluorescence. *Journal of Immunological Methods*. 283(1-2), 59–66 (2003).

118. Ndhlovu ZM, Angenendt M, Heckel D, Schneck JP, Griffin DE, Oelke M. Development of an artificial-antigen-presenting-cell-based assay for the detection of low-frequency virus-specific CD8(+) T cells in whole blood, with application for measles virus. *Clinical and Vaccine Immunology*. 16(7), 1066–73 (2009).

119. Kalamasz D, Long S a, Taniguchi R, Buckner JH, Berenson RJ, Bonyhadi M. Optimization of human T-cell expansion ex vivo using magnetic beads conjugated with anti-CD3 and Anti-CD28 antibodies. *Journal of immunotherapy (Hagerstown, Md. : 1997)*. 27(5), 405–18 (2004).

120. Earle KE, Tang Q, Zhou X, *et al.* In vitro expanded human CD4+CD25+ regulatory T cells suppress effector T cell proliferation. *Clinical immunology (Orlando, Fla.)*. 115(1), 3–9 (2005).

121. Porter DL, Levine BL, Bunin N, *et al.* A phase 1 trial of donor lymphocyte infusions expanded and activated ex vivo via CD3/CD28 costimulation. *Blood*. 107(4), 1325–31 (2006).

122. Thompson JA, Figlin RA, Sifri-steele C, Carcinoma C, Berenson RJ, Frohlich MW. A phase 1 trial of donor lymphocyte infusions expanded and activated ex vivo via CD3/CD28 costimulation. *Clinical Cancer Research*. 9, 3562–3570 (2003).

123. Astete CE, Sabliov CM. Synthesis and characterization of PLGA nanoparticles. *Journal of biomaterials science. Polymer edition*. 17(3), 247–89 (2006).

124. Saltzman WM, Olbricht WL. Building drug delivery into tissue engineering. *Nature reviews. Drug discovery*. 1(3), 177–86 (2002).

125. Semete B, Booysen L, Lemmer Y, *et al.* In vivo evaluation of the biodistribution and safety of PLGA nanoparticles as drug delivery systems. *Nanomedicine : nanotechnology, biology, and medicine*. 6(5), 662–71 (2010).

126. Steenblock E, Wrzesinski S, Flavell R, Fahmy T. Antigen presentation on artificial acellular substrates: modular systems for flexible, adaptable immunotherapy. (2009).

127. Shalaby WSW, Yeh H, Woo E, *et al.* Absorbable microparticulate cation exchanger for immunotherapeutic delivery. *Journal of biomedical materials research. Part B, Applied biomaterials*. 69(2), 173–82 (2004).

128. Walter E a, Greenberg PD, Gilbert MJ, *et al.* Reconstitution of cellular immunity against cytomegalovirus in recipients of allogeneic bone marrow by transfer of T-cell clones from the donor. *The New England journal of medicine*. 333(16), 1038–44 (1995).

129. Roncarolo M-G, Battaglia M. Regulatory T-cell immunotherapy for tolerance to self antigens and alloantigens in humans. *Nature reviews. Immunology*. 7(8), 585–98 (2007).

130. Turtle C. Artificial antigen presenting cells for use in adoptive immunotherapy. *Cancer journal (Sudbury, Mass.)*. 16(4) (2010).

131. Wrzesinski C, Paulos CM, Kaiser A, *et al.* Increased intensity lymphodepletion enhances tumor treatment efficacy of adoptively transferred tumor-specific T cells. *Journal of Immunotherapy*. 33(1), 1–7 (2010).

132. Gattinoni L, Finkelstein SE, Klebanoff C a, *et al.* Removal of homeostatic cytokine sinks by lymphodepletion enhances the efficacy of adoptively transferred tumor-specific CD8+ T cells. *The Journal of experimental medicine*. 202(7), 907–12 (2005).

133. Dudley ME, Yang JC, Sherry R, *et al.* Adoptive cell therapy for patients with metastatic melanoma: evaluation of intensive myeloablative chemoradiation preparative regimens. *Journal of clinical oncology : official journal of the American Society of Clinical Oncology*. 26(32), 5233–9 (2008).

134. Klebanoff C a, Khong HT, Antony P a, Palmer DC, Restifo NP. Sinks, suppressors and antigen presenters: how lymphodepletion enhances T cell-mediated tumor immunotherapy. *Trends in immunology*. 26(2), 111–7 (2005).

135. Jenkins MK, Moon JJ. The Role of Naive T Cell Precursor Frequency and Recruitment in Dictating Immune Response Magnitude. *The Journal of Immunology*. 188(9), 4135–4140 (2012).

136. La Rosa C, Wang Z, Lacey SF, *et al.* In vitro expansion of polyclonal T-cell subsets for adoptive immunotherapy by recombinant modified vaccinia Ankara. *Experimental hematology*. 34(4), 497–507 (2006).

137. Klebanoff C a, Gattinoni L, Palmer DC, *et al.* Determinants of successful CD8+ T-cell adoptive immunotherapy for large established tumors in mice. *Clinical cancer research : an official journal of the American Association for Cancer Research*. 17(16), 5343–52 (2011).

138. Chapuis A, Ragnarsson G. Transferred WT1-reactive CD8+ T cells can mediate antileukemic activity and persist in post-transplant patients. *Science translational …*. 27 (2013).

139. Gajewski TF, Fuertes M, Spaapen R, Zheng Y, Kline J. Molecular profiling to identify relevant immune resistance mechanisms in the tumor microenvironment. *Current opinion in immunology*. 23(2), 286–92 (2011).

140. Mazzarella T, Cambiaghi V, Rizzo N, *et al.* Ex vivo enrichment of circulating anti-tumor T cells from both cutaneous and ocular melanoma patients: clinical implications for adoptive cell transfer therapy. *Cancer immunology, immunotherapy : CII*. 61(8), 1169–82 (2012).

141. Valmori D, Pittet MJ, Rimoldi D, *et al.* An Antigen-targeted Approach to Adoptive Transfer Therapy of Cancer An Antigen-targeted Approach to Adoptive Transfer Therapy of Cancer 1. , 2167–2173 (1999).

142. Bouquié R, Bonnin A, Bernardeau K, *et al.* A fast and efficient HLA multimer-based sorting procedure that induces little apoptosis to isolate clinical grade human tumor specific T lymphocytes. *Cancer immunology, immunotherapy : CII*. 58(4), 553–66 (2009).

143. Cobbold M, Khan N, Pourgheysari B, *et al.* Adoptive transfer of cytomegalovirus-specific CTL to stem cell transplant patients after selection by HLA-peptide tetramers. *The Journal of experimental medicine*. 202(3), 379–86 (2005).

144. Walkey CD, Chan WCW. Understanding and controlling the interaction of nanomaterials with proteins in a physiological environment. *Chemical Society reviews*. (2011).

145. Venkataraman S, Hedrick JL, Ong ZY, *et al.* The effects of polymeric nanostructure shape on drug delivery. *Advanced Drug Delivery Reviews*. (2011).

146. Manolova V, Flace A, Bauer M, Schwarz K, Saudan P, Bachmann MF. Nanoparticles target distinct dendritic cell populations according to their size. *European Journal of Immunology*. 38(5), 1404–13 (2008).

147. Sharma G, Valenta DT, Altman Y, *et al.* Polymer particle shape independently influences binding and internalization by macrophages. *Journal of Controlled Release*. 147(3), 408–412 (2010).

148. Champion J a, Walker A, Mitragotri S. Role of particle size in phagocytosis of polymeric microspheres. *Pharmaceutical research*. 25(8), 1815–21 (2008).

149. Huang J, Zarnitsyna VI, Liu B, *et al.* The kinetics of two-dimensional TCR and pMHC interactions determine T-cell responsiveness. *Nature*. 464(7290), 932–6 (2010).

150. Fahmy TM, Bieler JG, Schneck JP. Probing T cell membrane organization using dimeric MHC-Ig complexes. *Journal of Immunological Methods*. 268(1), 93–106 (2002).

151. Delon J, Grégoire C, Malissen B, *et al.* CD8 expression allows T cell signaling by monomeric peptide-MHC complexes. *Immunity*. 9(4), 467–73 (1998).

152. Lebowitz MS, O'Herrin SM, Hamad a R, *et al.* Soluble, high-affinity dimers of T-cell receptors and class II major histocompatibility complexes: biochemical probes for analysis and modulation of immune responses. *Cellular Immunology*. 192(2), 175–84 (1999).

153. Stone JD, Stern LJ. CD8 T cells, like CD4 T cells, are triggered by multivalent engagement of TCRs by MHC-peptide ligands but not by monovalent engagement. *Journal of Immunology*. 176(3), 1498–505 (2006).

154. Maus M, Riley JL, Kwok WW, Nepom GT, June CH. HLA tetramer-based artificial antigen-presenting cells for stimulation of CD4+ T cells. *Clinical Immunology*. 106(1), 16–22 (2003).

155. Gottschalk R a., Hathorn MM, Beuneu H, *et al.* Distinct influences of peptide-MHC quality and quantity on in vivo T-cell responses. *Proceedings of the National Academy of Sciences*. , 1–6 (2012).

156. Bullock TNJ, Mullins DW, Engelhard VH. Antigen density presented by dendritic cells in vivo differentially affects the number and avidity of primary, memory, and recall CD8+ T cells. *Journal of Immunology*. 170(4), 1822–9 (2003).

157. Gottschalk R a., Corse E, Allison JP. TCR ligand density and affinity determine peripheral induction of Foxp3 in vivo. *Journal of Experimental Medicine*. 207(8), 1701–1711 (2010).

158. Leignadier J, Labrecque N. Epitope density influences CD8 memory T cell differentiation. *PloS one*. 5(10), e13740 (2010).

159. Sykulev Y, Joo M, Vturina I, Tsomides TJ, Eisen HN. Evidence that a single peptide-MHC complex on a target cell can elicit a cytolytic T cell response. *Immunity*. 4, 565 (1996).

160. Purbhoo M a, Irvine DJ, Huppa JB, Davis MM. T cell killing does not require the formation of a stable mature immunological synapse. *Nature Immunology*. 5(5), 524–30 (2004).

161. Walter S, Herrgen L, Schoor O, Wernet D, Bühring H, Stevanovic S. Cutting Edge: Predetermined Avidity of Human CD8 T Cells Expanded on Calibrated MHC/Anti-CD28-Coated Microspheres. *Journal of Immunology*. 171, 4974–4978 (2003).

162. Fahmy TM, Bieler JG, Edidin M, Schneck JP. Increased TCR avidity after T cell activation: a mechanism for sensing low-density antigen. *Immunity*. 14(2), 135–43 (2001).

163. Kumar R, Ferez M, Swamy M, *et al.* Increased Sensitivity of Antigen-Experienced T Cells through the Enrichment of Oligomeric T Cell Receptor Complexes. *Immunity*. 35(3), 375–87 (2011).

164. Tolar P. Inside the microcluster: antigen receptor signalling viewed with molecular imaging tools. *Immunology*. 133(3), 271–7 (2011).

165. Dustin ML, Groves JT. Receptor signaling clusters in the immune synapse. *Annual review of biophysics*. 41, 543–56 (2012).

166. Fooksman DR, Grönvall GK, Tang Q, Edidin M. Clustering class I MHC modulates sensitivity of T cell recognition. *Journal of Immunology*. 176(11), 6673–80 (2006).

167. Alarcón B, Swamy M, van Santen HM, Schamel WW a. T-cell antigen-receptor stoichiometry: pre-clustering for sensitivity. *EMBO reports*. 7(5), 490–5 (2006).

168. Giannoni F, Barnett J, Bi K. Clustering of T cell ligands on artificial APC membranes influences T cell activation and protein kinase C θ translocation to the T cell plasma membrane. *The Journal of ….* 174, 3204–3211 (2005).

169. Sunshine JC, Green JJ. Nanoengineering approaches to the design of artificial antigen-presenting cells. *Nanomedicine (London, England)*. 8(7), 1173–89 (2013).

170. Dustin ML. T-cell activation through immunological synapses and kinapses. *Immunol. Rev*. 221, 77–89 (2008).

171. Chang JT, Palanivel VR, Kinjyo I, *et al.* Asymmetric T lymphocyte division in the initiation of adaptive immune responses. *Science*. 315(5819), 1687–91 (2007).

172. Irvine DJ, Doh J. Synthetic surfaces as artificial antigen presenting cells in the study of T cell receptor triggering and immunological synapse formation. *Seminars in immunology*. 19(4), 245–54 (2007).

173. Maeda H. The enhanced permeability and retention (EPR) effect in tumor vasculature: the key role of tumor-selective macromolecular drug targeting. *Advances in enzyme regulation*. 41(00), 189–207 (2001).

174. Greish K. Enhanced permeability and retention of macromolecular drugs in solid tumors: a royal gate for targeted anticancer nanomedicines. *Journal of drug targeting*. 15(7-8), 457–64 (2007).

175. Rabinovich G a, Gabrilovich D, Sotomayor EM. Immunosuppressive strategies that are mediated by tumor cells. *Annual review of immunology*. 25, 267–96 (2007).

176. Lee K-H, Holdorf AD, Dustin ML, Chan AC, Allen PM, Shaw AS. T cell receptor signaling precedes immunological synapse formation. *Science*. 295(5559), 1539–42 (2002).

177. Lin M-L, Zhan Y, Villadangos J a, Lew AM. The cell biology of cross-presentation and the role of dendritic cell subsets. *Immunology and cell biology*. 86(4), 353–62 (2008).

178. Gratton SE a, Ropp P a, Pohlhaus PD, *et al.* The effect of particle design on cellular internalization pathways. *Proceedings of the National Academy of Sciences of the United States of America*. 105(33), 11613–8 (2008).

179. Champion J a, Katare YK, Mitragotri S. Particle shape: a new design parameter for micro- and nanoscale drug delivery carriers. *Journal of Controlled Release*. 121(1-2), 3–9 (2007).

180. Champion J a, Mitragotri S. Role of target geometry in phagocytosis. *Proceedings of the National Academy of Sciences of the United States of America*. 103(13), 4930–4 (2006).

181. Yoo J-W, Mitragotri S. Polymer particles that switch shape in response to a stimulus. *Proceedings of the National Academy of Sciences of the United States of America*. 107(25), 11205–10 (2010).

182. Barua S, Yoo J. Particle shape enhances specificity of antibody-displaying nanoparticles. *Proceedings of the ….* (2013).

1.3 Adoptive Cell Transfer for Cancer Immunotherapy

The transfer of large numbers of tumor-specific lymphocytes into cancer patients can mediate complete, durable regressions of metastatic tumors. The remarkable series of clinical trials demonstrating the effectiveness of adoptive immunotherapy has spurred large-scale interest in both the clinical and basic aspects of adoptive immunotherapy for cancer.

From a theoretical standpoint, cancer immunotherapy using T cells has long been of interest. Adaptive immunity has numerous beneficial properties that make it amenable for cancer treatment: 1) T cell responses are specific, and can thus potentially distinguish between healthy and cancerous tissue; 2) T cells responses are robust, undergoing up to 1,000-fold clonal expansion after activation ; 3) T cell response can traffic to the site of antigen, suggesting a mechanism for eradication of distant metasteses; and 4) T cell responses have memory, maintaining therapeutic effect for many years after initial treatment.

Despite this theoretical interest, cancer immunotherapy could not proceed until it was established that immunity could distinguish tumor from healthy tissue[1]. Unlike microbial pathogens, tumors are fundamentally "self," and belief in immune recognition cancer has waxed and waned since the cancer immunosurveillance hypothesis was first proposed. The identification of human tumor associated antigens (TAA's) [2] was the culmination of a renewed interest in tumor immunology spurred by tumor transplant models in the mouse[3], and provided definitive proof that specific anti-tumor responses could be generated under the right conditions.

The next hurdle to be addressed was the identification of a readily accessible pool of tumor-specific lymphocytes. Using modern techniques, T cells with anti-tumor cytotoxic activity can be

identified in tumor samples of up to 80% of melanoma patients[4] (but less frequently in other cancers). It is now clear that the T cell infiltration and inflammation are "hallmarks" of cancer[5]. Still, the immune surveillance hypothesis remains controversial, and whether Tumor Infilitrating Lymphocytes (TILs) are spectators to cell death and dysfunction or actively mediating rejection of human cancers is open to debate. Furthermore, the very co-existence of tumor-specific T cells and large tumors casts doubt on the effectiveness of these responses in cancer eradication. However, while the question of whether immunity *does* control cancer remains a matter of some debate, adoptive cell therapy has conclusively demonstrated that under the right therapeutic conditions, ACT *can* eradicate tumors.

1.3.1 ACT Can Eradicate Tumors

Adoptive cell therapy involves the isolation of T cells from a patient or compatible donor; *ex vivo* expansion, manipulation, or enrichment of these cells; and subsequent re-infusion. While the mechanism of action was not initially understood, allogeneic stem cell transplantation (HSCT) for hematological malignancies represents the earliest adoptive transfer of T cells with tumoricidal activity in cancer patients[6]. Rather than simply replacing leukemic bone marrow with a healthy transplant, donor cells mediate a graft-vs.-tumor effect against allogeneic antigens present on leukemic cells[7], which reduces tumor burden and prevents recurrence[8]. Unfortunately, lack of specificity in the allogeneic responses makes it challenging to separate the graft effect on tumor from the graft effect on host. Thus, developments in HCST have paralleled ACT development in general, as outlined below.

The earliest trials of ACT using lymphocytes isolated from cancer samples were conducted at the surgical branch of the NCI in 1988[9], following the demonstration in 1987 that TILs could be cultured in the lymphotrophic cytokine IL-2 and exhibited cytotoxic activity against cancer cells

in vitro[10]. Objective responses by RECIST criteria were observed in 11 of 20 patients with metastatic melanoma, and in 34% of patients of a larger follow-up report in 1994[11]. Unfortunately, only 5 of the 29 responses were complete, and the median duration of response in these early studies was only 4 months.

A major breakthrough occurred with the addition of lymphodepletion prior to ACT. The benefits of total body irradiation and lymphodepleting chemotherapy were first illustrated in mouse models of B16 melanoma[12], demonstrating the value of pre-clinical animal models of ACT. As discussed in greater detail below, lymphodepletion enhances ACT by reducing competition for cytokines and eliminating the multiple layers of immunosuppression that stifle productive tumor responses. The addition of lymphodepletion to ACT increased response rates in Stage IV melanoma patients to 49%, 52%, and 72% with three sequential protocols of increasing intensity total body irradiation [13–15]. Complete responses were achieved in 20 of 93 patients treated, and 19 of these 20 responses have persisted for at least 5 years. Comparable results have now been achieved have now been achieved outside of the NCI, with 48% response (4 complete, 11 partial) in a trial that utilized a lymphodepleting chemotherapy regimen but no TBI [16,17].

While these results represented a stunning breakthrough in melanoma treatment, the protocol could not be applied to patients that lacked readily cultured T cell responses, or to cancers other than melanoma in which TIL culture remained a challenge. While both breast and colon cancer, for example, do contain TILs, their antigen specificities are still incompletely defined, and a significant proportion of those lymphocytes have suppressive rather than anti-tumor activity[18,19].Several approaches have thus been developed to increase the proportion of patients and cancers which can be treated using ACT.

Tumor-specific T cell clones can be generated from repeated antigen-specific stimulation of patient-derived (autologous) or donor-derived (allogeneic) T cells *in vitro*[20]. For example, a recent pilot study explored the use of allogeneic CD8+ T cells with activity against the Wilms tumor antigen 1 (WT1) in leukemia patients who relapsed after HSCT[21]. Clones were generated by leukophoresis of HLA-matched donor cells and repeated stimulation with peptide-pulsed, autologus Dendritic Cells over several months. This approach can be described as an attempt to uncouple the Graft-vs.-Tumor effect from the Graft-vs.-Host effect of hematopoietic cell transfer by generating T cells of a single antigen-specificity from donors. Adoptively transferred lymphocytes remained detectable in patient blood long-term, and transient responses were observed in 2/11 of these high relapse-risk patients, with stable disease observed in 3 others. Similar approaches have been applied to CTL clones in melanoma[22,23] and ovarian cancer[24].

A potentially limitless source of T cells with almost any desired specificity can be derived from autologous lymphocytes genetically engineered to express the relevant TCR (reviewed in [25]). Tumor-reactive TCR must first be identified in T cells isolated from patients with naturally occurring anti-tumor activity, and can be engineered to increased affinity specificity by changes to complementarity-determining regions [26]. Antigen-specific TCR may also be derived from mice engineered to express human antigens[27]. Retroviral or lentiviral transfection is then used to transfer cDNA encoding the desired TCR specificity to T cells isolated from the patient[28]. A key theoretical concern with this approach is that engineered T cells contain both endogenous and engineered TCR (and thus dual specificity), which may lead to cross-reactivity after activation. TCR chains from native and engineered TCR could also pair to create novel TCR

with new specificities. Despite this concern, side effects of genetically engineered T cell therapy have primarily been due to on-target effects of tumor antigen expressed on healthy tissue.

In melanoma, genetically-engineered T cells have not been as successful as TIL-derived ACT [29], with only 2/18 patients showing partial response and sustained levels of circulating cells at one year. A subsequent study of two additional TCR specificities showed objective response rates of 19-30%[27]. However, the use of genetic engineering has vastly expanded the range of potential cancers amenable to ACT therapy, including neuroblastoma[30], synovial cell sarcoma[31], and colorectal cancer[32], among others. However, the use of TCR derived from responses in other patients eliminates the contribution of central tolerance, increasing the risk of autoimmune toxicity[31]. Despite the comparatively weak responses and safety concerns, interest in this approach is high due to its ability to treat a variety of cancers and the potential to improve results by additional genetic modifications, as will be discussed later.

While gene-modified T cells can be generated against many tumor antigens, TCR are still HLA-restricted, meaning that new specificities must be described for each tumor antigen and HLA allele. The development of chimeric antigen receptors (CARs) provided a more universal approach to targeting tumor antigens that are expressed on the membrane of cancer cells. Now on their third generation, CARs are hybrid receptors formed by the fusion of an extracellular tumor-specific antibody fragments, CD3-derived ITAM signaling chain, and a co-stimulatory signaling domain [33]. CARs have been explored with moderate success against carbonic anhydrase in Renal Cell Carcinoma[34] and L1 Adhesion molecule (CD171) in neuroblastoma[35], among other antigens (reviewed in [25]). The most promising results have been achieved in hematologic malignancies [36,37], where CD19-targeted CARs can recapitulate the mechanism of rituximab therapy without the need for repeated antibody administration.

Two decades after the first trials demonstrated the feasibility of large-scale adoptive cell transfer, a series of approaches have been developed to generate antigen-specific T cells against cancer. Attention has turned toward making ACT more safer, more effective, and more reliable. In the sections that follow, I will attempt to synthesize knowledge derived from these trials to generate steps towards the design of optimal adoptive cellular therapy.

1.3.2 Selection of Tumor Antigens

A primary goal in the design of all cancer therapeutics is the selection of targets that are present on tumor but not healthy cells. In immunotherapy, this means identifying tumor-associated antigens (TAAs) which are expressed solely or preferentially on cancer cells. With the development of *in vitro* antigen-stimulated clones, TCR-engineering, and CARs as sources of antigen-specific T cells, the choice of antigen has become an explicit first step in the development of many ACT protocols.

Tumor-Associated Antigens

TAAs can be classified into four major groups[38]: 1) Antigens over-expressed in tumors: these antigens arise from non-mutated proteins which are present on healthy tissue, but are over-expressed in cancer, often because they provide a growth advantage to the cell. Central tolerance mechanisms [39]ensure that T cell responses against these antigens are largely poorly immunogenic and low-affinity[40], as will be discussed in further detail below. Prototypical antigens include HER-2/Neu in breast and ovarian cancer, and RAGE-1 in renal cell carcinoma. 2) Melanoma differentiation genes: antigens derived from differentiation proteins specific to the melanocyte lineage are overexpressed in melanoma and are recognized by TILs in many patients. While they are also found on healthy melanocytes, differentiation antigens are highly immunogenic and may explain the unique success of TIL therapy in this disease. Protoypical

antigens in this category include gp100/pmel117, Melan-A/MART-1, and TRP-2. 3) Antigens resulting from mutations: these so-called *neo-epitopes* arise from somatic mutations in cancer. Mutation patterns are unique to each patient [41,42] and may occur as 'driver' mutations central to oncogenesis, or passenger proteins accumulated during tumor progression [43]. Because they result in novel antigenic eptitopes that are not regulated by Central Tolerance, neo-antigens are more likely to generate high affinity T cell responses. 4) Cancer-germline antigens: many cancers share common expression of cancer-germline (aka cancer-testis) proteins that are only expressed on male germline cells, which reside in an immunoprivileged site and are thus less vulnerable to autoimmune T cell targeting. This expression appears to be due to a common de-differentiation program associated with genome-wide demethylation. Prototypical antigens include the MAGE family genes and NY-ESO1.

Databases of known tumor antigens classified by category are now widely available to guide selection [44]. An ideal target would have minimal off-target effects and expression on healthy tissue; would be widely shared by many patients in many cancers; would permit the generation of high avidity T cell responses against it; and would be critical to tumor progression, reducing the likelihood of loss of expression and immune escape. A comparison of these desired traits to the categories of tumor antigens above immediately suggests that no antigen will constitute a perfect target. However, numerous trials now exist whose results guide target selection, and they will be referenced throughout the remainder of this review.

Off-Target Effects

A key determinant of the success of ACT in melanoma is a well-tolerated and controlled side-effect profile. The loss of skin pigmentation due to melanocyte destruction, vitiligo, is

disfiguring but not life-threatening, and was one of the first indicators of ACT activity[45]. The presence of melanocytes in the eye and ear can trigger mild uveitis and hearing loss that can be controlled by topical steroids. This permits the use of TILs and T cells specific for melanoma differentiation antigens, which are of high affinity but mediate autoimmune melanocyte destruction.

Side effects of ACT in other cancer histologies similarly depend on expression of tumor antigen on healthy tissue. The use of CAR against CD19 in B cell leukemias leads to B cell aplasia and hypogammaglobulinema due to CD19 expression on B cells [37]. Tissue damage may also increase with higher affinity/sensitivity of the adoptively transferred cells, as described in greater detail below[46].

Unfortunately, off-target effects cannot always be predicted based on available pre-clinical knowledge; TCR targeting carcinoembryonic antigen was predicted to have limited toxicity in mouse models[47], but induced severe transient colitis in trials[32]. The use of TCR-engineering permits the use and re-use of defined TCR specificities, and the gradual development of well-described safety profiles. This knowledge, however, comes at a price, and may only be discovered after significant toxicity has occurred; for example, the previously unrecognized expression of MAGE isoforms in the brain led to neuronal cell destruction using an anti-MAGE-A3 TCR [31]. A high affinity anti-MAGE-A3 TCR also induced myocardial damage even without MAGE-A3 expression in the heart due to cross-reactivity [48]. As a means of limiting unexpected toxicities, TCR-engineered T cells can also be engineered to express a “kill-switch” that can be used to eliminate cells following transfer: these include sensitivity to gancyclovir through expression of HSV-TK[49], or rituximab by expression of CD20[50].

Multiple Antigens and Immune Escape

There is a theoretical concern that under selective pressure by T cells with a single antigen specificity, tumors could down-regulate antigen or MHC expression, as is known to occur during cancer development[51], as a mechanism of immune escape. In mouse models of B16 melanoma, tumor recurrence is associated with loss of antigen expression [52,53], whereas adoptive transfer of T cells with multiple specificities can prevent this process and enhance treatment [54].

In humans, TIL-derived ACT transfer remains the most clinically effective form of adoptive immunotherapy; this could be due to the transfer of polyclonal T cells against many antigens, but also to the inherent immunogenicity of cancers such as melanoma from which TILs can be cultured. Within TIL trials, the most successful results were achieved when patients had multiple persistent antigen-specific responses [55][56], which is again suggestive but may again be explained through numerous mechanisms. Furthermore, loss of MHC expression has been observed following immunotherapy[57]. Thus, there is reason to believe ACT would benefit from multiple simultaneous antigenic targets, but thus far no direct evidence from trials.

CD4 T cells in ACT

CD4 T cell "help" provided to CD8 and APC is important for formation of productive immune responses, and particularly memory[58]. Furthermore, CD4 T cells are master regulators of the balance between rejection and suppression in the tumor microenvironment [59], coordinating responses primarily through secretion of inflammatory and suppressive cytokines. While CD4 T cells can directly lyse tumors such as melanoma which express antigen presented in the context

of MHC Class II[60], most tumors do not [59], and ACT has thus focused on Class I-restricted antigens.

Mouse models suggest that CD4 T cells are capable of enhancing the effect of adoptively transferred CD8 T cells and coordinating anti-tumor responses when adoptively transferred on their own[59]. In fact, CD4 cells can be more effective than CD8 cells under conditions of minimal manipulation and post-adoptive transfer support[61]. Helper cells can be skewed *in vitro* to a number of subsets associated with unique patterns of cytokine production and immune cell recruitment, and which may have different levels of anti-tumor activity; in melanoma, a Th17 polarized subset was superior to unskewed (Th0) and Th1 polarized cells[62]. Finally, T cells that can directly recognize antigen presented on tumors *and* have the superior immune regulatory functions of CD4 cells can be generated by engineering of Class I restricted TCR into CD4 cells[63,64].

CD4 use in clinical trials of ACT has thus far been limited by a lack of well-established Class II restricted antigens and techniques for reliability generating CD4 cells. A case report described a single patient with melanoma who received autologous CD4 cells engineered with an NY-ESO-1 TCR mediated a durable clinical remission[65]. A small trial of4 ovarian cancer patients treated with MUC1 stimulated CD4 cells generated responses in 2/4 patients[66]. However, CD8 enriched TIL are non-inferior to bulk TIL for melanoma treatment[67], and the efficacy of CD4 ACT compared to CD8 ACT remains unclear.

1.3.3 Parameters of T Cell Quality: Replicative Potential, Avidity, and Polyfunctionality

Replicative Potential

The effectiveness of ACT correlates with the number of TILs or antigen-specific T cells that are adoptively transferred in animal models [68,69] and some [17] (but not all [70]) clinical trials.

This common-sense observation, coupled with a belief that "more is better," led early investigators to repeatedly stimulate T cells *ex vivo* to induce repeated rounds of T cell division. The generation of tumor-specific T cells from polyclonal precursors similarly required multiple rounds of stimulation over several weeks to months until high antigen-specific frequencies were achieved.

Unfortunately, the production of high T cell *quantity* during *in vitro* culture often comes at the cost of T cell *quality.* In particular, repeated stimulation with high doses of antigen can drive T cells toward an effector phenotype that, while highly cytotoxic, is also terminally differentiated and has low replicative potential. T cell differentiation from naive to effector cell shares many features in common with stem cell differentiation, with cells classified as more 'stem-like' on the basis of surface phenotype (CD62Lhi, CD45RO, CCR7hi, IL-7Rhi, etc.), increased telomere length, and high overall replicative capacity (reviewed in [71]). Based on these characteristics, T cells can be described (from most stem-like to most-differentiated) as naive (T_n), central memory (T_{cm}), and effector memory (T_{em}).

Initial trials of TIL-derived ACT following lymphodepletion showed that tumor response and persistence in the host were correlated with telomere length prior to transfer [72]. Based in part on these observations, investigators set out to determine whether less-differentiated subsets might confer better anti-tumor activity. In mouse and primate models, naive T cells T cells were more than effective than effector or memory populations[73,74], and central memory cells outperformed effector memory cells[75–77]. Tumor response thus correlated with inversely with differentiation status.

As a result, numerous methods have been developed to maintain T cell stemness and replicative capacity while also generating sufficient antigen-specific T cells. The introduction of genetically engineered TCR allows the manufacture of large numbers of antigen-specific cells without the need to repeatedly stimulate polyclonal T cells with antigen[25]. New protocols for the rapid expansion of TILs have been developed that minimize time in culture prior to adoptive transfer[78]. Pharmacological inhibition of the Wnt-signaling during T cell activation generates a subset termed "T memory stem cell" that maintains high replicative capacity even after repeated division[79]. As will be reviewed in further detail below, the use of T cell growth supporting cytokines other than IL-2 can also maintain a more plastic phenotype. Finally, it is not yet clear whether differentiation status is a "one-way" street, and even highly cultured, repeatedly stimulated T cells clones generate cells with a T_{cm} phenotype after adoptive transfer into a lymphodepleted host[23].

Avidity

T cell avidity is a biophysical description of the strength of binding between TCR and its cognate MHC. It is most commonly measured by binding to soluble MHC constructs[80]. A related concept, functional avidity, describes the sensitivity of T cell responses to antigen, with T cells that secrete cytokine in response to low antigen doses described as "high functional avidity" cells. In general, higher avidity (aka structural avidity) and functional avidity are correlated with each other[81], and with stronger immune responses and better control of infection[82,83]. Similarly, the adoptive transfer of high avidity T cells in mouse models of cancer leads to more effective tumor rejection[84–86].

The use of genetically engineered TCR in ACT allows the selection of selection of high avidity T cell responses from a single patient, and further avidity enhancement by modification to the transferred TCR sequence [26,87,88]. For T cell populations derived by clonal selection, avidity can be tested and selected prior to cloning[20,89]. In general, stimulation with low doses of antigen is associated with the selection of higher-avidity clones [90] as well as increased avidity of individual clones by TCR and CD8 dependent mechanisms[91,92].

In an attempt to improve low response rates in trials of melanoma therapy using cells engineered with specificity against MART-1, a higher avidity anti-MART1 TCR was isolated and transferred into PBMC[93]. Using this higher avidity TCR, objective response rates increased from 14 [29] to 31 percent [46]. However, the higher avidity TCR was associated with significantly more toxicity, including a cytokine spike and serious skin rashes 3-5 days after transfer. A similar pattern of enhanced efficacy and toxicity was also observed with a high avidity TCR against MAGE-A3[31]. These results have motivated basic studies to understand the relationship between avidity, autoimmunity, and anti-tumor effectiveness. A study of *in vitro* and *in vivo* against melanoma by seven gp100-specific TCR, antitumor activity and autoimmunity were correlated across a range of avidities[94]. Thus, caution should be exercised when using high avidity TCR until off-target effects are better understood.

Polyfunctionality

Polyfunctionality is the capacity of T cells to produce many effector cytokines and chemokines (TNF-α, IFN-γ, MIP-1β, IL-2, etc.) simultaneously during effector responses. High levels of polyfunctionality among antigen-specific T cells are a marker of effective vaccine responses[95], and have been observed to correlate with effective control of chronic viral infections such as

HIV[96]. Polyfunctionality has also been proposed as a quality parameter that may explain why TCR-engineered T cells can persist in the host but fail mediate tumor rejection, but its role in determining the outcome of ACT is still unclear. In a small study of 3 melanoma patients, the functional profile of CD8+ Mart-1 specific engineered T cells varied over time, but no clear correlation with tumor response could be established[97].

Further study of polyfunctionality will depend on the generation of highly polyfunctional T cells with tumor-specificity. Enhanced polyfunctionality during *in vitro* culture can be generated by selecting optimal antigen dose **[YEN PAPER]**, or administration of kinase inhibitors and TLR agonists[98]. Alternatively, polyfunctionality can be enhanced after adoptive transfer by certain vaccine/adjuvant strategies [99]. CTLA-4 checkpoint blockade has also been shown to enhance polyfunctionality of endogenous immune responses[100], suggesting a possibility to integrate ACT with checkpoint blockade for melanoma.

1.3.4 The Importance of Lymphodepletion

The development of ACT was motivated in part by poor results with cancer vaccines, inducing tumor regression in only 4% of patients treated in early trials[101]. Subsequent work has suggested that this failure was due in part due multiple layers of immunosuppression found within the tumor microenvironment[102–104], explaining how tumor-specific responses could be found in patients but fail to reject cancer. This suppression is mediated by tumor cell production of immunosuppressive proteins such as TGF-β and PD-L1[105,106], as well as the recruitment of immunosuppressive immune cells such as regulatory T cells and Myeloid Derived Suppressor Cells[102,107]. These mechanisms represent T cell-*extrinsic* pathways of immune dysfunction (as compared to T cell-*intrinsic* pathways discussed earlier), and may be the consequence of peripheral tolerance mechanisms that control autoimmunity. Modulation of the

immunosuppressive tumor microenvironment is both a key therapeutic target and a tremendous challenge[108], with recent advances such as checkpoint blockade [109–111] seen as a means for unlocking the potential of cancer vaccines.

A significant comparative advantage of adoptive immunotherapy is that cultured T cells are physically separated from the suppressive cells in the patient, reducing the need to find targeted therapies that block immunosuppressive but not tumor-specific cells. Instead, highly non-specific therapies such as high intensity radiation or chemotherapy can be used to induce a transient lympho- and myeloablation that stimultaneously depletes both suppressive and active immune cells, which are then replaced by ACT. This process can be conceptualized as a "re-boot" of the immune system, where the dysfunctional, suppressed immune compartment is replaced by a highly active immune compartment generated *ex vivo*.

Lymphodepletion also enhances engraftment of adoptively transferred cells by reducing competition for lymphotrophic cytokines [112,113]. It has long been appreciated that T cells adoptively transferred into a lymphopenic environment undergo a robust, non-antigen driven homeostatic expansion driven by increased availability of the γ-chain cytokines IL-7, IL-15, and IL-21, and in some cases low affinity interactions with MHC [12,114,115]. MHC and γ-chain cytokine regulate the size of the T cell compartment by permitting T cell division and persistence normal conditions, and become scarce when the compartment is expanded following adoptive transfer. Lymphodepletion enhances the availability of homeostatic signals by reducing competition from host cells; for example, circulating levels of IL-15 are not detectable in patients prior to lymphodepletion, but high levels are detected immediately afterward [70].

Homeostatic expansion can greatly enhance T cell function in the context of adoptive immunotherapy; for example, transfer of LCMV-specific T cells into lymphodepeleted but not immunocompetent LCMV-infected mice eliminates virus in hosts[116]. In fact, the combination of regulatory cell depletion and homeostatic cell expansion is sufficient to induce anti-cancer activity in animal models, even without exogenous antigen-driven stimulation [117–119]. In clinical trials, less than 0.1% of adoptively transferred T cells persisted in the host at one week prior to the introduction of lymphodepletion[120], whereas patients could be identified to have multiple persistent TIL clonotypes 2-3 months following ACT after its introduction[55][56]. Furthermore, TIL persistence, and particularly the persistence of a wide variety of transferred clones, was significantly correlated with effective response.

Finally, it has been proposed that total body irradiation and chemotherapy can enhance host antigen presentation, triggering tissue damage that induces the production of inflammatory cytokines and upregulation of co-stimulatory molecules by professional APCs[121–123]. Of course, this is a double-edged sword, as professional APCs are significantly depleted five days after treatment[124,125]. Thus, the overall effect of conditioning on antigen presentation is time-dependent and incompletely understood, and the loss of APC may limit the effectiveness of vaccines used to boost T cell function after ACT.

1.3.5 Cytokine Support Following Adoptive Transfer

The cytokine IL-2 has a prominent role in the history of immunotherapy; it was the discovery that IL-2 could support TIL expansion *in vitro* that permitted the first trials of ACT against melanoma [10], and IL-2 has long been used as monotherapy in the treatment of melanoma, decreasing the size of lesions but not increasing survival[126,127]. Thus, IL-2 was a natural choice as cytokine support agent in melanoma treatment, and its administration to patients after

ACT can increase T cell expansion after adoptive transfer in animal models[68] and clinical trials[128]. In this context, IL-2 adminstration serves a similar purpose as lymphodepletion, increasing the availability of lymphotrophic cytokines (by increasing the available pool rather than reducing competition).

In many ways, however, IL-2 is not the optimal agent for supporting T cell proliferation. High-dose IL-2 can lead to severe flu-like symptoms and dose-limiting toxicities in patients[127]. It is also associated with activation induce cell death of T cells[129], and skews T cell proliferation away from long-live memory responses toward short lived effector responses[130,131].

A number of cytokines similarly function to support T cell expansion and even signal through common receptor components (CD132, the common gamma chain) as IL-2, including IL-7, IL-15, and IL-21. These cytokines, however, also appear to support memory formation and enhanced proliferative capacity [130–134] in T cell culture compared to IL-2. When administered *in vivo*, IL-15 improved survival and anti-tumor activity of adoptively transferred cells[76]. In a head-to-head comparison in a mouse melanoma model, all gamma chain cytokines were found to be capable of supporting anti-tumor activity of adoptively transferred CD8 T cells[68]. Thus, due to IL-2 cytotoxicity and the efficacy of other gamma chain cytokines in supporting persistet

1.3.6 Enhancing ACT Through Gene Engineering

The use of gene-engineered TCR has increased the range of cancers that can be targeted using ACT. Simultaneously, it has opened the possibility of further modifications to T cell function through the genetic engineering of other T cell behaviors to address existing limitations of ACT (reviewed extensively in [25]).

For example, the trafficking of lymphocytes to large solid tumors appears to be a rate-limiting step in tumor eradication. Intravital imaging has suggested that individual lymphocytes may interact with a given tumor cell for several hours[135], suggesting that large numbers of antigen-specific cells in the tumor are required. Numerous barriers exist to efficient trafficking, however, including low expression of trafficking ligands such as L-selectin on tumor microvasculature[136], and suppressive mechanisms mediated by cancer also appear to impair T cell penetration into tumor cores [137]. To improve trafficking, cells can be engineering with chemokine receptors such as CXCR2[138] or CCR4[139], which enhances therapeutic efficacy in mouse models.

As an alternative to intravenous administration of supportive cytokines, T cells can be genetically modified to express IL-2, IL7, IL-15, or IL-21[140–143]. As described previously, cytokine support is required for efficient engraftment of transferred cells, and autocrine delivery may eliminate the need for systemic administration and, particularly in the case of IL-2, a reduction in systemic toxicity.

1.3.7 The Path Forward

While the therapeutic potential of ACT in cancer has been conclusively demonstrated, much remains to be discovered and optimized. Tumor-specific cells can be generated from TILs, repeated stimulation with antigen, or genetic engineering, with each appropriate carrying advantages and drawbacks. T Cell quality in addition to quantity is emerging as a critical parameter of immunotherapeutic success, and strategies to improve avidity, safety, functionality, and persistence are required to expand on the promise of ACT.

1.3.8 References

1. Pardoll D. Does the immune system see tumors as foreign or self? *Annual review of immunology*. 21(Table 1), 807–39 (2003).

2. Robbins PF, Kawakamit Y. Human tumor antigens recognized by T cells. *Current opinion in immunology*. 8, 628–636 (1996).

3. Schreiber RD, Old LJ, Smyth MJ. Cancer Immunoediting: Integrating Immunity's Roles in Cancer Suppression and Promotion. *Science*. 331(6024), 1565–1570 (2011).

4. Dudley ME, Wunderlich JR, Shelton TE, Even J, Rosenberg SA. Generation of Tumor-Infiltrating Lymphocyte Cultures for Use in Adoptive Transfer Therapy for Melanoma Patients. *J Immunotherapy*. 26(4), 332–342 (2003).

5. Hanahan D, Weinberg RA. Hallmarks of Cancer: The Next Generation. *Cell*. 144(5), 646–674 (2011).

6. Welniak L a, Blazar BR, Murphy WJ. Immunobiology of allogeneic hematopoietic stem cell transplantation. *Annual review of immunology*. 25, 139–70 (2007).

7. Fabre JW. The allogeneic response and tumor immunity. *Nature medicine*. 7(6), 649–52 (2001).

8. Kolb HJ, Schattenberg a, Goldman JM, *et al.* Graft-versus-leukemia effect of donor lymphocyte transfusions in marrow grafted patients. *Blood*. 86(5), 2041–50 (1995).

9. Rosenberg SA, Packard BS, Aebersold PM, *et al.* Use of Tumor-Infiltrating Lymphocytes and Interleukin-2 in the Immunotherapy of Patients with Metastatic Melanoma. *New England Journal of Medicine*. 319(25), 1676–1680 (1988).

10. Muul LM, Spiess PJ, Director EP, Rosenberg SA. Identification of Specific Cytolytic Immune Responses Against Autologus Tumor in Humans Bearing Malignant Melanoma. *Journal of Immunology*. 138, 989–995 (1987).

11. Rosenberg SA, John R, Yang JC, *et al.* Treatment of Patients With Metastatic Melanoma With Autologous Tumor-Infiltrating Lymphocytes and Interleukin 2. *Journal of the National Cancer Institute*. 86(15), 1159–1166 (1994).

12. Gattinoni L, Finkelstein SE, Klebanoff C a, *et al.* Removal of homeostatic cytokine sinks by lymphodepletion enhances the efficacy of adoptively transferred tumor-specific CD8+ T cells. *The Journal of experimental medicine*. 202(7), 907–12 (2005).

13. Wrzesinski C, Paulos CM, Kaiser A, *et al.* Increased intensity lymphodepletion enhances tumor treatment efficacy of adoptively transferred tumor-specific T cells. *Journal of Immunotherapy*. 33(1), 1–7 (2010).

14. Dudley ME, Wunderlich JR, Yang JC, *et al.* A Phase I Study of Nonmyeloablative Chemotherapy and Adoptive Transfer of Autologous Tumor Antigen-Specific T Lymphocytes in Patients With Metastatic Melanoma. *Journal of Immunotherapy*. 25(3), 243–251 (2002).

15. Rosenberg S a, Yang JC, Sherry RM, *et al.* Durable complete responses in heavily pretreated patients with metastatic melanoma using T-cell transfer immunotherapy. *Clinical cancer research : an official journal of the American Association for Cancer Research*. 17(13), 4550–7 (2011).

16. Itzhaki O, Hovav E, Ziporen Y, *et al.* Establishment and Large-scale Expansion of Minimally Adoptive Transfer Therapy. *J Immunotherapy*. 34(2), 212–220 (2011).

17. Besser MJ, Shapira-Frommer R, Treves AJ, *et al.* Clinical responses in a phase II study using adoptive transfer of short-term cultured tumor infiltration lymphocytes in metastatic melanoma patients. *Clinical Cancer Research*. 16(9), 2646–55 (2010).

18. Woo EY, Yeh H, Chu CS, *et al.* Cutting edge: Regulatory T cells from lung cancer patients directly inhibit autologous T cell proliferation. *Journal of immunology (Baltimore, Md. : 1950)*. 168(9), 4272–6 (2002).

19. Curiel TJ, Coukos G, Zou L, *et al.* Specific recruitment of regulatory T cells in ovarian carcinoma fosters immune privilege and predicts reduced survival. *Nature medicine*. 10(9), 942–9 (2004).

20. Ho WY, Nguyen HN, Wolfl M, Kuball J, Greenberg PD. In vitro methods for generating CD8+ T-cell clones for immunotherapy from the naïve repertoire. *Journal of immunological methods*. 310(1-2), 40–52 (2006).

21. Chapuis A, Ragnarsson G. Transferred WT1-reactive CD8+ T cells can mediate antileukemic activity and persist in post-transplant patients. *Science translational …*. 27 (2013).

22. Vignard V, Lemercier B, Lim A, *et al.* Adoptive Transfer of Tumor-Reactive Melan-A-Specific CTL Clones in Melanoma Patients Is Followed by Increased Frequencies of Additional Melan-A-Specific T Cells. *Journal of Immunology*. 175, 4797–4805 (2005).

23. Chapuis AG, Thompson JA, Margolin KA, *et al.* Transferred melanoma-specific CD8 + T cells persist , mediate tumor regression , and acquire central memory phenotype. (2012).

24. Phillips CA, Townsend M, Philip R, Dobrzanski MJ, Lockwood-cooke PR, Robinson W. Cytotoxic T-lymphocyte Immunotherapy for Ovarian Cancer : A Pilot Study. 35(2), 196–204 (2012).

25. Kershaw MH, Westwood J a, Darcy PK. Gene-engineered T cells for cancer therapy. *Nature reviews. Cancer*. 13(8), 525–41 (2013).

26. Varela-Rohena A, Molloy PE, Dunn SM, *et al.* Control of HIV-1 immune escape by CD8 T cells expressing enhanced T-cell receptor. *Nature medicine*. 14(12), 1390–5 (2008).

27. Johnson L a, Morgan R a, Dudley ME, *et al.* Gene therapy with human and mouse T-cell receptors mediates cancer regression and targets normal tissues expressing cognate antigen. *Blood*. 114(3), 535–46 (2009).

28. Bonini C, Brenner MK, Heslop HE, Morgan R a. Genetic modification of T cells. *Biology of blood and marrow transplantation : journal of the American Society for Blood and Marrow Transplantation*. 17(1 Suppl), S15–20 (2011).

29. Morgan R a, Dudley ME, Wunderlich JR, *et al.* Cancer regression in patients after transfer of genetically engineered lymphocytes. *Science (New York, N.Y.)*. 314(5796), 126–9 (2006).

30. Pule M a, Savoldo B, Myers GD, *et al.* Virus-specific T cells engineered to coexpress tumor-specific receptors: persistence and antitumor activity in individuals with neuroblastoma. *Nature medicine*. 14(11), 1264–70 (2008).

31. Morgan RA, Chinnasamy N, Abate-daga D, *et al.* Cancer Regression and Neurological Toxicity Following Anti-Mage-A3 TCR Gene Therapy. *Journal of Immunotherapy*. 36(2), 133–151 (2013).

32. Parkhurst MR, Yang JC, Langan RC, *et al.* T cells targeting carcinoembryonic antigen can mediate regression of metastatic colorectal cancer but induce severe transient colitis. *Molecular therapy : the journal of the American Society of Gene Therapy*. 19(3), 620–6 (2011).

33. Cartellieri M, Bachmann M, Feldmann A, *et al.* Chimeric antigen receptor-engineered T cells for immunotherapy of cancer. *Journal of biomedicine & biotechnology*. 2010, 956304 (2010).

34. Lamers CHJ, Sleijfer S, Vulto AG, *et al.* Treatment of metastatic renal cell carcinoma with autologous T-lymphocytes genetically retargeted against carbonic anhydrase IX: first clinical experience. *Journal of clinical oncology : official journal of the American Society of Clinical Oncology*. 24(13), e20–2 (2006).

35. Park JR, Digiusto DL, Slovak M, *et al.* Adoptive Transfer of Chimeric Antigen Receptor Re-directed Cytolytic T Lymphocyte Clones in Patients with Neuroblastoma. 15(4), 825–833 (2007).

36. Grupp S a, Kalos M, Barrett D, *et al.* Chimeric antigen receptor-modified T cells for acute lymphoid leukemia. *The New England journal of medicine*. 368(16), 1509–18 (2013).

37. Porter DL, Levine BL, Kalos M, Bagg A, June CH. Chimeric antigen receptor-modified T cells in chronic lymphoid leukemia. *The New England journal of medicine*. 365(8), 725–33 (2011).

38. Vigneron N, Van den Eynde BJ. Insights into the processing of MHC class I ligands gained from the study of human tumor epitopes. *Cellular and molecular life sciences : CMLS*. 68(9), 1503–20 (2011).

39. Hogquist K a, Baldwin T a, Jameson SC. Central tolerance: learning self-control in the thymus. *Nature reviews. Immunology*. 5(10), 772–82 (2005).

40. McMahan RH, Slansky JE. Mobilizing the low-avidity T cell repertoire to kill tumors. *Seminars in cancer biology*. 17(4), 317–29 (2007).

41. Segal NH, Parsons DW, Peggs KS, *et al.* Epitope landscape in breast and colorectal cancer. *Cancer research*. 68(3), 889–92 (2008).

42. Koboldt DC, Fulton RS, McLellan MD, *et al.* Comprehensive molecular portraits of human breast tumours. *Nature*. , 1–10 (2012).

43. Bozic I, Antal T, Ohtsuki H, *et al.* Accumulation of driver and passenger mutations during tumor progression. *Proceedings of the National Academy of Sciences of the United States of America*. (2010).

44. Vigneron N, Stroobant V, Eynde BJ Van Den, Bruggen P Van Der. Database of T cell-defined human tumor antigens : the 2013 update. *Cancer Immunity*. 13(July), 1–6 (2013).

45. Overwijk WW, Theoret MR, Finkelstein SE, *et al.* Tumor regression and autoimmunity after reversal of a functionally tolerant state of self-reactive CD8+ T cells. *J. Exp. Med*. 198, 569–580 (2003).

46. Johnson L a, Morgan R a, Dudley ME, *et al.* Gene therapy with human and mouse T-cell receptors mediates cancer regression and targets normal tissues expressing cognate antigen. *Blood*. 114(3), 535–46 (2009).

47. Offringa R. Antigen choice in adoptive T-cell therapy of cancer. *Current opinion in immunology*. 21(2), 190–9 (2009).

48. Linette GP, Stadtmauer E a, Maus M V, *et al.* Cardiovascular toxicity and titin cross-reactivity of affinity enhanced T cells in myeloma and melanoma. *Blood*. (2013).

49. Berger C, Flowers ME, Warren EH, Riddell SR. Analysis of transgene-specific immune responses that limit the in vivo persistence of adoptively transferred HSV-TK-modified donor T cells after allogeneic hematopoietic cell transplantation. *Blood*. 107(6), 2294–302 (2006).

50. Vogler I, Newrzela S, Hartmann S, *et al.* An improved bicistronic CD20/tCD34 vector for efficient purification and in vivo depletion of gene-modified T cells for adoptive immunotherapy. *Molecular therapy : the journal of the American Society of Gene Therapy*. 18(7), 1330–8 (2010).

51. Seliger B. Molecular mechanisms of MHC class I abnormalities and APM components in human tumors. *Cancer immunology, immunotherapy : CII*. 57(11), 1719–26 (2008).

52. Kaluza KM, Thompson JM, Kottke TJ, Flynn Gilmer HC, Knutson DL, Vile RG. Adoptive T cell therapy promotes the emergence of genomically altered tumor escape variants. *International journal of cancer. Journal international du cancer*. 131(4), 844–54 (2012).

53. Jensen SM, Twitty CG, Maston LD, *et al.* Increased frequency of suppressive regulatory T cells and T cell-mediated antigen loss results in murine melanoma recurrence. *Journal of immunology (Baltimore, Md. : 1950)*. 189(2), 767–76 (2012).

54. Kaluza KM, Kottke T, Diaz RM, Rommelfanger D, Thompson J, Vile R. Adoptive transfer of cytotoxic T lymphocytes targeting two different antigens limits antigen loss and tumor escape. *Human gene therapy*. 23(10), 1054–64 (2012).

55. Zhou J, Dudley ME, Rosenberg S a, Robbins PF. Persistence of multiple tumor-specific T-cell clones is associated with complete tumor regression in a melanoma patient receiving adoptive cell transfer therapy. *Journal of immunotherapy (Hagerstown, Md. : 1997)*. 28(1), 53–62 (2005).

56. Robbins PF, Dudley ME, Wunderlich J, *et al.* Cutting edge: persistence of transferred lymphocyte clonotypes correlates with cancer regression in patients receiving cell transfer therapy. *Journal of immunology (Baltimore, Md. : 1950)*. 173(12), 7125–30 (2004).

57. Restifo N, Marincola FM, Kawakami Y, Taubenberger J, Yannelli JR, Rosenberg SA. Loss of functional beta2-microglobulin in metastatic melanomas from five patients receiving immunotherapy. *Journal of the …*. 88(2), 100–108 (1996).

58. Castellino F, Germain RN. Cooperation between CD4+ and CD8+ T cells: when, where, and how. *Annual review of immunology*. 24, 519–40 (2006).

59. Muranski P, Restifo NP. Adoptive immunotherapy of cancer using CD4(+) T cells. *Current opinion in immunology*. 21(2), 200–8 (2009).

60. Quezada S a, Simpson TR, Peggs KS, *et al.* Tumor-reactive CD4(+) T cells develop cytotoxic activity and eradicate large established melanoma after transfer into lymphopenic hosts. *The Journal of experimental medicine*. 207(3), 637–50 (2010).

61. Perez-Diez A, Joncker NT, Choi K, *et al.* CD4 cells can be more efficient at tumor rejection than CD8 cells. *Blood*. 109(12), 5346–54 (2007).

62. Muranski P, Boni A, Antony P a, *et al.* Tumor-specific Th17-polarized cells eradicate large established melanoma. *Blood*. 112(2), 362–73 (2008).

63. Xue S-A, Gao L, Ahmadi M, *et al.* Human MHC Class I-restricted high avidity CD4(+) T cells generated by co-transfer of TCR and CD8 mediate efficient tumor rejection in vivo. *Oncoimmunology*. 2(1), e22590 (2013).

64. Ray S, Chhabra A, Chakraborty NG, *et al.* MHC-I-restricted melanoma antigen specific TCR-engineered human CD4+ T cells exhibit multifunctional effector and helper responses, in vitro. *Clinical immunology (Orlando, Fla.)*. 136(3), 338–47 (2010).

65. Hunder NN, Wallen H, Cao J, *et al.* Treatment of metastatic melanoma with autologous CD4+ T cells against NY-ESO-1. *The New England journal of medicine*. 358(25), 2698–703 (2008).

66. Dobrzanski MJ, Rewers-Felkins K a, Samad K a, *et al.* Immunotherapy with IL-10- and IFN-γ-producing CD4 effector cells modulate "Natural" and "Inducible" CD4 TReg cell subpopulation levels: observations in four cases of patients with ovarian cancer. *Cancer immunology, immunotherapy : CII*. 61(6), 839–54 (2012).

67. Dudley ME, Gross C a, Somerville RPT, *et al.* Randomized selection design trial evaluating CD8+-enriched versus unselected tumor-infiltrating lymphocytes for adoptive cell therapy for patients with

melanoma. *Journal of clinical oncology : official journal of the American Society of Clinical Oncology*. 31(17), 2152–9 (2013).

68. Klebanoff C a, Gattinoni L, Palmer DC, *et al.* Determinants of successful CD8+ T-cell adoptive immunotherapy for large established tumors in mice. *Clinical cancer research : an official journal of the American Association for Cancer Research*. 17(16), 5343–52 (2011).

69. Wen F, Thisted R. A systematic analysis of experimental immunotherapies on tumors differing in size and duration of growth. …. (April), 172–178 (2012).

70. Dudley ME, Yang JC, Sherry R, *et al.* Adoptive cell therapy for patients with metastatic melanoma: evaluation of intensive myeloablative chemoradiation preparative regimens. *Journal of clinical oncology : official journal of the American Society of Clinical Oncology*. 26(32), 5233–9 (2008).

71. Gattinoni L, Klebanoff C a, Restifo NP. Paths to stemness: building the ultimate antitumour T cell. *Nature reviews. Cancer*. 12(10), 671–84 (2012).

72. Zhou J, Shen X, Huang J, Hodes RJ, Rosenberg S a, Robbins PF. Telomere length of transferred lymphocytes correlates with in vivo persistence and tumor regression in melanoma patients receiving cell transfer therapy. *Journal of immunology (Baltimore, Md. : 1950)*. 175(10), 7046–52 (2005).

73. Gattinoni L, Klebanoff C. Acquisition of full effector function in vitro paradoxically impairs the in vivo antitumor efficacy of adoptively transferred CD8+ T cells. *Journal of Clinical …*. 115(6) (2005).

74. Hinrichs CS, Borman Z a, Cassard L, *et al.* Adoptively transferred effector cells derived from naive rather than central memory CD8+ T cells mediate superior antitumor immunity. *Proceedings of the National Academy of Sciences of the United States of America*. 106(41), 17469–74 (2009).

75. Klebanoff C a, Gattinoni L, Torabi-Parizi P, *et al.* Central memory self/tumor-reactive CD8+ T cells confer superior antitumor immunity compared with effector memory T cells. *Proceedings of the National Academy of Sciences of the United States of America*. 102(27), 9571–6 (2005).

76. Klebanoff C a, Finkelstein SE, Surman DR, *et al.* IL-15 enhances the in vivo antitumor activity of tumor-reactive CD8+ T cells. *Proceedings of the National Academy of Sciences of the United States of America*. 101(7), 1969–74 (2004).

77. Berger C, Jensen MC, Lansdorp PM, Gough M, Elliott C, Riddell SR. Adoptive transfer of effector CD8 + T cells derived from central memory cells establishes persistent T cell memory in primates. 118(1) (2008).

78. Dudley M, Gross C, Langhan M. CD8+ enriched "young" tumor infiltrating lymphocytes can mediate regression of metastatic melanoma. *Clinical Cancer …*. 16(24), 6122–6131 (2010).

79. Gattinoni L, Lugli E, Ji Y, *et al.* A human memory T cell subset with stem cell-like properties. *Nature medicine*. (September) (2011).

80. Stone JD, Chervin AS, Kranz DM. T-cell receptor binding affinities and kinetics: impact on T-cell activity and specificity. *Immunology*. 126(2), 165–76 (2009).

81. Dutoit V, Rubio-Godoy V, Doucey M-A, *et al.* Functional avidity of tumor antigen-specific CTL recognition directly correlates with the stability of MHC/peptide multimer binding to TCR. *Journal of Immunology*. 168(3), 1167–71 (2002).

82. Derby M, Alexander-Miller M, Tse R, Berzofsky J. High-avidity CTL exploit two complementary mechanisms to provide better protection against viral infection than low-avidity CTL. *Journal of Immunology*. 166(3), 1690–7 (2001).

83. Walker LJ, Sewell a K, Klenerman P. T cell sensitivity and the outcome of viral infection. *Clinical and experimental immunology*. 159(3), 245–55 (2010).

84. Zeh HJ, Perry-Lalley D, Dudley ME, Rosenberg S a, Yang JC. High avidity CTLs for two self-antigens demonstrate superior in vitro and in vivo antitumor efficacy. *Journal of immunology (Baltimore, Md. : 1950)*. 162(2), 989–94 (1999).

85. Soto CM, Stone JD, Chervin AS, *et al.* MHC-class I-restricted CD4 T cells: a nanomolar affinity TCR has improved anti-tumor efficacy in vivo compared to the micromolar wild-type TCR. *Cancer immunology, immunotherapy : CII*. 62(2), 359–69 (2013).

86. Bullock T, Mullins D, Colella T, VH. Manipulation of avidity to improve effectiveness of adoptively transferred CD8+ T cells for melanoma immunotherapy in human MHC class I-transgenic mice. *The Journal of Immunology*. (167), 5824–5831 (2001).

87. Haidar JN, Pierce B, Yu Y, Tong W, Li M, Weng Z. Structure-based design of a T-cell receptor leads to nearly 100-fold improvement in binding affinity for pepMHC. *Proteins*. 74(4), 948–60 (2009).

88. Robbins P, Li Y, El-Gamil M. Single and dual amino acid substitutions in TCR CDRs can enhance antigen-specific T cell functions. *The Journal of ….* 180, 6116–6131 (2008).

89. Chapuis A, Ragnarsson G. Transferred WT1-reactive CD8+ T cells can mediate antileukemic activity and persist in post-transplant patients. *Science translational ….* 27 (2013).

90. Alexander-Miller M a, Leggatt GR, Berzofsky J a. Selective expansion of high- or low-avidity cytotoxic T lymphocytes and efficacy for adoptive immunotherapy. *Proceedings of the National Academy of Sciences of the United States of America*. 93(9), 4102–7 (1996).

91. Perica K, Bieler JG, Edidin M, Schneck J. Modulation of MHC binding by lateral association of TCR and coreceptor. *Biophysical journal*. 103(9), 1890–8 (2012).

92. Kroger CJ, Alexander-Miller M a. Dose-dependent modulation of CD8 and functional avidity as a result of peptide encounter. *Immunology*. 122(2), 167–78 (2007).

93. Johnson LA, Heemskerk B, Powell Jr DJ, *et al.* Gene transfer of tumor-reactive TCR confers both high avidity and tumor reactivity to nonreactive peripheral blood mononuclear cells and tumor-infiltrating lymphocytes. *The Journal of Immunology*. 177(9), 6548 (2006).

94. Zhong S, Malecek K. T-cell receptor affinity and avidity defines antitumor response and autoimmunity in T-cell immunotherapy. *Proceedings of the ….* 110(17) (2013).

95. Seder R a, Darrah PA, Roederer M. T-cell quality in memory and protection: implications for vaccine design. *Nature reviews. Immunology*. 8(4), 247–58 (2008).

96. Almeida JR, Price DA, Papagno L, *et al.* Superior control of HIV-1 replication by CD8+ T cells is reflected by their avidity, polyfunctionality, and clonal turnover. *The Journal of experimental medicine*. 204(10), 2473–85 (2007).

97. Ma C, Cheung AF, Chodon T, *et al.* Multifunctional T-cell Analyses to Study Response and Progession in Adoptive Cell Transfer Immunotherapy. *Cancer discovery*. 3(4), 418–29 (2013).

98. Marshall N a, Galvin KC, Corcoran A-MB, Boon L, Higgs R, Mills KHG. Immunotherapy with PI3K inhibitor and Toll-like receptor agonist induces IFN-γ+IL-17+ polyfunctional T cells that mediate rejection of murine tumors. *Cancer research*. 72(3), 581–91 (2012).

99. Aranda F, Llopiz D, Díaz-Valdés N, *et al.* Adjuvant combination and antigen targeting as a strategy to induce polyfunctional and high-avidity T-cell responses against poorly immunogenic tumors. *Cancer research*. 71(9), 3214–24 (2011).

100. Yuan J, Gnjatic S, Li H, *et al.* CTLA-4 blockade enhances polyfunctional NY-ESO-1 specific T cell responses in metastatic melanoma patients with clinical benefit. *Proceedings of the National Academy of Sciences of the United States of America*. 105(51), 20410–5 (2008).

101. Klebanoff CA, Restifo NP. Therapeutic cancer vaccines : are we there yet ? *Immunological Reviews*. 239, 27–44 (2011).

102. Hurwitz A a, Watkins SK. Immune suppression in the tumor microenvironment: a role for dendritic cell-mediated tolerization of T cells. *Cancer Immunology and Immunotherapy*. 61(2), 289–93 (2012).

103. Lindau D, Gielen P, Kroesen M, Wesseling P, Adema GJ. The immunosuppressive tumour network: myeloid-derived suppressor cells, regulatory T cells and natural killer T cells. *Immunology*. 138(2), 105–15 (2013).

104. Beyer M, Schultze JL. Regulatory T cells in Cancer. *Blood*. 108(3), 804–811 (2006).

105. Gorelik L, Flavell R a. Immune-mediated eradication of tumors through the blockade of transforming growth factor-beta signaling in T cells. *Nature medicine*. 7(10), 1118–22 (2001).

106. Taube JM, Anders R a, Young GD, *et al.* Colocalization of inflammatory response with B7-h1 expression in human melanocytic lesions supports an adaptive resistance mechanism of immune escape. *Science translational medicine*. 4(127), 127ra37 (2012).

107. Serafini P, Borrello I, Bronte V. Myeloid suppressor cells in cancer: recruitment, phenotype, properties, and mechanisms of immune suppression. *Seminars in cancer biology*. 16(1), 53–65 (2006).

108. Motz GT, Coukos G. Deciphering and reversing tumor immune suppression. *Immunity*. 39(1), 61–73 (2013).

109. Brahmer JR, Drake CG, Wollner I, *et al.* Phase I Study of Single-Agent Anti-Programmed Death-1 (MDX-1106) in Refractory Solid Tumors: Safety, Clinical Activity, Pharmacodynamics, and Immunologic Correlates. *Journal of clinical oncology : official journal of the American Society of Clinical Oncology*. 28(19), 3167–3175 (2010).

110. Topalian S, Hodi F. Safety, activity, and immune correlates of anti–PD-1 antibody in cancer. ... *England Journal of ...* , 2443–2454 (2012).

111. Hodi FS, O'Day SJ, McDermott DF, *et al.* Improved Survival with Ipilimumab in Patients with Metastatic Melanoma. *The New England journal of medicine*. , 1–13 (2010).

112. Restifo NP, Dudley ME, Rosenberg S a. Adoptive immunotherapy for cancer: harnessing the T cell response. *Nature reviews. Immunology*. 12(4), 269–81 (2012).

113. Klebanoff C a, Khong HT, Antony P a, Palmer DC, Restifo NP. Sinks, suppressors and antigen presenters: how lymphodepletion enhances T cell-mediated tumor immunotherapy. *Trends in immunology*. 26(2), 111–7 (2005).

114. Clarke SR, Rudensky a Y. Survival and homeostatic proliferation of naive peripheral CD4+ T cells in the absence of self peptide:MHC complexes. *Journal of Immunology*. 165(5), 2458–64 (2000).

115. Surh CD, Sprent J. Homeostasis of naive and memory T cells. *Immunity*. 29(6), 848–62 (2008).

116. Oehen S, Brduscha-Riem K. Naïve cytotoxic T lymphocytes spontaneously acquire effector function in lymphocytopenic recipients: A pitfall for T cell memory studies? *European journal of immunology*. 29(2), 608–14 (1999).

117. Kline J, Brown IE, Zha Y-Y, *et al.* Homeostatic proliferation plus regulatory T-cell depletion promotes potent rejection of B16 melanoma. *Clinical cancer research : an official journal of the American Association for Cancer Research*. 14(10), 3156–67 (2008).

118. Dummer W, Niethammer AG, Baccala R, *et al.* T cell homeostatic proliferation elicits effective antitumor autoimmunity. *Journal of Clinical Investigation*. 110(2), 157–159 (2002).

119. Kline J, Zhang L, Battaglia L, Cohen KS, Gajewski TF. Cellular and molecular requirements for rejection of B16 melanoma in the setting of regulatory T cell depletion and homeostatic proliferation. *Journal of immunology (Baltimore, Md. : 1950)*. 188(6), 2630–42 (2012).

120. Rosenberg S, Aebersold P. Gene transfer into humans—immunotherapy of patients with advanced melanoma, using tumor-infiltrating lymphocytes modified by retroviral gene transduction. ... *England Journal of ...* 323(9), 570–578 (1990).

121. Torihata H, Ishikawa F, Okada Y, *et al.* Irradiation up-regulates CD80 expression through two different mechanisms in spleen B cells, B lymphoma cells, and dendritic cells. *Immunology*. 112(2), 219–27 (2004).

122. Xun BCQ, Thompson JS, Jennings CD, Brown SA, Widmer MB. Effect of Total Body Irradiation, Busulfan-Cyclophosphamide, or Cyclophosphamide Conditioning on Inflammatory Cytokine Release and Development of Acute and Chronic Graft-Versus-Host Disease in H-2-Incompatible Transplanted SCID Mice. *Blood*. 83(8), 2360–2367 (1994).

123. Sherman ML. Regulation of Tumor Necrosis Factor Gene Expression by Ionizing Radiation in Human Myeloid Leukemia Cells and Peripheral Blood Monocytes. *Journal of Clinical Investigation*. 87(May), 1794–1797 (1991).

124. Zhang Y, Louboutin J, Zhu J, Rivera AJ, Emerson SG. Preterminal host dendritic cells in irradiated mice prime CD8 + T cell – mediated acute graft-versus-host disease. *The Journal of Clinical Investigation*. 109(10), 1335–1344 (2002).

125. Brown S, Konopa J, Zhou D, Thompson J. Expression of TNFalpha by CD3+ and F4/80+ cells following irradiation preconditioning and allogeneic spleen cell transplantation. *Bone marrow transplantation*. 33(4), 359–65 (2004).

126. Atkins MB, Lotze MT, Dutcher JP, *et al.* High-dose recombinant interleukin 2 therapy for patients with metastatic melanoma: analysis of 270 patients treated between 1985 and 1993. *Journal of clinical oncology : official journal of the American Society of Clinical Oncology*. 17(7), 2105–16 (1999).

127. Rosenberg SA, Yang JC, Topalian SL, *et al.* Treatment of 283 Consecutive Patients With Metastatic Melanoma or Renal Cell Cancer Using High-Dose Bolus Interleukin 2. *JAMA*. 271(12), 907–913 (1994).

128. Paolo B, Paciucci A, Holland JF, Glidewell O, Odchimar R. Recombinant Interleukin-2 by Continuous Infusion and Adoptive Transfer of Recombinant Interleukin-2-Activated Cells in Patients with Advanced Cancer. *Journal of Clinical Oncology*. 7(7), 869–878 (1989).

129. Refaeli Y, Van Parijs L, London C a, Tschopp J, Abbas a K. Biochemical mechanisms of IL-2-regulated Fas-mediated T cell apoptosis. *Immunity*. 8(5), 615–23 (1998).

130. Zhang X, Sun S, Hwang I, Tough DF, Sprent J. Potent and selective stimulation of memory-phenotype CD8+ T cells in vivo by IL-15. *Immunity*. 8(5), 591–9 (1998).

131. Yang S, Ji Y, Gattinoni L, *et al.* Modulating the differentiation status of ex vivo-cultured anti-tumor T cells using cytokine cocktails. *Cancer immunology, immunotherapy : CII*. 62(4), 727–36 (2013).

132. Surh CD, Sprent J. Homeostasis of naive and memory T cells. *Immunity*. 29(6), 848–62 (2008).

133. Hinrichs CS, Spolski R, Paulos CM, *et al.* IL-2 and IL-21 confer opposing differentiation programs to CD8+ T cells for adoptive immunotherapy. *Blood*. 111(11), 5326–33 (2008).

134. Zeng R, Spolski R, Finkelstein SE, *et al.* Synergy of IL-21 and IL-15 in regulating CD8+ T cell expansion and function. *The Journal of experimental medicine*. 201(1), 139–48 (2005).

135. Deguine J, Breart B, Lemaître F, Di Santo JP, Bousso P. Intravital Imaging Reveals Distinct Dynamics for Natural Killer and CD8(+) T Cells during Tumor Regression. *Immunity*. , 1–13 (2010).

136. Fisher DT, Chen Q, Appenheimer MM, *et al.* Hurdles to lymphocyte trafficking in the tumor microenvironment: implications for effective immunotherapy. *Immunological investigations*. 35(3-4), 251–77 (2006).

137. Peng W, Liu C, Xu C, *et al.* PD-1 Blockade Enhances T-cell Migration to Tumors by Elevating IFN-γ Inducible Chemokines. *Cancer research*. , 5209–5218 (2012).

138. Kershaw MH, Wang G, Westwood J a, *et al.* Redirecting migration of T cells to chemokine secreted from tumors by genetic modification with CXCR2. *Human gene therapy*. 13(16), 1971–80 (2002).

139. Di Stasi A, De Angelis B, Rooney CM, *et al.* T lymphocytes coexpressing CCR4 and a chimeric antigen receptor targeting CD30 have improved homing and antitumor activity in a Hodgkin tumor model. *Blood*. 113(25), 6392–402 (2009).

140. Singh H, Figliola MJ, Dawson MJ, *et al.* Reprogramming CD19-specific T cells with IL-21 signaling can improve adoptive immunotherapy of B-lineage malignancies. *Cancer research*. 71(10), 3516–3527 (2011).

141. Kaka A, Shaffer D. Genetic Modification of T Cells with IL-21 Enhances Antigen Presentation and Generation of Central Memory Tumor-Specific Cytotoxic T Lymphocytes. *Journal of …*. 32(7), 726–736 (2009).

142. Markley JC, Sadelain M. IL-7 and IL-21 are superior to IL-2 and IL-15 in promoting human T cell-mediated rejection of systemic lymphoma in immunodeficient mice. *Blood*. 115(17), 3508–19 (2010).

143. Dugast A-S, Haudebourg T, Coulon F, *et al.* Myeloid-derived suppressor cells accumulate in kidney allograft tolerance and specifically suppress effector T cell expansion. *Journal of Immunology*. 180(12), 7898–906 (2008).

2 Modulation of MHC Binding By Lateral Association of TCR and Coreceptor[1]

2.1 Introduction

T cells face the extraordinary challenge of finding as few as 1-10 cognate peptides presented in the context of Major Histocompatibility Complex (MHC) (1, 2), masked by thousands of irrelevant but structurally similar peptide/MHC on the opposing membrane. In addition, they must respond to complex environmental stimuli which heighten or dampen the response. As a result, T cell regulate the lateral organization of surface receptors to achieve optimal ligand recognition and activate downstream signaling cascades after binding (3, 4).

Antigen recognition by naïve T cells induces lateral reorganization of membrane proteins on several length scales (5). The co-receptor CD8, which binds an invariant region of the polymorphic MHC (6, 7), mediates the association of T Cell Receptor (TCR) with src-family tyrosine kinases to initiate downstream signaling (8). Robust activation subsequently induces the formation of TCR and adhesion structures, including "bulls-eye" shaped immune synapses (5, 9) and TCR microclusters 100's of nm in diameter (10), which function to generate, sustain and terminate TCR signals (11, 12).

TCR clusters can also be observed days after the initial antigen recognition event, long after the antigen has been cleared (13, 14). In activated T cells, TCR clustering has been reported to lead

[1] This chapter is reproduced in part from "Perica, K., Bieler, J. G., Edidin, M. & Schneck, J. Modulation of MHC binding by lateral association of TCR and coreceptor. *Biophysical journal* **103,** 1890–8 (2012)" with permission from the publisher.

to enhanced binding of soluble peptide-MHC (15). These studies stand in contrast with observations that activated T cells may also lose the ability to bind cognate soluble MHC (16–20). Changes in the CD8 coreceptor (20) have been implicated in loss of binding, but the precise signals regulating binding behavior are poorly understood. Furthermore, the contradiction between observations of enhanced binding and complete loss of binding after activation has not been explained.

Here, we resolve this contradiction and show that changes in nanoscale colocalization of TCR and CD8 determine changes in binding after antigen stimulation. Primary stimulation with a high dose but not low dose of antigen leads to a transient spatial segregation of TCR and CD8. This spatial segregation can impair CD8-dependent MHC binding antigen depending on antigen dose during primary stimulation. Thus, despite having identical TCR, activated T cells can have different MHC binding properties due to changes in membrane organization of TCR and CD8.

2.2 Materials and Methods

Mice and reagents:

2C TCR $Rag^{-/-}$ transgenic mice were maintained as heterozygotes by breeding on a C57/BL6 background. PMEL TCR/$Thy1^{a}$ Rag-/- transgenic mice were a gift from Nicholas Restifo (National Institutes of Health, Bethesda, MD) and maintained as homozygotes. Balb/C mice were purchased from Jackson Laboratories (Bar Harbor, ME). All mice were maintained according to Johns Hopkins University's Institutional Review Board. Peptides SIY (SIYRYYGL), SIIN (SIINFEKL), QL9 (QLSPFPFDL), mCMV (YPHFMPTNL), GP100 (KVPRNQDWL) and ASN (ASNENMETH) were purchased from Genscript (Piscataway, NJ). Fluorescently labeled monoclonal antibodies were purchased from BioLegend (San Diego, CA). MHC monomers were obtained from NIH Tetramer Facility (Bethesda, MD).

Cells:

Cells used were obtained from homogenized mouse spleens after depletion of RBC by hypotonic lysis. For Mixed Lymphocyte Reaction, $10x10^6$/ml 2C splenocytes were activated by co-culture with $18x10^6$/ml irradiated Balb/C splenocytes as allogeneic stimulator cells for 4-7 days in complete RPMI media supplemented with T cell factor, a cytokine cocktail harvested from human plasma (21). For peptide activation, $10x10^6$/ml 2C splenocytes were activated by incubation with cognate peptide at the indicated concentration in complete RPMI plus T cell factor.

Preparation of MHC-Ig Dimers

Soluble MHC-Ig dimers, K^b-Ig and L^d-Ig, were labeled fluorescently and loaded with peptide as described previously(22). Unless otherwise indicated, K^b-SIY and L^d-QL9 refer to soluble MHC-Ig dimer reagent of the corresponding allele loaded with the indicated peptide. Labeling with Alexa-488 or Alexa-657 succimidyl ester (Molecular Probes, Eugene, OR) was performed at pH 7.4 and labeled protein was purified by dialysis with a 50 kDa filter. Protein concentration was determined after labeling by size exclusion High Performance Liquid Chromatography. The efficiency of fluorophore labeling was calculated by measuring absorbance at 280 and fluorophore emission wavelength for the labeled proteins. Typically, approximately 1 dye molecule was attached per MHC-Ig molecule.

Alexa K^b-Ig molecules were loaded with peptide by stripping at alkaline condition (pH 11.5), and then refolded in the presence of 40 fold excess peptide. L^d-Ig molecules were stripped under mildly acidic conditions (pH 6.5) and refolded in the presence of 40 fold molar excess peptide and 2-fold molar excess of human β_2-microglobulin(23).

MHC-Ig Dimer Binding Assay:

MHC-Ig dimer binding assays were performed as previously described(24). Briefly, $CD8^+$ T cells were incubated at 4 °C at a concentration of 10^7cells/ml in FACS wash buffer (PBS + 2% FCS + .05% sodium azide). 15 µl aliquots of cells were mixed with varying concentrations of peptide loaded, fluorescently labeled MHC-Ig dimers for 60-90 min. Without any washing, cells were analyzed by flow cytometry on a BD Biosciences FACSCalibur flow cytometer and analyzed using FlowJo software (Treestar, Ashland, OR). The mean channel fluorescence (MCF) was a measure of the amount of MHC-Ig dimer bound on cells. A non-cognate dimer (K^b-SIIN or L^d-MCMV) was used to account for non-specific binding which was subtracted from the total binding to yield specific MHC-Ig binding. The specific binding was normalized to the plateau of the binding isotherm and plotted against the peptide MHC-Ig dimer concentration.

Confocal Microscopy

For confocal microscopy, T cells were stained with Alexa Fluor 488-labeled H57 anti-mouse TCR antibody and Alex Fluor 647-labeled 53.6.7 anti-mouse CD8α at a 1:100 dilution for 30 minutes on ice. Samples were washed and fixed immediately with 2% paraformaldehyde. Images were acquired on a Zeiss LSM 510 META (Zeiss, Oberkochen, Germany) laser scanning confocal at 100x magnification at the Johns Hopkins School of Medicine Microscopy Facility.

k-Space Image Correlation Spectroscopy

kICS imaging and analysis were performed as described previously(25). T cells were labeled using biotinylated L^d-QL9 monomer (NIH Tetramer Facility, Atlanta, GA) at a concentration of 2µg/2-5 x 10^6 T cells in 100µl PBS for 30 minutes on ice and then washed once with 2 ml PBS, followed by 10nM streptavidin coated Quantum Dots 655 (Life Technologies, Carlsbad CA) in

100 µl PBS incubated for 30 minutes at 4° C. Labeled cells were then washed 2x with 2 ml PBS before imaging.

Cells were imaged using a 3-I Marianas Live Cell Imaging Workstation equipped with dual Cascade II 512 EM cameras at the Johns Hopkins University Integrated Imaging Center. 150-300 images were obtained at 300 ms intervals.

Each image series was corrected for background intensity values using a top-hat transformation, segmented using the watershed transform, and filtered for immobile components. Degree of Aggregation was calculated by dividing mean image intensity by clusters of differentiation (CD), a function of the autocorrelation of fast fourier transformed (FFT) image series in k-space with a custom program written in MATLAB (Mathworks, Natick, MA) (26).

Forster Resonance Energy Transfer

TCR-CD8 FRET was assessed by flow cytometry (17). Approximately 10^6 T cells were incubated with a 1:100 dilution of unlabeled or PE-labeled 53.6.7 anti-mouse CD8α as donor and 500 nM uncoupled or Alexa Fluor 647-coupled L^d-QL9 in FACS buffer at 4° C for 30 minutes. Samples were stained with labeled L^d-QL9 and anti-CD8 antibody (E_{both}), labeled L^d-QL9 but unlabeled CD8 (E_{A647}), unlabeled L^d-QL9 but labeled anti-CD8 (E_{PE}), or both reagants unlabeled (E_{none}). FRET emission was assessed by flow cytometry on a BD FacsCalibur without compensation, with FL-3 channel for Alexa Fluor emission without direct laser excitation. FRET efficiency was calculated in FRET units(17, 27) as follows: FRET unit = $(E3_{both} - E3_{none}) - [(E3_{A647} - E3_{none}) \cdot (E2_{both}/E2_{A647})] - [(E3_{PE} - E3_{None}) \cdot (E1_{both}/E1_{PE})]$

where E1 is the fluorescence detected at 580nm upon excitation at 488 nm, E2 is the fluorescence detected at 670 nm upon excitation at 630 nm, and E3 is the fluorescence detected at 670 nm upon excitation at 488 nm.

Intracellular Cytokine Staining

Four or seven days after primary stimulation, T cell functional activity was assessed by re-challenge with artificial Antigen Presenting Cells (aAPCs). aAPCs were fabricated as described previously(28) by chemical coupling of MHC Dimer and anti-CD28 antibody to Dynal Magnetic Microbeads (Life Technologies, Carlsbad, CA).

200,000 T cells were incubated in complete RPMI with the indicated concentration of activator bead for 5 hours in a round bottom 96 well plate in the presence of 0.2 µl GolgiPlug (BD Biosciences, Mountain View, CA). Cells were washed and fixed using a BD Cytofix/Cytoperm kit (BD Biosciences) according to the manufacturer's instructions, then stained with anti-IL-2 Alexa Fluor 647 and anti-IFNγ PE (BioLegend). Cytokine staining was assessed by flow cytometry and frequency of cytokine functional cells was assessed by comparison with an unstimulated control in FlowJo (TreeStar).

2.3 Results

T Cells Stimulated with a High Dose of Peptide Transiently Lose MHC Binding

To evaluate the effects of peptide dose during stimulation on subsequent MHC-Ig binding, splenocytes from a 2C T Cell Receptor transgenic mouse (specific for peptide SIY presented in the context of MHC allele K^b) were activated with increasing amounts of the cognate peptide. Overall T cell expansion was equivalent and robust (approximately 10-15 fold) at all antigen doses used. Specific binding was characterized 4 days after activation as the difference between binding of cognate (SIY) and noncognate (SIIN) peptide-loaded K^b-Ig. Samples were not washed after binding which allowed for quantitative assessment of specific binding, as described in

Materials and Methods. As shown in **Figure 2.1a**, T cells stimulated with a high dose (100 uM) of peptide showed no measurable specific binding 4 Days after activation, while cells stimulated with a 6-log fold lower dose of peptide (100 fM) did. By Day 7, both high dose (HD) and low dose (LD) activated cells specifically bound K^b-SIY. Loss of binding is not unique to the 2C system, as PMEL TCR Transgenic T cells, which are specific for the melanoma antigen GP100 presented in D^b-Ig, show a similar loss and recovery when stimulated with a high dose of antigen (**Figure 2.1b**).

Loss of binding is not explained by changes in surface expression of TCR and CD8 co-receptor (**Figure 2.2**). Four days after activation, surface expression as measured by fluorescent antibody staining was similar for TCR (MFI of 539 FU compared to 522 FU for HD and LD cells, respectively), CD8α (455 FU and 600 FU), and CD8β (1071 FU and 1072 FU). Differences in the expression level of CD8α and CD8β, as described previously(29),(30), are prominent seven days after activation when binding has recovered and thus cannot account for loss of binding.

Equilibrium Binding Assays Suggest a Defect in CD8 Coreceptor Colocalization With TCR

To understand the role of TCR and CD8 in high-antigen dose induced loss of binding, we performed equilibrium binding experiments on HD, LD, and Mixed Lymphocyte Reaction (MLR, stimulated by allogeneic splenocytes) activated cells. On Day 4, HD cells bound lower amounts of K^b-SIY at all concentrations examined (**Figure 2.3a**). At high concentrations of K^b-SIY (250 nM), high peptide dose activated cells displayed six-fold lower binding than low dose activated cells.

Some TCR require CD8 engagement to specifically bind cognate MHC-peptide, while others are CD8-independent, and bind to MHC even in absence of CD8 or after CD8 blockade(31–33). The

2C TCR transgenic system has several cognate ligands, and the alloantigen L^d-QL9 peptide/MHC has been characterized as a CD8-independent binding partner(31, 32). HD cells, which could not specifically bind K^b-SIY at any concentration, bound 1 μM L^d-QL9 as well as LD or MLR stimulated cells (**Figure 2.3b**). However, K_d for binding L^d-QL9 to HD cells was 423 μM compared to 117 μM for LD cells. Day 7 recovery from loss of binding was seen with both K^b-SIY and L^d-QL9 ligands with complete recovery of K_d and a decreased off-rate for L^d-QL9 (**Figure 2.4**).

To confirm differential CD8 sensitivity, we incubated 500 nM of MHC-Ig either alone or with 20-fold molar excess of the CD8-blocking antibody CT-CD8a. As described previously (31, 32), CD8 blocking antibody CT-CD8a was able to completely inhibit all specific binding of Kb-SIY MHC-Ig for all three cell samples (**Figure 2.3c**). The relative CD8-independence of 2C for L^d-QL9 was confirmed by the insensitivity of L^d-QL9 binding to Day 4 stimulated cells in the presence of CD8 blocking antibody (**Figure 2.3d**).

Spatial Segregation of CD8 and TCR

The ability of high dose activated cells to bind the CD8-independent L^d-QL9 but not CD8-dependent K^b-SIY implicates the CD8 coreceptor in loss of binding. Since CD8-dependent binding was impaired but CD8 expression was unchanged, we examined the relative spatial organization of TCR and CD8. We hypothesized that four days after high dose peptide activation, TCR and CD8 may not be colocalized on the T cell membrane, and so CD8 could not assist in MHC binding.

The clustering of TCR and CD8 was examined with k-Space Image Correlation Spectroscopy (kICS), an image analysis technique that extends the ICS approach to quantum dot labels(26).

kICS allows the measurement of Degree of Aggregation (DA), with large DAs indicating that the labeled receptor is highly clustered at scales of 100's of nms (**Figure 2.5a**). DAs were normalized to naive cells and reported as fold-change from naive. HD cells had less clustered TCR than naive (0.57-fold naive). In contrast, LD (1.67) and MLR cells (2.20) had more clustered TCR (**Figure 2.5b**). For CD8, HD (2.19), LD (3.24), and MLR (2.90) cells were all more clustered than naive cells. This finding suggests that TCR and CD8 may be organized in different membrane subdomains on the surface of high dose activated T cells. By Day 7, both CD8 and TCR were more clustered on all activated samples compared to naive, such that the degree of TCR clustering correlated with K^b binding (Supplementary Figure 2).

Confocal microscopy was used to measure differences in CD8 and TCR colocalization. HD cells showed a significantly lower degree of colocalization (Pearson's Correlation coefficient 0.45 ± 0.02) between TCR and CD8 than LD cells (0.61 ± 0.03) on Day 4 (**Figure 2.6a**). On Day 7, when the binding defect had recovered, both HD and LD cells exhibit large Pearson's Correlation coefficients of 0.70 ± 0.02 and 0.74 ± 0.02, respectively.

CD8 and TCR Are Not Colocalized at the Nanoscale on High Dose Activated Cells

Since CD8 must be located within 10's of nms to TCR to assist in MHC binding, we assessed the colocalization of TCR and CD8 at the nanoscale by Forster Resonance Energy Transfer (FRET). FRET is the non-radiative transfer of energy from a directly excited donor fluorophore to an acceptor fluorophore; this only occurs when they are within 10 nm of each other, hence FRET is a measure of nanoscale colocalization(34). HD and LD cells were labeled with fluorescently-tagged L^d-QL9 and anti-CD8 antibody. FRET was observed as a relative increase in the fluorescence intensity of the acceptor fluorophore when MHC-Ig and CD8 were fluorescently labeled with the appropriate FRET pair. Approximately 97% of naive CD8 T cells showed

nanoscale colocalization of CD8 and TCR by FRET (**Figure 2.6a**). Similarly, a majority of LD and MLR activated cells displayed a FRET shift. However, only approximately 30% of HD cells displayed a FRET shift (**Figure 2.6a**), consistent with reduced CD8-TCR colocalization. The amount of nanoscale colocalization can be quantified in FRET units as a normalized shift in acceptor intensity(27). As shown in **Figure 2.6b**, HD cells have a decreased FRET intensity of 16 FRET units compared to LD (62 units) or naive (43 units) cells. Reduced FRET was not due to a decrease in CD8 or MHC-Ig binding in HD cells (**Figure 2.7**), since coreceptor expression is unchanged and CD8-indpendent L^d-QL9 does not display loss of binding.

FRET intensity recovered for HD cells from Day 4 to Day 7 (**Figure 2.6c**), while FRET was consistently high when observed on LD and MLR cells throughout. FRET thus uniquely reveals the loss of nanoscale localization between TCR and CD8 on high dose activated cells.

Production of Cytokine IFNy Correlates With CD8-Dependent Binding

The functional consequences of changes in binding of cognate ligand were assayed by intracellular cytokine staining assay, which measures T cell production of cytokine in response to antigen. Four or seven days after activation, T cells were re-challenged with an artificial antigen presenting cell (aAPC) (28), a bead-based T cell activation platform presenting MHC-Ig and a co-stimulatory signal (**Figure 2.8**).

As seen in **Figure 2.8a**, T cells were capable of producing the cytokine IFNγ when stimulated with PMA and ionomycin, stimuli that bypass the TCR. Thus, any functional defects observed when T cells are stimulated via their TCR are not due to downstream defects in T cell signaling, but to signals received by the TCR itself.

When T cells were re-stimulated with K^b-SIY aAPC four days after stimulation, less than 20% of HD cells produced IFNγ at all aAPC-cell ratios examined. In comparison, up to 55% of LD cells were responsive (**Figure 2.8b**). However, both cell populations were able to produce high levels of IFNγ in response to a L^d-QL9 presenting aAPC (**Figure 2.8c**). Functional response of HD cells to L^d-QL9 but not K^b-SIY correlates with observed binding on Day 4. Again, similarly to binding, HD cells recovered functionally by Day 7, when up to 42% of cells produced the cytokine in response to a K^b-SIY based aAPC (**Figure 2.8d**).

2.4 Discussion

In this study, we show that T cells dynamically regulate the organization of their receptor for antigen in response to activation signals, with consequences for MHC binding and thus functional response. T cells activated by a high dose of antigen bound CD8-independent but not CD8-dependent MHC-Ig. This difference was associated with a loss of colocalization at the nanoscale as measured by FRET between TCR and CD8. Decreased FRET in HD cells may be due to either a true loss of colocalization independent of MHC-Ig binding, or to a loss in the ability of MHC-Ig to induce TCR/CD8 clustering (35, 36). We observe no differences in the ability of MHC to independently bind TCR or CD8. Therefore, decreased FRET represents either a loss of colocalization in the resting state or an inability for CD8 and TCR to colocalize once they bind MHC. As a result, T cells are unable to produce cytokines in response to antigen challenge by CD8-sensitive antigen. The effect is transient, with colocalization, binding, and function recovering over time.

Thus, despite the presence of identical receptors, activated T cells derived from the same precursor may have different surface receptor organization and different antigen binding properties based on their history of antigen exposure. FRET and co-immunoprecipitation studies have shown TCR and CD8 are(37–39) and are not(27, 36, 40) colocalized at the nanoscale on resting T cells. We suggest that differences in antigen exposure and timing may be the source of conflicting results. Similarly, antigen exposure is likely responsible for conflicting reports of enhanced binding(15) or loss of binding(16–20) after activation.

The mechanism underlying dynamic T cell membrane organization remains unclear. TCR and CD8 (41, 42) are known to preferentially segregate in lipid rafts during stimulation and interact

with the galectin-glycan lattice(43). Recently, Demotte et al.(16) demonstrated that exogenous galectin treatment could reverse a tumor-induced defect in TCR-CD8 colocalization and binding, adding to evidence that interaction of galectins with N-linked glycosylation sites on TCR controls sensitivity of T cell responses(44). Long-term control of membrane organization could thus involve changes in lipid rafts, surface receptor glycosylation, and both endogenous and exogenous secretion of receptor-binding galectins. However, great care needs to be taken to identify mechanisms that operate seconds and minutes after T cell activation, as well as those mechanisms that control more persistent membrane changes.

Persistent TCR clustering and TCR-CD8 colocalization coexist with and may be mechanistically related to more transient changes that occur upon exposure to antigen. TCR on a resting naive T cell are organized in small nanoclusters(14, 45) which concatenate(10) when the T cell encounters antigen. These signaling microclusters are thought to represent early signaling platforms upon which downstream kinases and scaffolding proteins assemble and activate(46). With sustained, robust stimulation, signaling microclusters migrate to the center of the micro-scale immune synapse, where they are degraded(11, 12). Many days after stimulation, T cells' membranes retain memory of the previous activation event, with more highly clustered TCR than naive cells (13, 15, 25) and different levels of CD8 colocalization depending on the strength of initial stimulation. These membrane structures can potentially affect both binding of antigen and the activation of downstream signaling proteins.

It is well established that in chronic viral infections and cancer sustained exposure to low-dose antigen induces dysfunctional T cell responses(47, 48). We demonstrate that an acute exposure to high dose antigen *in vitro* can induce transient functional and binding defects, although this finding must be confirmed at physiological antigen doses *in vivo*. Long term antigen dose driven

responses also include binding-independent functional defects (29),(30) and a tendency toward effector compared to memory phenotypes as a result of acute high dose stimulation(49). We thus suggest that antigen-induced loss of binding is an intrinsic T cell response to high dose antigen stimulation, and need not be associated with the tumor microenvironment(17). Membrane organization induced loss of binding may serve as a regulatory mechanism to avoid excessive inflammation and immunopathology in response to aggressive infection.

2.5 Figures

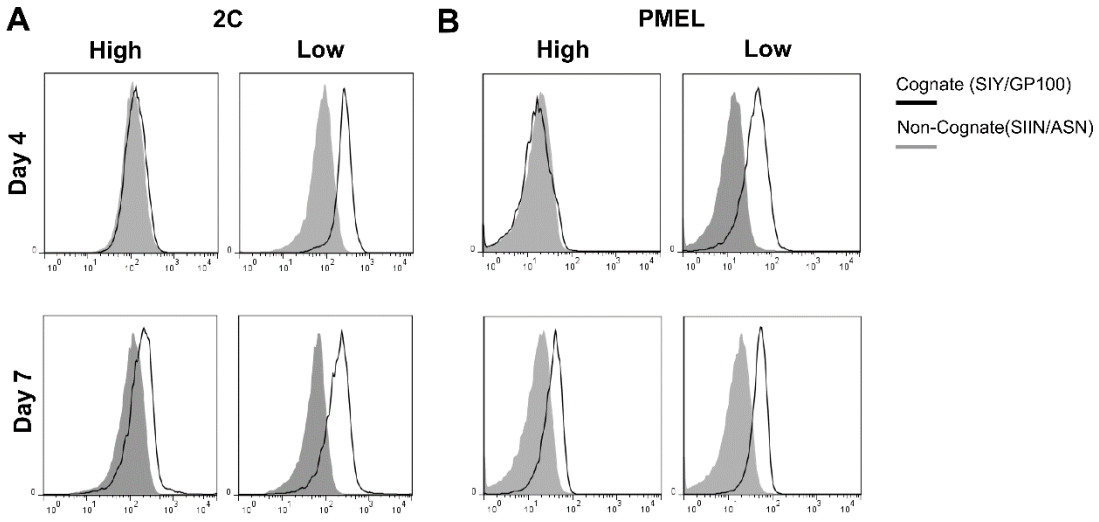

Figure 2-1. Transient Loss of Binding Induced By Stimulation With High Dose Antigen

(A) Specific Binding. Splenocytes from TCR transgenic mice bearing the 2C receptor were activated with high (100 ug/ml) or low (100 fg/ml) doses of cognate peptide. At Day 4, viability was greater than 70% for high and 90% for low dose stimulated cells, both of which had shown robust proliferation by Day 7 (10-15 fold). Specific binding was characterized at the indicated timepoints by comparing cognate (SIY loaded Kb, no fill) and noncognate (SIIN loaded Kb, gray fill) fluorescence intensity of 500 nM labeled MHC-Ig. While low dose stimulated T cells show a classic difference between cognate and non-cognate binding, high dose activated cells (top left) show no such difference on Day 4. Both high and low dose activated cells show specific binding on Day 7 (bottom row).
(B) Loss of binding is also observed for high but not low dose activated PMEL TCR transgenic splenocytes (top left). PMEL splenocytes were activated with 10 ug/ml and 10 pg/ml for high and low doses, respectively, and stained with 500 nM of Db-gp100 (cognate) and Db-ASN (noncognate) MHC-Ig dimer.

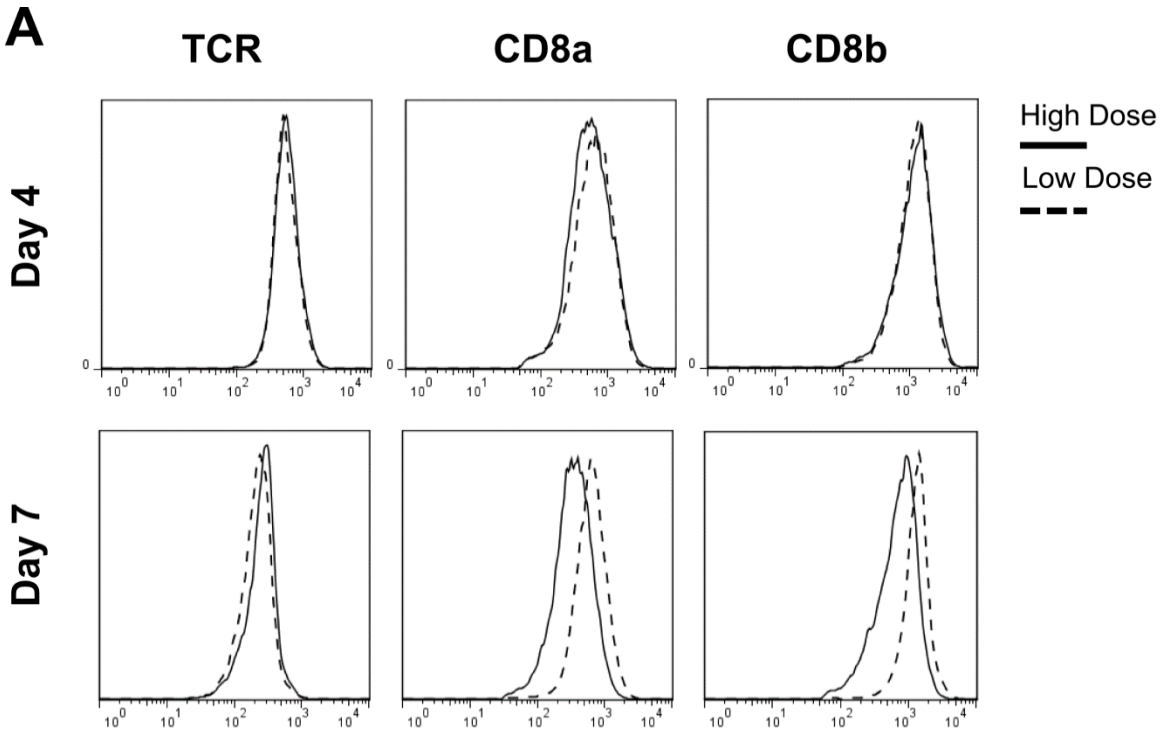

Figure 2-2 Equivalent surface expression of MHC binding receptors on high and low dose activated cells measured with fluorescently labeled antibodies

Four or seven days after activation, T cells were stained with anti-TCR (Clone H57), anti-CD8α, or anti-CD8β antibody. High dose (HD - solid line) and low dose (LD-dashed lined) activated T cells had equivalent receptor expression on Day 4, when loss of binding was observed. On Day 7, when loss of binding was not present, LD cells had higher expression of CD8α and CD8β but not TCR.

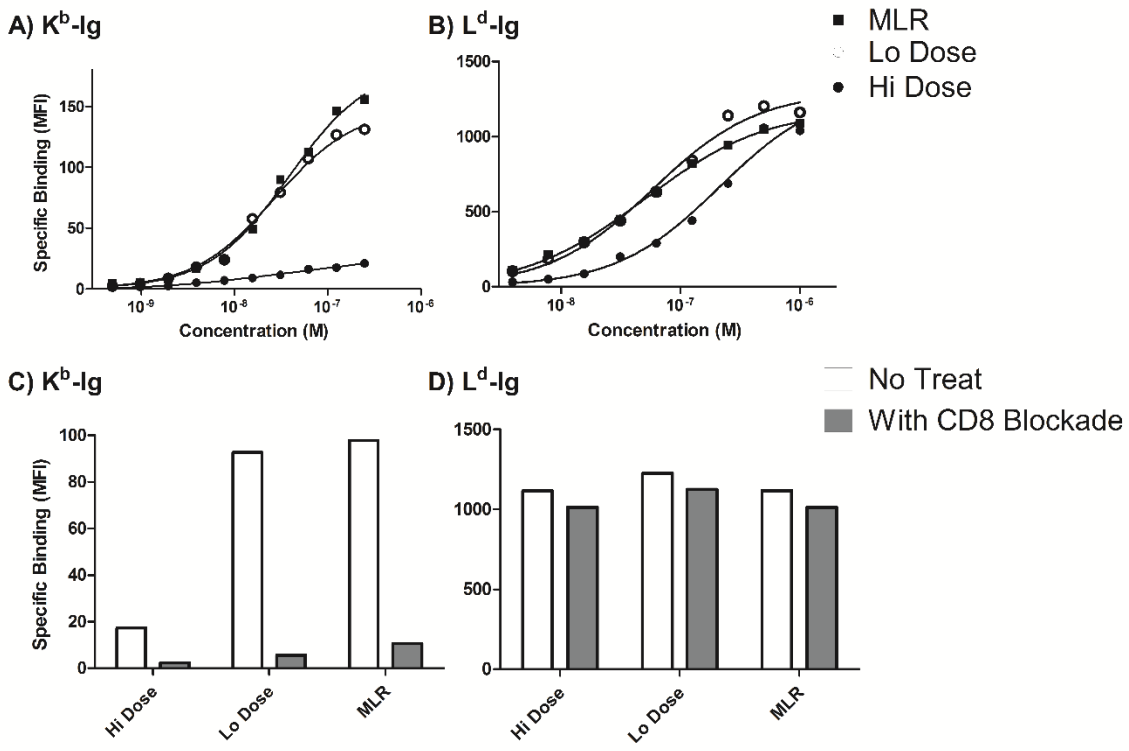

Figure 2-3 Loss of Binding is Ligand Sensitive

(A) K^b equilibrium binding is decreased on high dose activated cells. Mixed Lymphocyte Reaction (MLR, black square), high dose (HD, black circle), and low dose (LD, white circle) activated splenocytes were bound to increasing doses of cognate Kb-SIY and noncognate Kb-SIIN. Mean MFI was measured without washing and specific binding characterized as the difference between cognate and noncognate binding.
(B) L^d equilibrium binding is equivalent for HD, LD, and MLR activated cells at a high concentration of L^d (500 nM), but HD cells had four-fold higher K_d. Binding was calculated as difference between cognate (L^d–QL9) and noncognate (L^d–mCMV) fluorescense.
(C) Relative CD8 dependence of K^b and (D) independence of L^d binding to 2C T cells. Specific binding of 500 nM MHC-Ig was calculated as above with (filled) and without (white) simultaneous addition of CD8-blocking antibody CT-CD8a.

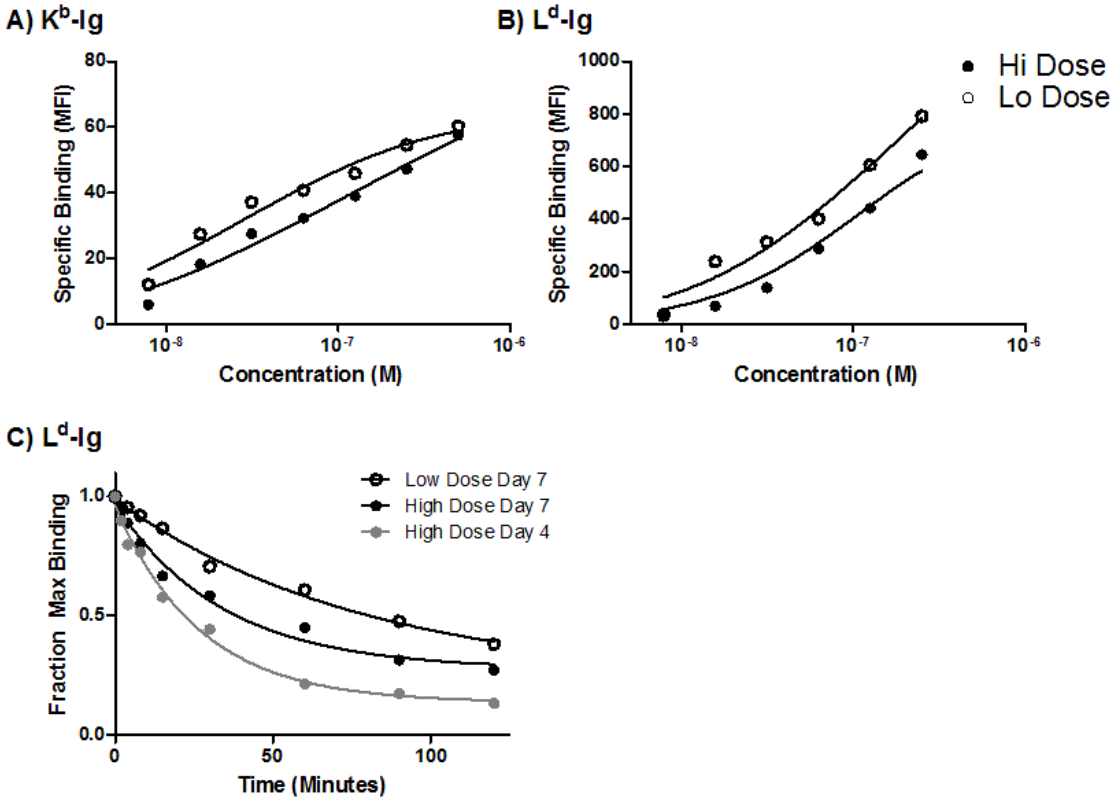

Figure 2-4. Kb Equilibrium binding recovers on Day 7

(A) Binding was measured by titration of Kb-Ig seven days after activation for HD (black circle) and LD (white circle) cells. Specific binding was defined as the difference in mean fluorescence intensity between cognate and noncognate binding. As expected, Kb binding recovers in HD samples by Day 7, with similar maximal binding when incubated with high amounts (500 nM) of MHC-Ig (57.6 MFI for HD compared to 60.3 MFI for LD).
(B) Ld equilibrium binding with cognate (Ld –QL9) and noncognate (Ld –mCMV) MHC-Ig on Day 7. As on Day 4, Ld is similar on Day 7 for HD and LD splenocytes on Day 7.
(C) Dimer binding off-rate. Four or seven days after activation, 2*106 HD (squares) or LD (circle) activated cells were incubated with 250 nM cognate or noncognate Ld and allowed to reach equilibrium. At time 0, a 30-fold molar excess of TCR blocking 1B2 antibody was added to prevent Dimer rebinding. Fluorescence intensity was measured at indicated timepoints and specific binding was measured as cognate MFI minus noncognate MFI. Results are presented as fraction of maximal binding (binding at time 0), and data were fit to a one phase exponential decay curve.
On Day 4, high dose activated cells had a rapid Dimer off-rate of 6.21 *10-4 sec-1, partially explaining their high disassociation constant. By Day 7, HD activated cells had partially recovered, with a slower decay constant of 4.90 *10-4 sec-1 compared to 2.08 *10-4 sec-1 for LD activated cells.

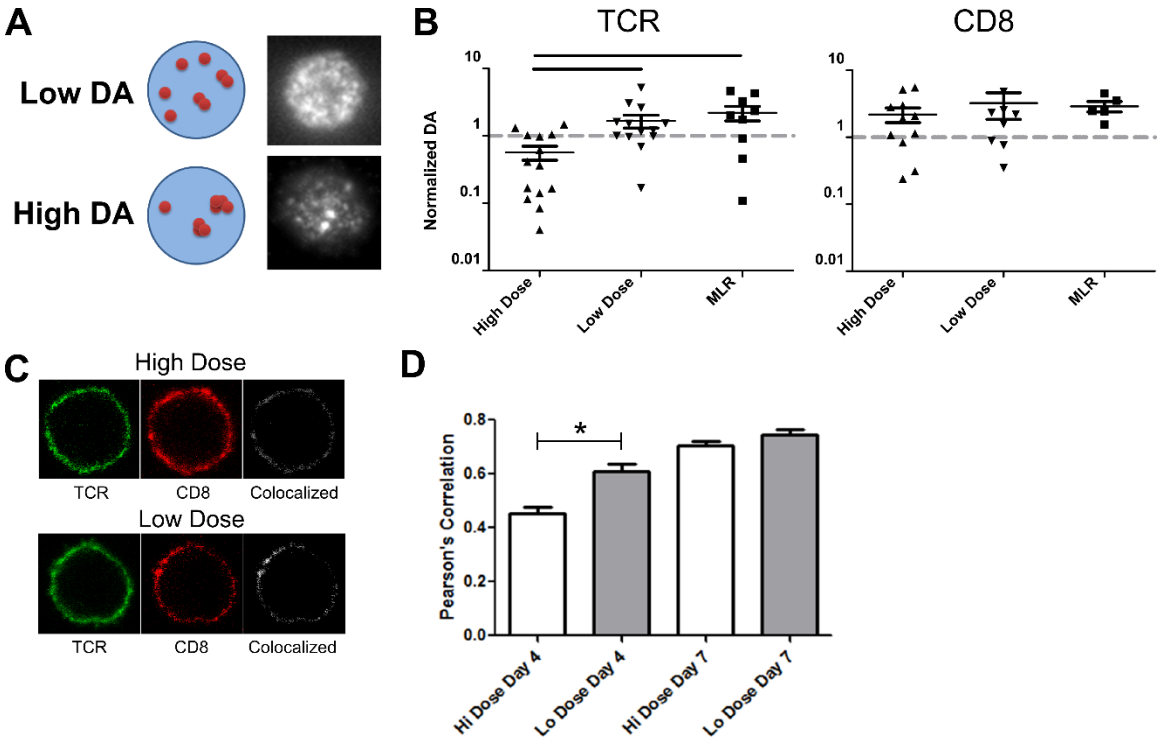

Figure 2-5. TCR and CD8 Colocalization and Clustering Characteristics at Optical Scales

(A) k-Space Image Correlation Spectroscopy (kICS). On left, schematic of receptor clusters illustrates Degree of Aggregation (DA) is calculated as mean image intensity divided by discrete receptor clusters measured on the cell. For a given cell, a high DA indicates that the fluorescently labeled receptors are aggregated into a small number of discrete clusters, and a low DA indicates that receptors are diffusely distributed across the cell. On top right, representative epifluorescent images used for kICS analysis show an HD stimulated cell with 0.98 DA, compared to 2.60 DA for the LD stimulated cell on bottom right.

(B) TCR but not CD8 are comparatively unclustered on HD cells. Four days after activation, HD, LD, and MLR activated splenocytes were assessed by kICS. DA for individual cells are represented in the dot plot, with median DA for the sample shown as a black bar. DA were normalized to the median DA for a sample of naive T cells, shown as a light gray dashed line. DA for TCR on HD cells was lower than naive and significantly different ($p<0.05$, black bars) from LD and MLR cells.

(C) Representative confocal images of HD (top) and LD (bottom) activated cell for TCR (green), CD8 (red), and colocalized TCR/CD8 (white).

(D) TCR/CD8 colocalization correlates with loss and recovery of binding. Degree of colocalization was calculated by Pearson's Correlation Coefficient on at least 15 cells four and seven days after activation. HD cells had significantly less colocalization ($p<0.05$, star) on Day 4 compared to LD cells. In contrast, both samples have relatively high colocalization on Day 7 when both can bind.

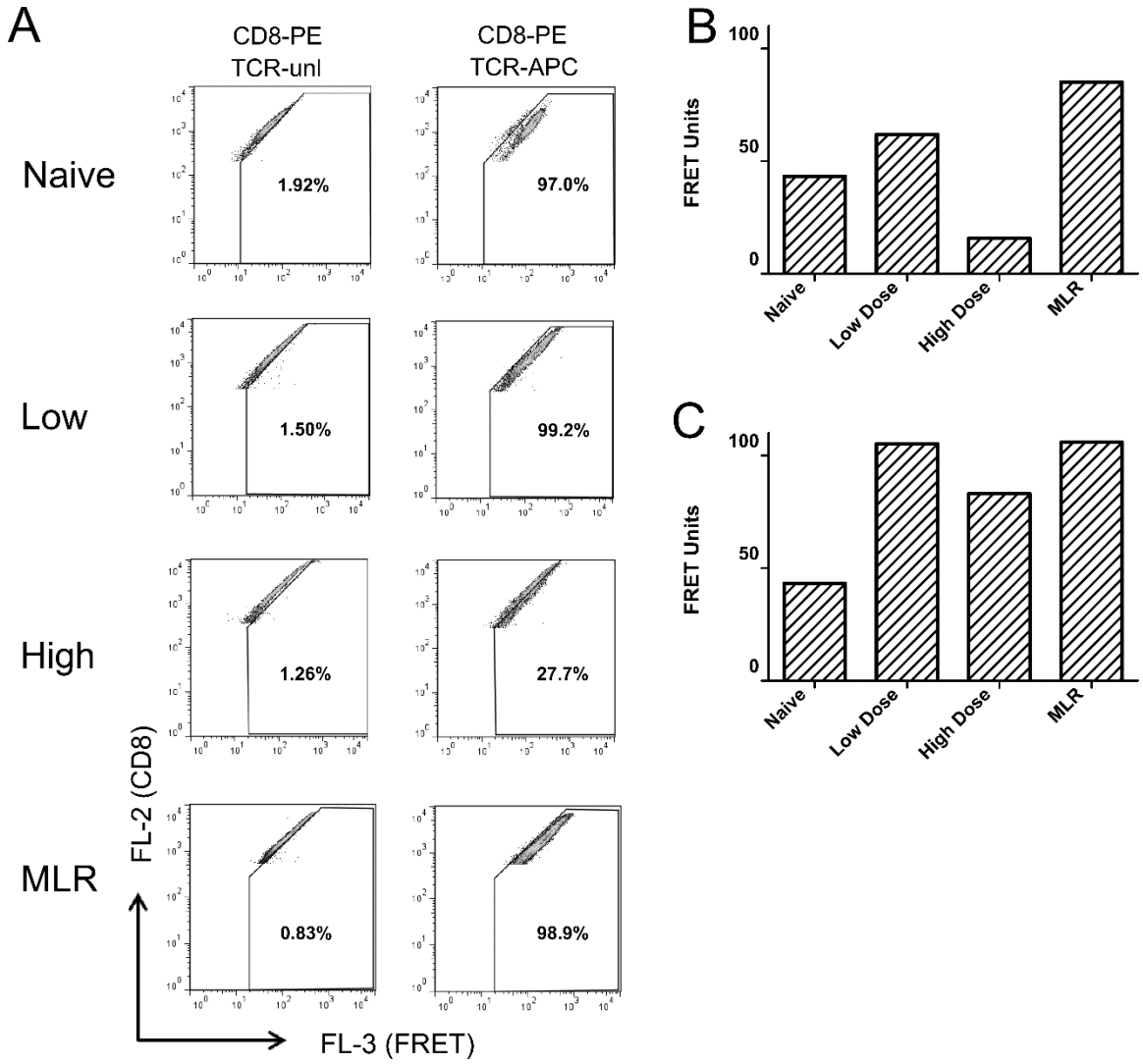

Figure 2-6 Reduced Nanoscale Colocalization of TCR and CD8 on High Dose Activated Cells Revealed by FRET.

(A) Four days after activation, naive, HD, LD and MLR activated T cells were bound to 500 nM L^d-QL9 Dimer and anti-CD8 antibody at 4°C. Background fluorescence was assessed with unlabeled acceptor (MHC-Ig) and PE-labeled donor (CD8) (left column). FRET manifests as a shift in fluorescence intensity in the FRET Channel (acceptor emission with no acceptor laser excitation) when both MHC-Ig and CD8 are labeled with fluorophore (right column). HD cells show the smallest shift as represented by the percentage of cells found in FRET gate.
(B) FRET units are a normalized measure of FRET shift (as described in Materials and Methods) for all samples. (B) FRET shift four days after activation. High dose activated cells show the lowest degree of FRET shift compared to naive, LD, or MLR. (C) Day 7 FRET units show recovery in high dose nanoscale colocalization which correlates with recovery in K^b binding.

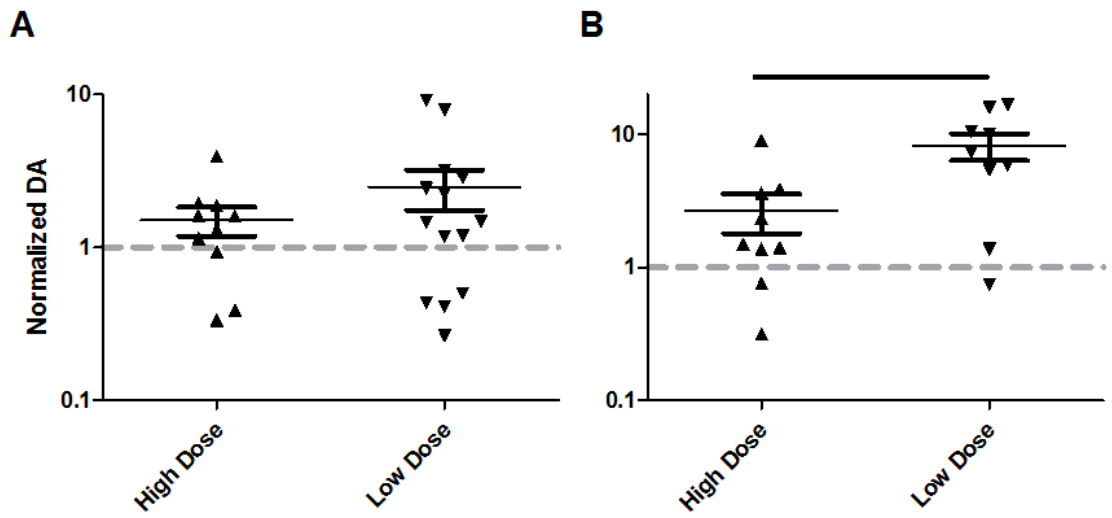

Figure 2-7. Day 7 DA Is Higher On All Samples Than on Naive Cells.

Seven days after activation, HD and LD activated splenocytes were labeled with (A) cognate monomeric MHC-biotin or (B) anti-CD8 fab, then streptavidin-quantum dots. Membranes were imaged as an epifluorescent time series and DA was assessed by kICS. At least 9 cells were collected for each sample. DA for individual cells are represented in the dot plot, with median DA for the sample shown as a black bar. DAs were normalized to the median DA for a sample of naive T cells, shown as a light gray dashed line. CD8 DA was significantly higher ($p<0.05$, black bar) on LD compared to HD cells, but clustering of TCR and CD8 on both LD and HD cells was enhanced on Day 7 compared to naive cells. This is consistent with a recovery in binding associated with changes in TCR spatial organization.

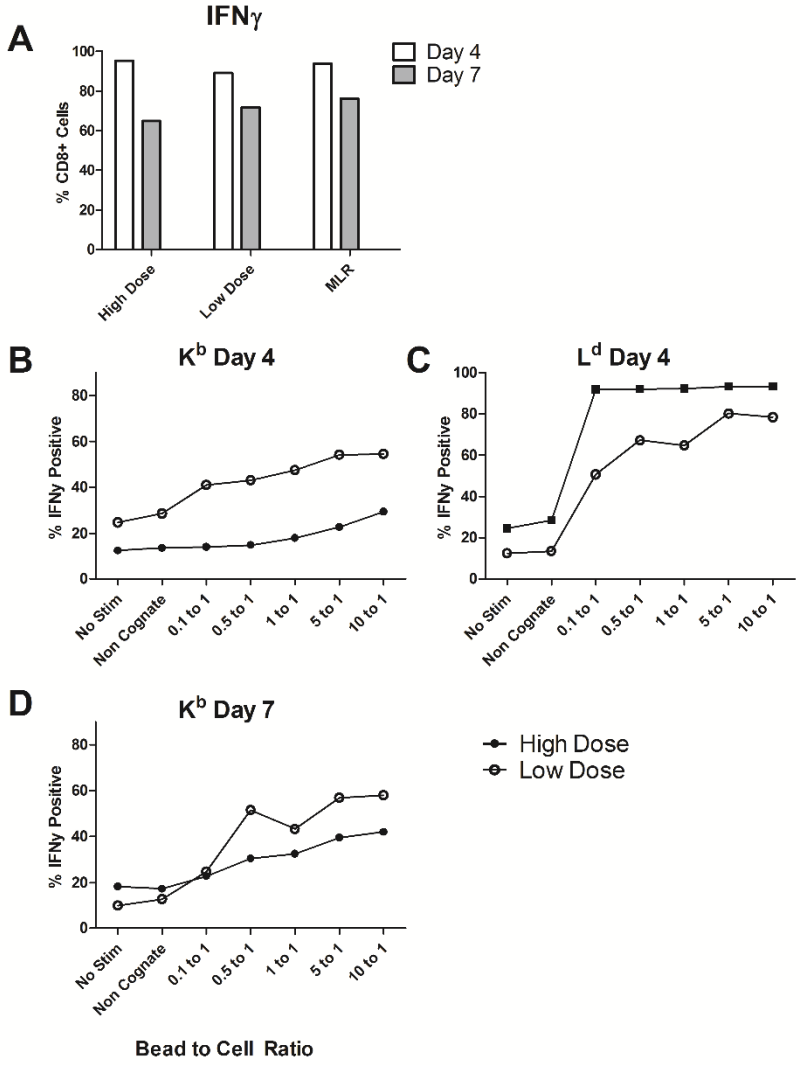

Figure 2-8. Functional Responses Correlate with Binding Defects.

(A) HD or LD cells are capable of producing the cytokine IFNγ when re-stimulated on Day 4 (white) or Day 7 (shaded) after activation with PMA and ionomycin, which activate T cells downstream of the TCR. IFNγ production was measured by Intracellular Cytokine Staining (ICS) and quantified as percentage of cells producing cytokine.
(B) T cells were re-stimulated with beads bearing L^d-QL9 or K^b-SIY dimer and CD28 costimulatory antibody on Days 4 or 7 at the indicated T cell to bead ratios (x axis). No stimulation and noncognate beads (at a 10 bead to 1 cell ratio) were used as negative control. With Day 4 K^b stimulation, LD cells showed dose-dependent IFNγ production that was significantly lower in high dose cells (top left). However, both HD and LD cells stimulated with L^d containing beads on Day 4 (bottom left) were able to produce cytokine. The difference between HD and LD cells had partially recovered on Day 7 (top right).

2.6 References

1. Irvine, D.J., M. a Purbhoo, M. Krogsgaard, and M.M. Davis. 2002. Direct observation of ligand recognition by T cells. Nature. 419: 845–9.

2. Sykulev, Y., M. Joo, I. Vturina, T.J. Tsomides, and H.N. Eisen. 1996. Evidence that a single peptide-MHC complex on a target cell can elicit a cytolytic T cell response. Immunity. 4: 565.

3. Groves, J.T., and J. Kuriyan. 2010. Molecular mechanisms in signal transduction at the membrane. Nature Structural & Molecular Biology. 17: 659–65.

4. Palmer, E., and D. Naeher. 2009. Affinity threshold for thymic selection through a T-cell receptor-co-receptor zipper. Nature reviews. Immunology. 9: 207–13.

5. Dustin, M.L. 2008. T-cell activation through immunological synapses and kinapses. Immunol. Rev. 221: 77–89.

6. Dutoit, V., P. Guillaume, M. Ayyoub, C.S. Hesdorffer, I.F. Luescher, et al. 2003. Decreased binding of peptides-MHC class I (pMHC) multimeric complexes to CD8 affects their binding avidity for the TCR but does not significantly impact on pMHC/TCR dissociation rate. The Journal of Immunology. 170: 5110.

7. Wooldridge, L., H.A. Van Den Berg, M. Glick, E. Gostick, B. Laugel, et al. 2005. Interaction between the CD8 Coreceptor and Major Histocompatibility Complex Class I Stabilizes T Cell Receptor-Antigen Complexes at the Cell Surface. J Biol Chem. 280: 27491–27501.

8. Davis, S.J., and P.A. van der Merwe. 2010. Lck and the nature of the T-cell receptor trigger. Trends in Immunology. 32: 1–5.

9. Monks, C.R.F., B.A. Freiberg, H. Kupfer, N. Sciaky, and A. Kupfer. 1998. Three-dimensional segregation of supramolecular activation clusters in T cells. Nature. 395: 82–86.

10. Lillemeier, B.F., M. a Mörtelmaier, M.B. Forstner, J.B. Huppa, J.T. Groves, et al. 2010. TCR and Lat are expressed on separate protein islands on T cell membranes and concatenate during activation. Nature Immunology. 11: 90–6.

11. Varma, R., G. Campi, T. Yokosuka, T. Saito, and M.L. Dustin. 2006. T cell receptor-proximal signals are sustained in peripheral microclusters and terminated in the central supramolecular activation cluster. Immunity. 25: 117–127.

12. Lee, K.-H., A.R. Dinner, C. Tu, G. Campi, S. Raychaudhuri, et al. 2003. The immunological synapse balances T cell receptor signaling and degradation. Science. 302: 1218–22.

13. Kumar, R., M. Ferez, M. Swamy, I. Arechaga, M.T. Rejas, et al. 2011. Increased Sensitivity of Antigen-Experienced T Cells through the Enrichment of Oligomeric T Cell Receptor Complexes. Immunity. 35: 375–87.

14. Alarcón, B., M. Swamy, H.M. van Santen, and W.W. a Schamel. 2006. T-cell antigen-receptor stoichiometry: pre-clustering for sensitivity. EMBO reports. 7: 490–5.

15. Fahmy, T.M., J.G. Bieler, M. Edidin, and J.P. Schneck. 2001. Increased TCR avidity after T cell activation: a mechanism for sensing low-density antigen. Immunity. 14: 135–43.

16. Demotte, N., D. Colau, S. Ottaviani, D. Godelaine, A. Van Pel, et al. 2002. A reversible functional defect of CD8+ T lymphocytes involving loss of tetramer labeling. European Journal of Immunology. 32: 1688–1697.

17. Demotte, N., V. Stroobant, P.J. Courtoy, P. Van Der Smissen, D. Colau, et al. 2008. Restoring the association of the T cell receptor with CD8 reverses anergy in human tumor-infiltrating lymphocytes. Immunity. 28: 414–24.

18. Drake III, D.R., R.M. Ream, C.W. Lawrence, and T.J. Braciale. 2005. Transient loss of MHC class I tetramer binding after CD8+ T cell activation reflects altered T cell effector function. The Journal of Immunology. 175: 1507–15.

19. Xiao, Z., M.F. Mescher, and S.C. Jameson. 2007. Detuning CD8 T cells: down-regulation of CD8 expression, tetramer binding, and response during CTL activation. The Journal of experimental medicine. 204: 2667–77.

20. Kao, C., M.A. Daniels, and S.C. Jameson. 2005. Loss of CD8 and TCR binding to Class I MHC ligands following T cell activation. International Immunology. 17: 1607–17.

21. Durai, M., C. Krueger, Z. Ye, L. Cheng, A. Mackensen, et al. 2009. In vivo functional efficacy of tumor-specific T cells expanded using HLA-Ig based artificial antigen presenting cells (aAPC). Cancer immunology, immunotherapy : CII. 58: 209–20.

22. Dal Porto, J., T.E. Johansen, B. Catipović, D.J. Parfiit, D. Tuveson, et al. 1993. A soluble divalent class I major histocompatibility complex molecule inhibits alloreactive T cells at nanomolar concentrations. Proceedings of the National Academy of Sciences of the United States of America. 90: 6671–5.

23. Lebowitz, M.S., S.M. O'Herrin, a R. Hamad, T. Fahmy, D. Marguet, et al. 1999. Soluble, high-affinity dimers of T-cell receptors and class II major histocompatibility complexes: biochemical probes for analysis and modulation of immune responses. Cellular Immunology. 192: 175–84.

24. Fahmy, T.M., J.G. Bieler, and J.P. Schneck. 2002. Probing T cell membrane organization using dimeric MHC-Ig complexes. Journal of Immunological Methods. 268: 93–106.

25. Boyle, S., D.L. Kolin, J.G. Bieler, J.P. Schneck, P.W. Wiseman, et al. 2011. Quantum Dot Fluorescence Characterizes the Nanoscale Organization of T Cell Receptors for Antigen. Biophysical Journal. 101: L57–L59.

26. Kolin, D.L., D. Ronis, and P.W. Wiseman. 2006. k-Space image correlation spectroscopy: a method for accurate transport measurements independent of fluorophore photophysics. Biophysical Journal. 91: 3061–75.

27. Doucey, M.-A., L. Goffin, D. Naeher, O. Michielin, P. Baumgärtner, et al. 2003. CD3 delta establishes a functional link between the T cell receptor and CD8. The Journal of Biological Chemistry. 278: 3257–64.

28. Oelke, M., and J.P. Schneck. 2010. Overview of a HLA-Ig based "Lego-like system" for T cell monitoring, modulation and expansion. Immunologic Research. 47: 248–56.

29. Kroger, C., and M.A. Alexander-Miller. 2007. Cutting edge: CD8+ T cell clones possess the potential to differentiate into both high-and low-avidity effector cells. The Journal of Immunology. 179: 748.

30. Kroger, C.J., and M. a Alexander-Miller. 2007. Dose-dependent modulation of CD8 and functional avidity as a result of peptide encounter. Immunology. 122: 167–78.

31. Holler, P.D., and D.M. Kranz. 2003. Quantitative analysis of the contribution of TCR/pepMHC affinity and CD8 to T cell activation. Immunity. 18: 255–64.

32. Cho, B.K., K.C. Lian, P. Lee, A. Brunmark, C. McKinley, et al. 2001. Differences in antigen recognition and cytolytic activity of CD8(+) and CD8(-) T cells that express the same antigen-specific receptor. Proceedings of the National Academy of Sciences of the United States of America. 98: 1723–7.

33. Sykulev, Y., Y. Vugmeyster, a Brunmark, H.L. Ploegh, and H.N. Eisen. 1998. Peptide antagonism and T cell receptor interactions with peptide-MHC complexes. Immunity. 9: 475–83.

34. Batard, P., J. Szollosi, I. Luescher, J.-C. Cerottini, R. MacDonald, et al. 2002. Use of phycoerythrin and allophycocyanin for fluorescence resonance energy transfer analyzed by flow cytometry: advantages and limitations. Cytometry. 48: 97–105.

35. Lee, P.U.Y., and D.M. Kranz. 2003. Allogeneic and syngeneic class I MHC complexes drive the association of CD8 and TCR on 2C T cells. Molecular immunology. 39: 687–95.

36. Block, M.S., a J. Johnson, Y. Mendez-Fernandez, and L.R. Pease. 2001. Monomeric class I molecules mediate TCR/CD3 epsilon/CD8 interaction on the surface of T cells. Journal of Immunology. 167: 821–6.

37. Arcaro, A., C. Grégoire, T.R. Bakker, L. Baldi, M. Jordan, et al. 2001. CD8beta endows CD8 with efficient coreceptor function by coupling T cell receptor/CD3 to raft-associated CD8/p56(lck) complexes. The Journal of experimental medicine. 194: 1485–95.

38. Osono, E., N. Sato, K. Yokomuro, and M.K. Saizawa. 1997. Changes in arrangement and in conformation of molecular components of peripheral T-cell antigen receptor complex after ligand binding: analyses by co-precipitation profiles. Scandinavian Journal of Immunology. 45: 487–93.

39. Beyers, a D., L.L. Spruyt, and a F. Williams. 1992. Molecular associations between the T-lymphocyte antigen receptor complex and the surface antigens CD2, CD4, or CD8 and CD5. Proceedings of the National Academy of Sciences of the United States of America. 89: 2945–9.

40. Yachi, P.P., J. Ampudia, N.R.J. Gascoigne, and T. Zal. 2005. Nonstimulatory peptides contribute to antigen-induced CD8-T cell receptor interaction at the immunological synapse. Nature Immunology. 6: 785–92.

41. Cho, J.-H., H.-O. Kim, C.D. Surh, and J. Sprent. 2010. T cell receptor-dependent regulation of lipid rafts controls naive CD8+ T cell homeostasis. Immunity. 32: 214–26.

42. Kabouridis, P.S. 2006. Lipid rafts in T cell receptor signalling. Molecular Membrane Biology. 23: 49–57.

43. Garner, O.B., and L.G. Baum. 2008. Galectin-glycan lattices regulate cell-surface glycoprotein organization and signalling. Biochemical Society Transactions. 36: 1472–7.

44. Kuball, J., B. Hauptrock, V. Malina, E. Antunes, R.-H. Voss, et al. 2009. Increasing functional avidity of TCR-redirected T cells by removing defined N-glycosylation sites in the TCR constant domain. The Journal of experimental medicine. 206: 463–75.

45. Molnár, E., S. Deswal, and W.W. a Schamel. 2010. Pre-clustered TCR complexes. FEBS Letters. 584: 4832–7.

46. Bunnell, S.C. 2009. A view to a kill: how ligand quality controls lethal hits. Immunity. 31: 531–3.

47. Shin, H., and E.J. Wherry. 2007. CD8 T cell dysfunction during chronic viral infection. Current opinion in immunology. 19: 408–15.

48. Wherry, E.J. 2011. T cell exhaustion. Nature Immunology. 131: 492–499.

49. Wherry, E.J., M.J. McElhaugh, and L.C. Eisenlohr. 2002. Generation of CD8(+) T cell memory in response to low, high, and excessive levels of epitope. Journal of Immunology. 168: 4455–61.

3 Nanoscale Artificial Antigen Presenting Cells for T Cell Immunotherapy[2]

3.1 Introduction

The induction of specific cytotoxic T lymphocyte (CTL) responses is a powerful therapy for pathogens and tumors. Specific CTL populations expand several logs to produce robust responses and generate long-term memory that can prevent recurrence of disease[1]. CTL can be directly activated *in vivo*, as in some vaccines [2], or generated *in vitro* and adoptively transferred into a patient [3–5].

We have previously developed a cell-sized T cell expansion platform by coupling proteins that deliver two necessary and sufficient T cell activation signals to 4.5 μm diameter ("microscale") beads [6,7]. Signals present on APC that are required for T cell activation include signal 1, a cognate antigenic peptide presented in the context of major histocompatibility complex (MHC) that binds the TCR [8], and signal 2, a group of co-stimulatory receptors that modulate T cell response. In our system, signal 1 is delivered by a chimeric MHC-immunoglobulin dimer (MHC-Ig) loaded with a specific peptide, and signal 2 is either B7.1 (the natural ligand for the T cell receptor CD28) or an activating antibody against CD28. Both proteins can be directly chemically coupled to the surface of microscale beads to create artificial antigen presenting cells (aAPC).

[2] This chapter is reprinted in part from "Perica, K. *et al.* Nanoscale Artificial Antigen Presenting Cells for T Cell Immunotherapy. *Nanomedicine : nanotechnology, biology, and medicine* **[Epub Ahead of Primt],** (2013).", with permission.

The *in vivo* delivery and biodistribution of bead-based therapeutics is determined primarily by particle size [9–11]. Microscale particles have limited lymphatic drainage from their injection site and are preferentially cleared by and targeted to certain phagocytic subsets[12–14]. Nanoparticle platforms have different trafficking properties which would open new immunotherapeutic delivery strategies, but the appropriateness of nanoparticles for T cell activation has been questioned.

Studies have suggested that only beads larger than 2 microns in diameter are able to induce T cell proliferation [15,16]. As a result, nanoparticles have traditionally been developed for antigen or drug delivery [17,18], or to study biophysical aspects of TCR-MHC binding [19,20]. When T cell activation was examined directly, Steenblock et al.[21] demonstrated that polymer-based nanoparticles were much less efficient than microbeads in inducing short-term functional responses, with no reported proliferation.

Here, we present nanoscale, particle-based T cell activation platforms based on either paramagnetic iron-oxide particles 50-100 nm in diameter or quantum dot nanocrystals approximately 30 nm in diameter. We show these platforms induce antigen specific T cell proliferation and functional responses from murine and human T cells *in vitro*. Finally we show that nano-aAPC can prime CTL to attenuate tumor growth *in vivo* in a mouse melanoma model.

3.2 Materials and Methods

Mice and reagents

2C TCR transgenic mice were maintained as heterozygotes by breeding on a C57/BL6 background. pMEL TCR/Thy1^a Rag-/- transgenic mice were a gift from Nicholas Restifo (National Institutes of Health, Bethesda, MD) and maintained as homozygotes. C57BL/6j and Nu/J mice were purchased from Jackson Laboratories (Bar Harbor, ME). All mice were maintained according to Johns Hopkins University's Institutional Review Board. Fluorescently labeled monoclonal antibodies were purchased from BioLegend (San Diego, CA).

Preparation of MHC-Ig Dimers

Soluble MHC-Ig dimers, K^b-Ig and D^b-Ig, were prepared and loaded with peptide as described[50]. Briefly, K^b-Ig molecules were loaded with peptide by stripping at alkaline condition (pH 11.5), and then refolded in the presence of 50 fold excess peptide. D^b-Ig molecules were stripped under mildly acidic conditions (pH 6.5) and refolded in the presence of 50 fold molar excess peptide and 2-fold molar excess of human β_2-microglobulin. Human A2-Ig was passively loaded in the presence of excess M1 peptide [51]. Peptides SIY (SIYRYYGL, synthetic), SIIN (SIINFEKL, derived from ovalbumin protein), GP100 (KVPRNQDWL, from melanocyte GP100 protein) ASN (ASNENMETH, from influenza A nucleoprotein), and M1 (GILGFVFTL, from influenza A M1 protein) were purchased from Genscript (Piscataway, NJ). Protein concentration was determined after labeling by size exclusion high performance liquid chromatography (HPLC).

Nano-aAPC Synthesis

Nanoscale iron-dextran aAPC were manufactured in one of two ways. 2 μM biotinylated MHC-Ig dimer and an equimolar concentration of biotinylated anti-CD28 antibody were incubated with

100 μL of anti-biotin Miltenyi Microparticles (Miltenyi Biotec) for at least 1 hour with gentle agitation at 4ºC. Unbound protein was washed using a MS magnetic enrichment column (Miltenyi Biotec). Particle concentration was measured by absorbance at 405 nm using a Beckman Coulter AD340 plate reader. Alternatively, MHC-Ig dimer and B7.1-Ig were directly chemically coupled to biodegradable particles (Miltenyi Biotec). Total protein content was assessed by Bradford assay. Unless otherwise stated, "iron-dextran aAPC" refers to particles directly chemically coupled to MHC and B7.1, rather than anti-biotin coupling.

Nanoscale quantum dot aAPC were manufactured by incubating 5 μM biotinylated MHC-Ig dimer and an equimolar concentration of biotinylated anti-CD28 antibody with 100 μL of 1 μM streptavidin coated quantum dots (Life Technologies) for 2 hours at at 4ºC. Quantum dots were washed and concentrated using a Sartorius Vivaspin membrane with a 300,000 molecular weight cutoff. Quantum dot concentration was measured by absorbance at 405 nm using a Beckman Coulter AD340 plate reader.

Micro-aAPC Synthesis

Micro-aAPCs were fabricated as described previously[7] by direct chemical coupling of protein to 4.5 μm Dynal Magnetic Microbeads (Life Technologies, Carlsbad, CA). For the initial coupling step, 25 μg anti-biotin antibody (Sigma, St. Louis, MO) was added to 100 million Microbeads in 0.1 M sodium borate buffer. After washing in a magnetic column, biotin labeled MHC-Ig and CD28 were added in equimolar amounts to form aAPC.

In Vitro Cell Expansion

For murine cell culture, cells were obtained from homogenized mouse spleens followed by hypotonic lysis of RBC. Cytotoxic lymphocytes were isolated using a CD8 no-touch isolation kit and magnetic enrichment column from Miltenyi Biotec (Cologne, Germany) and if necessary

labeled with carboxyfluorescein succinimidyl ester (CFSE) for 15 minutes at 37ºC, then washed extensively. One million CD8+ T cells and particles at the indicated dosages were mixed and cultured in 96 well round bottom plates for 4-7 days in complete RPMI media supplemented with T cell factor (TF), a cytokine cocktail of conditioned media harvested from stimulated human PBMC [6].CFSE fluorescence was measured on Day 4 using a BD FacsCalibur flow cytometer and analyzed in FlowJo (TreeStar). CFSE is diluted with each round of T cell division, and division thus manifests as a one half-fold decrease in CFSE fluorescence.

For human cell culture, PBMCs from healthy HLA*0201 positive donors were isolated by Ficoll-Paque PLUS gradient centrifugation following the manufacturer's protocol (GE Healthcare). CD8+ T cells were further purified from fresh PBMC using the CD8+ T cell negative selection kit (Miltenyi Biotec). The purity of CD8+ T cells was higher than 95%, as determined by flow cytometry. Three million CD8+ T cells and particles at the indicated dosages were mixed and cultured in 96-well round bottom plates for up to 14 days in complete RPMI media supplemented with TF. On day 7 after stimulation, T cells were harvested, counted and replated at the same T cell:nano-aAPC density. Antigen specificity was determined using HLA-M1-specific, A*0201 PE or APC tetramers (Beckman Coulter) according to manufacturer's protocol.

Near-Infrared Imaging

Anti-biotin coated micro- and nano-particles were labeled with IRDye 680 RD or 800CW Protein labeling kits from LI-COR Biosciences (Lincoln, Nebraska). Beads were washed in a magnetic column and biotin labeled MHC-Ig and anti-CD28 were added to form aAPC. pMEL T cells were labeled with CellVue NIR 815 labeling kits from LI-COR Biosciences according manufacturer's instructions.

Nu/J mice were injected with 2 $\times 10^5$B16 melanoma cells on the right flank. Four days later, 5 $\times 10^5$ micro-aAPC and a fluorescence intensity equivalent amount of nano-aAPC were injected into the tail vein, ipsilateral flank, or hindlimb, as indicated. T cells were injected into tail vein. Biodistribution of injected aAPC was visualized with LI-COR Pearl Impulse imaging system (Johns Hopkins Molecular Imaging Center, Baltimore, MD). Area of distribution was calculated using thresholding of the NIR channel in the ImageJ application (NIH, Bethesda, MD).

Effect of Nano-aAPC on Subcutaneous Tumor Growth In Vivo

For QD aAPC experiment, 2 $\times 10^6$ naive CD8+ pMEL T cells were adoptively transferred into 8 week old C57BL/6 male mice by tail vein injection, except for control mice which received no T cells or aAPC treatment. The same day, B16 melanoma cells (2 $\times 10^5$) were injected subcutaneously into the right flank. The following day, 5 mice per group were treated with either 20 μL cognate QD aAPC, 20 μL non-cognate QD aAPC, or 20 μL PBS. Mice were treated days 3, 4, and 5 with 30,000 units intraperitoneal IL-2. Tumor growth was monitored at 2 day intervals, using digital calipers, until tumor size was ~200 mm^2 at which point animals were euthanized.

For iron-dextran aAPC experiment, 2 $\times 10^6$ naive CD8+ pMEL T cells were adoptively transferred as before. Four days later, mice in the treatment group received 25 μL cognate HD nano-aAPC either intravenously, *iv* or subcutaneously, *sc*, with eight mice per group. Three days later, aAPC were injected either *sc* or *iv*. B16 melanoma cells (2 $\times 10^5$) were injected *sc* four days later, and a second injection of aAPC were given four days after tumor, either *iv* or *sc* on the ipsilateral flank. Tumor tracking and animal euthanasia proceeded as above.

Tumor growth for each mouse was summarized as Area Under Curve calculated using trapezoidal approximation. Statistical analysis was performed in GraphPad Prism.

3.3 Results

Iron-Dextran Nano-aAPC Induce Antigen Specific T Cell Expansion

Nanosized iron-oxide core, dextran coated particles produced by Miltenyi Biotec were selected as a nanoscale particle platform due to their extensive characterization and biocompatibility6. To produce nanoscale aAPC, soluble dimeric MHC-Ig loaded with an appropriate peptide (signal 1) and chimeric B7.1-Ig fusion protein (signal 2) were covalently coupled in a 1:1 ratio to the particle surface (**Figure 3.1a**). Alternatively, particles were manufactured by coupling biotinylated MHC-Ig and biotinylated anti-CD28 to an anti-biotin coated iron-dextran particle (**Figure 3.1b**).

Iron-dextran aAPC were confirmed to be monodisperse with an average diameter of 50-100 nM in diameter using Nanoparticle Tracking Analysis (NTA, **Figure 3.1c**). Particles were suspended at a concentration of 8.3 nM (5×10^{12} particles/mL), and all subsequent volumes refer to particles at this concentration. By titrating the amount of protein present during the coupling reaction, we synthesized particles presenting a high density, HD (65 μg protein/mL of particles), or low density, LD (16 μg protein/mL of particles), of protein as measured by Bradford Assay.

To evaluate aAPC-induced T cell expansion, we utilized two TCR transgenic mouse models: 2C mice, whose T cells recognize the SIY peptide presented in the context of MHC Class I H2-K^b, and pMEL mice, whose T cells recognize a peptide derived from melanoma differentiation antigen GP100 presented in the context of MHC Class I H2-$D^{b,}$. Four types of anti-biotin coupled iron-dextran particles were manufactured, presenting either K^b or D^b loaded respectively with either the cognate peptide described above or a non-cognate peptide (SIIN for K^b, ASN for D^b). T cells were incubated with particles and proliferation was evaluated seven days later.

Particle based expansion was antigen-specific, as 2C cells only proliferated in the presence of K^b-SIY particles, and pMEL cells only proliferated in the presence of D^b-GP100 particles (**Figure 3.2A**). Nano-aAPC mediated expansion is therefore antigen specific. Furthermore, both signal 1 and signal 2 were required for optimal expansion, and anti-biotin particles carrying either MHC-Ig or CD28 alone were not as effective at inducing robust T cell proliferation (**Figure 3.2B**).

Soluble MHC-Ig and anti-CD28 are known to mediate weak T cell expansion *in vitro* [25,26]. To demonstrate that coupling of Signal 1 and 2 to solid support enhanced activation [27], nano-aAPC mediated T cell expansion was compared to equivalent amounts soluble MHC-Ig and anti-CD28. 10 ng of protein coupled to nano-aAPC induced greater T cell expansion than several orders of magnitude more soluble protein (**Figure 3.3**). Furthermore, soluble protein induced maximal expansion at an intermediate dose of 100 ng, whereas nano-aAPC mediated expansion was dose-dependent, reaching up to 30-fold expansion at a dose of 10 μg protein.

Both the amount [28,29] and density [30,31] of antigen presented by APC influence downstream T cell behavior such as proliferation and cell death, and may thus be important parameters for aAPC stimulation. HD and LD particles were used to evaluate the effect of antigen density on T cell expansion and both sets of particles were titrated to evaluate the effect of antigen dose. Proliferation was characterized three days after stimulation by dilution of the vital dye carboxyfluorescein succinimidyl ester (CFSE). Seven days after stimulation, T cells were counted to characterize the overall balance between proliferation and death.

Both HD and LD particles were able to induce pMEL T cell proliferation in a dose-dependent fashion (**Figure 3.2C**). As measured by CFSE dilution, HD particles induced proliferation in

79%, 98%, and 99% of cells for 1, 5, and 20 μLs of particles, respectively, per 1 million cells, while identical amounts of LD particles induced proliferation in 4%, 40%, and 93% of cells. By day 7, HD and LD particles had induced an overall expansion of T cells on the order of 5-30 fold, with a minimum threshold of approximately 5 μL of LD particles and less than 0.5 μL of HD particles required to induce expansion (**Figure 2D**). Both CFSE proliferation and cell counts demonstrated that at any given quantity of particles, HD nano-aAPC induced greater expansion than LD. For example, at 5 μL of particles, HD particles induced 21-fold expansion, while LD particles induced only 7-fold expansion.

To assess whether the increased amount of protein on HD particles fully accounted for the proliferation advantage, LD and HD particles were incubated with T cells at equal protein concentrations (that is, approximately 5-fold more LD particles at a given concentration of HD). Once aAPC were normalized for protein concentration, HD and LD particles induced similar expansion as measured by CFSE dilution on Day 3 (**Figure 3.2E**) or overall expansion on Day 7 (**Figure 3.2F**). For example, 20 uL of LD particles or 3.5 uL of HD particles both induced proliferation in 94% of cells by Day 3, and approximately 17-fold expansion after 7 days of growth. Thus, at the antigen doses and densities evaluated, expansion was driven by total protein presented on aAPC, and not particle dose or protein density.

Generating sufficient numbers of antigenic-specific T cells is a critical goal of immunotherapy. However, CTL can become anergic or even suppressive under certain stimulation conditions[32], so expanded lymphocytes must also be evaluated for their ability to produce critical effector cytokines, such as IFNγ, and to secrete cytotoxic granules, as indicated by surface expression of the degranulation marker CD107a. Seven days after particle-based stimulation, CTL were

harvested and re-challenged with peptide-pulsed splenocytes and assessed for functional response by intracellular cytokine assay (**Figure 3.4)**.

Functional responses were robust and equivalent for all three particle doses. CTL of all groups expressed high levels of CD107a, with up to 90% of cells degranulating and expressing high levels of IFNγ when re-challenged with peptide (**Figure 3.4A-C**). Thus, while particle to T cell ratio and protein quantity on particles influence the degree of CTL expansion, the resulting T cells displayed similar, strong effector responses regardless of particle dose. CTL phenotype was also assessed by expression of effector and memory surface markers CD44 and CD62L. After activation with either HD or LD nano-aAPC, naive CD44lo CD62Lhi T cells upregulated CD44, forming both CD62Lhi "Central Memory" (T_{cm}) phenotype and CD62Llo "Effector Memory" (T_{em}) phenotypes (**Figure S2D-E**).

We next compared nano-aAPC mediated T cell expansion to our micro-aAPC platform [7], which is based on 4.5 μm diameter iron-dextran beads. The total dose of protein was normalized between micro- and nano-aAPC. Micro- and nano-aAPC mediated robust, dose-dependent, and comparable levels of proliferation of pMEL T cells with acquisition of effector phenotype during three weeks of re-stimulation *in vitro* (**Supplementary Figure 3.5**). After one week, micro-aAPC induced approximately 15-fold expansion, and nano-aAPC induced approximately 20-fold expansion at a high dose of aAPC. After three weeks, fold expansion of CTL as high as 650-fold expansion with nano-aAPC and 450-fold expansion with micro-aAPC was observed. Both sizes of aAPC induced upregulation of CD44 and downregulation of CD62L consistent with effector phenotypes. Total amounts of proliferation observed is consistent with previous studies [33] and illustrates that nano-aAPC induce robust proliferation comparable to micro-aAPC.

Quantum Dot Nano-aAPC

To evaluate nano-aAPC based stimulation at an even smaller scale, and to demonstrate that nano-aAPC are not platform-exclusive, we obtained commercially available quantum dot core, avidin coated nanocrystals approximately 30 nm in diameter from Life Technologies. Biotin labeled dimeric D^b-GP100 (signal 1) and anti-CD28 antibody (signal 2) were bound in a 1:1 molar ratio to the nanocrystal surface to form a quantum dot nano-aAPC (QD-aAPC) (**Figure 3.6A**).

QD aAPC induced dose-dependent, antigen specific T cell expansion *in vitro* (**Figure 3.6B**). At the highest dose evaluated, T Cells expanded 14.6 fold after 7 days, while T cells stimulated with non-cognate control QD aAPC did not expand.

Nano-aAPC Expansion of Endogenous Human T Cell Responses

Antigen-specific precursor T cells exist as low-frequency, heterogeneous populations of peripheral blood mononuclear cells (PBMC). Thus, immunotherapy ultimately depends on the expansion of antigen-reactive CTL from a polyclonal pool of endogenous precursors. Antigen-specific T cells in a polyclonal pool can be identified as cells that bind fluorescent MHC tetramer of the appropriate allele carrying the peptide of interest [34].

Anti-biotin iron-dextran aAPC were synthesized bearing the human HLA allele A2 loaded with the immunodominant T cell epitope derived from influenza protein M1 (signal 1) and anti-CD28 (signal 2). PBMC were incubated with increasing doses of nano-aAPC and antigen-specific T cell expansion was assessed by tetramer staining after two consecutive stimulations.

Before stimulation, M1 specific precursor frequency in the peripheral blood was low, with 0.4% specific CD8+ PBMC (**Figure 3.7A, top row)**. Incubation with nano-aAPC for one (middle row) or two (bottom row) weeks resulted in a dose-dependent increase in the percentage of antigen specific T cells. These data are summarized in **Figure 3.7B.** The highest dose (30 μL) of nano-aAPC induced up to 44% of antigen specific T cells after one week or 80% after two weeks (left panel). This was associated with a dose-dependent increase in the total amount of antigen-specific T cells (right panel), with up to 150-fold expansion after one week and 800-fold expansion after two weeks at the highest particle dose. Nano-aAPC thus induced large populations of antigen-specific T cells from small endogenous precursor populations.

Enhanced Distribution of Nano- Compared to Micro-aAPC

As discussed, nanoscale particles are expected to drain more efficiently via lymphatics than microscale particles[14,35], motivating our interest in developing a nanoscale aAPC. To assess biodistribution after subcutaneous injection, we injected near-infrared (NIR) labeled iron-dextran nano- and micro-aAPC into the right flanks of B16 melanoma bearing Nu/J (nude) mice.

Twenty-four hours after subcutaneous injection, micro-aAPC remained largely confined to the injection site (**Figure 3.8A, left**). No significant drainage was observed up to 72 hours after injection. In contrast, nano-aAPC had spread diffusely across a larger area of the right flank, with most drainage occurring within the first 24 hours (**Figure 3.8A, right**). However, neither nano- nor micro-aAPC were observed to spread to the tumor itself. Distribution was quantified by measuring the area of particle distribution in the NIR channel above a certain fluorescence threshold. Twenty-four hours post-injection, nano-aAPC were visible in a 5-fold larger area than micro-aAPC (**Figure 3.8B**).

Enhanced drainage could lead to colocalization of antigen-specific T cells and nano-aAPC in lymph nodes. To simultaneously visualize T cell and aAPC biodistribution, we labeled pMEL T cells with a NIR membrane dye and injected them in the tail veins of Nu/J mice (**Figure 5c**). aAPC were labeled and injected subcutaneously as before. Forty-eight hours after injection, T cells were visible in axillary, inguinal, and cervical lymph nodes, as well as spleen. Nano-APC drained broadly from the injection site and a portion of particles were localized to the inguinal lymph nodes, where they could contact cognate T cells. Micro-aAPC, in contrast, were confined to the injection site, and not present at the same location as T cells.

Nano-aAPC Inhibit Tumor Growth In Vivo

A mouse model of subcutaneous melanoma was chosen to demonstrate the functional efficacy of nanoscale aAPC for immunotherapy when injected directly *in vivo*. To evaluate QD-aAPC, naive TCR transgenic pMEL CTL were adoptively transferred into wild-type B6 mice, and mice were challenged the same day with B16 melanoma cells injected subcutaneously *(sc)* on the right flank (**Figure 3.9A, top**). The following day, mice were injected with either 20 μL of cognate QD aAPC or 20 μL of non-cognate QD aAPC or PBS as control. One injection of QD aAPC significantly inhibited tumor growth (**Figure 3.9A, bottom**). After 16 days, mice treated with T cells and cognate QD aAPC had the smallest tumor burden, with an average tumor size of 22.1 mm^2 +/- (sd) 2.3, compared to 111.1 mm^2 +/- 29.4 for T cell + noncognate aAPC treated mice, 141.1 mm^2 +/- 9.6 for T cells alone and 133.1 mm^2 +/- 7.6 for untreated mice. Total tumor growth over the course of the experiment was summarized as area under the curve (AUC). Mice treated with cognate QD-aAPC had significantly less ($p=0.028$) overall tumor growth by AUC (33.1 mm^2 +/- 7.8) than mice treated with control, non-cognate aAPC (373.6 mm^2 +/- 227.0).

The route of particle administration is likely to affect bead trafficking, with subcutaneously deposited beads more likely to drain to local lymph nodes [36] and intravenously injected particles more likely to be filtered by the spleen. To test the impact of route of aAPC administration as well as the *in vivo* efficacy of iron-dextran aAPC, particles were injected either intravenously or subcutaneously three days after pMEL adoptive transfer. B16 Tumors were injected subcutaneously on right flank four days later, and a second injection of aAPC were given four days after tumor, either *iv* or *sc* on the ipsilateral flank. Thus, there were three treatment groups: mice receiving two *iv* bead injections, mice receiving one *iv* and one *sc* injection, and mice receiving two *sc* injections (**Figure 6B, top**). Control mice injected with non-cognate aAPC received one *iv* and one *sc* injection.

All three treatment groups had less tumor growth than mice injected with control bead (**Figure 3.9B, bottom**). After 16 days, mice treated with one *sc* and one *iv* injection (*sc/iv*) showed the least tumor growth (48.0 mm^2 +/- 31.16), followed by *sc/sc* treated (73.7 mm^2 +/- 37.44), *iv/iv* treated (89.4 mm^2 +/- 69.5), no treatment (88.4 mm^2 +/- 17.8) and non-cognate treated (113 mm^2 +/- 39.4). Over the entire course of the experiment, *sc/iv* treated mice (AUC 52.6 mm^2 +/- 29.7) and *sc/sc* mice (AUC 73.1 mm^2 +/- 36.1) showed significantly less ($p<0.02$) tumor growth than control mice (AUC 162.7 mm^2 +/- 77.6). Mice treated with two *iv* injections had less total tumor burden (AUC 103.0 +/- 86.1) than control, but did not reach the significance threshold ($p = 0.19$). Thus, mice treated with at least one dose of nano-aAPC delivered subcutaneously had significantly less tumor than control. This was consistent with observations that sc injected nano-aAPC drained from the injection site and were retained for several days after injection, whereas iv injected nano-aAPC were more likely to be rapidly cleared by renal excretion or filtered by the liver and spleen (**Figure 3.10**).

3.4 Discussion

We have described two nanoscale T cell activation platforms, termed artificial antigen present cells (aAPCs), based on coupling signal 1, peptide-MHC, and signal 2, B7.1-Ig or anti-CD28, to iron-dextran nanoparticles and quantum dot nanocrystals. Nano-aAPC induced T cell expansion from both TCR transgenic mouse splenocytes and human, polyclonal peripheral blood T cells, generating CTL with a robust effector phenotype that inhibited tumor growth *in vivo*. Both 30 nm quantum nanocrystals and 50-100 nm iron oxide nanoparticles were effective aAPC platforms, indicating that bead based aAPC can be explored at a range of nano-scales.

Previous work suggested that nanoparticles were incapable of providing the robust activating signals necessary for T cell proliferation [15,16,21]. This is the first description of a nanoscale particle-based T cell stimulation platform that can effectively induce antigen-specific T cell proliferation *in vitro* and anti-tumor activity *in vivo*. Our success may be due in part to our use of MHC-Ig dimers, whose flexible hinge region and nanoscale MHC dimerization may provide more optimal TCR/MHC interactions than MHC monomer [15,37].

Microscale, cell-sized bead platforms were initially chosen as aAPC to mimic structures that form between T cells-APC conjugates during activation [38]. For example, the immune synapse is a pattern of surface receptor reorganization several microns in diameter, with centrally located TCR and peripherally located adhesion molecules. The synapse, while not absolutely required for activation, does modulate antigen search and recognition [39]. A related process, asymmetric cell division, is hypothesized to regulate memory development by providing a microscale scaffold that induces polarity during cell division [40]. It has not been shown that aAPC of any size can recapitulate these structures, which seem to at least partly depend on coordinated

rearrangement of both the APC and T cell membrane. Furthermore, it is particularly unlikely that nano-aAPC will drive the formation of structures that seem to depend on microscale cell-cell interactions. The nature of T cell activation by nano-aAPC may thus have important consequences for T cell function and memory development.

Nanoscale structures, such as clusters of TCR form on the T cell membrane even prior to formation of microscale structures [41,42], are also thought to be important regulators of T cell responses. However, even on the nanoscale level, the mechanism of TCR triggering by nano-aAPC is not clear. aAPC activate T cells through specific receptor-ligand binding at the cell-bead interface. Such interactions are not well defined when one of the participants is nanoscale [43]. The geometry of the nanobead, such as high local curvature at the interface, may preclude multiple productive receptor-ligand interactions. Alternatively, nanoscale platforms may preferentially interact with nano-clustered receptors such as the TCR [44,45]. Nanoscale bead-cell interaction platforms thus represent not just a novel approach to immunotherapy, but a tool for studying the delivery of biological signals at the cell membrane [19].

Nano-aAPC are better suited than micro-aAPC for *in vivo* administration and thus, allow the exploration of new particle-based immunotherapy strategies. Two potential sites where aAPC might be most effective are the lymph node, where naive and memory T cells reside and the tumor itself. Nanoparticles of approximately 50-100 nm diameter can be taken up by lymphatics and transported to the lymph nodes [14,36] thus gaining access to a larger pool of T cells. Nano-aAPC were more efficiently distributed from the injection site than micro-aAPC, were found to co-localize with antigen-specific T cells in inguinal lymph nodes, and inhibited tumor growth when injected subcutaneously. This suggests drainage of nano-aAPC to lymph nodes is a

potential mechanism for optimal *in vivo* T cell activation, and the possibility of further tuning size [46] and particle surface properties[36] to enhance lymph node trafficking.

In addition, nanoscale delivery vehicles preferentially accumulate in tumors through enhanced permeability retention due to poorly formed tumor vasculature[47,48]. In this study, nano-aAPC delivered subcutaneously were not observed to drain into the tumor environment directly, whereas future work will focus on delivery strategies that lead to intratumoral aAPC accumulation. By delivering an immunostimulatory signal *in situ,* aAPC in the tumor microenvironment may address one of the most prominent hurdles in cancer immunotherapy, the immunosuppressive tumor microenvironment [49]. Although our work demonstrates that nano-aAPC can induce anti-tumor effector T cells from naive populations *in vivo*, it does not explore the capability of nano-aAPC to mediate rejection of established tumors in highly immunosuppressive microenvironments. Thus, whether a local stimulatory signal can overcome multiple layers of tumor immunosuppresion, or whether aAPC based stimulation can synergize with immunomodulatory therapies like checkpoint blockade, remains unknown. The enhanced drainage properties of nano-aAPC compared to micro-aAPC provides a system for examining the optimal distribution of aAPC for tumor rejection, and allows the exploration of new *in vivo* delivery strategies.

3.5 Figures

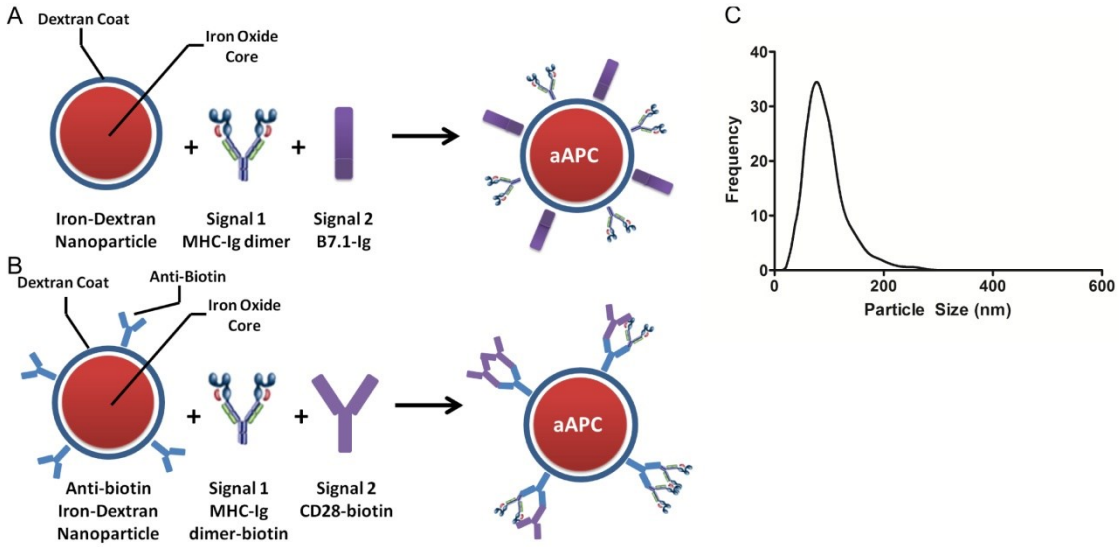

Figure 3-1 Synthesis and Characterization of Iron-Dextran Nano-aAPC .

Nano-aAPC were synthesized in one of two ways: **(A)** Direct chemical coupling of soluble MHC-Ig dimer (signal 1) and B7.1-Ig (signal 2) in a 1:1 molar ratio to the surface of a paramagnetic iron-oxide, dextran-coated particle. **(B)** Binding of biotinylated MHC-Ig dimer (signal 1) and biotinylated anti-CD28 (signal 2) in a 1:1 molar ratio to anti-biotin coated particles.
(C) Nanoparticle tracking analysis confirms that nano-aAPC are a monodisperse mixture of particles with a mean diameter of 50-100 nm suspended at a concentration of 8.3 nM.

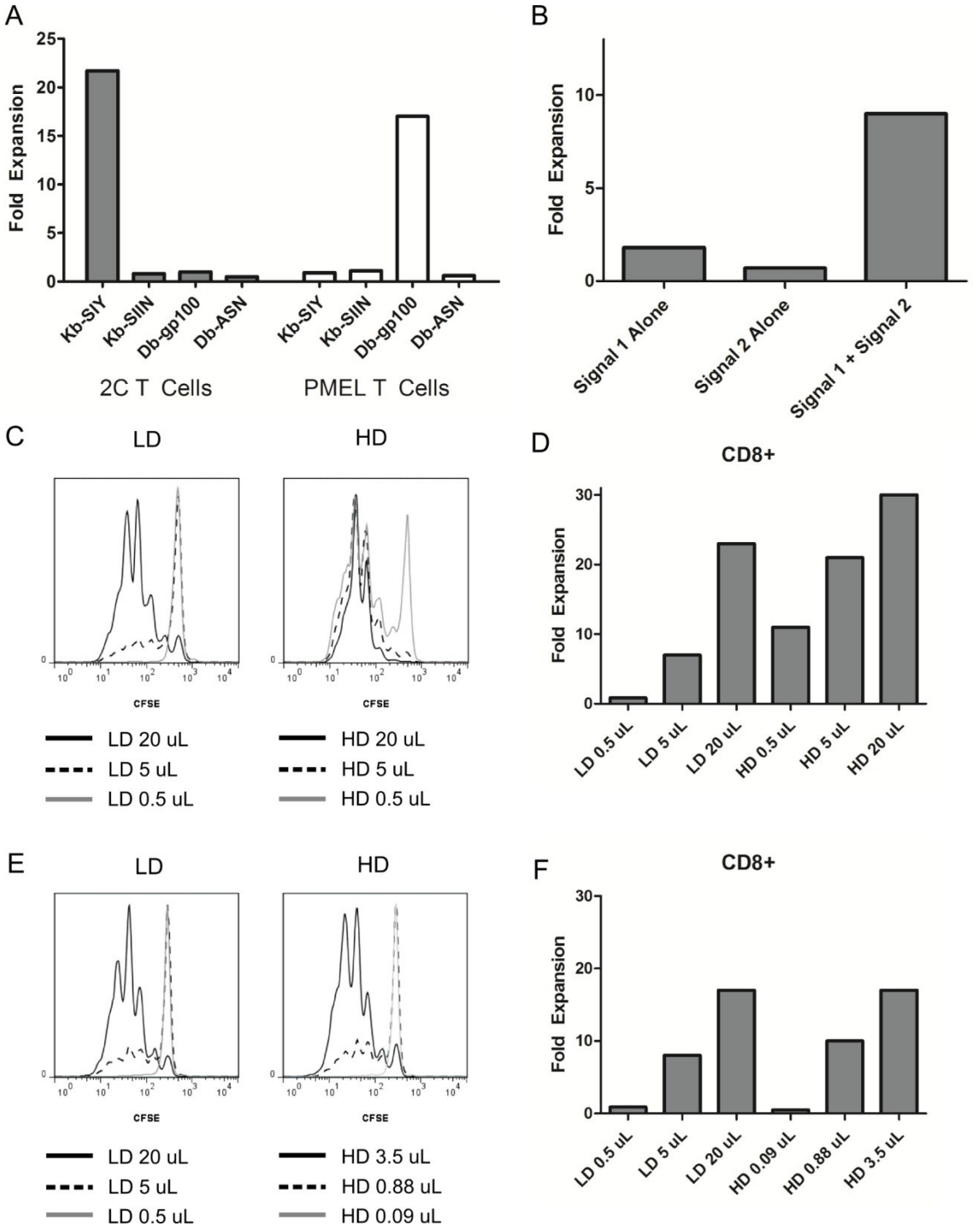

Figure 3-2. Nano aAPC Induced Proliferation is Antigen-Specific and Dose-Dependent

(A) Antigen specific nano-aAPC induce proliferation. T cells were counted seven days after stimulation with anti-biotin coated nano-aAPC to calculate fold expansion from day 0. TCR transgenic 2C (grey) and pMEL (white) T cells proliferated only when incubated with nanoparticles bearing cognate MHC/peptide (22-fold and 16-fold, respectively), and not in the presence of nnaoparticles bearing either non-cognate peptide or non-cognate MHC (<3-fold).

(B) Addition of both signal 1 and signal 2 leads to optimal T cell expansion. At a dose of 10 μL particles per $1*10^6$ T cells, only anti-biotin particles bearing both MHC-Ig and anti-CD28 induced robust T cell expansion.
Proliferation of CD8+ CTL induced by Low Density, LD (16 μg protein/mL particles), and High Density, HD (65 μg protein/mL), particles. Results are representative of three experiments.
(C) Equivalent doses of HD and LD particles were used to stimulate pMEL T cells. Proliferation was measured by dilution of CFSE three days after stimulation. Decreased fluorescence indicates increased proliferation. Equivalent volumes of HD particles induce greater proliferation than LD particles, with 0.5 uL LD particles inducing almost no expansion.
(D) Fold expansion on day 7 of samples of dose equivalent samples shows a similar pattern. Proliferation is dose-dependent and 2-4 fold greater for HD particles compared to an equivalent dose of LD particles (21-fold compared to 7-fold at 5 μL).
(E) Day 3 CFSE dilution of CD8+ CTL induced by LD and HD particles at equivalent protein concentrations, with approximately 5.5-fold more LD than HD at a given dose. When particle doses are normalized to equivalent protein concentrations, particles induce similar amounts of CFSE dilution.
(F) Fold expansion on day 7 of samples demonstrates equivalent expansion for HD and LD particles at an equivalent protein dose (17-fold at 3.5 μL of HD and 20 μL of LD). A threshold of about 0.5 uL LD particles or 0.08 uL HD particles is required to induce detectable expansion.

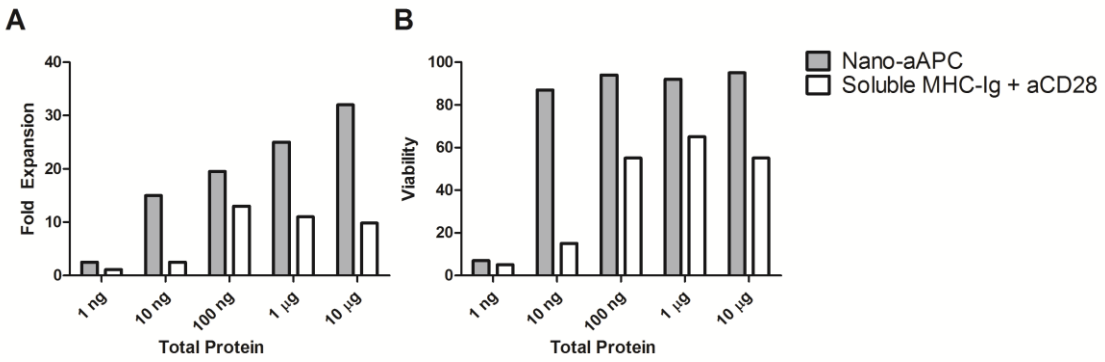

Figure 3-3. Coupling of MHC-Ig and anti-CD28 to Nanoparticles Enhances T Cell Stimulation.

HD nano-aAPC, at 65 µg of total protein/ml, were incubated at titrated doses with $1x10^6$ isolated CD8+ T cells. Equivalent doses of equimolar MHC-Ig and anti-CD28 antibody were compared in parallel. Fold expansion was assessed with cell counts seven days after activation. Data are representative of three experiments.
(A) Nano-aAPC bearing 10 µg of total protein (D^b-GP100 + CD28) were able to induce greater-fold T cell proliferation (15x) than any dose of soluble protein. Nano-aAPC mediated expansion increased in a dose-dependent manner, reaching up to 32-fold expansion, whereas soluble protein mediated expansion peaked at 13 fold for 100 ng, then decreased for increasing protein concentration.
(B) Cell viability was assessed by exclusion of Trypan Blue dye. Greater than 90% viability was observed for all nano-aAPC doses that induced T cell stimulation. In contrast, soluble peptide based stimulation showed decreased cell viability.

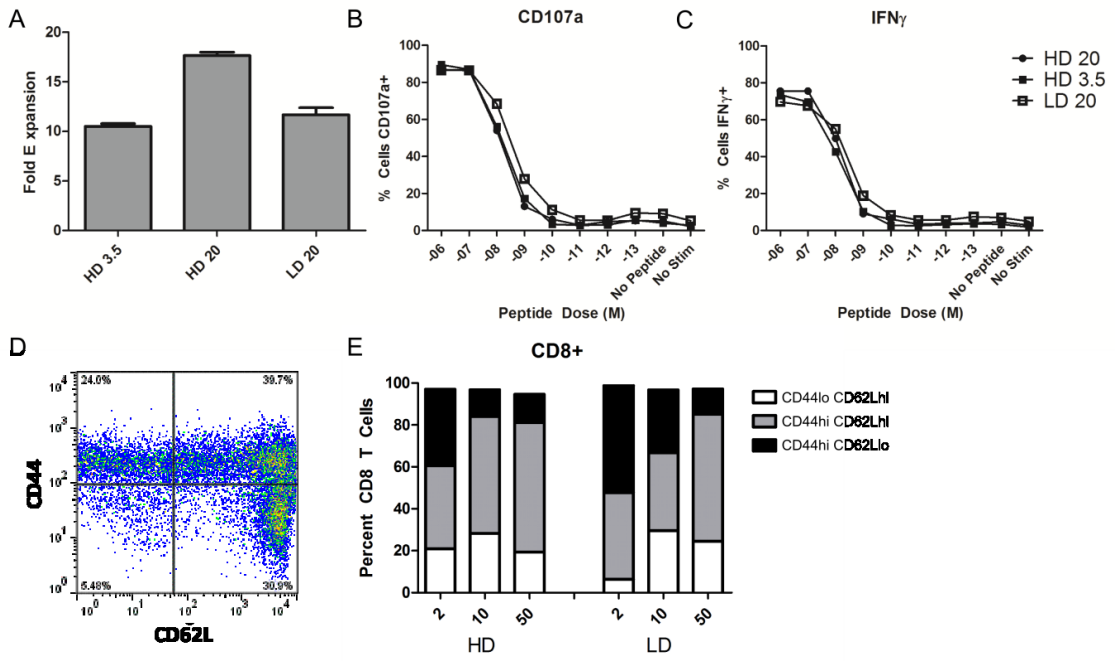

Figure 3-4. T Cell Functional Characterization

(A-C) Intracellular Cytokine Staining. **(A)** CD8+ T Cells were expanded using HD and LD particles. Particle doses were chosen to induce either roughly equivalent expansion by HD and LD particles (3.5 uL and 20 uL, respectively) or more robust expansion (HD 20 uL). **(B & C)** Samples were re-stimulated on day 7 and assessed for effector function by intracellular cytokine staining assay. 20 uL HD sample (black circles), 3.5 uL HD sample (black filled square), and 20 uL LD samples (unfilled square) all induced robust, equivalent, and dose-dependent **(B)** degranulation measured by CD107a and **(C)** IFNγ production.
(**B**). Functional responses were robust and equivalent for all three particle doses. CTL of all groups expressed high levels of CD107a, with up to 90% of cells degranulating when re-challenged with a high dose of peptide (**C**)Similarly, all three groups displayed high levels of IFNγ responsiveness.
(D) Representative FACS plot shows three populations seven days after nano-aAPC stimulation. T cells were stained with anti-CD44 and anti-CD62L to characterize effector phenotype. **(E)** T cells were stimulated with 2, 10 and 50 μL of LD or HD iron-oxide nano-aAPC and characterized seven days later. Bar plots show percentage of naive (unfilled), T_{cm} (grey fill), and T_{em} (black fill) cells generated after stimulation. Lower doses of particles generated a higher proportion of CD62Llo CD44hi T_{em} cells, with 2 uL of LD and 2 uL of HD generating 51% and 36% T_{em}, respectively.

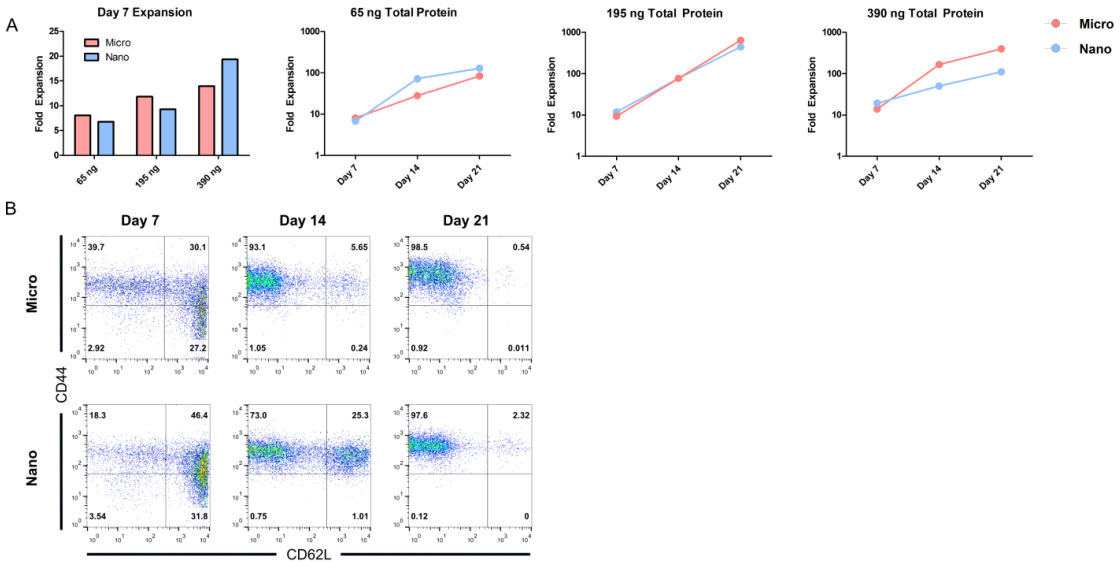

Figure 3-5. Micro- vs. Nano-aAPC Mediated T Cell Prolieration

Proliferation induced by micro- and nano-aAPC with repeated re-stimulation in culture. aAPC doses were normalized to total dose of protein (MHC-Ig and anti-CD28).
(**A**) Seven days after stimulation, proliferation was assessed by cell count and reported as fold expansion from Day 0. Data are representative of four experiments. Both micro- and nano-aAPC induce dose-dependent T cell expansion, with a maximal expansion of 13-fold for nano-aAPC and 19-fold for micro-aAPC at the highest dose examined here. Over two subsequent weeks of re-stimulation (on Days 7 and 14), T cell proliferation continued in a dose-dependent fashion. An optimal dose of 195 nanograms induced the most robust overall expansion with both platforms, reaching 644-fold expansion with nano-aAPC and 446-fold expansion with micro-aAPC after 21 days.
(**B**) Effector phenotype induced micro- and nano-aAPC during *in vitro* culture. After repeated stimulation with aAPC, nearly all T cells acquire a CD62Llo CD44hi effector phenotype. Representative FACS plots are shown for aAPC stimulation with the optimal dose of protein (195 ng).

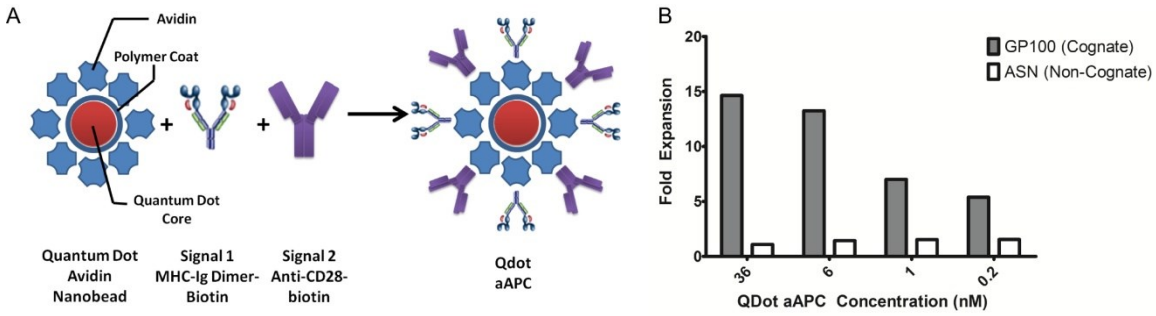

Figure 3-6. Synthesis and Characterization of Quantum Dot Nano-aAPC

(A) Quantum Dot (Qdot) Nano-aAPC were constructed by avidin-biotin mediated coupling of soluble MHC-Ig dimer (signal 1) and anti-CD28 antibody (signal 2) in a 1:1 ratio to the surface of a polymer-coated quantum dot particle.
(B) Qdot Nano-aAPC expansion in whole CD8+ T cells. Fold expansion on Day 7 is dose dependent and antigen-specific. Non cognate particles did not induce any expansion, whereas the highest dose of cognate QD aAPC (D^b-GP100) induced approximately 15 fold expansion of CTL. Results are representative of 3 experiments.

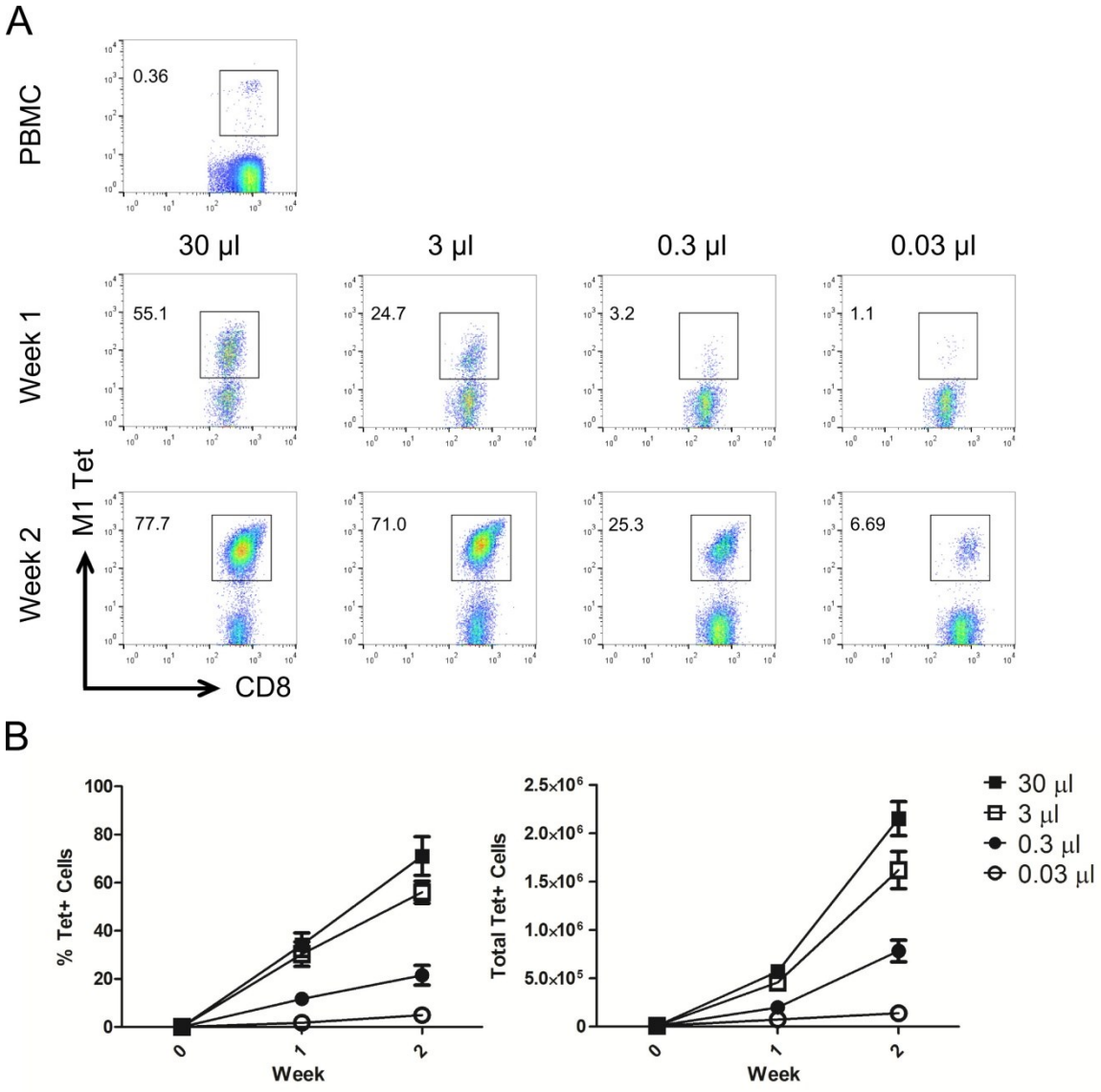

Figure 3-7. Antigen-specific Human T Cell Expansion From Endogenous Precursors

(A) CD8+ T cells were isolated from PBMC by magnetic enrichment and incubated with increasing doses of iron-dextran nano-aAPC bearing A2-Ig complexes loaded with antigen derived from the immunodominant epitope of the influenza M1 protein, and assessed for antigen-specificity by tetramer staining before stimulation (PBMC, top row) and after one (middle row) or two (bottom row) weeks of stimulation. Numbers in top left represent percentage of CD8+ cells that were tetramer positive (gated).The size of the M1 specific population increases with repeated rounds of stimulation (top to bottom) and increasing dose of nano-aAPC (left to right), from 0.36% of CD8+ PBMC to 77.7% at the highest dose. Plots are representative of results from three separate experiments, summarized in panel B. **(B)** Percentage of CD8+ PBMC binding HLA-A2 M1 tetramers increases with repeated stimulation and increasing dose of nano-aAPC (left panel). The total number of tetramer positive cells (right panel) similarly increases

with rounds of stimulation and particle dose, expanding up to 800-fold over the initial precursor population.

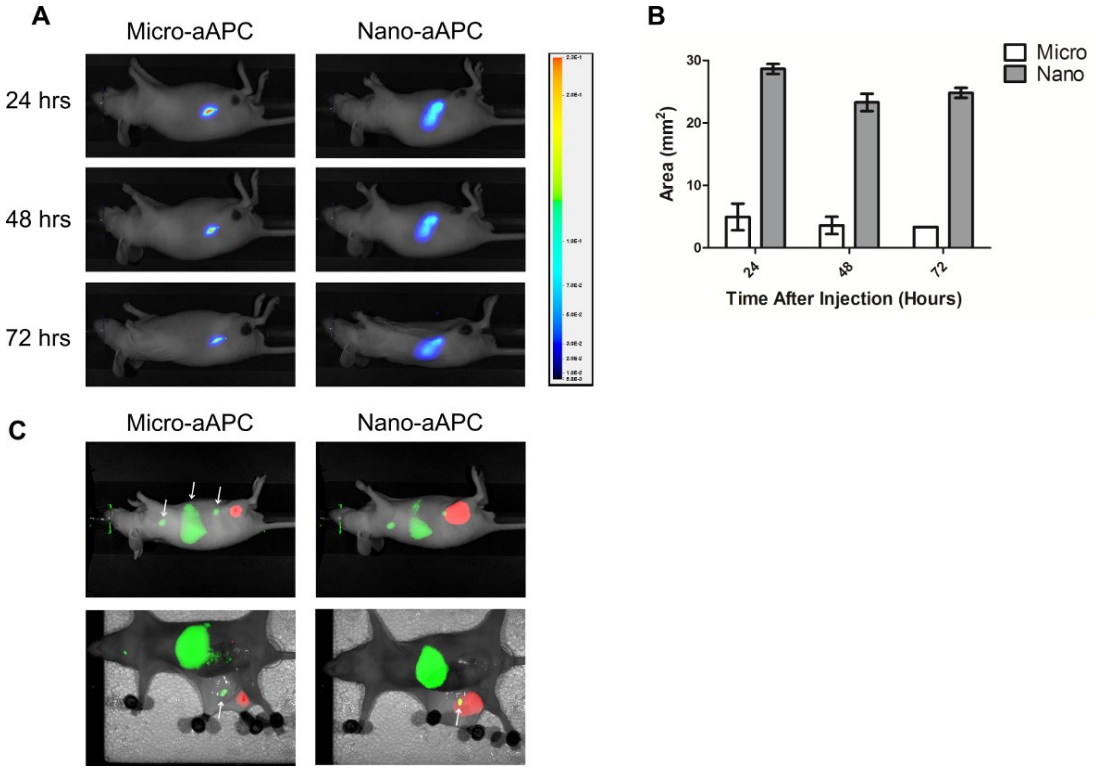

Figure 3-8Enhanced Drainage of Nano- Compared to Micro-aAPC.

(A) Visualization of drainage of near infrared labeled micro-aAPC (left) compared to nano-aAPC (right) after subcutaneous injection on right flank. Right flank views are shown for representative mice (3 mice/group) at the indicated timepoints after injection. Legend at right relates color in image to arbitrary fluorescence units. Micro-aAPC are confined largely to injection site, whereas local drainage of Nano-aAPC is more pronounced. (B) Biodistribution is quantified as area of visible drainage at indicated timepoints. Nano-aAPC have five-fold greater area of drainage than micro-aAPC at equivalent timepoints. (C) Simultaneous NIR images of biodistribution for pMEL T cells (green) and aAPC (red). Forty-eight hours after intravenous injection, T cells are visible in axillary lymph nodes, spleen, inguinal lymph nodes (white arrows, left to right) and cervical lymph nodes (not pictured). Right flank view (top row) shows nano-aAPC which were injected in right hindlimb 48 hrs. earlier reach inguinal lymph node, whereas micro-aAPC do not. This is even more pronounced after dissection (bottom row); aAPC signal is stronger and can be seen in the area of the inguinal lymph node (white arrow) for nano- but not micro-aAPC. Images are representative of three mice.

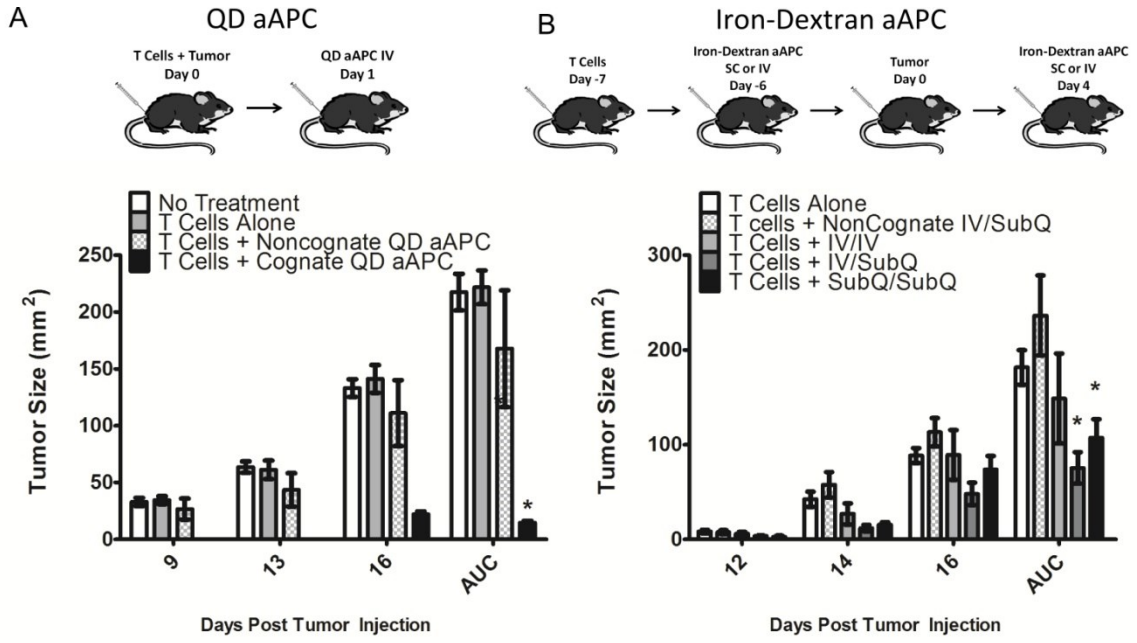

Figure 3-9. Nano-aAPC Inhibit Tumor Growth *In Vivo*

(A) QD aAPC. B16 Tumors were injected subcutaneously on day 0, with injection of naive pMEL T cells on the same day. One day later, QD aAPC were injected intravenously (*iv*). IL-2 was administered on days 3, 4, and 5. Tumor size was measured as surface area (mm^2) on indicated days, with area under the curve (AUC) shown at right. Mice treated with pMEL T cells and cognate QD aAPC (black bars) had less tumor growth compared to no treatment (white), T cells alone (light grey), and T cells + noncognate QD aAPC (checkered) (4 mice per group). Significance was characterized over entire experiment by AUC ($p<0.001$ by ANOVA with Tukey's Post-Test, * indicates significant difference from no treatment group).
(B) Iron-Dextran aAPC. Naive pMEL T cells were injected intravenously on day -7. One day later, iron-dextran aAPC were injected either *iv* or subcutaneously (*sc*) on the right flank. B16 tumors were injected *sc* on right flank on day 0. Mice in treatment arms were given an additional injection on day 4 post tumor injection either *iv* or *sc*, to form four treatment groups: noncognate aAPC *iv* (day -6) then *sc* (day 4) (checkered), cognate aAPC *iv* then *iv* (light grey), cognate aAPC *iv* then *sc* (dark grey), and cognate aAPC *sc* then *sc* (black). Mice treated with pMEL T cells and cognate Iron-Dextran aAPC *iv/sc* or *sc/sc* (filled squares) had less tumor growth compared to noncognate aAPC (7 mice per group, $p<0.02$ by ANOVA with Tukey's Post-Test, * indicates significant difference from no treatment group).

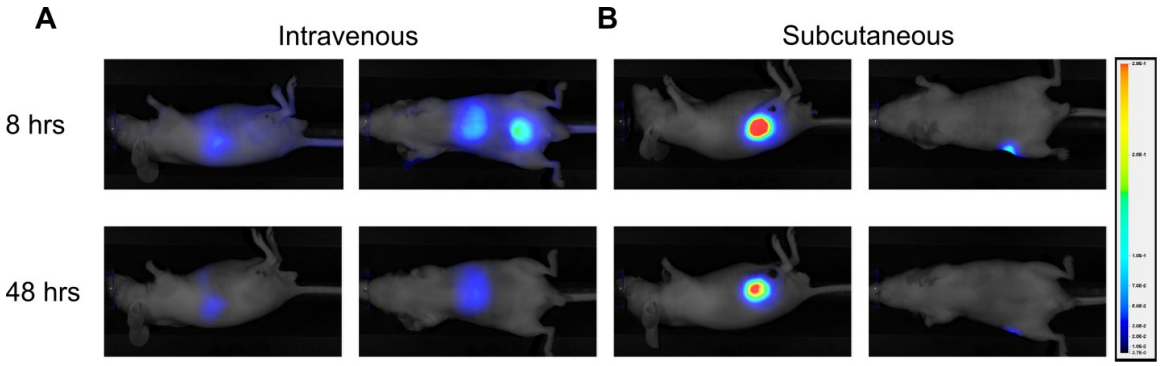

Figure 3-10. Biodistribution of Nano-aAPC After Intravenous (iv) and Subcutaneous (sc) Injection.

Nu/J mice were injected with 2 $\times 10^5$ B16 melanoma cells on the right flank. Four days later, 25 µL of 8.3 nM nano-aAPC were injected either iv tail vein, or sc into the ipsilateral flank several cm from tumor. Images are representative of three mice per group.
(**A**) Eight hours after injection, distribution of iv nano-aAPC is consistent with filtration by liver and spleen, as well as significant renal excretion. 48 hours later, nano-aAPC are only visible in liver and spleen, and intensity is significantly decreased, likely due to clearance. (**B**) In contrast, sc nano-aAPC are visible with high intensity 8 and 48 hours after injection, forming a depot on the right flank that drains from the injection site.

3.6 References

1. Zhang N, Bevan MJ. CD8(+) T cells: foot soldiers of the immune system. *Immunity*. 35(2), 161–8 (2011).

2. Ahlers JD, Belyakov IM. Memories that last forever: strategies for optimizing vaccine T-cell memory. *Blood*. 115(9), 1678–89 (2010).

3. Wrzesinski C, Paulos CM, Kaiser A, *et al.* Increased intensity lymphodepletion enhances tumor treatment efficacy of adoptively transferred tumor-specific T cells. *Journal of Immunotherapy*. 33(1), 1–7 (2010).

4. Mehrotra S, Al-Khami A a, Klarquist J, *et al.* A coreceptor-independent transgenic human TCR mediates anti-tumor and anti-self immunity in mice. *Journal of immunology (Baltimore, Md. : 1950)*. 189(4), 1627–38 (2012).

5. Turtle CJ, Riddell SR. Genetically retargeting CD8+ lymphocyte subsets for cancer immunotherapy. *Current opinion in immunology*. 23(2), 299–305 (2011).

6. Durai M, Krueger C, Ye Z, *et al.* In vivo functional efficacy of tumor-specific T cells expanded using HLA-Ig based artificial antigen presenting cells (aAPC). *Cancer immunology, immunotherapy : CII*. 58(2), 209–20 (2009).

7. Oelke M, Schneck JP. Overview of a HLA-Ig based "Lego-like system" for T cell monitoring, modulation and expansion. *Immunologic Research*. 47, 248–56 (2010).

8. Smith-Garvin JE, Koretzky G a, Jordan MS. T cell activation. *Annual review of immunology*. 27, 591–619 (2009).

9. He C, Hu Y, Yin L, Tang C, Yin C. Effects of particle size and surface charge on cellular uptake and biodistribution of polymeric nanoparticles. *Biomaterials*. 31(13), 3657–66 (2010).

10. Decuzzi P, Godin B, Tanaka T, *et al.* Size and shape effects in the biodistribution of intravascularly injected particles. *Journal of controlled release : official journal of the Controlled Release Society*. 141(3), 320–7 (2010).

11. Semete B, Booysen L, Lemmer Y, *et al.* In vivo evaluation of the biodistribution and safety of PLGA nanoparticles as drug delivery systems. *Nanomedicine : nanotechnology, biology, and medicine*. 6(5), 662–71 (2010).

12. Sharma G, Valenta DT, Altman Y, *et al.* Polymer particle shape independently influences binding and internalization by macrophages. *Journal of Controlled Release*. 147(3), 408–412 (2010).

13. Champion J a, Walker A, Mitragotri S. Role of particle size in phagocytosis of polymeric microspheres. *Pharmaceutical research*. 25(8), 1815–21 (2008).

14. Manolova V, Flace A, Bauer M, Schwarz K, Saudan P, Bachmann MF. Nanoparticles target distinct dendritic cell populations according to their size. *European Journal of Immunology*. 38(5), 1404–13 (2008).

15. Mescher MF. Surface contact requirements for activation of cytotoxic T lymphocytes. *Journal of Immunology*. 149(7), 2402–5 (1992).

16. Steenblock ER, Wrzesinski SH, Flavell R a, Fahmy TM. Antigen presentation on artificial acellular substrates: modular systems for flexible, adaptable immunotherapy. *Expert opinion on biological therapy*. 9(4), 451–64 (2009).

17. Balmert SC, Little SR. Biomimetic delivery with micro- and nanoparticles. *Advanced materials (Deerfield Beach, Fla.)*. 24(28), 3757–78 (2012).

18. Hubbell J a, Thomas SN, Swartz M a. Materials engineering for immunomodulation. *Nature*. 462(7272), 449–60 (2009).

19. Anikeeva N, Lebedeva T, Clapp AR, *et al.* Quantum dot/peptide-MHC biosensors reveal strong CD8-dependent cooperation between self and viral antigens that augment the T cell response. *Proceedings of the National Academy of Sciences of the United States of America*. 103(45), 16846–51 (2006).

20. Boyle S, Kolin DL, Bieler JG, Schneck JP, Wiseman PW, Edidin M. Quantum Dot Fluorescence Characterizes the Nanoscale Organization of T Cell Receptors for Antigen. *Biophysical Journal*. 101(11), L57–L59 (2011).

21. Steenblock ER, Fahmy TM. A comprehensive platform for ex vivo T-cell expansion based on biodegradable polymeric artificial antigen-presenting cells. *Molecular therapy : the journal of the American Society of Gene Therapy*. 16(4), 765–72 (2008).

22. Kunzmann A, Andersson B, Thurnherr T, Krug H, Scheynius A, Fadeel B. Toxicology of engineered nanomaterials: Focus on biocompatibility, biodistribution and biodegradation. *Biochimica et biophysica acta*. 1810(3), 361–373 (2010).

23. Dobrovolskaia M a, McNeil SE. Immunological properties of engineered nanomaterials. *Nature nanotechnology*. 2(8), 469–78 (2007).

24. Nune SK, Gunda P, Majeti BK, Thallapally PK, Forrest ML. Advances in lymphatic imaging and drug delivery. *Advanced drug delivery reviews*. (2011).

25. Motta I, Lone YC, Kourilsky P. In vitro induction of naive cytotoxic T lymphocytes with complexes of peptide and recombinant MHC class I molecules coated onto beads: role of TCR/ligand density. *European journal of immunology*. 28(11), 3685–95 (1998).

26. Ge Q, Stone JD, Thompson MT, *et al.* Soluble peptide-MHC monomers cause activation of CD8+ T cells through transfer of the peptide to T cell MHC molecules. *Proceedings of the National Academy of Sciences of the United States of America*. 99(21), 13729–34 (2002).

27. Curtsinger J, Deeths MJ, Pease P, Mescher MF. Artificial cell surface constructs for studying receptor-ligand contributions to lymphocyte activation. *Journal of immunological methods*. 209(1), 47–57 (1997).

28. Hosken N, Shibuya K, Heath A, KM. The effect of antigen dose on CD4+ T helper cell phenotype development in a T cell receptor-alpha beta-transgenic model. *The Journal of*. 182(November), 20– 22 (1995).

29. Alexander-Miller M a, Leggatt GR, Sarin A, Berzofsky J a. Role of antigen, CD8, and cytotoxic T lymphocyte (CTL) avidity in high dose antigen induction of apoptosis of effector CTL. *The Journal of experimental medicine*. 184(2), 485–92 (1996).

30. González P a, Carreño LJ, Coombs D, *et al.* T cell receptor binding kinetics required for T cell activation depend on the density of cognate ligand on the antigen-presenting cell. *Proceedings of the National Academy of Sciences of the United States of America*. 102(13), 4824–9 (2005).

31. Bullock TNJ, Mullins DW, Engelhard VH. Antigen density presented by dendritic cells in vivo differentially affects the number and avidity of primary, memory, and recall CD8+ T cells. *Journal of Immunology*. 170(4), 1822–9 (2003).

32. Mescher MF, Popescu FE, Gerner M, Hammerbeck CD, Curtsinger JM. Activation-induced non-responsiveness (anergy) limits CD8 T cell responses to tumors. *Seminars in cancer biology*. 17(4), 299–308 (2007).

33. Oelke M, Maus MV, Didiano D, June CH, Mackensen A, Schneck JP. Ex vivo induction and expansion of antigen-specific cytotoxic T cells by HLA-Ig–coated artificial antigen-presenting cells. *Nature medicine*. 9(5), 619–625 (2003).

34. Altman J, Davis M. MHC □Peptide Tetramers to Visualize Antigen Specific T Cells. *Current Protocols in Immunology*. , 1–33 (2003).

35. Fifis T, Gamvrellis A, Crimeen-Irwin B, *et al.* Size-dependent immunogenicity: therapeutic and protective properties of nano-vaccines against tumors. *Journal of Immunology*. 173(5), 3148–54 (2004).

36. Cai S, Yang Q, Bagby TR, Forrest ML. Lymphatic drug delivery using engineered liposomes and solid lipid nanoparticles. *Advanced drug delivery reviews*. 63(10-11), 901–08 (2011).

37. Lebowitz MS, O'Herrin SM, Hamad a R, *et al.* Soluble, high-affinity dimers of T-cell receptors and class II major histocompatibility complexes: biochemical probes for analysis and modulation of immune responses. *Cellular Immunology*. 192(2), 175–84 (1999).

38. Moon JJ, Huang B, Irvine DJ. Engineering nano- and microparticles to tune immunity. *Advanced materials (Deerfield Beach, Fla.)*. 24(28), 3724–46 (2012).

39. Dustin ML. T-cell activation through immunological synapses and kinapses. *Immunol. Rev*. 221, 77–89 (2008).

40. Chang JT, Palanivel VR, Kinjyo I, *et al.* Asymmetric T lymphocyte division in the initiation of adaptive immune responses. *Science*. 315(5819), 1687–91 (2007).

41. Varma R, Campi G, Yokosuka T, Saito T, Dustin ML. T cell receptor-proximal signals are sustained in peripheral microclusters and terminated in the central supramolecular activation cluster. *Immunity*. 25, 117–127 (2006).

42. Lillemeier BF, Mörtelmaier M a, Forstner MB, Huppa JB, Groves JT, Davis MM. TCR and Lat are expressed on separate protein islands on T cell membranes and concatenate during activation. *Nature Immunology*. 11(1), 90–6 (2010).

43. Nel AE, Mädler L, Velegol D, *et al.* Understanding biophysicochemical interactions at the nano-bio interface. *Nature materials*. 8(7), 543–57 (2009).

44. Fahmy TM, Bieler JG, Edidin M, Schneck JP. Increased TCR avidity after T cell activation: a mechanism for sensing low-density antigen. *Immunity*. 14(2), 135–43 (2001).

45. Kumar R, Ferez M, Swamy M, *et al.* Increased Sensitivity of Antigen-Experienced T Cells through the Enrichment of Oligomeric T Cell Receptor Complexes. *Immunity*. 35(3), 375–87 (2011).

46. Reddy ST, Van der Vlies AJ, Simeoni E, *et al.* Exploiting lymphatic transport and complement activation in nanoparticle vaccines. *Nature biotechnology*. 25(10), 1159–64 (2007).

47. Maeda H. The enhanced permeability and retention (EPR) effect in tumor vasculature: the key role of tumor-selective macromolecular drug targeting. *Advances in enzyme regulation*. 41(00), 189–207 (2001).

48. Greish K. Enhanced permeability and retention of macromolecular drugs in solid tumors: a royal gate for targeted anticancer nanomedicines. *Journal of drug targeting*. 15(7-8), 457–64 (2007).

49. Rabinovich G a, Gabrilovich D, Sotomayor EM. Immunosuppressive strategies that are mediated by tumor cells. *Annual review of immunology*. 25, 267–96 (2007).

50. Schneck JP, Slansky JE, O'Herrin SM, Greten TF. Monitoring antigen-specific T cells using MHC-Ig dimers. *Current protocols in immunology / edited by John E. Coligan ... [et al.]*. Chapter 17, Unit 17.2 (2001).

51. Chiu Y-L, Schneck JP, Oelke M. HLA-Ig based artificial antigen presenting cells for efficient ex vivo expansion of human CTL. *Journal of visualized experiments : JoVE*. (50), 1–5 (2011).

4 Magnetic Field-Induced T Cell Receptor Clustering By Nanoparticles Enhances T Cell Activation and Stimulates Anti-Tumor Activity In Vivo

4.1 Introduction

Nanoparticles functionalized with surface ligands are frequently used for targeted delivery of drugs, proteins, and genes to cells bearing specific receptors[1,2]. Since receptor binding can trigger downstream signaling in the target cell, nanoparticle engagement of membrane receptors can also be used to directly induce biological responses.

We have previously described nanoscale artificial Antigen Presenting Cells (nano-aAPC), 50-100 nm in diameter, as the first nanoparticles shown to initiate antigen-specific T cell activation by presenting peptide in the context of Major Histocompatability Complex (MHC) to cognate T cell receptors (TCR)[3]. While TCR-MHC interactions have been extensively studied for MHC presented on cells[4] and cell-sized, MHC-coated particles[5–8], receptor-ligand interactions at the cell-nanoparticle interface are not well understood and are likely to have unique properties[9]. For example, T cell activation induces a state of persistently enhanced nanoscale TCR clustering[10–13] and nanoparticles might be sensitive to this clustering in a way that larger particles are not.

Furthermore, nanoparticle interactions with TCR clusters could be exploited to control or enhance receptor triggering. T cell activation is mediated by aggregation of signaling proteins[14], with ‘signaling microclusters’, 100’s of nms across, initially forming at the periphery of the T cell-APC contact site and migrating inward[15]. We hypothesized that an

external magnetic field could drive aggregation of paramagnetic nano-aAPC bound to TCR, resulting in aggregation of TCR clusters and enhanced activation of naïve T cells.

Magnetic bead clustering has been used to study effects of mechanical stress[16] and receptor clustering[17,18] in a variety of systems. Magnetic fields can exert appropriately strong forces on paramagnetic particles, but are otherwise biologically inert, making them a powerful tool to control particle behavior[19,20]. In our approach, T cells bound to paramagnetic nano-aAPC are activated in the presence of an externally applied magnetic field. Nano-aAPC are thus themselves magnetized, and will be attracted to both the field source and to nearby nanoparticles in the field[17,20], inducing bead and thus TCR aggregation to boost aAPC-mediated activation.

We show that nano-aAPC bound more TCR on and induced greater activation of previously activated compared to naive T cells. Application of an external magnetic field induced aAPC aggregation on naive cells, enhancing T cells proliferation *in vitro* and following adoptive transfer *in vivo*. In a melanoma adoptive immunotherapy model, T cells activated by nano-aAPC in a magnetic field mediated greater tumor rejection than T cells activated by nano-aAPC alone.

4.2 Methods

Mice and reagents

2C TCR transgenic mice were maintained as heterozygotes by breeding on a C57/BL6 background. Pmel TCR/Thy1^{a} Rag-/- transgenic mice were a gift from Nicholas Restifo (National Institutes of Health, Bethesda, MD) and maintained as homozygotes. C57BL/6j mice were purchased from Jackson Laboratories (Bar Harbor, ME). All mice were maintained according to Johns Hopkins University's Institutional Review Board. Fluorescently labeled monoclonal antibodies were purchased from BioLegend (San Diego, CA).

Preparation of MHC-Ig Dimers and Nano-aAPC

Soluble MHC-Ig dimers, K^b-Ig and D^b-Ig, were prepared and loaded with peptides as described[5],see supplementary methods. Nano-aAPC were manufactured by direct conjugation of MHC-Ig dimer and anti-CD28 antibody (37.51; BioLegend) to MACS Microbeads (Miltenyi Biotec) as described[3]. Protein bound to nanoparticles was measured by fluorescence as described in supplementary methods.

In Vitro Cell Expansion

Cells were obtained from homogenized mouse spleens and lymph nodes followed by hypotonic lysis of RBC. Cytotoxic lymphocytes were isolated using a CD8 no-touch isolation kit and magnetic enrichment column from Miltenyi Biotec (Cologne, Germany). CD44-biotin antibody was added to primary cocktail to isolate CD44lo, naive cells. Where applicable, cells were labeled with carboxyfluorescein succinimidyl ester (CFSE) for 15 minutes at 37^{o}C, then washed extensively.

CD8+ T cells and nano-aAPC, at the indicated dosages, were mixed and cultured in 24 well flat-bottom or 96 well round bottom plates for 4-7 days in complete RPMI media supplemented with T cell factor (TF), a cytokine enriched cocktail of conditioned media harvested from stimulated human PBMC [21]. Where indicated, culture plates were fixed between two Neodynium N52 disk magnets between ¼ and ¾ inches in length (K&J Magnetics, Jamison, PA). CFSE fluorescence was measured at indicated timepoints using a BD FacsCalibur flow cytometer and analyzed in FlowJo (TreeStar). Fold expansion was assessed by cell counts seven days after stimulation. Expansion of endogenous antigen-specific cells was assessed by staining with 400 nM fluorescently labeled MHC-Ig dimer seven days after activation.

Particle Binding Assays

For equilibrium particle binding assays, $CD8^+$ T cells were incubated at 4°C at a concentration of 10^7cells/ml in FACS wash buffer (PBS + 2% FCS + .05% sodium azide). 30 μl aliquots of cells were mixed with varying concentrations of nanoparticles bearing fluorescently labeled MHC-Ig dimer for 60-90 min. After washing, cell-bound fluorescence was measured by flow cytometer and MCF (mean channel fluorescence) was calculated using FlowJo.

For particle off-rate binding assays, cells and a saturating dose of nanoparticle or soluble MHC-Ig dimer were bound to steady-state as described above. MCF was measured at Time 0, followed by the addition of excess clonotypic 1B2 blocking antibody to prevent re-binding. MCF was measured at the indicated timepoints, and effective off-rate was calculated for exponential decay in GraphPad Prism (La Jolla, CA). Cell-particle contacts were estimated as described in **Table 2**.

Microscopy

T cells were bound to nano-aAPC for 60 minutes at 4ºC. Cells were subsequently transferred to a 96-well plate at 37ºC in the presence or absence of a magnetic field generated by Neodymium N52 disk magnets. After 30 minutes, cells were washed and stained at 4ºC with Alexa488 anti-LFA1, monoclonal PE anti-mouse IgG1, and Alexa 647 anti-CD3ε. Samples were washed and fixed immediately with 2% paraformaldehyde. Images were acquired on a Zeiss LSM 510 META (Zeiss, Oberkochen, Germany) laser scanning confocal at 100x magnification at the Johns Hopkins School of Medicine Microscopy Facility. CD3ε cluster size was determined using a particle-detection algorithm written in ImageJ (National Institutes of Health) using the built-in Particle Analyzer.

Effect of Nano-aAPC on In Vivo T cell Expansion and Inhibition of Subcutaneous Tumor Growth

CD44lo, CD8+ cells were isolated from pmel spleen and lymph nodes using a magnetic

enrichment column and activated for 24 hours in the presence or absence of a magnetic field as described above. 1 $\times 10^6$ Thy1.1+ pmel cells were adoptively transferred into B6 Thy1.2+ wild type hosts (n = 6 mice per group). Mice were treated both the day of and the day after adoptive transfer with 30,000 units intraperitoneal IL-2. Seven and twenty-days after adoptive transfer, three mice per group were sacrificed and lymphocytes were isolated from peripheral blood, spleen, and inguinal, cervical, and axillary lymph nodes, and then stained with anti-Thy1.1 antibody.

Tumor rejection experiments were performed as above, except $3x10^5$ B16 melanoma cells were injected subcutaneously ten days prior to T cell adoptive transfer. Transient lymphopenia was induced by sublethal irradiation (500 cGy) one day before adoptive transfer with a MSD Nordion Gammacell dual Cs137 source (Johns Hopkins Molecular Imaging Center) as irradiation induced lymphopenia is thought to remove immunosuppressive host cells and reduce competition for lymphotrophic cytokines[22], and significantly enhances the effect of immunotherapy for melanoma in clinical trials[23]. Tumor growth was monitored at 2 day intervals using digital calipers, until tumor size was ~150 mm^2, at which point animals were euthanized.

Preparation of MHC-Ig Dimers

Soluble MHC-Ig dimers, K^b-Ig and D^b-Ig, were prepared and loaded with peptide as described [2]. Briefly, K^b-Ig molecules were loaded with peptide by stripping at alkaline condition (pH 11.5), and then refolded in the presence of 50 fold excess peptide. D^b-Ig molecules were stripped under mildly acidic conditions (pH 6.5) and refolded in the presence of 50 fold molar excess peptide and 2-fold molar excess of human β_2-microglobulin [3]. Peptides SIY (SIYRYYGL, synthetic), SIIN (SIINFEKL, derived from ovalbumin protein), GP100 (KVPRNQDWL, from melanocyte GP100 protein) and ASN (ASNENMETH, from influenza A nucleoprotein) were

purchased from Genscript (Piscataway, NJ). Protein concentration was determined after labeling by size exclusion high performance liquid chromatography (HPLC).

Micro-aAPC Synthesis

Micro-aAPCs were fabricated as described previously[4] by direct chemical coupling of protein to 4.5 μm Dynal Magnetic Microbeads (Life Technologies, Carlsbad, CA). For the initial coupling step, 25 μg anti-biotin antibody (Sigma, St. Louis, MO) was added to 100 million microbeads in 0.1 M sodium borate buffer. After washing in a magnetic column, biotin labeled MHC-Ig and CD28 were added in equimolar amounts to form aAPC.

Nanoparticle Tracking Analysis

A Nanosight LM10 equipped with a sensitive CCD camera was used for characterizing the size distribution of nano-aAPC by NTA. 50 μL of diluted nanoparticle solution was loaded into the sample chamber, which was connected to a 405 nm laser source. A 60 s movie containing the Brownian motion tracking of the scattering centroids (particles) was recorded using NTA software (Version 2.0). The movie was processed using the manufacturer recommended auto settings with manual adjustment of the gain, blur and brightness as recommended. The nanoparticle solution was diluted in phosphate buffered saline to adjust the sample concentration to 5×10^{12} particles mL^{-1}.

4.3 Results

Nano-aAPC Preferentially Stimulate Activated T Cells

T cell stimulation requires two activating signals delivered by endogenous APC: signal 1, a cognate antigenic peptide presented in the context of MHC that binds the TCR, and signal 2, one of a number of co-stimulatory receptors that modulate T cell responses[24]. Nano-aAPC are

synthesized by coupling chimeric MHC-Ig dimer (signal 1) and anti-CD28 antibody (signal 2) to 50-100 nm paramagnetic iron-dextran nanoparticles (**Figure 4.1A**), which were selected as a nanoscale particle platform due to their extensive characterization and biocompatibility[25]. Protein coupling to particles was characterized by labeling with a fluorescent antibody against the protein of interest (**Figure 4.2**). Nano-aAPC present 13 ± 3 MHC-Ig dimers and 12 ± 5 anti-CD28 antibodies per particle, for a protein density of 96 ± 10 and 92 ± 12 protein/ μm^2, respectively (**Table 5.1**).

To compare stimulation of naive versus activated T cells, we used CD44 depleted naive CD8+ splenocytes isolated from either pmel TCR or 2C TCR transgenic mice as a source of homogenous naïve T cells with defined antigenic specificities (**Figure 4.3A**). Activated cells were generated by stimulating CD8+ splenocytes for seven days with soluble peptide, GP100 for pmel T cells and SIY for 2C T cells.

Three days after stimulation with a low dose of nano-aAPC, 8 ng total MHC-Ig, naive pmel T cells had not proliferated as measured by CFSE (**Figure 4.1B - left**), a vital dye that is diluted with each cell division. At the same dose, however, activated cells proliferated robustly (**Figure 4.1B – right**). Nano-aAPC titration showed that naive cells had a higher threshold for nano-aAPC-induced proliferation (8-10 ng of total MHC-Ig) than activated cells (less than 1.5 ng of total MHC-Ig) (**Figure 4.1C**).

As control for aAPC size, we assessed T cell proliferation induced by cell-sized, 4.5 μm diameter iron-dextran micro-aAPCs. Micro-aAPC induced naive T cell proliferation at lower doses (1.5-8 ng MHC-Ig) than nano-aAPC as measured by CFSE dilution on day 3 (**Figure 4.3B**), with approximately 10-20 fold expansion on day 7 (**Figure 4.3C**).

Thus, while activated cells respond equivalently to nano- and micro-aAPC, naive cells have a higher threshold for nano-aAPC based stimulation. This difference was not driven by differences in protein density between micro- and nano-aAPCs, as micro-aAPCs with higher density (HD) and lower density (LD) than nanoparticles based aAPC induced identical proliferation when normalized for total MHC-Ig (**Figure 4.3D-E**). Since response was sensitive to particle size, we hypothesized that the difference in responses was due to differences in nanoparticle interactions with TCR nanoclusters on naive versus activated cells.

Nano-aAPC Bind More TCR on Activated Than Naive Cells

To examine nanoparticle binding to TCR, we synthesized nanoparticles bearing MHC-Ig alone, thus removing the binding contribution of anti-CD28. Binding experiments were performed on naive and activated T cells, which bound nanoparticles bearing cognate MHC-Ig specifically and with low background (**Figure 4.4A**).

Nanoparticles were bound to naive and activated cells to equilibrium, followed by the addition of the anti-clonotypic 1B2 blocking antibody to prevent re-binding. Nanoparticles showed faster disassociation from naive cells (half life of 531 seconds ± 149) than activated cells (984 s ± 221) (**Figure 4.1D, Table 5.2**).

Disassociation rates can be used to estimate the number of contacts between cells and multivalent ligands, with more contacts leading to slower disassociation[26]. Nanoparticle disassociation from cells was modeled as an exponential stochastic process, with disassociation of soluble MHC-Ig dimer used to derive parameters and validate the approach (see **Table 5.2** for details). The off-rate of a single TCR-MHC contact was measured for soluble MHC-Ig dimer binding to naive cells (**Figure 4.4C**), which is effectively monovalent[10]. As expected, MHC-Ig

dimers disassociated more slowly from activated cells, leading to 1.7 estimated contacts (**Figure 4.1E**), consistent with previous reports[10,26].

Nanoparticle disassociation from naive cells was significantly slower than free MHC-Ig (**Figure 4.4C**), and 2-fold slower from activated cells than naive. Nano-aAPC thus made an estimated 6.8 contacts with naive cells, compared to approximately double (12.6) on activated cells **(Figure 4.1E, Table 5.2**). These numbers represent 11% and 22% of MHC-Ig dimers, respectively, attached to the surface of nano-aAPC.

Increased TCR-MHC contacts per particle could lead to fewer available TCR, inhibiting binding and limiting the total amount of nanoparticles that bind to an individual cluster. Consistent with this prediction, activated cells bound two-fold fewer nanoparticles at equilibrium than naive cells across a wide range of particle concentrations (**Figure 4.1F**). This difference was not due to T cell receptor expression, which was equivalent on naive and activated T cells (**Figure 4.3B**).

Together the two-fold increase in total nano-aAPC bound and two-fold decrease of the TCR-MHC contacts engaged by naive cells suggest the binding model shown schematically in **Figure 4.1G**. Naive cells bind more nano-aAPC utilizing fewer MHC contacts due to the small scale of TCR clusters prior to cell-nanoparticle contact. Activated cells, in contrast, bind fewer nanoparticles because each particle makes contact with more TCR.

Magnetic Fields Drive Aggregation of aAPC and TCR/CD3

Based on the hypothesis that nano-aAPC bound to small scale TCR clusters, we took advantage of nanoparticle binding to T cells to control TCR cluster aggregation, and thus T cell activation. An exogenous magnetic field was used to drive aggregation of paramagnetic nano-aAPC bound to naive cells. Nano-aAPC were bound to naive T cells at 4^{o}C, then cultured at 37 ^{o}C between

two neodymium disk magnets generating a maximum field strength of 0.2 T. We predicted that, in an external magnetic field, paramagnetic iron-dextran aAPC would be magnetically polarized and attracted to each other[18], driving aggregation of TCR (**Figure 4.5A**).

Cluster formation was assessed by confocal microscopy. After one hour of binding at 4^{o}C, we either stained and fixed cells immediately (Time 0), or transferred cells to a 37 ^{o}C incubator for 30 minutes in the absence or presence of a magnetic field. Cells were then stained with antibodies against LFA-1 (green), an adhesion molecule used as a control; CD3ε (magenta), a signaling component associated with TCR; and MHC-Ig (red), to visualize the nano-aAPC. Finally, cells were fixed and imaged.

Prior to incubation at 37^{o}C, aAPC and CD3ε were distributed in a punctate pattern on the membrane, with small clusters diffusely distributed across the cell surface (Time 0, **Figure 4.5B top left**). LFA-1 was uniformly distributed across the cell. The LFA-1 and CD3ε staining patterns were identical to those at Time 0 after thirty minutes of incubation with non-cognate K^{b}-SIINF particles (Non-Cognate, **Figure 4.5B top right**). In the absence of a magnetic field, incubation with cognate nano-aAPC did not drastically alter the distribution of either LFA-1, aAPC, or CD3ε (No Magnet, **Figure 4.5B bottom left**). However, after 30 minutes in a magnetic field, large aggregates of nano-aAPC formed on the membrane (Magnet, **Figure 4.5B bottom right**). These clusters of nano-aAPC co-localized with similarly sized clusters of CD3ε. The control molecule LFA-1 maintained a diffuse pattern across the membrane, indicating that CD3ε aggregation was due to its association with aAPC.

To characterize the size and number of aggregates induced by aAPC, a particle-identification program was developed in ImageJ. The program was able to identify both diffuse, punctuate

clusters from Time 0 cells (**Figure 4.5C left**), and larger aggregates induced by magnetic fields (**Figure 4.5C right**).

Incubation in a magnetic field significantly increased TCR aggregation, beyond that seen after incubation with nano-aAPC alone, and led to larger CD3 complex aggregates on cells. Mean cluster area prior to incubation at 37°C was 0.30 ± 0.03 μm^2, and this did not change after incubation with non-cognate nano-aAPC (**Figure 4.5D**). aAPC alone increased cluster size to a mean of 0.52 ± 0.06 μm^2 ($p<0.001$). Clustering was further enhanced in a magnetic field to a mean size of 0.73 ± 0.11 μm^2 ($p<0.001$ compared to No Magnet). The mean number of clusters per cell decreased from 6.5 ± 0.6 at Time 0 to 3.0 ± 0.2 with a magnetic field (**Figure 4.5E**). Nano-aAPC disassociation rate after culture in a magnetic field did not increase (**Figure 4.4D**), suggesting aggregate formation was not associated with an increase in TCR/MHC contacts, but rather aggregation of TCR nanoclusters bound to aAPC. In summary, aAPC aggregation induced by a magnetic field led to a 2-fold increase in TCR/CD3 aggregate size and a 2-fold decrease in the number of aggregates per cell.

Activation in a Magnetic Field Enhances Proliferation of Naïve T cells

To assess whether activation of T cells by aAPC was enhanced by culture in a magnetic field, CFSE-labeled pmel T cells were incubated with increasing doses of Db-GP100 nano-aAPC and cultured with or without an external magnetic field. Naïve T cells proliferated in a magnetic field at doses of nano-aAPC that induced minimal proliferation otherwise (**Figure 4.6A**). After incubation with nano-aAPC bearing 5 ng MHC-Ig, 29% of cells in culture had proliferated, compared to 89% of cells in a magnetic field. Proliferation at day 7 was up to 4 fold greater

compared to no magnet controls (**Figure 4.6B**). Culture in a magnetic field without aAPC did not lead to T cell proliferation (*data not shown*).

The duration and strength of magnetic field stimulation required for optimal expansion were assessed by the addition and removal of neodymium magnets of varying size. One to three hours in a magnetic field **(Figure 3C-3D)** and a field strength of 0.2 T or more **(Figure 4.6E-5.6F; Figure 4.7)** drove 10-fold T cell expansion after one week.

Magnetic field enhanced aAPC stimulation also enhanced expansion of antigen-specific T cells from endogenous, polyclonal T cell populations. We synthesized nano-aAPC bearing the Kb-Ig dimer loaded with the Trp2 peptide, which is specific for the Trp2 melanoma antigen. CD8+ splenocytes from wild type B6 mice were cultured with a limiting dose of aAPC and, after seven days, antigen-specific T cells were analyzed . Nano-aAPC alone, at this dose, did not induce expansion of antigen-specific T cells, as determined by comparing cognate Kb-Trp2 binding to non-cognate Kb-SIINF binding (Figure 3G and **Figure 4.8**). When incubated with T cells in a magnetic field, however, aAPC generated approximately 3.4% antigen specific T cells after a single week (**Figure 4.6G**). This resulted in approximately 36,000 Trp-2 specific cells generated from a pool of $10x10^6$ precursor cells (**Figure 4.6H**). With CD8 precursor frequencies estimated to be on the order of 10-800 per 10 million[27], this suggests 450 to 3,600-fold expansion in culture, comparable to the 1000-fold precursor expansion seen with viral infection *in vivo*[28].

Magnetic Field Enhanced T cell Activation for Adoptive Immunotherapy

The potential for enhancing stimulation of antigen-specific cells led us to study magnetic field enhanced aAPC stimulation prior to adoptive transfer *in vivo*. Thy 1.1+ pmel T cells were activated *in vitro* with aAPC in the presence or absence of a magnetic field and adoptively

transferred into wild type, Thy1.2+ recipient mice (see schematic **Figure 4.9A**). Seven or twenty-one days after adoptive transfer, mice were sacrificed and assessed for adoptively transferred, Thy1.1+ cells.

Magnetic field enhanced nano-aAPC stimulation resulted in robust expansion of the transferred T cell population. On day 7, 3.1% of T cells in the spleen were Thy1.1+ for T cells stimulated in a magnetic field, compared with 0.6% for cells stimulated with aAPC but no magnetic field, and 0.2% for untreated T cells alone that were not stimulated prior to adoptive transfer ($p<0.01$, **Figure 4.9B-C**). The largest percentage of cells was observed in the spleen on day 7 (**Figure 4.9C**). The total Thy1.1+ cells in all organs examined reached approximately 1×10^6 for the magnetic field enhanced group (**Figure 4.9D**) on day 7, compared to less than 2×10^5 for the no magnet group. This 5-fold enhancement was roughly consistent with the enhancement seen *in vitro*. While fewer cells were seen on day 21, T cells activated by aAPC in a magnetic field established a detectable population in lymph nodes (0.15%), compared to 0.04% from T cells activated by aAPC alone and 0.01% from cells that were not stimulated at all ($p<0.05$, **Figure 4.9B-D**).

The functional consequences of magnetic field enhanced T cell stimulation were studied by treatment of B16 melanoma, a poorly immunogenic tumor with a high threshold for immune rejection[29]. Pmel T cells were adoptively transferred into mice bearing established subcutaneous B16 tumors ten days after tumor injection (**Figure 4.9E**) and transient lymphopenia was induced by sublethal irradiation (500 cGy) of mice one day before adoptive transfer as per standard approaches to adoptive immunotherapy[22,23].

Tumor-specific T cells activated by aAPC in a magnetic field strongly inhibited tumor growth compared to no treatment controls, T cells alone and T cells stimulated by aAPC without a magnetic field ($p<0.0001$ treatment effect by two-way ANOVA, **Figure 4.9F**). At day 18, mice treated with magnetic field enhanced T cells had 8 to 10-fold smaller tumors than untreated or no magnet T cell treated mice. Similarly, magnetic field enhanced T cells significantly improved host survival, with 6/8 mice surviving and 4/8 having no detectable tumor at Day 28 post injection ($p<0.001$, Mantel-Cox, **Figure 4.9F**).

4.4 Discussion

Receptor triggering by nanoparticles depends on poorly understood interactions at the membrane-nanoparticle interface[9], with unique features not present in other systems. We demonstrate that nanoparticles but not cell-sized particles are sensitive to TCR clustering controlled by the T cell activation state. Based on this hypothesis, we show that an applied magnetic field leads to aggregation of TCR clusters, and in turn enhanced T cell proliferation *in vitro* and *in vivo*. Thus, nanoscale T cell activation platforms can be used to sense and manipulate the spatial organization of the T cell membrane.

Particle size considerations also include the high degree of local curvature on a nanoparticle compared to microparticle surface, which limits the interaction of neighboring ligands with the cell membrane. Furthermore, cell-sized platforms may mimic the stable contact surface and directional cues observed during cell-cell contact, as seen during asymmetric cell division[30,31] or immune synapse formation[32]. In contrast to micron-sized interactions, many nanoparticles can engage a single cell, providing multi-directional spatial cues with no single contact surface. These features motivate the design of approaches like magnetic clustering, which both compensate for the weaknesses and exploit the unique strengths of nanoscale particles.

Despite the challenges of designing nanoparticle platforms, their biocompatibility makes them a preferred platform for adoptive immunotherapy, as they are less likely than larger particles to induce tissue infarction or inflammation when co-injected intravenously with T cells[33]. Iron-dextran nanoparticles are available in GMP-grade formulations, and cell isolation using magnetic enrichment followed by infusion is already a staple of cellular therapy[34,35]. The magnetic

fields generated for cell isolation are stronger than those used in this study, and magnet induced receptor aggregation could thus be incorporated into already-existing immunotherapy protocols.

The use of nano-aAPC with an applied magnetic field allowed us to activate naive T cell populations, which were otherwise poorly responsive to stimulation. Naive T cells have been shown to be more effective than more differentiated subtypes for cancer immunotherapy[36–38], with higher proliferative capacity and greater ability to generate strong, long-term T cell responses. However, naive precursors are rare, at approximately 1 in 10^5 CD8+ cells[39], and there exists a need for methods that can rapidly generate large numbers of antigen specific cells without repeated stimulation, which exhausts proliferative capacity[40]. Thus, nano-aAPC could potentially be coupled to magnetic enrichment protocols to increase the yield of antigen-specific T cells expanded from naive precursors, improving cellular therapy for cancer.

4.5 Figures

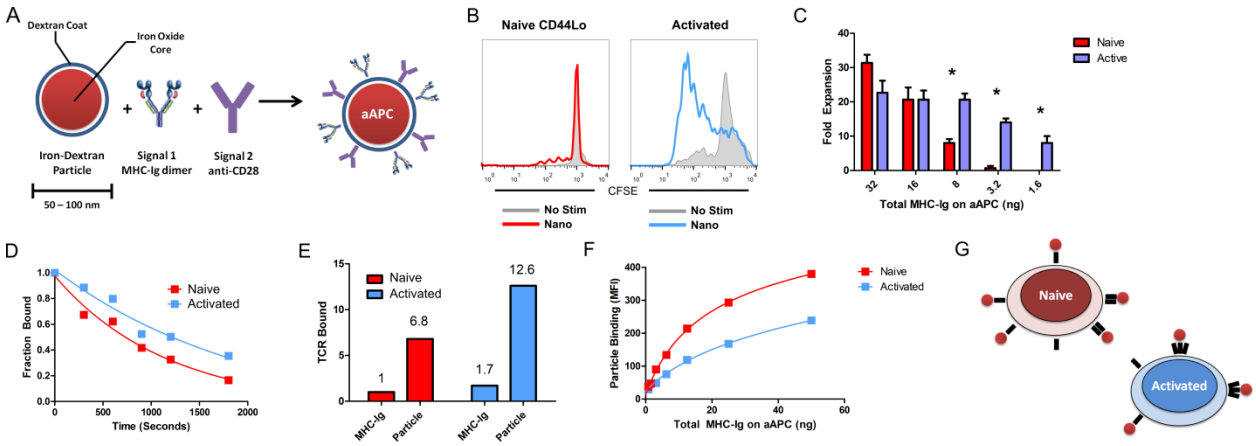

Figure 4.1: Nano-aAPC Binding to Naive and Activated Cells

(A) Schematic of nano-aAPC synthesis by coupling MHC-Ig dimers and co-stimulatory anti-CD28 to iron-dextran nanoparticles. (B) Proliferation of naive (left) and activated (right) pmel T cells measured by CFSE dilution 3 days after stimulation with nano-aAPC presenting 8 ng of Db-GP100 to 10^6 T cells. Unstimulated controls are shown in grey. (C) Naive (red) and activated (blue) cells were counted to measure fold expansion seven days after stimulation with titrated doses of nano-aAPC. Nano-aAPC presenting 8 ng or less of MHC-Ig induced minimal proliferation in naive cells (*, $p < 0.01$) compared to activated T cells. (D) Disassociation of Alexa-647, Kb-SIY labeled nanoparticles; time 0 represents addition of 1B2 blocking antibody to prevent re-binding. Data representative of three experiments, see Supplementary Table 1. (E) Mean TCR-MHC contacts made between Kb-SIY dimers (MHC-Ig) and Kb-SIY nanoparticles (Particle) with naive (red) and activated (blue) cells as estimated from disassociation data (see Supplementary Table 1). (F) Equilibrium binding of increasing doses of nano-aAPC (measured by total MHC-Ig presented) to naive (red) and activated (blue) cells. (G) A binding model that explains increased equilibrium binding and increased particle off-rate observed with naive cells. Naive cells bind more beads with fewer contacts per bead than activated cells.

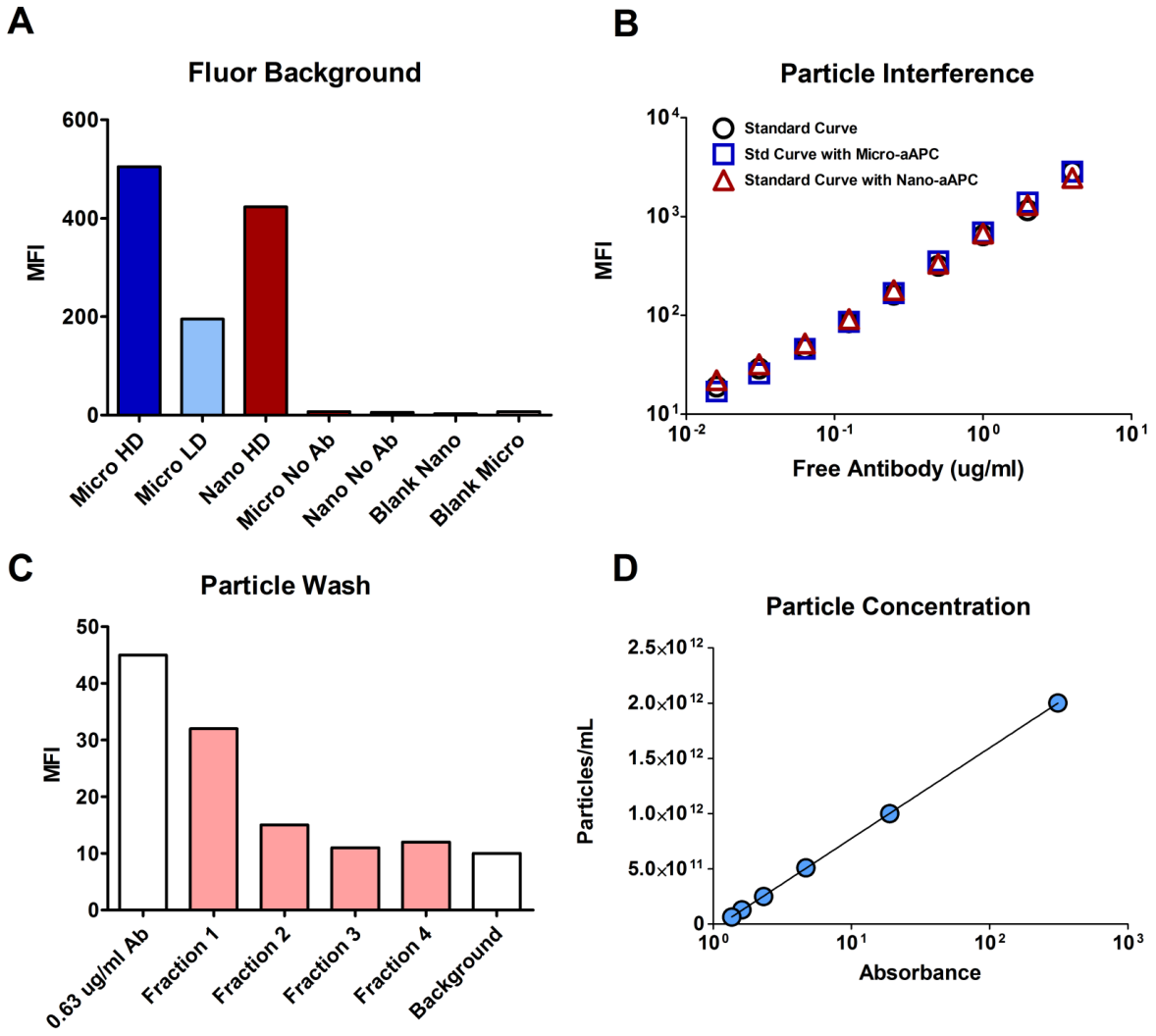

Figure 4.2. Characterization of Protein Bound to Nano- and Micro-aAPC By Fluorescence.

(A) Mean fluorescence intensity (MFI) of antibody bound to nanoparticles and controls. Nano-aAPC and Micro-aAPC (cell-sized) particles were incubated with excess of monoclonal anti-mouse IgG1 (for MHC-Ig) and anti- antibody conjugated with PE for 30 minutes, and washed on a magnetic column. Fluorescent antibody bound to particles was detectable above background samples, including micro- and nano- particles not stained with anti-IgG1 (No Ab) and particles which were not coupled to protein and stained with anti-IgG1 (Blank). Protein concentration in solution was determined by comparison to an IgG1-PE standard curve. Fluorescence is shown for anti-IgG1 and is representative of three experiments. HD – High Density. LD – Low Density. (B) Particles in solution do not interfere with antibody fluorescence. Soluble anti-IgG1 PE antibody was titrated and measured for fluorescence. Similar fluorescence emission was observed when soluble antibody was measured in the presence of blank micro- and nano-particles. (C) Washing in magnetic column was sufficient to remove free antibody. After three washes (Fraction 3), fluorescence is not detectable above background. Fluorescence of 0.63

ug/ml free antibody is provided for comparison. (D) Nanoparticle concentration was characterized by iron absorbance at 405 nm. Particle concentrations were determined by Nanoparticle Tracking Analysis. Titrations of nanoparticles were measured for absorbance and a standard curve was calculated to determine particle concentration.

Table 4.1

Particle	Particle Mean Diameter (μm)	MHC-Ig Dimers per Particle	MHC-Ig Density (protein/ μm^2)	Anti-CD28 per Particle	Anti-CD28 Density (protein/ μm^2)
Nano-aAPC	0.1	13 ± 3	96 ± 10	12 ± 5	92 ± 12
Kb-SIY Alone Nanoparticle	0.1	29 ± 6	214 ± 12	--	--
Micro HD	4.5	49,900 ± 2800	196 ± 11	27,200 ± 4600	107 ± 18
Micro LD	4.5	15,300 ± 1000	60 ± 11	14,400 ± 4500	56 ± 17

The amount and density of MHC-Ig and anti-CD28 on the surface of micro- (cell-sized) and nano-aAPC. Protein was quantified as described in Supplementary Figure 1, and particle concentration determined by counts (micro-aAPC) or Nanoparticle Tracking Analysis (nano-aAPC). High (HD) and low (LD) density particles were synthesized by varying amount of protein per particle during synthesis. Signal 1 nanoparticles were synthesized without anti-CD28.

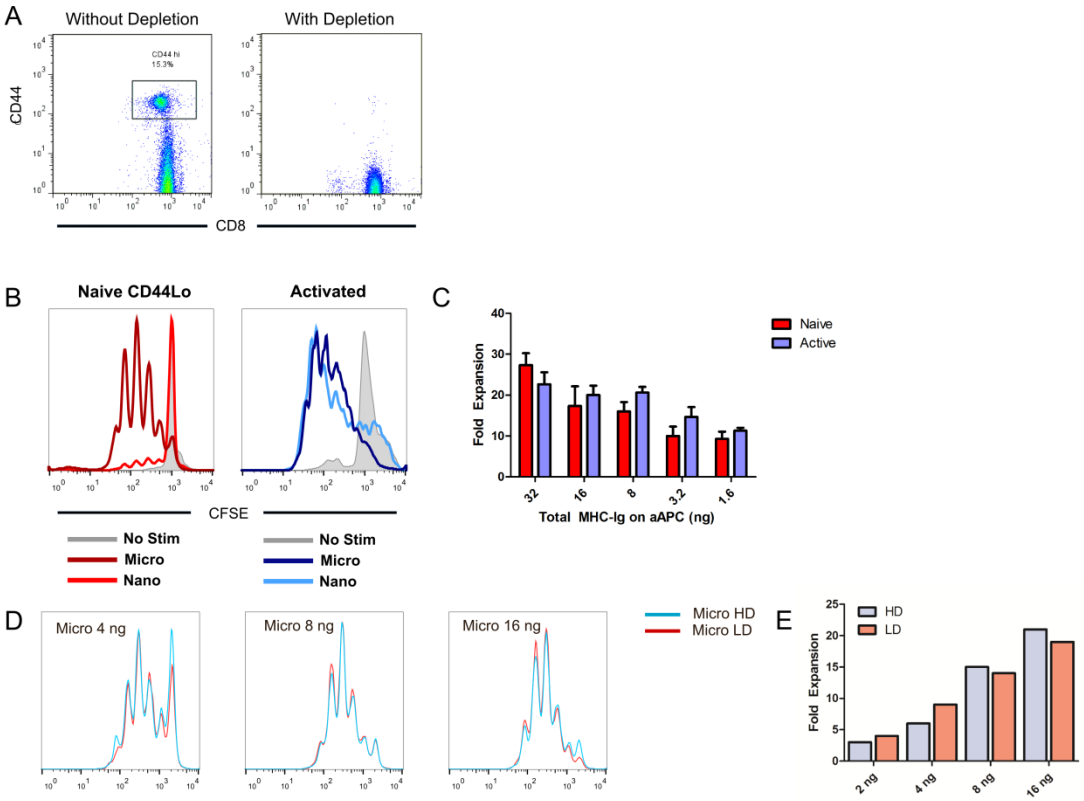

Figure 4.3. pMEL T cell Proliferation Induced by Micro-aAPC

(A) CD8+ pMEL splenocytes include a population of memory-phenotype, CD44 positive cells (representative percentage shown as percentage of CD8, left). CD44lo naive cells were isolated by a no-touch negative selection enrichment with anti-CD44 antibody in a magnetic enrichment column. (B) Proliferation of Naive CD44lo (left) and activated (right) cells by CFSE dilution stimulated three days with micro-aAPC (dark red and blue lines) and nano-aAPC (light red and blue lines) or unstimulated (grey lines). Micro- and nano-aAPC were used at doses presenting equivalent total amount of MHC-Ig (8 ng). Nano-aAPC data are re-produced from Figure 1. (C) Proliferation of naive (red) and active (blue) cells seven days after stimulation with indicated doses of micro-aAPC. (D) Effect of MHC-Ig density on micro-aAPC induced stimulation. High density (HD, blue) and low density (LD, red) micro-aAPC were normalized for total MHC-Ig (4-16 ng). See Supplementary Table 1 for density. Proliferation assessed by CFSE dilution three days after activation. (E) Fold expansion of samples shown in **D** seven days after activation, representative of three experiments.

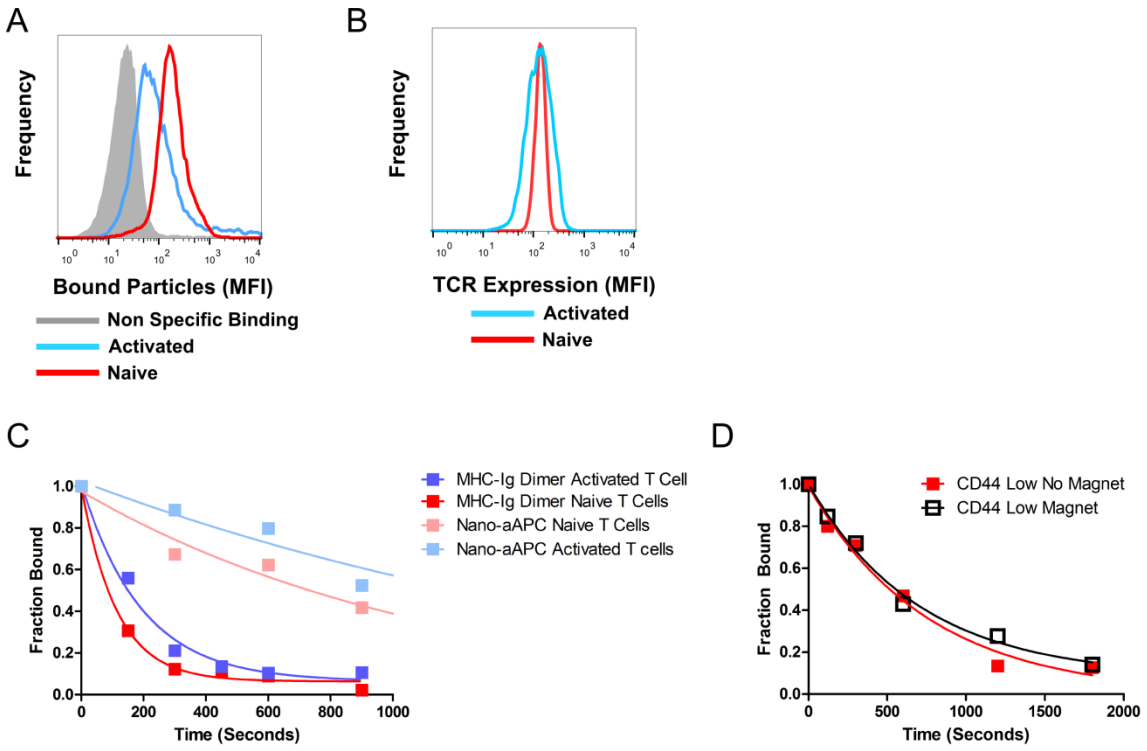

Figure 4.4. Additional Binding Figures

(A) Kb-SIY only nanoparticles binding to cognate 2C T cells. Binding to activated cells, seven days after peptide activation (activated, blue, MFI 89) as compared to naive, CD44lo isolated 2C T cells (naive, red, MFI 179) and control non-cognate CD44lo pmel T cells (non-specific binding, grey, MFI 21). Binding is characterized as mean fluorescence intensity of Alexa 647 labeled particles bound to cells. (B) Surface TCR expression of naive (MFI 137) and activated (MFI 128) cells measured with fluorescent anti-TCRβ. (C) Disassociation of Kb-SIY MHC-Ig dimers from activated (dark blue) and naive (dark red) cells. Disassociation of nano-aAPC from activated (light blue) and naive (light red) cells are reproduced from Figure 1 for comparison. (D) Disassociation curves of nano-aAPC bound to naive CD44low cells before (red) and after (black) one hour of incubation in a magnetic field. Figure is representative of 2 experiments.

Table 4.2

Ligand	**T Cells**	**Off-Rate (s^{-1}) [A]**	**Half-Life (s) [B]**	**TCR-MHC Contacts[C]**
MHC-Ig Dimer	Naive	8.9×10^{-3}	78	1
	Activated	5.2×10^{-3}	112	1.7
Nanoparticle	Naive	$(2.0 \pm 0.5) \times 10^{-3}$	531 ± 149	6.8
	Activated	$(0.9 \pm 0.2) \times 10^{-3}$	984 ± 221**	12.6

[A]Off-rates experiments were performed by incubating naive or activated 2C TCR transgenic T cells with APC-labeled MHC-Ig or APC-labeled nanoparticles bearing K^b-SIY alone. After incubation for one hour at 4°C, cells were washed, a Time 0 fluorescence measurement was taken, and 1B2, an anti-clonotypic antibody, was added to prevent re-binding. Fluorescence measurements were then repeated at 2-10 minute intervals. Off-rates were calculated from a one-dimensional exponential fit in GraphPad Prism.

[B]Half-lives were derived from off-rates in column A. Particles bound to activated cells had a significantly longer half-life ($p<0.02$ by paired t-test, where measurements were paired by experiment) than particles bound to naive cells. Three experiments were performed for each condition.

[C]Unbinding of individual MHC-Ig on either dimer or particle can be stochastically modeled as a Poisson (aka memoryless or exponential) Process. For a Poisson Process with rate constant *r*, the departure time of the *n*th event is characterized by a gamma distribution with shape parameter *n* and single-event rate parameter *r* :

$$f_n(t) = r^n \frac{t^{n-1}}{(n-1)!} e^{-rt}, \qquad 0 \leq t < \infty$$

The mean of this distribution $E[t] = {}^{n}/_{r}$. If MHC-Ig dimer is assumed to make one contact with a naive T cell [1], then r can be estimated from the off-rate of MHC-Ig on naive cells (8.9×10^{-3}). Thus, for any given condition, $E[t]$ is derived from the half-life of MHC-Ig dimer or particle on naive or active cells ($t_{1/2}$), and r is assumed constant. The number of TCR-MHC contacts is estimated as n:

$$n = \frac{t_{1/2} * r}{\ln(2)}$$

The true number of contacts is likely to be higher than this estimate, as MHC-Ig are likely to make more than one contact with naive cells.

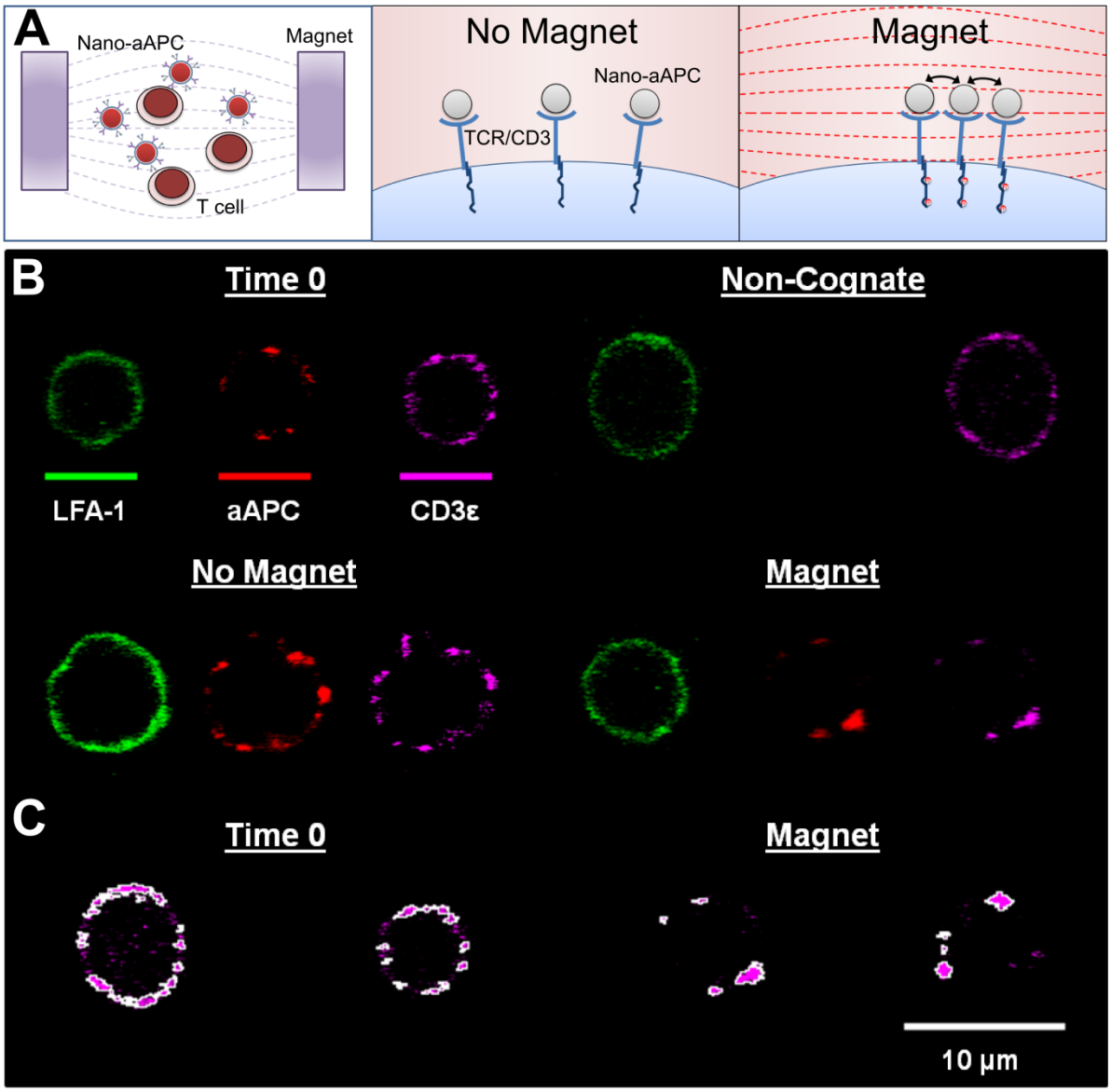
A
Nano-aAPC
Magnet
T cell
No Magnet
Nano-aAPC
TCR/CD3
Magnet
B
Time 0
Non-Cognate
LFA-1
aAPC
CD3ε
No Magnet
Magnet
C
Time 0
Magnet
10 μm

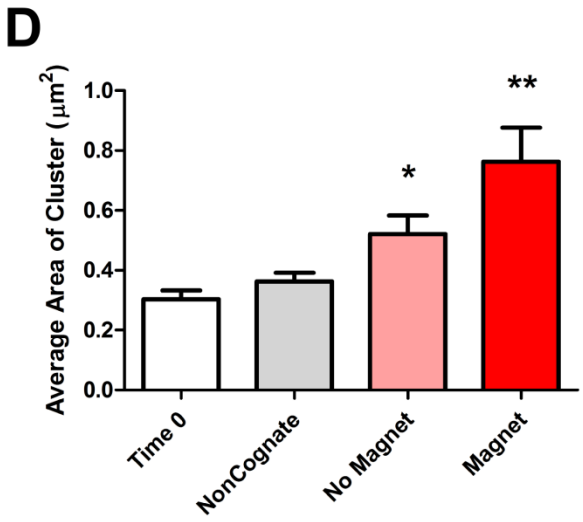
D
Average Area of Cluster (μm²)
1.0
0.8
0.6
0.4
0.2
0.0
*
**
Time 0
NonCognate
No Magnet
Magnet

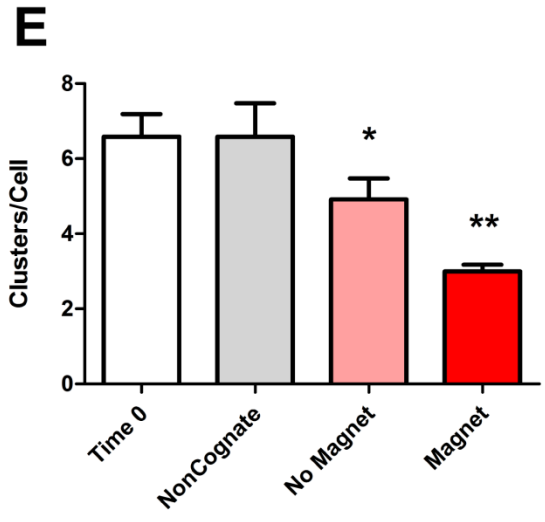
E
Clusters/Cell
8
6
4
2
0
*
**
Time 0
NonCognate
No Magnet
Magnet

Figure 4.5. **Clustering of aAPC and CD3ε Induced by a Magnetic Field**

(A) Schematic of magnet-induced clustering. We hypothesized that an external magnetic field generated by neodymium disc magnets (left) would induce aggregation of receptors bound to polarized paramagnetic beads (right). (B) After nano-aAPC binding (Time 0), cells were incubated for thirty minutes in the presence or absence of a magnetic field. Cells were subsequently stained with antibodies against LFA-1 (green), MHC-Ig on nano-aAPC (red), and CD3ε (magenta) and fixed prior to confocal imaging. Representative images are shown for cells prior to incubation (Time 0, top left), cells incubated with non-cognate particles (Non-Cognate, top right), cells incubated with cognate nano-aAPC (No Magnet, bottom left), and cells incubated with cognate nano-aAPC in a magnetic field (Magnet, bottom right). (C) Aggregate detection shown for representative images from Time 0 group (two on left) and Magnet group (two on right). White outlines represent borders of CD3 clusters (magenta) identified by algorithm. (D) Average cluster area identified with cluster detection algorithm (15 cells/group). The No Magnet group had significantly larger clusters than Time 0 (*, mean difference 0.22 μm^2), and the Magnet group had significantly larger clusters than both Time 0 (**, mean difference 0.46 μm^2, $p < 0.0001$ by ANOVA with Tukey post-test) and No Magnet (**, mean difference 0.24 μm^2). (E) Cells in No Magnet group had fewer clusters per cell than Time 0 (*, mean difference 5.8 clusters) and Magnet group cells had fewer clusters per cell than No Magnet (**, mean difference 1.9 clusters, $p < 0.001$ by ANOVA with Tukey post-test).

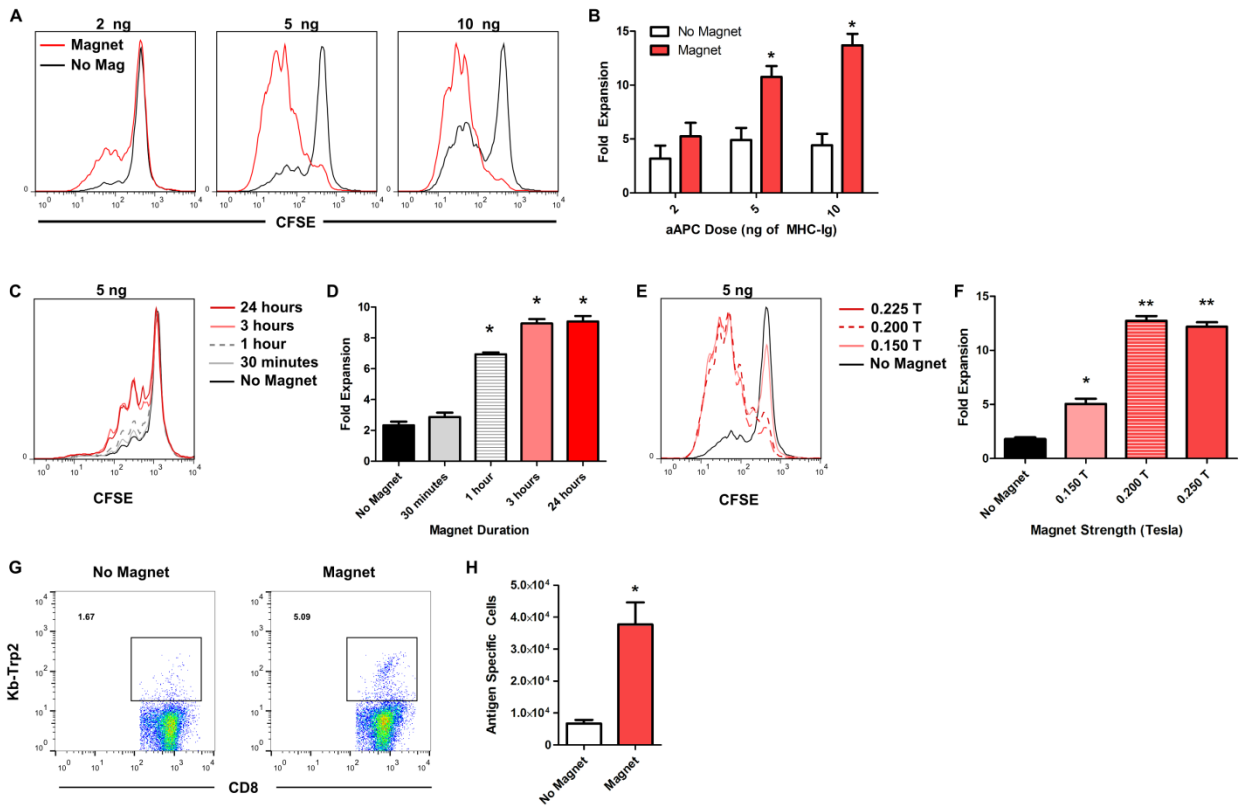

Figure 4.6: Magnet-enhanced Nano-aAPC Stimulation Leads to Robust T cell Proliferation In Vitro.

(**A**) Pmel T cell proliferation assessed by CFSE dilution three days after stimulation with doses of nano-aAPC presenting a total of 2, 5, and 10 ngs of MHC-Ig in the presence (red) or absence (black) of a 0.2 T external magnetic field. (**B**) Fold expansion of samples described in A assessed by cell counts seven days after stimulation. (**C**) Pmel T cells incubated with 5 ng MHC-Ig dose of nano-aAPC and 0.2 T magnetic field for 0-24 hours. Proliferation assessed by CFSE dilution at day 3. (**D**) Fold expansion of samples from C seven days after stimulation. (*, $p<0.001$ by ANOVA with Tukey post-test) (**E**) Pmel T cells incubated with 5 ng MHC-Ig dose of nano-aAPC and magnetic fields of increasing maximal strength (0.15-0.225 T) generated by neodymium magnets of increasing thickness for twenty-four hours. (**F**) Proliferation of samples from E seven days after stimulation (* greater than no magnet, ** greater than 0.15 T magnet, $p<0.001$ by ANOVA with Tukey post-test). (**G**) Antigen-specific expansion of endogenous CD8+ lymphocytes from wild type mice after stimulation with Kb-Trp2 nano-aAPC in the presence or absence of a 0.2 T magnetic field for twenty-four hours. (**H**) Quantity of Kb-Trp2 antigen specific cells generated by nano-aAPC stimulation in presence (red) or absence (white) of magnet ($p<0.01$ by t-test).

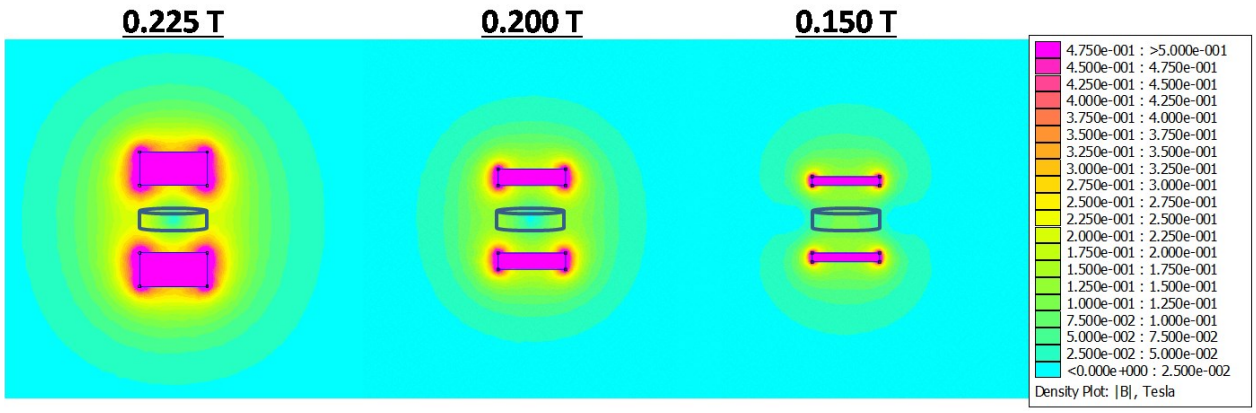

Figure 4.7: Magnetic Field Strength Generated in Culture By Neodynium Disk Magnets

Density plots of field strength in culture as estimated by finite element analysis with FEMM (Finite Element Method Magnetics) software. Disk magnets (magenta) ¾", ½", and ¼" in thickness were used to generate fields of up to 0.225 T, 0.200 T, and 0.150 T, respectively.

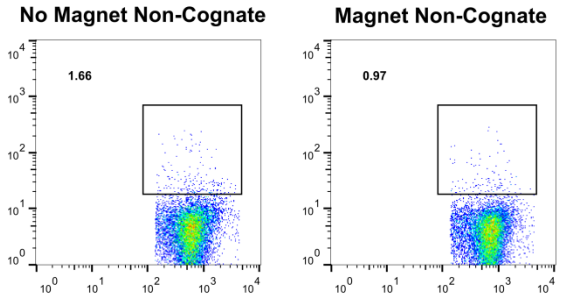

Figure 4.8. Non-cognate MHC Binding After Nano-aAPC Stimulation.

Non-cognate (Kb-SIINF) staining of wild-type CD8+ lymphocytes after stimulation with Kb-Trp2 nano-aAPC in the presence or absence of a 0.2 T magnetic field for twenty-four hours. Seven days after stimulation, cells were stained with Kb-SIINF dimer to identify non-specific binding.

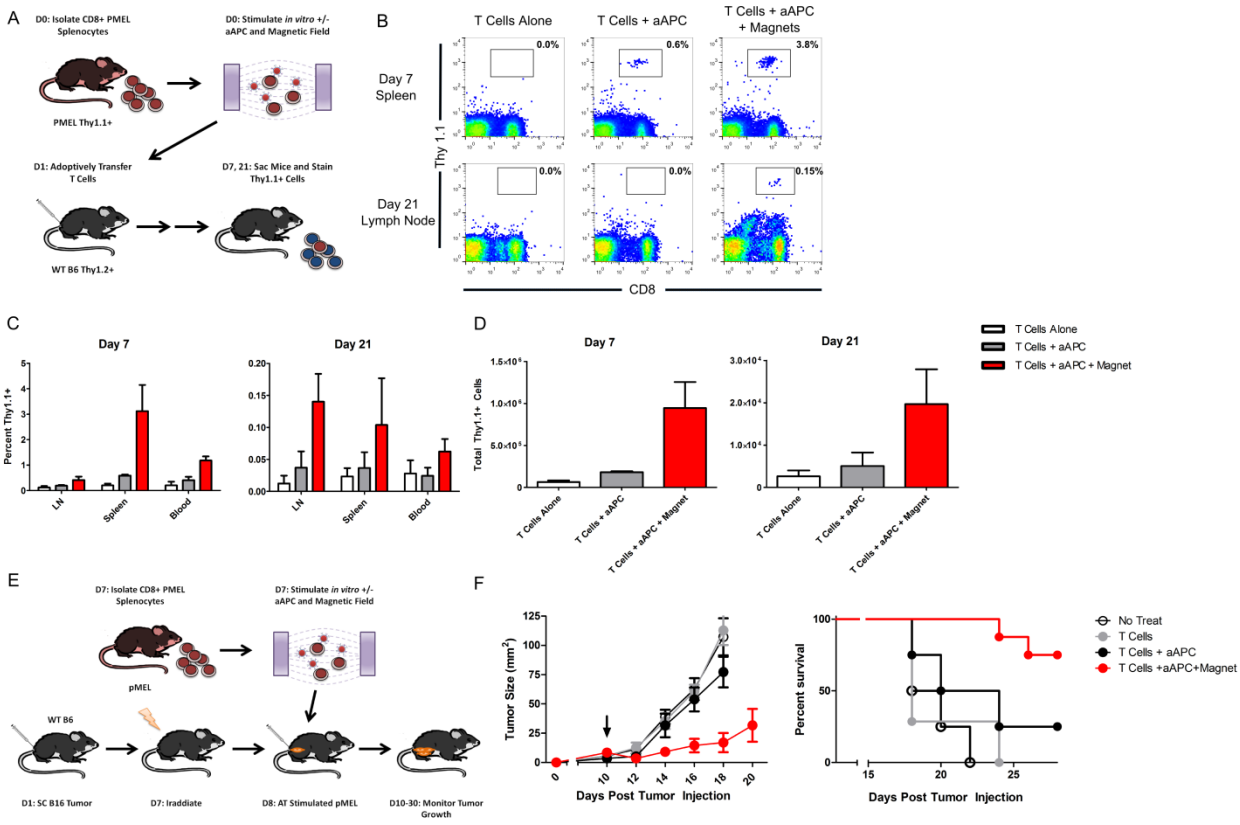

Figure 4.9: Magnet-Enhanced T Cell Expansion *In Vivo* and Increased Efficacy of Adoptive Immunotherapy

(A) Schematic of adoptive immunotherapy model. CD44lo, CD8+ T cells from Thy1.1+ pmel TCR transgenic mice were stimulated *in vitro* for 24 hours in the presence or absence of nano-aAPC (5 ng total MHC-Ig) and magnetic field prior to being adoptively transferred into wild type, Thy1.2+ B6 recipient mice (6 mice per group). Mice received recombinant IL-2 ip on days 1 and 2. Seven and twenty-one days after adoptive transfer, recipient mice were sacrificed (3 per timepoint) and cells from peripheral blood, inguinal lymph nodes, and spleen were stained for CD8 and Thy1.1 to quantify expansion of transferred cells. **(B)** Representative FACS plots from day 7 spleens and day 21 lymph nodes are shown, with frequencies of Thy1.1 cells reported as percentage of CD8+ cells. (**C**) Frequencies of Thy1.1+ cells were significantly higher in mice given T cells stimulated with nano-aAPC in a magnetic field (red) compared to nano-aAPC with no magnet (grey) and no stimulation (white) ($p<0.001$ for treatment effect by two-way ANOVA for day 7 and 21). (**D**) Total Thy1.1+ cells in all organs combined on Day 7 and Day 21. Five-fold more cells were observed in the nano-aAPC + Magnet group than nano-aAPC alone group on day 7 ($p < 0.05$ by student's t-test), but did not reach significance on Day 21 ($p = 0.15$). (**E**) Schematic of treatment of established tumors with magnetic field enhanced adoptive immunotherapy. B16 melanoma tumors were injected subcutaneously into B6 mice, and mice were treated with partially myeloablative total body irradiation on day 9. 5×10^5 CD44lo, CD8+ pmel T cells stimulated for 24 hours with either nano-aAPC (5 ng total MHC-Ig) in a magnetic field (red) or nano-aAPC with no magnet (black) were transferred on Day 10. T cell alone (grey)

and untreated (unfilled) groups were used as control (8 mice per group). Mice received recombinant IL-2 ip on days 10 and 11. (**F**) Treatment with magnet-enhanced nano-aAPC activated T cells led to attenuated tumor growth compared to no magnet and control groups ($p<0.0001$ for treatment effect by two-way ANOVA). Arrow indicates timepoint of adoptive transfer (day 10). Mice were censored if dead or tumors were greater than 150 mm^2. Treatment led to increased survival in T cells + nano-aAPC + Magnet group ($p<0.001$ by Mantel-Cox log-rank test).

4.6 References

1. Fay F, Scott C. Antibody-targeted nanoparticles for cancer therapy. *Immunotherapy*. 3, 381–394 (2011).

2. Moon JJ, Huang B, Irvine DJ. Engineering nano- and microparticles to tune immunity. *Advanced materials (Deerfield Beach, Fla.)*. 24(28), 3724–46 (2012).

3. Perica K, De León Medero A, Durai M, *et al.* Nanoscale Artificial Antigen Presenting Cells for T Cell Immunotherapy. *Nanomedicine : nanotechnology, biology, and medicine*. [Epub Ahea (2013).

4. Van der Merwe PA, Dushek O. Mechanisms for T cell receptor triggering. *Nature reviews. Immunology*. 11(1), 47–55 (2010).

5. Oelke M, Maus M V, Didiano D, June CH, Mackensen A, Schneck JP. Ex vivo induction and expansion of antigen-specific cytotoxic T cells by HLA-Ig-coated artificial antigen-presenting cells. *Nature medicine*. 9(5), 619–24 (2003).

6. Ugel S, Zoso A, De Santo C, *et al.* In vivo administration of artificial antigen-presenting cells activates low-avidity T cells for treatment of cancer. *Cancer Research*. 69(24), 9376–84 (2009).

7. Oelke M, Schneck JP. Overview of a HLA-Ig based "Lego-like system" for T cell monitoring, modulation and expansion. *Immunologic Research*. 47, 248–56 (2010).

8. Steenblock E, Wrzesinski S, Flavell R, Fahmy T. Antigen presentation on artificial acellular substrates: modular systems for flexible, adaptable immunotherapy. (2009).

9. Nel AE, Mädler L, Velegol D, *et al.* Understanding biophysicochemical interactions at the nano-bio interface. *Nature materials*. 8(7), 543–57 (2009).

10. Fahmy TM, Bieler JG, Edidin M, Schneck JP. Increased TCR avidity after T cell activation: a mechanism for sensing low-density antigen. *Immunity*. 14(2), 135–43 (2001).

11. Kumar R, Ferez M, Swamy M, *et al.* Increased Sensitivity of Antigen-Experienced T Cells through the Enrichment of Oligomeric T Cell Receptor Complexes. *Immunity*. 35(3), 375–87 (2011).

12. Boyle S, Kolin DL, Bieler JG, Schneck JP, Wiseman PW, Edidin M. Quantum Dot Fluorescence Characterizes the Nanoscale Organization of T Cell Receptors for Antigen. *Biophysical Journal*. 101(11), L57–L59 (2011).

13. Perica K, Bieler JG, Edidin M, Schneck J. Modulation of MHC binding by lateral association of TCR and coreceptor. *Biophysical journal*. 103(9), 1890–8 (2012).

14. Lillemeier BF, Mörtelmaier M a, Forstner MB, Huppa JB, Groves JT, Davis MM. TCR and Lat are expressed on separate protein islands on T cell membranes and concatenate during activation. *Nature Immunology*. 11(1), 90–6 (2010).

15. Varma R, Campi G, Yokosuka T, Saito T, Dustin ML. T cell receptor-proximal signals are sustained in peripheral microclusters and terminated in the central supramolecular activation cluster. *Immunity*. 25, 117–127 (2006).

16. Hughes S, El Haj AJ, Dobson J. Magnetic micro- and nanoparticle mediated activation of mechanosensitive ion channels. *Medical engineering & physics*. 27(9), 754–62 (2005).

17. Cho MH, Lee EJ, Son M, *et al.* A magnetic switch for the control of cell death signalling in in vitro and in vivo systems. *Nature materials*. 11(12), 1038–1043 (2012).

18. Dobson J. Remote control of cellular behaviour with magnetic nanoparticles. *Nature nanotechnology*. 3(3), 139–43 (2008).

19. Lee J-H, Kim ES, Cho MH, *et al.* Artificial control of cell signaling and growth by magnetic nanoparticles. *Angewandte Chemie (International ed. in English)*. 49(33), 5698–702 (2010).

20. Mannix RJ, Kumar S, Cassiola F, *et al.* Nanomagnetic actuation of receptor-mediated signal transduction. *Nature nanotechnology*. 3(1), 36–40 (2008).

21. Durai M, Krueger C, Ye Z, *et al.* In vivo functional efficacy of tumor-specific T cells expanded using HLA-Ig based artificial antigen presenting cells (aAPC). *Cancer immunology, immunotherapy : CII*. 58(2), 209–20 (2009).

22. Wrzesinski C, Paulos CM, Kaiser A, *et al.* Increased intensity lymphodepletion enhances tumor treatment efficacy of adoptively transferred tumor-specific T cells. *Journal of Immunotherapy*. 33(1), 1–7 (2010).

23. Restifo NP, Dudley ME, Rosenberg S a. Adoptive immunotherapy for cancer: harnessing the T cell response. *Nature reviews. Immunology*. 12(4), 269–81 (2012).

24. Smith-Garvin JE, Koretzky G a, Jordan MS. T cell activation. *Annual review of immunology*. 27, 591–619 (2009).

25. Kunzmann A, Andersson B, Thurnherr T, Krug H, Scheynius A, Fadeel B. Toxicology of engineered nanomaterials: Focus on biocompatibility, biodistribution and biodegradation. *Biochimica et biophysica acta*. 1810(3), 361–373 (2010).

26. Fahmy TM, Bieler JG, Schneck JP. Probing T cell membrane organization using dimeric MHC-Ig complexes. *Journal of Immunological Methods*. 268(1), 93–106 (2002).

27. Jenkins MK, Moon JJ. The Role of Naive T Cell Precursor Frequency and Recruitment in Dictating Immune Response Magnitude. *The Journal of Immunology*. 188(9), 4135–4140 (2012).

28. Blattman JN, Antia R, Sourdive DJD, *et al.* Estimating the precursor frequency of naive antigen-specific CD8 T cells. *The Journal of experimental medicine*. 195(5), 657–64 (2002).

29. Klebanoff C a, Gattinoni L, Palmer DC, *et al.* Determinants of successful CD8+ T-cell adoptive immunotherapy for large established tumors in mice. *Clinical cancer research : an official journal of the American Association for Cancer Research*. 17(16), 5343–52 (2011).

30. Chang JT, Palanivel VR, Kinjyo I, *et al.* Asymmetric T lymphocyte division in the initiation of adaptive immune responses. *Science*. 315(5819), 1687–91 (2007).

31. King CG, Koehli S, Hausmann B, Schmaler M, Zehn D, Palmer E. T Cell Affinity Regulates Asymmetric Division, Effector Cell Differentiation, and Tissue Pathology. *Immunity*. 37(4), 709–720 (2012).

32. Dustin ML. T-cell activation through immunological synapses and kinapses. *Immunol. Rev*. 221, 77–89 (2008).

33. Naahidi S, Jafari M, Edalat F, Raymond K, Khademhosseini A, Chen P. Biocompatibility of engineered nanoparticles for drug delivery. *Journal of controlled release : official journal of the Controlled Release Society*. 166(2), 182–94 (2013).

34. Grützkau A, Radbruch A. Small but mighty: how the MACS-technology based on nanosized superparamagnetic particles has helped to analyze the immune system within the last 20 years. *Cytometry. Part A : the journal of the International Society for Analytical Cytology*. 77(7), 643–7 (2010).

35. Dvorak CC, Gilman a L, Horn B, *et al.* Positive selection and transplantation of autologous highly purified CD133(+) stem cells in resistant/relapsed chronic lymphocytic leukemia patients results in rapid hematopoietic reconstitution without an adequate leukemic cell purging. *Bone marrow transplantation*. 48(4), 508–13 (2013).

36. Hinrichs CS, Borman Z a, Gattinoni L, *et al.* Human effector CD8+ T cells derived from naive rather than memory subsets possess superior traits for adoptive immunotherapy. *Blood*. 117(3), 808–14 (2011).

37. Hinrichs CS, Borman Z a, Cassard L, *et al.* Adoptively transferred effector cells derived from naive rather than central memory CD8+ T cells mediate superior antitumor immunity. *Proceedings of the National Academy of Sciences of the United States of America*. 106(41), 17469–74 (2009).

38. Klebanoff C a, Gattinoni L, Restifo NP. Sorting through subsets: which T-cell populations mediate highly effective adoptive immunotherapy? *Journal of immunotherapy (Hagerstown, Md. : 1997)*. 35(9), 651–60 (2012).

39. Jenkins MK, Chu HH, McLachlan JB, Moon JJ. On the composition of the preimmune repertoire of T cells specific for Peptide-major histocompatibility complex ligands. *Annual review of immunology*. 28, 275–94 (2010).

40. Wherry EJ. T cell exhaustion. *Nature Immunology*. 131(6), 492–499 (2011).

5 Streamlined Enrichment and Expansion Using Nano-aAPC for Adoptive Immunotherapy

5.1 Introduction

The adoptive transfer of large numbers of tumor-specific T cells can mediate rejection of otherwise treatment resistant cancers[1,2]. Antigen-specific cells can be isolated and expanded from tumor specimens, or generated by repeated *in vitro* stimulation with antigen followed by T cell cloning [3,4]. The addition of high intensity lymphodepletion with chemotherapy or radiation prior to T cell transfer has significantly enhanced therapeutic efficacy [1,5,6] by depleting immunosuppressive regulatory cells and decreasing competition for lymphoproliferative signals such as common gamma chain cytokines [2,7].

Decreased competition for cytokines in a lymphopenic environment triggers a burst of antigen-independent proliferation termed "homeostatic expansion." In an adoptive immunotherapy setting, this competition can come from either reconstituting host T cells, or irrelevant T cells that are adoptively transferred simultaneously with the antigen-specific cells of interest. For example, the co-transfer of 10-50 million bystander T cells into a sublethally irradiated host significantly attenuates homeostatic expansion of both CD4+ and CD8+ T cells in a dose-dependent manner [8–10]. This motivates a desire to transfer highly pure populations of antigen-specific T cells.

Unfortunately, the repeated stimulation and 4-6 weeks of *in vitro* culture necessary to generate T cell cultures of high antigen-specific number and frequency also exhaust T cell proliferative capacity[11]. Exhaustion manifests as a terminally differentiated effector phenotype with

telomere shortening, characteristics associated with treatment failure in clinical trials[6,12]. In contrast, naive or "stem-like" T cells which proliferate robustly in the host are more potent mediators of tumor regression[11,13,14].

Lengthy culture also increases the cost and labor of adoptive immunotherapy, which limits applicability outside the research setting. Furthermore, existing T cell culture techniques rely on endogenous APC or feeder cells, which are themselves a complex biologic that must be generated for each individual patient[15]. The dendritic-cell based vaccine Provenge, the first FDA-approved immunotherapy for prostate cancer, costs approximately $93,000/patient[16].

Thus, optimal T cell populations would be derived from naive cells, have a high frequency of antigen-specific cells, would not require use of endogenous APC, and have not gone through repeated stimulations and prolonged culture. We hypothesized that this could be accomplished by enrichment of tumor-specific cells prior to activation with a synthetic bead-based platform. To streamline and simplify this procedure, we developed a nanoscale artificial Antigen Presenting Cell platform (nano-aAPC) capable of inducing antigen-specific T cell expansion *in vitro* and *in vivo* [17]. Nano-aAPC are functionalized with MHC-peptide that can bind and activate TCR, iron-oxide cores to capture bound cells in a magnetic column, and co-stimulatory anti-CD28, thus enriching and expanding cognate cells simultaneously. We show that this process, termed enrichment and expansion, can generate large numbers of high-frequency T cells from naive precursors. Furthermore, we explore T cell expansion after adoptive transfer and the ability of generated T cells to mediate tumor rejection.

5.2 Materials and Methods

Mice and reagents

2C TCR transgenic mice were maintained as heterozygotes by breeding on a C57/BL6 background. pMEL TCR/Thy1^a Rag-/- transgenic mice were a gift from Nicholas Restifo (National Institutes of Health, Bethesda, MD) and maintained as homozygotes. C57BL/6j and Nu/J mice were purchased from Jackson Laboratories (Bar Harbor, ME). All mice were maintained according to Johns Hopkins University's Institutional Review Board. Fluorescently labeled monoclonal antibodies were purchased from BioLegend (San Diego, CA).

Preparation of MHC-Ig Dimers

Soluble MHC-Ig dimers, K^b-Ig and D^b-Ig, were prepared and loaded with peptide as described[50]. Briefly, K^b-Ig molecules were loaded with peptide by stripping at alkaline condition (pH 11.5), and then refolded in the presence of 50 fold excess peptide. D^b-Ig molecules were stripped under mildly acidic conditions (pH 6.5) and refolded in the presence of 50 fold molar excess peptide and 2-fold molar excess of human β_2-microglobulin. Human A2-Ig was passively loaded in the presence of excess M1 peptide [51]. Peptides SIIN (SIINFEKL, derived from ovalbumin protein), and GP100 (KVPRNQDWL, from melanocyte GP100 protein) were purchased from Genscript (Piscataway, NJ). Protein concentration was determined after labeling by size exclusion high performance liquid chromatography (HPLC).

Nano-aAPC Synthesis

Nanoscale iron-dextran aAPC were made by direct chemical coupling of MHC-Ig dimer and B7.1-Ig to biodegradable particles (Miltenyi Biotec). *Micro-aAPC Synthesis*

Micro-aAPCs were fabricated as described previously[7] by direct chemical coupling of protein to 4.5 μm Dynal Magnetic Microbeads (Life Technologies, Carlsbad, CA). For the initial

coupling step, 25 μg anti-biotin antibody (Sigma, St. Louis, MO) was added to 100 million Microbeads in 0.1 M sodium borate buffer. After washing in a magnetic column, biotin labeled MHC-Ig and CD28 were added in equimolar amounts to form aAPC.

Enrichment and Expansion

For murine cell culture, cells were obtained from homogenized mouse spleens followed by hypotonic lysis of RBC. Cytotoxic lymphocytes were isolated using a CD8 no-touch isolation kit and magnetic enrichment column from Miltenyi Biotec (Cologne, Germany) and if necessary labeled with carboxyfluorescein succinimidyl ester (CFSE) for 15 minutes at 37^{o}C, then washed extensively. Ten million CD8+ T cells and 20 μL of nano-aAPC bearing the antigen of interest were incubated in 300 μL of B media for one hour at 4^{o}C. The resulting mixture was passed over a Miltenyi MACS MS column and the positive fraction eluted in media and directly cultured without washing. Media was based on RPMI media supplemented with T cell factor (TF), a cytokine cocktail of conditioned media harvested from stimulated human PBMC [6]. Frequency of antigen-specific cells was characterized seven days later by staining with cognate Pentamer (ProImmune) or MHC-Ig dimer.

Effect of Nano-aAPC on In Vivo T cell Expansion and Inhibition of Subcutaneous Tumor Growth

Thy1.1+ pmel or WT T cells were adoptively transferred into B6 Thy1.2+ wild type hosts. Mice were treated both the day of and the day after adoptive transfer with 30,000 units intraperitoneal IL-2. Seven days adoptive transfer, three mice per group were sacrificed and lymphocytes were isolated from peripheral blood, spleen, and inguinal, cervical, and axillary lymph nodes, and tumor, then stained with anti-Thy1.1 antibody.

Tumor rejection experiments were performed as above, except $3x10^5$ B16 melanoma cells were injected subcutaneously ten days prior to T cell adoptive transfer. Transient lymphopenia was

induced by sublethal irradiation (500 cGy) one day before adoptive transfer with a MSD Nordion Gammacell dual Cs137 source (Johns Hopkins Molecular Imaging Center). Tumor growth was monitored at 2 day intervals using digital calipers, until tumor size was ~150 mm^2, at which point animals were euthanized.

5.3 Results

Enrichment of Antigen-Specific Cells

Enrichment and expansion are performed by incubating polyclonal CD8+ lymphocytes with nano-aAPC, passing the cell-particle mixture through a magnetic column, and eluting then culturing the magnet-bound fraction (**Figure 5.1a**). To assess efficacy of enrichment, a known number of Thy1.1+ pmel TCR transgenic T cells specific for Db-GP100 melanoma antigen were incubated at a 1:1000 ratio with Thy1.2+ CD8 T cells from B6 mice. The frequency of antigen-specific cells increased more than 10-fold from 0.09% to 1.17% after enrichment with the highest dose of Db-GP100 nano-aAPC assessed (**Figure 5.1b**). Titration of nano-aAPC of particles incubated with T cells increased the enrichment frequency and resulted in recovery of up 95% of pmel cells added to culture (**Figure 5.1c**).

Enrichment of wild-type Db-GP100 cells from polyclonal CD8 splenocytes was assessed by staining with soluble MHC pentamer. Frequency of Db-GP100 cells was below detectable frequencies prior to enrichment, but increased to 0.30% afterward. The frequency of non-specific Kb-Trp2 cells did not increase (**Figure 5.1d**).

Although micro-aAPC made from a 4.5 μm diameter iron-dextran particles mediated antigen-specific T cell expansion, T cells formed frequently formed conjugates with non-cognate micro-aAPC, resulting in little to no enrichment of antigen-specific cells (**Figure 5.2**). In contrast, nano-aAPC bound T cells with high specificity and low background; thus, nano-aAPC are a uniquely effective reagent for antigen-specific enrichment.

Expansion of Antigen-Specific Cells Following Enrichment

We next sought to characterize antigen-specific T cell expansion after enrichment. Magnet-bound fractions of enriched cells and nano-aAPC were eluted and cultured *in vitro* (positive fraction). To explore the effect of enrichment on proliferation, the enrichment procedure was "undone" in a control sample by collecting the negative fraction and adding it back to the positive fraction (**Figure 5.3a**). Seven days after enrichment with a Kb-Trp2 nano-aAPC, 17.6% of cells expanded from the positive fraction were Kb-Trp2 specific, compared to 1.46% of cells from the negative+positive, not enriched group (**Figure 5.3b**). Although the negative+positive sample contained more cells total, the enrichment procedure resulted in a 2-3 fold increase in total antigen-specific cells (**Figure 5.3c**). By analogy to enhanced expansion seen with lymphodepletion *in vivo*, we suggest this may be due to reduced competition for lymphotropic cytokines.

After one week, $1.5x10^5$ Trp2-specific cells were generated from 10^7 polyclonal CD8 T cells. Precursor frequencies for CD8 responses to foreign antigen range from $10\text{-}100/10^7$[18], and may be even lower for the melanoma self-antigen Trp2; thus, a lower end estimate of Trp2-specific proliferation is between 1000 fold, comparable to proliferation after viral infection *in vivo*.

Enrichment and expansion similarly yielded large numbers and high purity of cells specific for melanoma antigen Db-GP100, model antigen Kb-SIIN, and mammary carcinoma antigen Ld-A5 (**Figures 5.3d, 5.3e**). Precursor frequencies for Db-GP100 have been estimated at 10 in 10 million [19], indicating up to 5,000 fold proliferation, and 20-350 in 10 million for Kb-SIINF[20], indicating up to 6,000 fold expansion.

Under selective pressure by the immune system, tumors down-regulate antigen or MHC expression, as is known to occur during cancer development[21], as a mechanism of immune escape. In mouse models of B16 melanoma, tumor recurrence is associated with loss of antigen expression [22,23], whereas adoptive transfer of T cells with multiple specificities can prevent this process and enhance treatment [24]. A streamlined procedure for generating T cells against three separate antigens was developed by enriching and expanding cells with a combined batch of Db-GP100, Kb-SIINF, and Kb-TRP2 bearing nano-aAPC. All three antigens generated robust responses when cultured simultaneously (**Figure 5.3F**). Although frequencies for each antigen generated during "triple-expansion" were lower than those observed when cultured individually, the total frequency of tumor-specific cells in the population was increased, and the number of antigen-specific cells generated was the same (**Figure 5.3G**).Thus, the effect of simultaneous culture of three antigens was additive.

Magnet-Induced Clustering of nano-aAPC

The robust expansion induced by nano-aAPC may be due in part to the effect of the magnetic field used during enrichment. We have previously shown that nano-aAPC bound to T cells in a magnetic field aggregate on the cell surface, inducing CD3 clustering, strong T cell activation and increased proliferation (**Chapter 4**). We thus visualized clustering of CD3ε and aAPC before and after passage through a magnetic enrichment column (**Figure 5.4**). CD3ε clusters increased in area from 0.43 ± 0.03 μm^2 to 1.22 ± 0.34 μm^2 during passage. Notably, cells spend only 5-10 minutes in a magnetic column at room temperature; incubating the cells for 30 minutes at 37^{o}C did not lead to further increases in cluster size. Magnetic fields generated by the MACS enrichment magnet are quite strong, at approximately 1 T, which may explain why clustering was relatively rapid.

Future work to validate the effect of magnetic fields on enhancing proliferation will compare the Positive and Positive+Negative fractions of magnetic enrichment to cells which have not passed through a magnetic column.

Nano-aAPC Induced Expansion of Co-Infused T cells

The ultimate goal of enrichment and expansion is to generate an antigen-specific T cell population that can be re-infused for cancer immunotherapy. At Day 7, T cell cultures can be re-enriched to further increase the frequency of antigen-specific cells. Re-enrichment increased antigen-specific frequency 4-fold, generated a 40% Trp2-specific population (**Figure 5.5**). 90% of antigen-specific cells were recovered after re-enrichment. Furthermore, nano-aAPC were retained in the positive fraction of the magnetic column and may be co-administered with T cells. Thus, re-enrichmet after one week of culture generates a combined product of nano-aAPC cell and 40% tumor specific for *in vivo* administration.

The capacity of nano-aAPC to further expand T cells after co-administration *in vivo* was verified using pmel T cells as a model. The administration of one million pmel T cells with cognate nano-aAPC led to 4% antigen specificity in peripheral blood 3 days after administration, although frequencies rapidly decreased thereafter (**Figure 5.6A**). T cells co-administered with nano-aAPC alone resulted in approximately 1% antigen-specificity. Furthermore, only T cells co-administered with cognate nano-aAPC inhibited growth of B16 lung metastases administered three days previously, indicating nano-aAPC activation induced effector function (**Figure 5.6B**).

As discussed, lymphodepletion prior to adoptive transfer improves retention of adoptively transferred cells by removing competition for proliferative cytokines. This phenomenon has been ascribed to antigen-independent homeostatic expansion. However, to demonstrate that decreased

competition can also enhance nano-aAPC-induced, *antigen-driven* expansion, we developed a pmel model where irrelevant cells in the host were removed by lymphodepletion, and the frequency of irrelevant bystander cells was varied in the donor cells. 10^5 pmel cells were co-administered with either 10^6 or 10^7 bystander B6 cells to mimic the effects of nano-aAPC enrichment. Cells were transferred into either untreated animals or animals lymphodepleted the previous day with 500 cGy gamma radiation. Furthermore, all populations received nano-aAPC to drive antigen-specific expansion after transfer.

Both lymphodepletion and decreasing bystander cells enhanced expansion. Frequency of pmel cells was approximately 5-fold higher in spleen and lymph nodes seven days after transfer (**Figure 5.6C**) with 10^6 bystanders compared to 10^7. Both sets of lymphodepleted animals had significantly higher frequencies of pmel cells (10-50 fold) than immunocompetent animals.

As expected, increased numbers of total CD8+ lymphocytes were recovered from immunocompetent animals (21.4 million ± 1.7) compared to lymphodepleted animals (5.7 million ± 1.2) ($p<0.001$ by t-test). Furthermore, lymphodepleted animals that received 10^7 bystanders had slightly larger numbers of lymphocytes than those that received 10^6 bystanders (6.8 million ± 1.3 vs. 4.9 million ± 0.81, not significant). Nevertheless, the total numbers of antigen-specific cells generated was greater with lymphodepletion and decreased bystander animals by 16- and 4-fold, respectively (**Figure 5.6D**).

Ogoing experiments seek to determine the relative contributions of homeostatic and antigen-driven proliferation, as well as the effect of the enrichment and expansion protocol on expansion of endogenous antigen-specific cells.

Tumor Rejection By Adoptive Transfer of Enriched+Expanded Cells

The inhibition of established B16 melanoma by adoptive transfer requires on the order of 10^5 tumor-specific transgenic pmel cells[25]. Comparable numbers are achieved by Enrichment+Expansion from 10 million CTL WT naive precursors after one week in culture. Thus, we treated animals bearing 8 day established B16 melanoma with lymphocytes expanded for 5 days with Kb-Trp2 and Db-GP100 nanoparticles simultaneously. Mice were irradiated with gamma irradiation one day prior to adoptive transfer.

Enrichment+Expansion treated animals had significantly less tumor growth than untreated or non-cognate (Kb-SIINF) treated animals (**Figure 5.7**). 2/8 treated animals completely eliminated tumor 30 days after treatment, whereas all animals in control groups were euthanized. This established than Enrichment+Expansion can generate sufficient cells to treat established melanoma after just one week.

Ongoing experiments compare tumor rejection from Enriched (Positive) and Not Enriched (Positive+Negative) and No Magnet activated T cells.

Immediate Reinfusion Without In Vitro Culture Is Not Sufficient For Tumor Rejection

An even more streamlined approach to adoptive immunotherapy would involve the immediate re-infusion of enriched lymphocytes on Day 0 into hosts, since nano-aAPC can induce T cell expansion when co-injected with T cells. However, since CTL precursors exist on the order of 10-100 per mouse, there may not be sufficient tumor-specific cells adoptively transferred using this strategy.

10 million Thy1.1+ donor lymphocytes were enriched and immediately co-infused with Kb-Trp2 nano-aAPC into irradiated, WT Thy1.2+ tumor-bearing mice. Seven days later, mice were sacrificed and the frequency of Thy1.1+, Kb-Trp2 binding T cells was assessed in the spleen and

tumor (**Figure 5.8A**). Although large numbers of adoptively transferred Thy1.1+ cells were detectable, no animal had greater than 0.11% Trp2-specific CTL in spleen; this animal is shown in Figure 5A. Most animals (4/6) had no detectable Trp2+ cells. Despite inducing robust expansion of co-injected pmel T cells (**Figure 5.6**), nano-aAPC did not induce robust antigen-specific expansion.

Furthermore, Enriched and immediately re-infused lymphocytes could not inhibit established B16 melanoma. Fourteen days after tumor injection, treated and untreated animals had similar subcutaneous tumor size (**Figure 5.8B**).

To verify the need for the threshold of tumor-specific cell number required to inhibit melanoma growth in our hands, we assessed inhibition of established B16 melanoma using increasing numbers of pmel T cells. 10^5 but not 10^4 or 10^3 pmel CTL co-infused with nano-aAPC significantly inhibited tumor growth (**Figure 5C**), validating the requirement to generate sufficient numbers of cells prior to transfer. T cells at all three doses could not inhibit tumor growth without co-infusion of nano-aAPC.

5.4 Conclusions

Adoptive cell transfer can mediate sustained, complete tumor rejection in melanoma. However, the expansion of ACT beyond the research setting requires the development of less expensive, streamlined approaches to generating tumor-specific T cells. aAPC are an off-the-shelf platform for simplifying T cell culture by eliminating the need to simultaneously culture autologous dendritic or feeder cells, which are themselves a complex biologic that must be assessed for safety and reliability.

Several sources of tumor-specific cells exist for adoptive immunotherapy. Tumor-infiltrating lymphocytes have been highly effective in trials, but cannot be cultured from all patients or most cancers. Polyclonal cell populations can be genetically engineered to express anti-cancer TCR; however, these TCR are derived from high-avidity responses in model patients or even humanized mouse responses. Thus, they have not undergone Central Tolerance mechanisms and can mediate destructive off- and on-target toxicity[26,27]. Cells derived from naive precursors have been described as the most effective immunotherapy subset, and autologous lymphocytes are likely to have a better safety profile than engineered TCR, but the process of generating tumor-specific T cells requires extensive culture that exhausts proliferative capacity and increases cost.

We propose to uncouple this trade-off using enrichment prior to expansion, quickly generating a autologous T-cell/nano-aAPC product of large number and purity for infusion into cancer patients. While antigen-specific T cells can be enriched using MHC tetramers after T cell expansion [28,29], our platform simplifies this process by coupling enrichment and expansion in a single reagent. Furthermore, cross-linking of TCR by multimeric MHC in the absence of co-stimulation can induce T cell apoptosis or anergy [30]. Thus, the use of a single platform for both T cell enrichment and activation has significant advantages over existing approaches.

Furthermore, our approach attempts to generate maximal expansion *after* adoptive transfer by removing irrelevant cells. We show here for the first time that removal of bystander cells and lymphodepletion also improve antigen-specific (and not only homeostatic) expansion, presumably by reducing competition for proliferative cytokines. While antigen-specific expansion in the host could also potentially be enhanced by vaccination, professional APCs are significantly depleted as a result of lymphodepleting treatments [31,32]. Thus an artificial APC

couples with lymphodepletion to induce extensive antigen-specific T cell expansion after transfer.

5.5 Figures

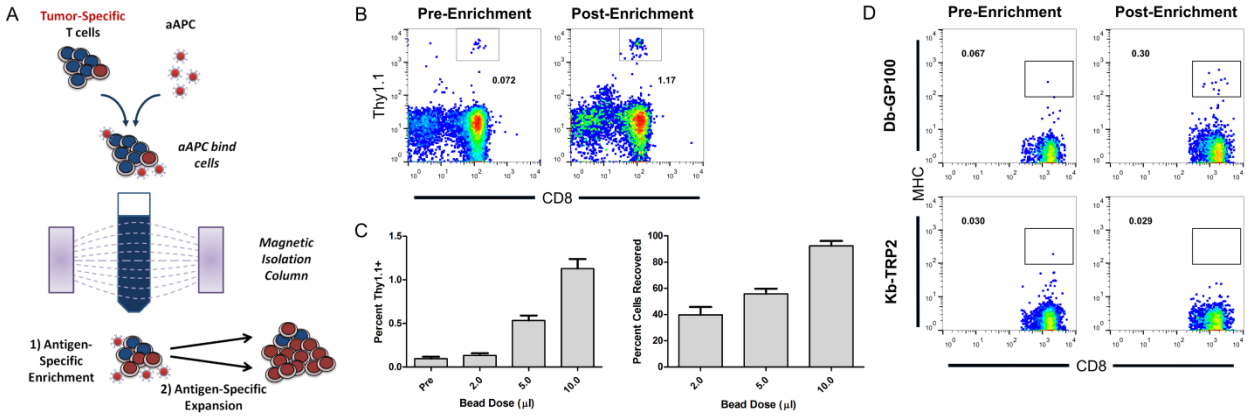

Figure 5.1. Nano-aAPC Mediated Enrichment of Antigen-Specific T Cells

A) Schematic of magnetic enrichment and expansion. Antigen-specific CD8+ T cells bound to aAPC are retained in a magnetic column in the "enrichment" step. Enriched cells are then activated by aAPC and proliferate in the "expansion" step. B) Nano-aAPC mediate antigen-specific enrichment of cognate, Thy1.1+ pmel cells from a pool of thousand-fold more polyclonal, Thy1.2+ B6 splenocytes. C) Summary antigen-specific cell frequency and percent cells recovered after pMEL enrichment performed as in **C** with increasing amounts of nano-aAPC. D) Enrichment of endogenous Db-GP100 splenocytes by nano-aAPC (top). Frequency of non-cognate Kb-Trp2 cells does not increase after enrichment (bottom).

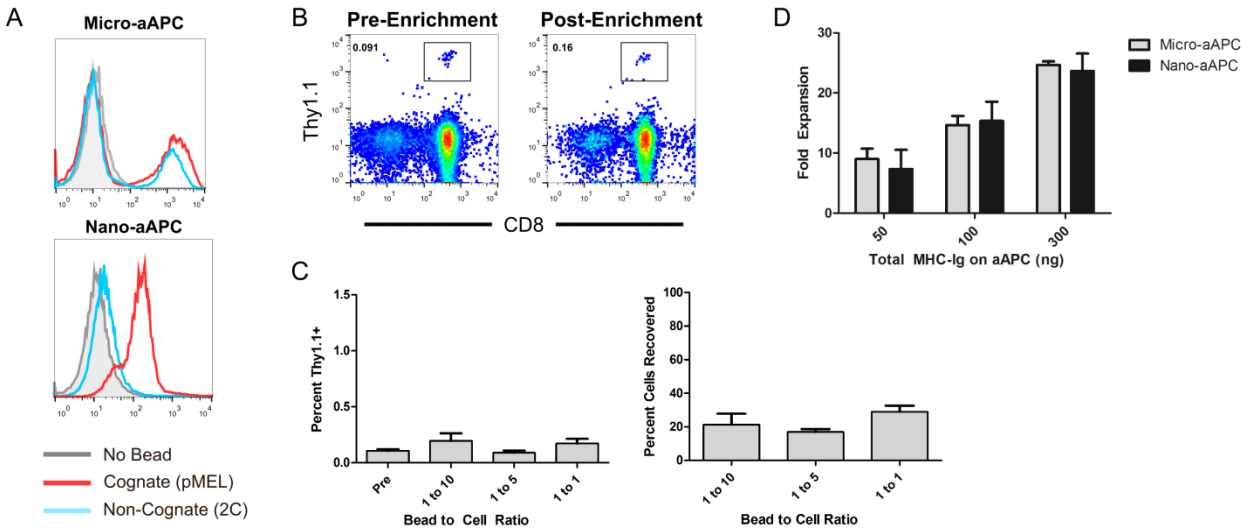

Figure 5.2. Micro-aAPC Are Not Effective For Antigen-Specific Enrichment

A) Binding of Micro- (top) and Nano- (bottom) aAPC to cognate pMEL (red) or non-cognate 2C (blue) CD8+ T cells, characterized by fluorescent labeling of bound beads. No bead (grey) background is shown as control. B) Micro-aAPC do not enrich cognate cells. Thy1.1+ pmel cells were incubated at a 1:1000 ratio with polyclonal, Thy1.2+ B6 splenocytes, and enrichment was attempted using Db-GP100 microparticles. Frequency of Thy1.1+ cells did not significantly increase after enrichment. C) Summary antigen-specific cell frequency and percent of cells recovered, performed as in **C** with increasing amounts of micro-aAPC. D) Both micro-aAPC and nano-aAPC induce dose-dependent expansion of pmel cells. Particle amounts were normalized to total amount of MHC-Ig presented by particles as described in **Chapter 4**.

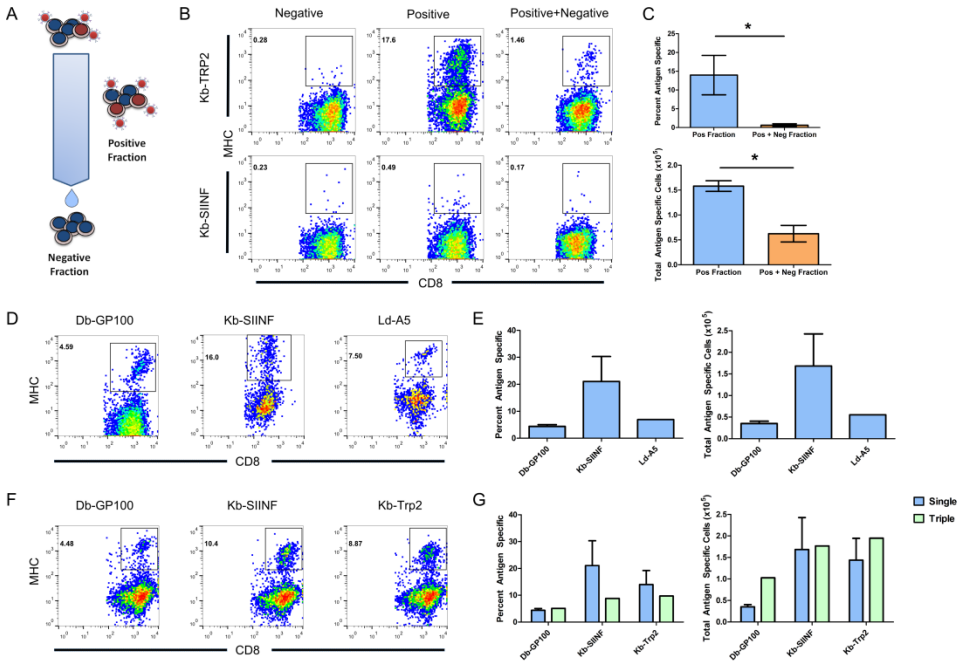

Figure 5.3. Expansion of Antigen-Specific T cells After Enrichment.

A) Schematic of cell fractions used to assess expansion of cells after enrichment. Bead-bound antigen-specific T cells are bound to a magnetic column (positive fraction), whereas unbound cells pass through (negative fraction). The negative fraction can be added back to the positive fraction to un-do the effect of enrichment. B) Increased frequency of antigen-specific cells generated after seven days of culture by Kb-Trp2 nano-aAPC as a result of enrichment. Negative (left), positive (middle), and negative added back to positive (right) fractions were eluted and cultured for seven days, then stained with cognate Kb-Trp2 (top) and control Kb-SIINF (bottom) dimer. C) 10-15 fold increase in frequency of Kb-Trp2 cells (*, $p<0.001$ by t-test) and 2-3 fold increase in total Kb-Trp2 cells ($p<0.05$) when cells are enriched. D) Representative FACS plots (3 experiments each) of Db-GP100, Kb-SIINF, and Ld-A5 dimer expansion seven days after enrichment with cognate nano-aAPC. E) Summary of percent antigen-specific cells (left) and total antigen specific cells (right) after enrichment and activation with indicated nano-aAPC. F)

Three antigens (Db-GP100, Kb-SIINF, Kb-Trp2) enriched and expanded simultaneously. Representative FACS plots of antigen-specificity for each antigen from the same T cell culture. G) Comparison of antigen-specificity (left) and total antigen-specific cells (right) generated for the three indicated antigens when enriched and expanded individually (Single, blue) or together (Triple, green).

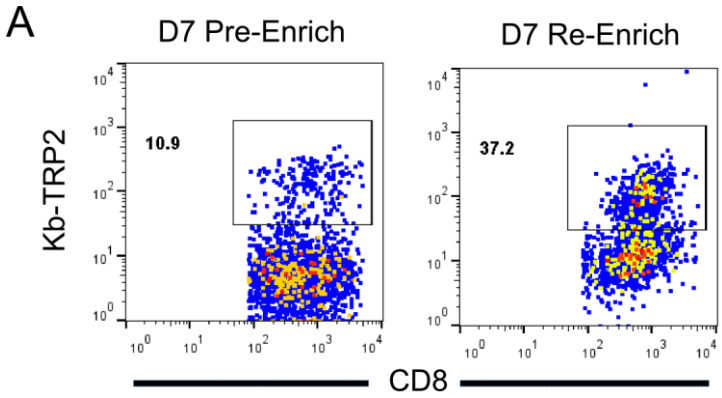

Figure 5.4: Re-Enrichment on Day 7

(A) A T cell culture enriched and expanded using Kb-Trp2 nano-aAPC seven days previously was harvested and re-enriched. Antigen-specific T cell frequency increased from 10% to approximately 40%.

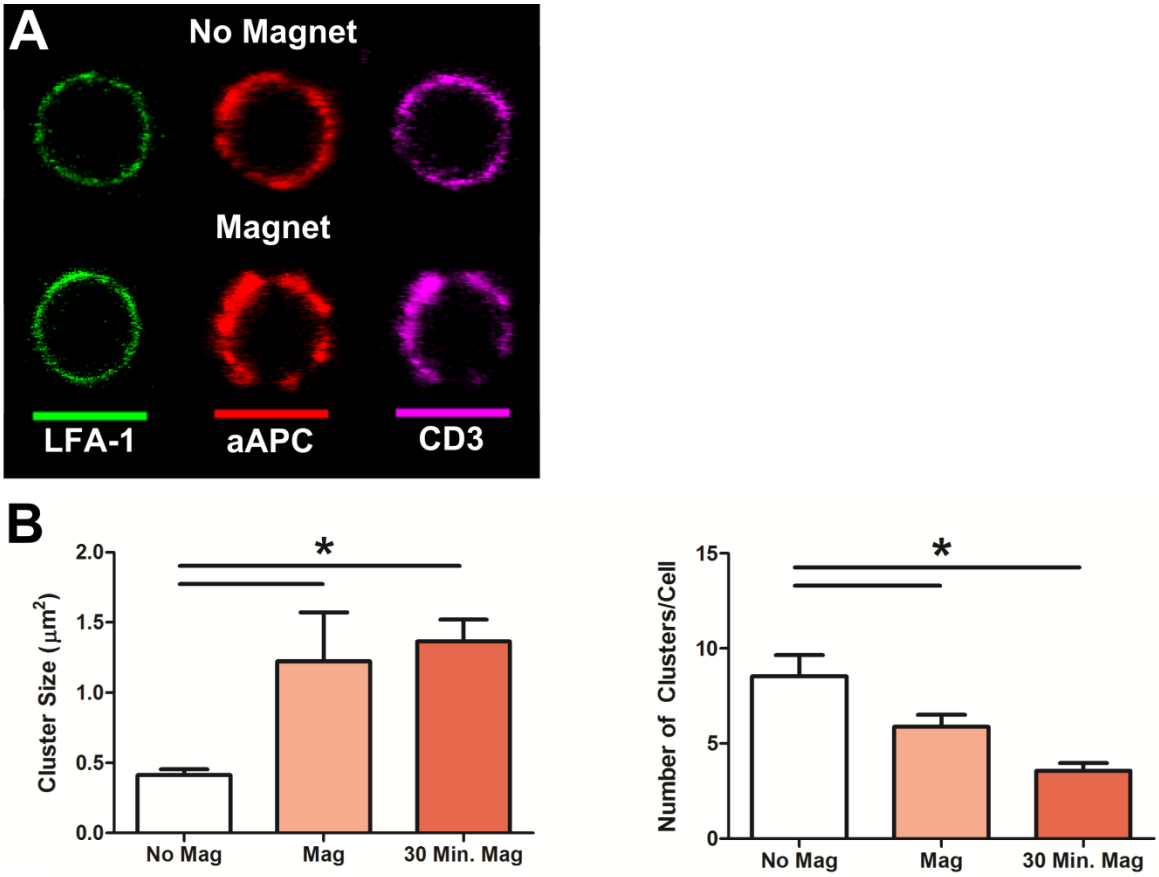

Figure 5.5: CD3 Aggregation Induced By Magnetic Enrichment Column

(A) Representative images of cells stained for LFA-1 (green), MHC-Ig on nano-aAPC (red), and CD3ε (magenta) before (top) and after (bottom) passage through a magnetic enrichment column (B) Average cluster area identified with cluster detection algorithm (20 cells/group). The Magnet and 30 Minutes in Magnet groups had significantly larger clusters than No Mag ($p < 0.01$ by ANOVA with Tukey post-test). The Magnet and 30 Minutes in Magnet groups also had significantly fewer clusters than No Mag ($p < 0.01$ by ANOVA with Tukey post-test).

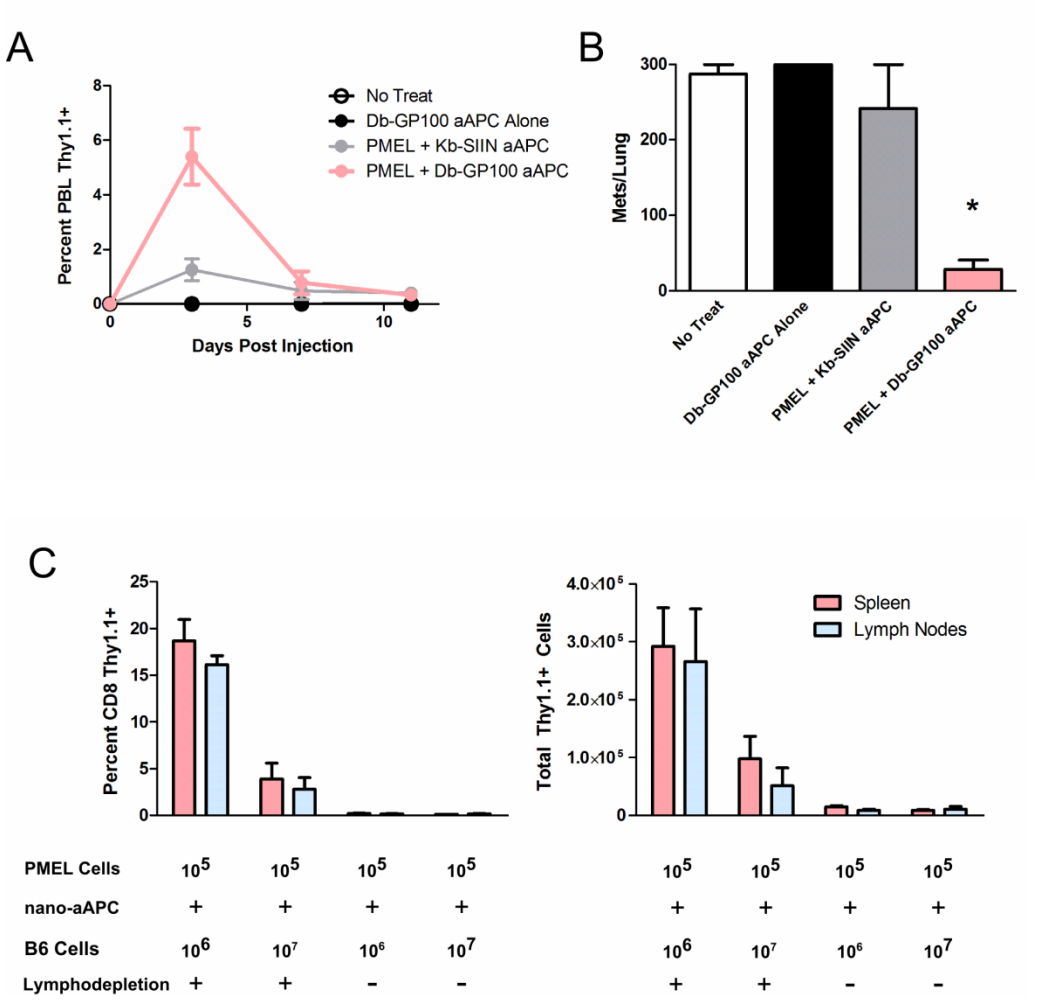

Figure 5.6: Expansion After Adoptive Transfer

(A) Expansion of one million Thy1.1+ pmel T cells after co-administration with cognate Db-GP100 nano-aAPC (pink) was significantly greater than after co-admistration with non-cognate Kb-SIIN nano-aAPC, as measured by frequency in blood. (B) Cognate nano-aAPC stimulated pmel cells led to decreased numbers of melanoma metastases in animals given B16 iv three days prior to treatment. Animals treated with non-cogante aAPC + T cells, cognate aAPC had significantly larger numbers of metastases per lung. (C) Effect of depletion and decreased

bystander competition on expansion after adoptive transfer. B6 mice were untreated or lymphodepleted with 500 cGy gamma radiation one prior to adoptive transfer of pmel T cells. The effect of enrichment was modeled by the co-administration of either 10^6 or 10^7 irrelevant B6 cells. Both lymodepletion and administration of fewer bystander cells increased the frequency (left) and total number (right) of pmel T cells recovered from spleen (pink) and lymph nodes (blue).

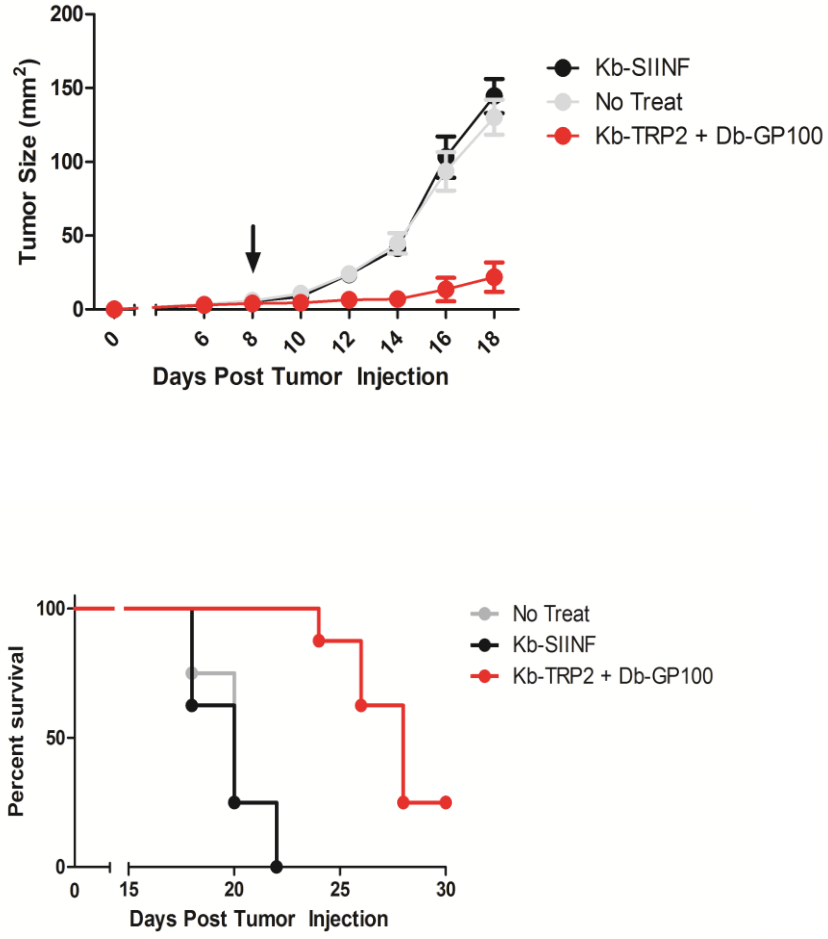

Figure 5.7: Treatment of Established Melanoma With Enriched and Expanded CTL

A) Cognate Kb-Trp2 and Db-GP100 Enriched+Expanded lymphocytes cultured for 5 days prior to adoptive transfer inhibited melanoma growth ($p<0.01$ by two-way ANOVA, 8 mice/group, red). Mice were injected with subcutaneous melanoma eight days prior and irradiated with 500 cGy gamma irradiation one day prior. Non-cognate Enriched+Expanded lymphocytes (black) did not inhibit tumor growth (compraed to untreated, gray). (B) Survival of animals from A; animals were euthanized when tumors reach greater than 150 mm^2. 2/8 mice showed complete

rejection of tumors in the Kb-Trp2 and Db-GP100 treated group, which had significantly longer survival compared to non-cognate and untreated groups ($p<0.01$ by Mantel-Cox).

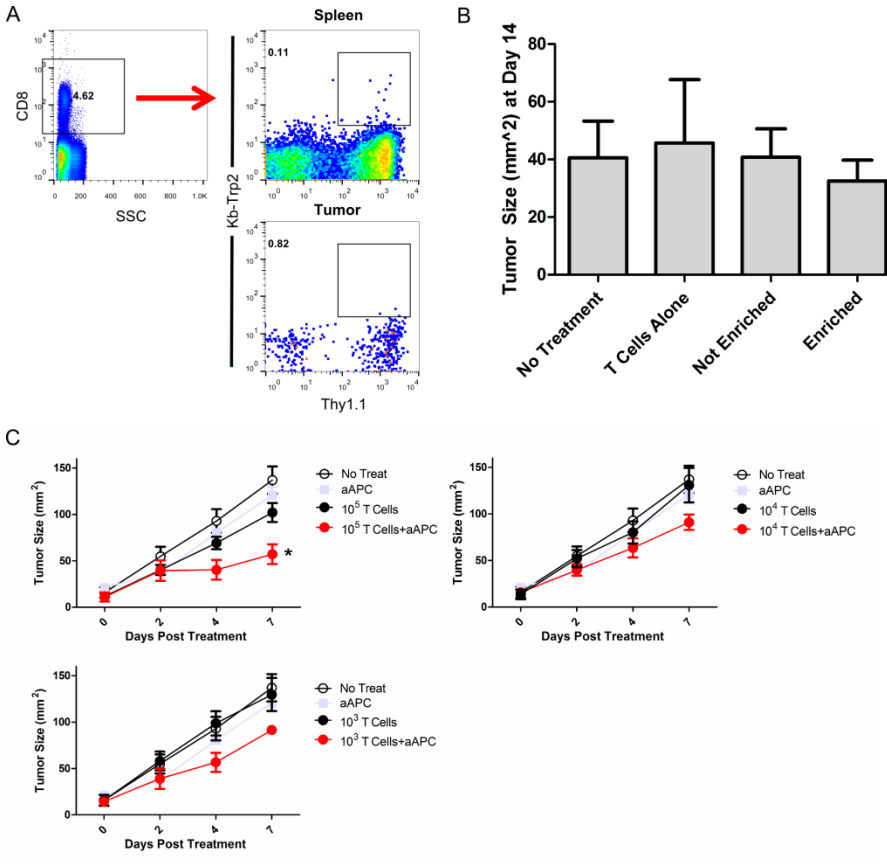

Figure 5.8. Immediate Reinfusion of Day 0 Cells in Tumor Treatment

A) FACS plots characterizing specificity of adoptively transferred Thy1.1 positive enriched and expanded cells. Cells from spleen (top right) and tumor (bottom right) were gated for CD8 lymphocytes (left); antigen specificity was assessed by Kb-Trp2 pentamer and Thy1.1 antibody staining. The highest frequency measured, 0.11%, is shown. (B) Treatment of eight day established melanoma in mice irradiated one day prior with 500,000 Enriched, Kb-Trp2 nano-aAPC co-infused cells. Tumor sizes at day 14 are shown. Controls include reconstituted Positive+Negative fractions (*not enriched),* unstimulated T cells, and untreated animals (5

animals/group). C) Subcutaneous B16 melanoma tumors treated with 10^5 , 10^4, or 10^3 pMEL cells +/- nano-aAPC. Co-transfer of 10^5 or 10^3 pMEL cells with aAPC inhibited tumor growth compared to T cells alone (*, $p < 0.05$ by two-way ANOVA), whereas 10^4 cells with aAPC was not significant compared to 10^4 cells alone, but was significantly less than no treatment (**, $p<0.05$ by two-way ANOVA).

5.6 References

1. Wrzesinski C, Paulos CM, Kaiser A, *et al.* Increased intensity lymphodepletion enhances tumor treatment efficacy of adoptively transferred tumor-specific T cells. *Journal of Immunotherapy*. 33(1), 1–7 (2010).

2. Restifo NP, Dudley ME, Rosenberg S a. Adoptive immunotherapy for cancer: harnessing the T cell response. *Nature reviews. Immunology*. 12(4), 269–81 (2012).

3. Dudley M, Gross C, Langhan M. CD8+ enriched "young" tumor infiltrating lymphocytes can mediate regression of metastatic melanoma. *Clinical Cancer …*. 16(24), 6122–6131 (2010).

4. Rosenberg S a, Yang JC, Sherry RM, *et al.* Durable complete responses in heavily pretreated patients with metastatic melanoma using T-cell transfer immunotherapy. *Clinical cancer research : an official journal of the American Association for Cancer Research*. 17(13), 4550–7 (2011).

5. Gattinoni L, Finkelstein SE, Klebanoff C a, *et al.* Removal of homeostatic cytokine sinks by lymphodepletion enhances the efficacy of adoptively transferred tumor-specific CD8+ T cells. *The Journal of experimental medicine*. 202(7), 907–12 (2005).

6. Dudley ME, Yang JC, Sherry R, *et al.* Adoptive cell therapy for patients with metastatic melanoma: evaluation of intensive myeloablative chemoradiation preparative regimens. *Journal of clinical oncology : official journal of the American Society of Clinical Oncology*. 26(32), 5233–9 (2008).

7. Klebanoff C a, Khong HT, Antony P a, Palmer DC, Restifo NP. Sinks, suppressors and antigen presenters: how lymphodepletion enhances T cell-mediated tumor immunotherapy. *Trends in immunology*. 26(2), 111–7 (2005).

8. Ernst B, Lee D, Chang JM, Sprent J, Surh CD, Cd I. The Peptide Ligands Mediating Positive Selection in the Thymus Control T Cell Survival and Homeostatic Proliferation in the Periphery. 11, 173–181 (1999).

9. Dummer W, Ernst B, Leroy E, Surh CD, Lee D. Autologous Regulation of Naive T Cell Homeostasis Within the T Cell Compartment. *Journal of Immunology*. 166, 2460–2468 (2001).

10. Wu Z, Bensinger SJ, Zhang J, *et al.* Homeostatic proliferation is a barrier to transplantation tolerance. *Nature medicine*. 10(1), 87–92 (2004).

11. Gattinoni L, Klebanoff C a, Restifo NP. Paths to stemness: building the ultimate antitumour T cell. *Nature reviews. Cancer*. 12(10), 671–84 (2012).

12. Zhou J, Shen X, Huang J, Hodes RJ, Rosenberg S a, Robbins PF. Telomere length of transferred lymphocytes correlates with in vivo persistence and tumor regression in melanoma patients receiving cell transfer therapy. *Journal of immunology (Baltimore, Md. : 1950)*. 175(10), 7046–52 (2005).

13. Hinrichs CS, Borman Z a, Gattinoni L, *et al.* Human effector CD8+ T cells derived from naive rather than memory subsets possess superior traits for adoptive immunotherapy. *Blood*. 117(3), 808–14 (2011).

14. Hinrichs CS, Borman Z a, Cassard L, *et al.* Adoptively transferred effector cells derived from naive rather than central memory CD8+ T cells mediate superior antitumor immunity. *Proceedings of the National Academy of Sciences of the United States of America*. 106(41), 17469–74 (2009).

15. Itzhaki O, Hovav E, Ziporen Y, *et al.* Establishment and Large-scale Expansion of Minimally Adoptive Transfer Therapy. *J Immunotherapy*. 34(2), 212–220 (2011).

16. Paller CJ, Antonarakis ES. Sipuleucel-T for the treatment of metastatic prostate cancer. *Human Vaccines and Immunotherapeutics*. 8(4), 509–519 (2012).

17. Perica K, De León Medero A, Durai M, *et al.* Nanoscale Artificial Antigen Presenting Cells for T Cell Immunotherapy. *Nanomedicine : nanotechnology, biology, and medicine*. [Epub Ahea (2013).

18. Jenkins MK, Moon JJ. The Role of Naive T Cell Precursor Frequency and Recruitment in Dictating Immune Response Magnitude. *The Journal of Immunology*. 188(9), 4135–4140 (2012).

19. Rizzuto G a, Merghoub T, Hirschhorn-Cymerman D, *et al.* Self-antigen-specific CD8+ T cell precursor frequency determines the quality of the antitumor immune response. *The Journal of experimental medicine*. 206(4), 849–66 (2009).

20. Obar JJ, Khanna KM, Lefrançois L. Endogenous naive CD8+ T cell precursor frequency regulates primary and memory responses to infection. *Immunity*. 28(6), 859–69 (2008).

21. Seliger B. Molecular mechanisms of MHC class I abnormalities and APM components in human tumors. *Cancer immunology, immunotherapy : CII*. 57(11), 1719–26 (2008).

22. Kaluza KM, Thompson JM, Kottke TJ, Flynn Gilmer HC, Knutson DL, Vile RG. Adoptive T cell therapy promotes the emergence of genomically altered tumor escape variants. *International journal of cancer. Journal international du cancer*. 131(4), 844–54 (2012).

23. Jensen SM, Twitty CG, Maston LD, *et al.* Increased frequency of suppressive regulatory T cells and T cell-mediated antigen loss results in murine melanoma recurrence. *Journal of immunology (Baltimore, Md. : 1950)*. 189(2), 767–76 (2012).

24. Kaluza KM, Kottke T, Diaz RM, Rommelfanger D, Thompson J, Vile R. Adoptive transfer of cytotoxic T lymphocytes targeting two different antigens limits antigen loss and tumor escape. *Human gene therapy*. 23(10), 1054–64 (2012).

25. Klebanoff C a, Gattinoni L, Palmer DC, *et al.* Determinants of successful CD8+ T-cell adoptive immunotherapy for large established tumors in mice. *Clinical cancer research : an official journal of the American Association for Cancer Research*. 17(16), 5343–52 (2011).

26. Morgan RA, Chinnasamy N, Abate-daga D, *et al.* Cancer Regression and Neurological Toxicity Following Anti-Mage-A3 TCR Gene Therapy. *Journal of Immunotherapy*. 36(2), 133–151 (2013).

27. Linette GP, Stadtmauer E a, Maus M V, *et al.* Cardiovascular toxicity and titin cross-reactivity of affinity enhanced T cells in myeloma and melanoma. *Blood*. (2013).

28. Lu X, Jiang X, Liu R, Zhao H, Liang Z. Adoptive transfer of pTRP2-specific CTLs expanding by bead-based artificial antigen-presenting cells mediates anti-melanoma response. *Cancer letters*. 271(1), 129–39 (2008).

29. Cobbold M, Khan N, Pourgheysari B, *et al.* Adoptive transfer of cytomegalovirus-specific CTL to stem cell transplant patients after selection by HLA-peptide tetramers. *The Journal of experimental medicine*. 202(3), 379–86 (2005).

30. Bouquié R, Bonnin A, Bernardeau K, *et al.* A fast and efficient HLA multimer-based sorting procedure that induces little apoptosis to isolate clinical grade human tumor specific T lymphocytes. *Cancer immunology, immunotherapy : CII*. 58(4), 553–66 (2009).

31. Zhang Y, Louboutin J, Zhu J, Rivera AJ, Emerson SG. Preterminal host dendritic cells in irradiated mice prime CD8 + T cell – mediated acute graft-versus-host disease. *The Journal of Clinical Investigation*. 109(10), 1335–1344 (2002).

32. Brown S, Konopa J, Zhou D, Thompson J. Expression of TNFalpha by CD3+ and F4/80+ cells following irradiation preconditioning and allogeneic spleen cell transplantation. *Bone marrow transplantation*. 33(4), 359–65 (2004).

6 Particle Shape Dependence of CD8+ T cell Activation by Artificial Antigen Presenting Cells[3]

6.1 Introduction

Geometry and spatial organization are critical components in many biological systems. The cytoskeleton, its organization, and the physical cues that it can transmit, result in dramatic

[3] This chapter is reproduced in part from **[add citation]** with permission from the publisher, written in collaboration with Joel Sunshine and Jordan Green.

effects on cell fate[1]. This is seen within the immune system in a variety of ways including during the interaction of a T cell with an antigen presenting cell (APC), which is a critical determinant of T cell fate and effector function. With activation, APC such as dendritic cells have major changes in their cell morphology resulting in significant increases in their overall cell surface area facilitating interaction with naïve T cells to direct T cell fate. Once an initial contact has been made by a T cell and an APC or some other target cell, T cell activation is further modulated by the formation of the immune synapse, a large surface area of close membrane apposition between the DC and T cell membrane, with concomitant cytoskeletal rearrangement and clustering of surface proteins[2-6]. Materials science approaches have helped to elucidate how the spatial organization and clustering of ligands that make up this synapse are important[7]. Thus, taking into account the geometry and spatial organization at cell-cell interfaces is important in studying biological responses.

Reductionist systems have facilitated the study of effective immune responses. One such system is the acellular artificial antigen presenting cell (aAPC). aAPCs have been made by coupling proteins required for T cell activation to particles. Minimally, T cell activation requires two sets of receptor-receptor interactions. One interaction, Signal 1, is the binding of major histocompatibility complexes (MHC) or a surrogate, such as anti-CD3, to bind the T cell receptor (TCR). A second interaction, Signal 2, is the binding of co-stimulatory receptors on the APC, such as B7.1, to ligands on the T cell, such as CD28. aAPC have been generated by coupling proteins that deliver Signal 1 and 2 to the surface of particles (**Fig. 6.1A**) made from a range of materials, including magnetic microparticles[8, 9], polystyrene particles[10], and PLGA microparticles[11-13]. Such systems have been broadly applied to tumor immunotherapy,

vaccination, and immunosuppression, and are amenable to *in vivo* or *ex vivo* T cell stimulation and offer possible novel translational approaches to immunotherapy[9, 14-19].

While useful, the Signal 1 and 2 paradigms alone do not capture aspects of spatial organization or the geometry of interactions. Previous work developing aAPCs have not attempted to re-capitulate these aspects of APC behavior. As a result, all aAPCs tested thus far have used spherical particles for their aAPC platforms, which unlike DCs minimize surface area for a given volume (**Fig. 6.1B**).

Further aAPC development may require incorporation of additional biomimetic cues beyond the presentation of signal 1 and signal 2 such as biomimicry of the surface density, dynamic protein spatial organization, and the geometry of the interface between the aAPC and the target. These cues could potentially be incorporated into next-generation aAPCs by nanoengineering approaches including presentation of cues on fluid membranes or in a patterned manner and by utilizing non-spherical particle shapes[19, 20].

Particle shape has only recently become a design parameter of interest in the field of material design for drug delivery. Shape can play a role in tuning the rate and mechanism of cellular uptake[21], can dramatically reduce internalization by phagocytic cells such as macrophages[22, 23], can change the biodistribution of the drug delivery vehicle[24, 25], and has been posited as potentially modulating the ability of a particle to bind a cell in part by increasing the surface area for interaction[24, 26]. In fact, a recent study by Barua et al. showed that antibody coated polystyrene nanorods had higher specific and reduced non-specific cellular uptake than spherical counterparts, demonstrating a significant relationship between particle shape and cell binding/unbinding [27].

A key consideration in cancer immunotherapy remains the efficient stimulation of antigen (Ag)-specific CTLs. *In vivo*, a criticial interaction for generation of activated, effector CD8+ T cells is the interaction between antigen presenting cells, such as dendritic cells or macrophages, with CD8+ T cells. In the development of acellular systems for T cellsstimulation, previous literature has focused predominantly on the proteins involved in the interaction between APCs and T cells[8, 9, 13, 28-30], and recent studies extended this to release of cytokines[12, 31]. However, the biological interaction between T cells and their targets is distinctly not an interaction most appropriately represented by two interacting spheres. We hypothesized that non-spherical aAPCs would offer improved activation of CD8+ T cells. To test this hypothesis, we adapted a film-stretching method for controlling the shape of microparticles made from poly (lactic-co-glycolic) acid (PLGA)[32] to generate ellipsoidal aAPCs with varying long axis lengths and aspect ratios (ARs)(**Fig. 6.1C,D**). To explore how particle shape might interact with particle dose and surface antigen density, we synthesized spherical and ellipsoidal aAPCs at different antigen densities, and then varied the particle dose, antigen density, and aAPC shape used to activate the T cells *in vitro*. To investigate the mechanism behind these effects, we performed confocal imaging to analyze aAPC:T cell conjugate formation. Finally, we compared the ability of spherical and ellipsoidal aAPCs in an *in vivo* melanoma tumor prevention model.

6.2 Materials and Methods

Film formation and particle stretching

Lyophilized PLGA microparticles that were synthesized by single emulsion (see supplemental methods) were added to a solution containing 10% PVA and 2% glycerol by weight at 5 mg/ml (particles/ml solution). The solution was poured on a flat surface and allowed

to dry overnight. After drying, strips of the resulting film were cut out and placed on an aluminum-stretching device consisting of two aluminum blocks that can be separated by sliding on aluminum rods. The film and custom-made stretcher were placed in a 90°C oven for 10 minutes and then the film was slowly stretched inside of the oven to the desired stretch ratio by separating the two blocks. After allowing the film to cool down to room temperature, the film was removed and dissolved in 10 ml of deionized water, then the particles were centrifuged (4000 rpm for 5 min) and washed 3x, and finally resuspended in deionized water, frozen, and lyophilized. Spherical particles in all experiments were also prepared similarly; they were heated along side of the ellipsoidal particles but simply not stretched.

aAPC synthesis

Soluble MHC-Ig dimers were prepared and loaded with peptide as described (see supplemental methods)[33]. Spherical and ellipsoidal microparticles were resuspended in coupling buffer (0.1M MES pH 6.0), and activated with EDC (1-Ethyl-3-(3-dimethylaminopropyl)carbodiimide, Sigma-Aldrich) and sulfo-NHS (N-hydroxysulfosuccinimide). As an example, 5 mg of microparticles were resuspended in 1 ml of coupling buffer and activated with 10 mg of EDC and 13 mg of sulfo-NHS for 15 min at 1000 rpm on a multitube vortexer (VWR). Activated microparticles were then centrifuged, the supernatant was removed, and the activated particles were resuspended in 1 ml PBS (pH 7.4) and transferred to a 5 mL glass scintillation vial for coupling. As an example, 8 µg of MHC-dimer and 10 µg of anti-CD28 antibody (always in this ratio) were added to 2 µg of activated PLGA microparticles, and then the reaction was allowed to proceed in the cold room (4°C) for 4 hours. After 4 hours, the aAPCs (here, 2 mg of aAPCs) were centrifuged and washed 2x with PBS, then

centrifuged, re-suspended in 200 µl of 0.2 mm-filtered sterilized 100 mg/ml endotoxin-free sucrose solution, frozen, and lyophilized overnight.

In vitro CTL induction and CFSE dilution

pMEL TCR/Thy1^a Rag-/- transgenic mice were a gift from Nicholas Restifo (National Institutes of Health, Bethesda, MD) and maintained as homozygotes. C57BL/6j were purchased from Jackson Laboratories (Bar Harbor, ME). All mice were maintained according to Johns Hopkins University's Institutional Review Board. The pMEL T cells used were obtained from homogenized pMEL mouse spleens after depletion of RBC by hypotonic lysis. CD8+ T cells were isolated using a CD8-negative isolation kit and magnetic enrichment column from Miltenyi Biotec (Cologne, Germany) and labeled with carboxyfluorescein succinimidyl ester (CFSE) for 15 minutes at 37°C, then washed extensively. Cells and aAPCs at the indicated amounts and dosages were mixed and cultured for 4-7 days in complete RPMI media supplemented with T cell factor, a cytokine cocktail harvested from human plasma[34]. Cell proliferation was quantified by manual cell counting, and final T cell count was divided by the initial T cell count for fold-change data.

aAPC-T cell conjugate formation evaluation

For confocal imaging, PLGA microparticles with encapsulated 5(6)-carboxy-tetramethylrhodamine dye (TAMRA, Nova Biochem, San Diego, CA) were synthesized (see supplemental methods). These labeled particles were then cast into a film, and the film stretching and subsequent sythesis of aAPC from spherical and ellipsoidal TAMRA-loaded particles were done as before. $1x10^6$ CFSE-labeled CD8+ T cells were incubated with 1 mg spherical or ellipsoidal aAPC for 60 minutes at 37ºC in a No. 1.5 glass bottom dish (MatTek, Ashland, MA).

Images were acquired on a Zeiss LSM 510 META (Zeiss, Oberkochen, Germany) laser scanning confocal at 40x magnification at the Johns Hopkins School of Medicine Microscopy Facility. aAPC/T cell areas of contact were quantitated by image analysis on ImageJ.

In vivo activity of aAPCs

We performed a subcutaneous B16 melanoma tumor prevention mouse model (**Fig 6a**). The animals were preinjected intravenously (i.v.) with naïve pMEL CD8+ T cells (day -1, $2x10^6$ cells/animal), subcutaneously (s.c.) in the flank with aAPCs (day 0, 2 mg aAPCs/animal), then injected with $2x10^5$ tumor cells in the hindlimb (day 3). Responses were boosted with subsequent s.c. injection of a second aAPC batch (day 6, 2 mg aAPCs/animal), and tumor growth over the course of the experiment was followed by measurement with external calipers. Once the tumor size reached 200 cm^2, the mice were sacrificed. Treatment groups consisted of ellipsoidal and spherical cognate aAPC (n=8), and control groups consisted of ellipsoidal non-cognate (n=8) and CD8+ T cell alone groups (n=5).

Statistics

All statistics were performed in GraphPad Prism. For analysis of surface protein quantification, we performed pairwise t-tests. For analysis of specific CD8+ T cell proliferation in response to specified aAPC dose, protein density, and shape of aAPC, we performed two-tailed t-tests with a Bonferroni correction for multiple comparisons. For analysis of quantification of cognate formation and area of contact between aAPCs and CD8+ T cells, we performed pairwise t-tests. For analysis of tumor size, we performed a 1-way ANOVA with Tukey post-test. For *in vivo* survival analysis, we used the Log-rank (Mantel-Cox) test. Data in text are presented as mean ± SEM.

Microparticle fabrication

The poly(lactide-glycolide) (PLGA) microparticles were made by dissolving 200 mg of acid-terminated PLGA (50:50 LA/GA, MW 38,000-54,000, Sigma-Aldrich) in 5 ml of dicholoromethane (ACS grade, Sigma-Aldrich). The dissolved PLGA was then added dropwise to 50 ml of an ice-cold 1% poly(vinyl alcohol) (PVA) solution, which was homogenized at 5,000 rpm. After dropwise addition, the solution was allowed to homogenize for an additional minute, and then added to a 100 ml solution of 0.5% PVA which was stirring at 500 rpm in the cold room (at 4°C). After stirring for 4 hours to allow for solvent evaporation, the particles were centrifuged (4000 rpm for 5 min) and washed 3x, resuspended in 5 mL of deionized water and lyophilized.

For confocal imaging, tetramethyl rhodamine (TAMRA) loaded microparticles were synthesized via single emulsion as follows: The TAMRA was dissolved in dichloromethane at 1 mg/ml. 200 mg of acid-terminated PLGA was dissolved in 4.9 ml of DCM and 100 µl of TAMRA solution was added to the PLGA DCM phase. Particle synthesis otherwise followed the same protocol as the single emulsion particles above.

Preparation of MHC-Ig Dimers

Briefly, Db-Ig molecules were stripped under mildly acidic conditions (pH 6.5) and refolded in the presence of 40 fold molar excess peptide and 2-fold molar excess of human β2-microglobulin. Peptides GP100 (KVPRNQDWL; the "cognate" peptide) and ASN (ASNENMETH; a "non-cognate" peptide) were purchased from Genscript (Piscataway, NJ). Protein concentration was determined after labeling by size exclusion High Performance Liquid Chromatography.

Characterization of aAPCs:

Measuring size and aspect ratio by SEM

Lyophilized particle samples were spread on conductive carbon tape mounted on aluminum SEM mounts (Eletron Microscopy Sciences, Hatfield, PA). Samples were sputter coated with a chromium sputter coater and imaged on a Leo/Zeiss Field emission SEM in the Johns Hopkins Core Microscopy facility. Particle size and aspect was quantified using ImageJ software. For spherical particles, a single diameter was measured for each particle. For ellipsoidal particles, two diameters were measured (long-axis and short-axis) and the aspect ratio was calculated by dividing the two.

Surface protein quantification and release

Surface protein quantification was performed by conjugation of unlabeled anti-CD28 mAb and fluorescently labeled MHC-IgG dimer and anti-CD28 antibody to the surface of EDC/sulfo-NHS pre-activated (or not pre-activated) 2-fold stretched (AR 2.8) ellipsoidal or spherical PLGA microparticles for 4 hours at 4°C. These aAPC were centrifuged washed 3x, and then their fluorescence was characterized on a Synergy 2 plate reader (Biotek, Winooski, VT) and by confocal microscopy. Colocalization analysis was done in ImageJ using "Just Another Colocalization Plugin (JaCoP)" with at least 10 particles/sample.

Release from surface was characterized by incubating 10 mg of aAPC (spherical, ellipsoidal) with labeled dimer in 500 µl PBS at 37°C for 1 week. At 3 days and 7 days, the particles were centrifuged and the supernatant was removed and stored for subsequent analysis. At 7 days, the supernatant was removed, and then the aAPC were resuspended the fluorescence was characterized.

Intracellular cytokine staining

Six days after primary stimulation with aAPC, T cell functional activity was assessed by re-challenge with peptide-pulsed C57Bl/6j splenocytes. Splenocytes were pulsed with the indicated concentration of peptide for 2 hours at 37°C then washed. 200,000 aAPC-activated T cells were incubated in complete RPMI with 200,000 splenocytes for 4 hours in a round bottom 96 well plate in the presence of 0.2 μl GolgiPlug, 0.2 ul GolgiStop, and anti-CD107a-fitC (BD Biosciences, Mountain View, CA). Cells were washed and fixed using a BD Cytofix/Cytoperm kit (BD Biosciences) according to the manufacturer's instructions, then stained with anti-IFNγ PE (BioLegend). Cytokine staining was assessed by flow cytometry and frequency of cytokine functional cells was assessed by comparison with an unstimulated control in FlowJo (TreeStar).

6.3 Results and Discussion

Ellipsoidal aAPC synthesis and characterization

Ellipsoidal, biodegradable aAPCs were synthesized by first fabricating PLGA microparticles which were then stretched into ellipsoids using a film stretching method. This method offers the advantage of allowing a direct comparison of particle shape and surface area, while retaining equivalent volumes.

The single emulsion PLGA (50:50 LA/GA, MW 38,000-54,000) microparticle synthesis resulted in spherical microparticles (**Fig. 6.1D, spheres**) with a number-weighted average diameter of 4.3 μm and a volume-weighted diameter of 6.7 μm (**Fig. 6.1E**). We were able to control the aspect ratio (AR) of ellipsoidal microparticles with a high degree of accuracy by imposing different degrees of stretch (STR) onto the film (**Fig. 6.1D**). This technique exhibits a

high correlation between predicted AR and empirically measured AR (by SEM) for a fixed volume ellipsoid that has been elongated in one direction ($AR = STR^{1.5}$) (**Fig. 6.1F**). This indicates that particle stretching is a feasible, controllable process that allows for flexibility in specifying the shape of the resulting particles. Ellipsoidal and spherical microparticles were then made into aAPCs by EDC/sulfo-NHS mediated covalent coupling of a dimeric MHC-Ig fusion protein[35] and an antibody against CD28 to free carboxyl groups on the particle surface.

Key parameters to evaluate these aAPCs include characterizing the total protein on the surface, the protein density, the dimer/anti-CD28 antibody ratio and the surface distribution on the spherical and ellipsoidal aAPCs. To characterize the conjugation efficiency with different amounts of protein added, we synthesized spherical and ellipsoidal (STR 2/AR 2.8) aAPC with fluorescently labeled MHC-Ig dimer and unlabeled anti-CD28 antibody, and characterized the particles by fluorimetry (**Fig. 6.1G**). By increasing the amount of MHC-Ig used during synthesis, we achieved protein coupling of up to 0.75 □g MHC-Ig/mg PLGA (**Fig. 6.1G**). Coupling efficiency was 15-20% over the entire range of protein analyzed, and there were no statistically significant differences between spherical and ellipsoidal aAPC in terms of their total protein content or protein density ($p > 0.35$ for all comparisons) (**Fig. 6.1G**). PLGA microparticles showed only minor auto-fluorescence and did not interfere with dye emission (**Fig. 6.2**). Of note, while total surface area increases modestly with stretching, with a modest increase of only 16% for AR 2.8 particles and maximum increase in net surface area of the aAPCs of 50% for AR 6.6 aAPCs (**Table 6.1C**), stretching the aAPCs dramatically increases surface flatness along the long axis of the aAPCs, with the radius of curvature increasing 23-fold over the same range (**Table 6.1E**).

To evaluate whether spherical or ellipsoidal aAPCs might show differences in dimer/anti-CD28 antibody ratio or surface distribution of the two proteins, we synthesized spherical and ellipsoidal aAPCs with fluorescently labeled MHC-Ig dimer and labeled anti-CD28 antibody, and characterized the particles by fluorimetry and by confocal microscopy (**Fig. 6.3**). Spherical and ellipsoidal aAPC did not show significant differences in MHC-dimer amount or density, anti-CD28 amount or density, or MHC-dimer/anti-CD28 ratio (**Fig. 6.3**). Approximately 85-90% of the protein on the surface required the EDC/NHS pre-activation step and non-specific protein adsorption was low and equivalent between aAPC shapes (**Fig. 6.3**). The fluorescence signals from the two proteins were co-localized in both cases (quantified here by the Pearsons correlation), and the distribution pattern was equivalent between the two groups (**Fig. 6.3**). Taken together with the only modest increase in total surface area (16%) for 2-fold stretched particles (AR 2.8) as compared to spherical particles (**Table 6.1**), the protein surface characterization data indicate that the spherical and ellipsoidal particles are equivalent with respect to protein density, total protein amount, protein ratio, protein organization and co-localization, and surface release.

While bulk polymer degradation from PLGA microparticles has been well investigated in the drug delivery field[36-38], the effect of degradation on release of surface-coupled proteins is less well studied. For aAPCs, presentation of immobilized proteins are critical for cytotoxic T cell (CTL) activation and thus it is important to study release of these proteins[10]. To characterize surface degradation, aAPCs bearing fluorescently labeled MHC-Ig were incubated for varying amounts of time in PBS at 37°C. Supernatants were recovered through centrifugation of the aAPCs and released protein quantified by protein fluorescence. For both spherical aAPCs and ellipsoidal aAPCs, 60-70% of the protein that was conjugated to the surface

was released over 7 days, with 30-40% of the protein released in the first 3 days. At 7 days, 30-40% of the protein remained on the surface of the aAPCs, as quantified by total fluorimetry from the particles (**Fig. 6.1H**). There was no significant difference in this release profile between ellipsoidal and spherical aAPCs.

We characterized the stability of the ellipsoidal aAPC shape by analyzing their relaxation rate to the more stable spherical shape. Previous studies have indicated that relaxation rates are dependent on surface characteristics, molecular weight, polymer composition, and temperature[32]. We observed very little shape relaxation for high aspect ratio ellipsoidal aAPC over 1 week at 37°C in PBS, indicating that the shape transition is slow for ellipsoidal aAPCs with the chosen lactide to glycolide ratio (**Fig. 6.4**). This agrees with published relaxation timescales for high aspect ratio PLGA with hydrophilic surfaces, such as those used here[32].

Effect of aAPC shape, dose, and antigen density on T cell activation

In order to assess the impact of particle elongation, we measured the ability of aAPC to induce antigen specific CD8+ T cell expansion of pMEL TCR transgenic CD8+ T cells. Spherical and 2-fold stretched (AR = 2.8) ellipsoidal aAPCs were synthesized at 3 different cognate MHC-peptide densities by adding 4, 1, and 0.5 μg of Db-Ig GP100/mg PLGA with corresponding amounts of anti-CD28 antibody, resulting in spherical and ellipsoidal aAPC with 0.75, 0.14, and 0.08 μg of MHC-dimer/mg PLGA (**Fig. 6.1G**). Spherical aAPCs bearing non-cognate Db-Ig ASN at the highest protein density were used as a negative control. The aAPCs were added to pMEL TCR transgenic CD8+ T cells at 3 aAPC to cell ratios (1, 0.1 and 0.01 mg aAPC/10^5 cells). Proliferation was assessed at day 4 by CFSE dilution (see methods for details)

and on day 7 by cell counts. Day 4 CFSE dilution for a representative Db-Ig density (0.75 ug Db-Ig/mg PLGA) is shown at each aAPC:cell ratio (**Fig. 6.5A**), while day 7 fold proliferation data are shown for all three parameters of aAPC shape, aAPC:cell ratio, and Db-Ig density (**Fig. 6.5B**).

At a subsaturating dose of aAPC, 0.01 mg/10^5 cells, ellipsoidal but not spherical aAPCs induced CD8+ T cell proliferation as measured by CFSE dilution (**Fig. 6.5A 0.01mg**). This was reflected in Day 7 cells counts, with only ellipsoidal aAPC bearing 0.75 or 0.14 μg Db-Ig/mg PLGA inducing CD8+ T cell expansion, of 22-fold and 11-fold expansion, respectively (**Fig. 6.5B 0.01mg;** $p<0.001$ and $p<0.01$ for 0.75 and 0.14 μg Db-Ig/mg, respectively**)**. At an intermediate aAPC:cell ratio (0.1 mg/10^5 cells), ellipsoidal aAPC also induced higher levels of CFSE dilution (**Fig. 6.5A 0.1mg**) than spherical aAPC. Cell counts indicated ellipsoidal aAPC conferred an approximately 3-fold increase in total CD8+ T cell expansion by day 7 compared to spherical aAPCs (**Fig. 6.5B 0.1mg;** $p<0.001$ and $p<0.01$ for 0.75 and 0.14 μg Db-Ig/mg, respectively). At saturating high aAPC:cell ratios (1 mg/10^5 cells) and the highest Db-Ig density, differences between ellipsoidal and spherical aAPCs were substantially smaller but still statistically significant ($p<0.05$) (**Fig. 6.5A/2B, 1mg**). However, when Db-Ig density on aAPC was titered to 0.1 □g Db-Ig/mg PLGA, ellipsoidal aAPC regained their advantage, stimulating significantly more CD8+ T cell expansion than spherical aAPC ($p<0.001$). aAPC bearing non-cognate MHC-peptide did not induce CFSE dilution or CD8+ T cell proliferation (**Fig. 6.5A left**).

Two parameters that are important in T cell activation are total amount of antigen-MHC complex and antigen density[39-41]. We wanted to study the impact of shape independent of total antigen-MHC complex or antigen density. To separate the effect of shape from the effect of

total antigen-MHC dose or antigen density, we replotted the expansion data from **Fig. 6.5B** versus total antigen-MHC dose (**Fig. 6.5C**) and antigen density (**Fig. 6.5D**). Increasing total dose results in increased CTL expansion, but at all total doses, ellipsoidal aAPC (in red) outperform their spherical counterparts (in black) (**Fig. 6.5C**). For example, at a total dose of MHC near 0.1 $\mu g/10^5$ cells, all 3 ellipsoidal formulations showed higher fold-expansion than the 3 spherical formulations. There is also a positive correlation between increased antigen density and CD8+ T cell proliferation at a given particle dose (**Fig. 6.5D**), but across the probed density ranges, ellipsoidal particles (in red) show higher fold-expansion than comparable spherical particles (in black). For example, in **Fig. 6.5D 0.1mgs**, ellipsoidal particles with an MHC density of 400±140 and 240±70 MHC-Ig dimer/μm^2 displayed higher fold expansion (19.7±0.7 and 6.3±0.8 fold respectively) than spherical particles with a similar MHC density of 350±60 MHC-Ig dimer/μm^2 (2.3±1 fold expansion). Thus, across a range of total antigen doses and protein densities, when controlling for dose and density, ellipsoidal aAPC were more efficient at inducing CD8+ T cell expansion than spherical aAPC.

To further study the importance of AR on CD8+ T cell stimulation, PLGA microparticles were synthesized, stretched varying amounts, and made into aAPCs. There was a striking correlation between increased AR and increased CD8+ T cell proliferation (**Fig. 6.6**). Interestingly, the greatest gain in CD8+ T cell numbers was seen by increasing the aspect ratio of the ellipsoidal aAPC by increasing the applied stretch from 1.5-fold to 2-fold, which resulted in approximately 2 fold CD8+ T cell expansion up to approximately 20 fold CD8+ T cell expansion at a 0.01 mg aAPC/10^5 cells dose (**Fig. 6.6C**). Analysis of the number of divisions from the CFSE dilution data (**Fig. 6.6A**) revealed that increasing AR further resulted in a larger percentage of cells going through a significantly greater number of divisions (**Fig. 6.6B**). The

fraction of non-responders (generations 0-1) progressively decreases with increasing AR, eventually resulting in only 11% non-responders for the 3.5-fold stretched (AR 6.6) aAPCs. The number of cells undergoing 4-5 or 6-7 divisions also increases with every additional .5-fold increase in applied film stretch. This effect was also saturable with very high doses of aAPCs (**Fig. 6.7**). Therefore, increasing aspect ratio of the aAPCs resulted in increased CD8+ T cell expansion consistently up to 3.5 fold stretched aAPCs (AR 6.6), with the greatest improvement in overall CD8+ T cell expansion seen when going from 1.5-fold to 2-fold applied stretch, which corresponds to a change in AR from 1.8 to 2.8.

Thus, increasing aspect ratio of ellipsoidal aAPC results in improved CD8+ T cell activation, and this enhanced proliferation that is mediated by ellipsoidal aAPC is primarily dependent on aAPC geometry rather than any differences in the density or amount of conjugated surface protein.

T cell quality, as reflected by the amount and diversity of cytokines and cytotoxic markers produced when T cells are re-challenged by antigen, is a critical parameter for assessing responses[42]. To determine the functional status of the expanded CD8+ T cell population, we re-challenged aAPC-activated CD8+ T cells with peptide-pulsed splenocytes and measured the production of a key cytokine, IFNγ, as well as measured the degranulation marker, CD107a in an intracellular cytokine staining (ICS) assay. Function tracked with proliferation; there was no significant difference in the quality of CD8+ T cells generated from spherical or ellipsoidal aAPCs as determined by IFNγ or CD107a expression (**Fig. 6.8**). There was no significant difference when comparing CD8+ T cell quality after equal doses of aAPCs (which resulted in higher proliferation with the ellipsoidal aAPC) or when comparing equal proliferation (from lower doses of ellipsoidal aAPC).

aAPC aspect ratio and T cell conjugate formation

Antigen recognition on APC is known to trigger coordinated cytoskeletal rearrangements in both T cells and APCs, leading to close apposition of their cellular membranes. The resulting interactions mediate T cell activation and, when visualized by imaging or flow cytometry, are termed cell-cell conjugates[43].

To evaluate the formation of T cell-aAPC conjugates, naïve CD8+ T cells were incubated at 37°C with spherical or ellipsoidal aAPCs. Cell-aAPC interactions were visualized after a one-hour incubation by confocal imaging. In the presence of ellipsoidal aAPCs bearing cognate MHC/peptide, T cell membranes could be observed in close apposition to the aAPC's long but not short axis, creating a T cell "cap", characteristic of conjugate formation (**Fig. 6.7A**).

Conjugate formation was observed for CD8+ T cells incubated in the presence of either ellipsoidal (**Fig. 6.7B**) or spherical (**Fig. 6.7C**) aAPC. Importantly, conjugate formation was a process driven by recognition of cognate antigen, as neither spherical nor ellipsoidal aAPCs bearing non-cognate MHC/peptide induced cap formation (**Fig. 6.7D, E**). When quantitated, conjugate formation was approximately 2.5-fold more frequent with ellipsoidal aAPC, with 4.6 ± 0.9% of the CD8+ T cells forming conjugates with the ellipsoidal aAPC compared to 1.8 ± 0.4% with spherical aAPC ($p = 0.01$, **Fig. 6.8F**). In addition to being 2.5-fold more frequent, we observed a significant increase ($p = 0.01$, **Fig. 6.8G**) in the contact length between the CD8+ T cells and the ellipsoidal aAPC (3.6 ± 0.6 μm/interface) as compared to spherical aAPC (1.9 ± 0.2 μm/interface).

Time-lapsed imaging revealed a striking reorientation and rearrangement of the CD8+ T cell surface against the aAPC long axis. Initially, the CD8+ T cell appears to contact the aAPC

along the short axis but with time migrates along the long axis rearranging its membrane against the long axis of the ellipsoidal aAPCs (**Fig. 6.7H**). Membrane reorientation and alignment against the long axis of ellipsoidal aAPC strongly suggests a preference for the flat surface presented by the long axis of ellipsoidal aAPC. We thus observe that ellipsoidal aAPCs generate increased biomimetic interactions with T cells compared to spherical aAPCs, and suggests that the improved T cell expansion seen *in vitro* is due to increased frequency and size of T cell-aAPC contact along the long axis of the ellipsoidal aAPCs.

Effect of aAPC shape in vivo

To test the activity of high aspect ratio aAPCs *in vivo*, we utilized a subcutaneous B16 melanoma tumor model. We injected a dose of aAPC subcutaneously 3 days before and a second dose 3 days after tumor injection into the hindlimb (see **Fig. 6.9A**). Treatment with either ellipsoidal ($p = 0.0009$ vs. non-cognate) or spherical ($p = 0.02$ vs. non-cognate) cognate aAPCs led to significant reductions in tumor size as compared to controls that received control non-cognate aAPCs or CD8+ T cells alone (**Fig. 6.9B**). By day 19, cognate ellipsoidal aAPC treated tumors had only reached a size of 42.5 ± 14.9 mm^2, compared to 90.5 ± 33.8 mm^2 for cognate spherical, 164.5 ± 28.6 mm^2 for non-cognate ellipsoidal, and 154.4 ± 35.4 mm^2 for CD8+ T cell alone treated mice. Area under the curve (AUC) of tumor growth over the course of the entire experiment showed a similar pattern, with tumors growing a total of 44.3 ± 15.6 mm^2, compared to 105.3 ± 34.7 mm^2 for cognate spherical, 251.0 ± 46.6 mm^2 for non-cognate ellipsoidal, and 238.0 ± 46.6 mm^2 for CD8+ T cell alone treated mice. Cognate ellipsoidal aAPCs thus reduced tumor size more than spherical aAPCs, but this effect did not achieve statistical significance ($p = 0.13$).

Survival studies revealed statistically significant differences in survival between mice injected with ellipsoidal cognate aAPC over spherical cognate aAPC (**Fig. 5C**)(p=0.05), as well as ellipsoidal non-cognate control aAPCs (p=0.004). 25% of the animals in the cognate ellipsoidal aAPC group completely cleared tumor by day 19 and survived the course of the experiment, which did not occur in any other treatment or control groups. Furthermore, ellipsoidal aAPC treatment led to a significant delay in tumor growth, with no mice reaching substantial tumor burden until 22 days after tumor injection, compared to 19 days for the other three groups.

Critically, this research demonstrates that increased aspect ratio acellular aAPCs, which only differ in their shape (and have equivalent volume, antigen dose, antigen co-localization, and antigen density) as compared to spherical controls, not only engender enhanced antigen specific activation *in vitro* but *in vivo* as well, and this enhanced activation has functional consequences which lead to reduced tumor burden and enhanced survival.

6.4 Conclusions

Previous aAPC systems have utilized spherical particles, yet the biological interaction between T cells and APCs is dramatically dissimilar from two spheres interacting. In this study, we investigated how engineering the shape of an aAPC might enhance aAPC activity both *in vitro* and *in vivo*. When antigen dose, antigen density, protein ratio, protein co-localization, and particle volume were held equivalent between spherical and ellipsoidal aAPCs, high aspect ratio ellipsoidal aAPCs showed significantly enhanced activity over spherical aAPCs. Increasing the aspect ratio of ellipsoidal aAPCs led to enhanced activity up to AR 6.6. This enhanced activity was also observed *in vivo*, where ellipsoidal cognate aAPCs caused increased survival in mice

compared to ellipsoidal non-cognate aAPCs ($p=0.004$) as well as cognate spherical aAPCs ($p=0.05$). Additionally, confocal imaging suggests that the observed improvement in CD8+ T cell activation is due to increased interaction along this flatter, long axis of the biomimetic, ellipsoidal aAPCs. These findings indicate that shape matters and that aAPC geometry is a critical design criterion to consider in the synthesis of biomimetic acellular aAPC systems. aAPCs that more closely mimic endogenous cell-cell interactions may provide a more complete understanding of the underlying biological processes, such as the role of close membrane apposition and a large surface area of contact in the APC/T cell interaction. aAPCs thus may not only be an enabling tool for antigen-specific immunotherapy, but also for studying basic aspects of T cell biology.

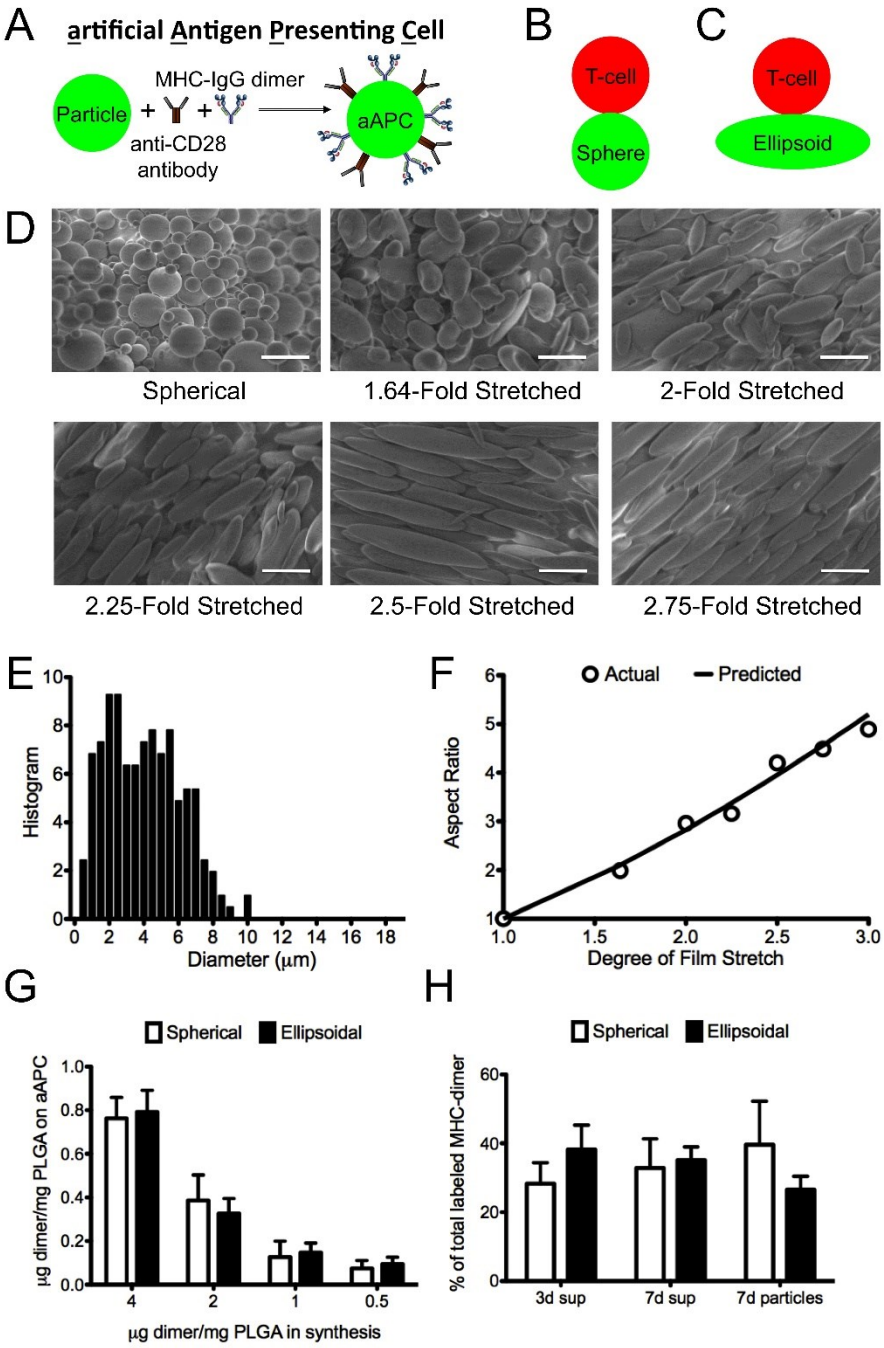

Figure 6.1: **Particle Shape and Size**

(A) Schematic of an aAPC. (B-D) Schematic of the interaction between a T cell, modeled as a sphere, interacting with (B) a sphere; (C) an ellipsoid (AR 2.83; stretch ratio 2). (D) Characterization by SEM (2000x magnification) of spherical and ellipsoidal aAPCs. Scale bar

corresponds to 10 μm. (E) Size distribution of aAPCs. (G) Comparison of degree of stretch imposed on the film (STR) with the aspect ratio (AR) of the generated ellipsoidal aAPCs. Predicted $AR = STR^{3/2}$ (F) Coupling efficiency for protein during synthesis of aAPC from spherical and ellipsoidal microparticles (n=2). (G) Protein release from the surface of aAPC at 37°C in PBS (pH 7.4) over the course of 1 week.

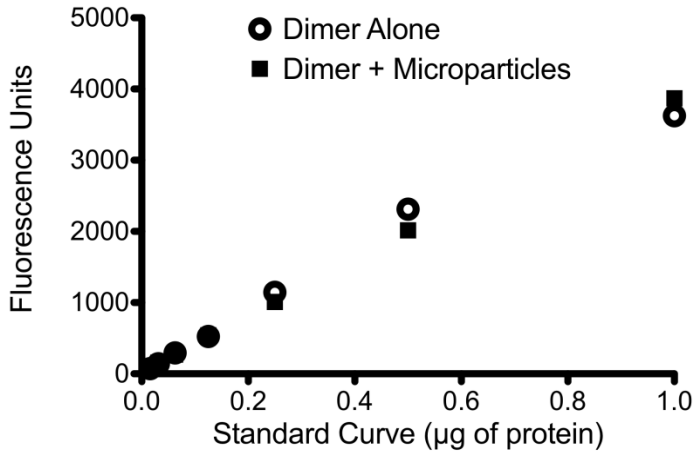

Figure 6.2: Fluorescence Standard Curves

Linear range of MHC-Ig fluorescence used as standard curves for quantifying labeled MHC dimer bound to PLGA microparticles. 2 mg microparticles per measurement.

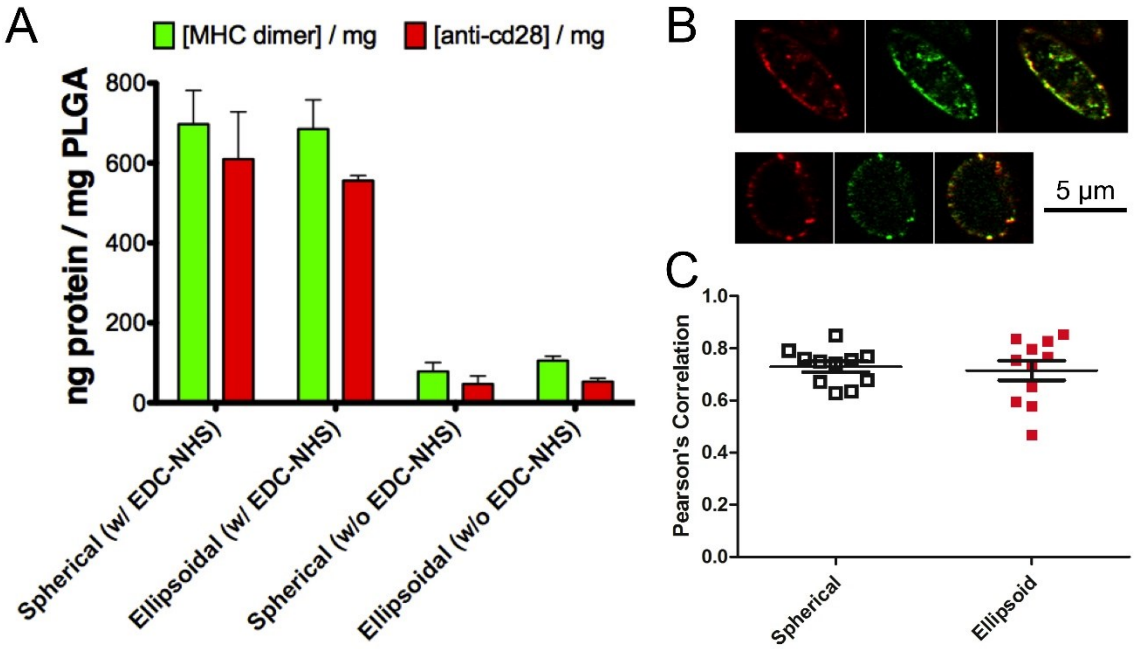

Figure 6.3: Quantification of Protein Labeling

Surface MHC-dimer (fluorescently labeled with alexa 488) and anti-CD28 (fluorescently labeled with APC) quantification by fluorescence. (A) Spherical and ellipsoidal aAPC synthesized with EDC/NHS chemistry did not have significant differences in MHC-dimer amount ($p = 0.92$) or density ($p = 0.42$), anti-CD28 amount ($p = 0.70$) or density ($p = 0.39$), or MHC-dimer/anti-CD28 ratio ($p = 0.72$). Approximately 85-90% of the protein on the surface required the EDC/NHS pre-activation step. (B) Representative confocal images of ellipsoidal and spherical aAPC showing anti-CD28 (red), MHC-dimer (green), and overlay of the two channels. (C) Pearson's correlation between the red and green channels for spherical and ellipsoidal aAPC (mean 0.73 for spherical, 0.71 for ellipsoidal; $p = 0.74$ for comparison). At least 10 particles were used per sample. Colocalization analysis was performed using Just Another Colocalization Plugin in ImageJ (Bethesda, MD, USA).

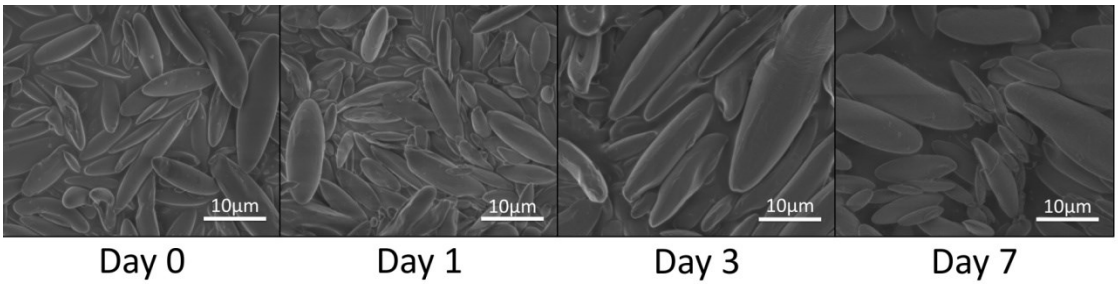

Figure 6.4: Particle Shape Characterized by TEM

aAPCs do not change their shape in physiological conditions over one week. SEM of freshly prepared aAPCs (a) and aAPCs incubated in PBS at 37°C for (b) 1 day, (c) 3 days, and (d) 7 days. The calculated ARs were (a) 3.57, (b) 3.31, (c) 3.34, and (d) 3.23.

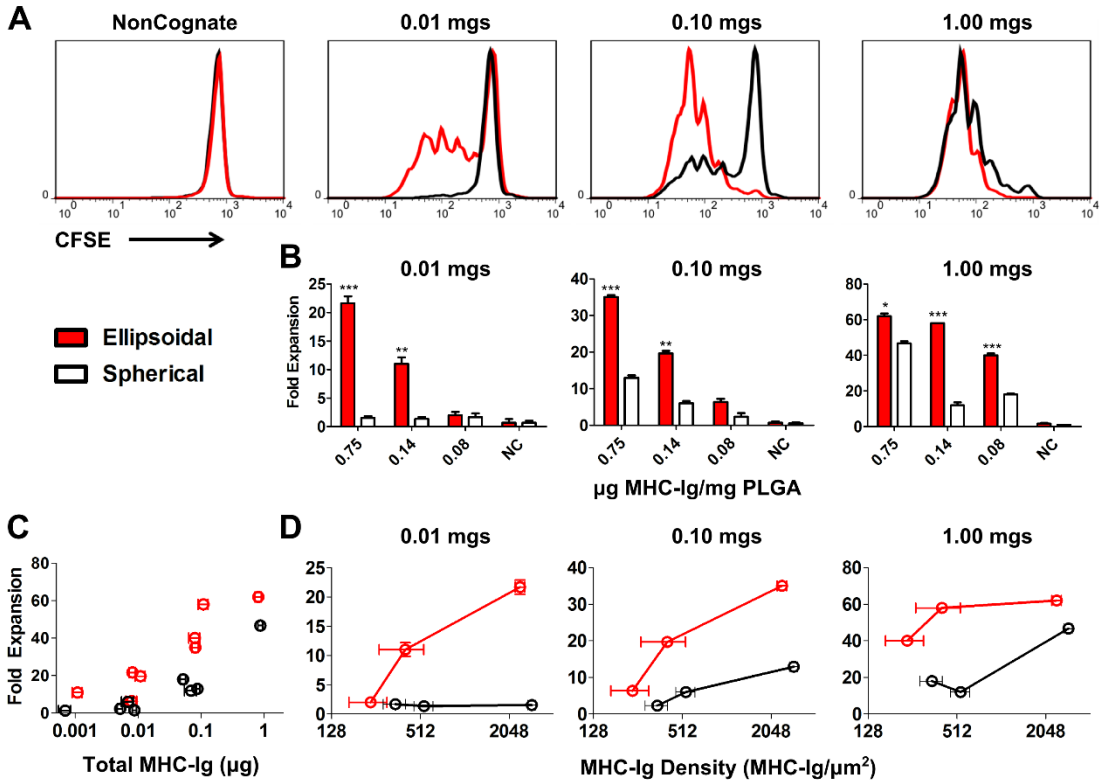

Figure 6.5: **T Cell Expansion and Particle Shape**

Specific CD8+ T cell proliferation in response to specified aAPC dose, protein density, and shape of aAPC. (A) CFSE dilution data for ellipsoidal (red) and spherical aAPC (black) at the highest protein dose (0.75 µg dimer/mg PLGA) at 3 doses of aAPC (0.01 mg, 0.1mg, and 1mg/10^5 $CD8^+$ *pmel* CD8+ T cells) compared to non-cognate. (B) CD8+ T cell proliferation (fold expansion/10^5 cells) 7 days after aAPC addition to T cells with indicated doses, shapes (ellipsoidal in red, spherical in white), and protein densities. (For comparison of ellipsoid vs. spherical, * $p<0.05$, ** $p<0.01$, *** $p<0.001$; n=3). (C) CD8+ T cell proliferation (fold expansion/10^5 cells) versus total MHC-dimer dose (in µg) for ellipsoidal (red) and spherical (black) aAPCs. (D) CD8+ T cell proliferation (fold expansion/10^5 cells) versus MHC-dimer density (in MHC-Ig/µm^2) for ellipsoidal (red) and spherical (black) aAPC at 3 doses of aAPC (0.01 mg, 0.1mg, and 1mg/10^5 $CD8^+$ *pmel* CD8+ T cells).

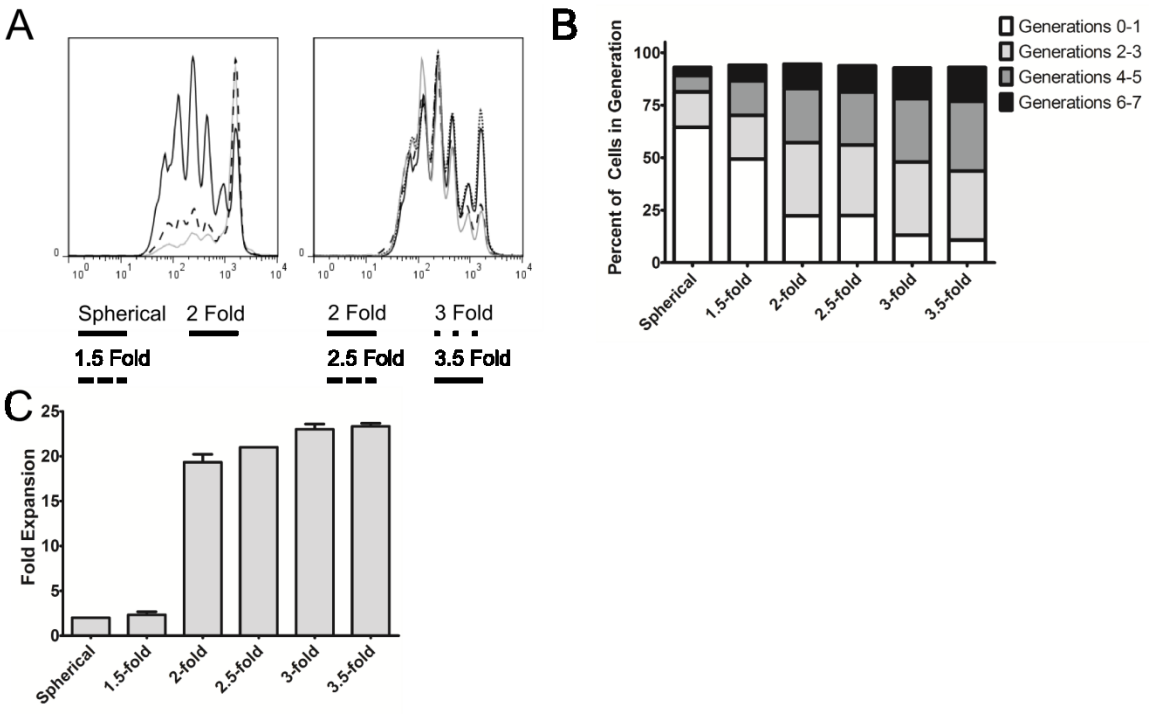

Figure 6.6: **Response to differential stretching.**

Specific CD8+ T cell proliferation in response to 0.01 mg particles/100,000 cell dose for ellipsoidal aAPCs with different applied stretch compared to spherical aAPCs. (A) CFSE dilution after aAPC addition to CD8+ T cells. (B) Fraction of cells which underwent 0-1, 2-3, 4-5, 6-7 rounds of proliferation after aAPC addition to CD8+ T cells. (C) CD8+ T cell proliferation (fold expansion/100,000 cells) 7 days after aAPC addition to CD8+ T cells.

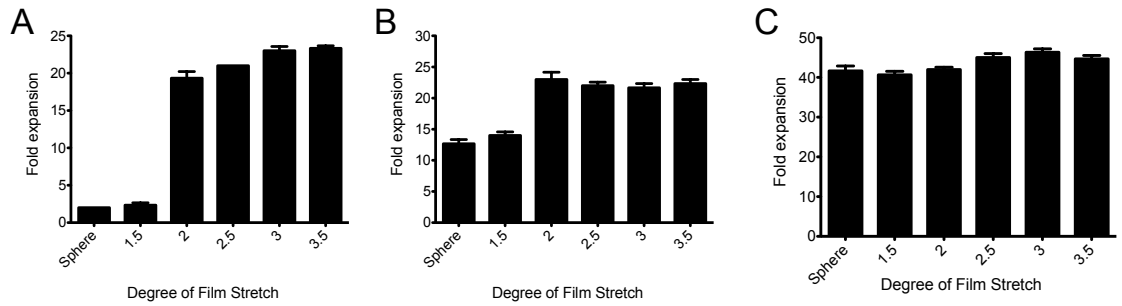

Figure 6.7: Titration of Particle Stretching

Fold expansion of PMEL T cells post incubation with (A) 0.01 mg / 100,000 cells, (B) 0.1 mg / 100,000 cells, and (C) 1 mg / 100,000 cells of differentially stretched ellipsoidal aAPC as indicated. Negative controls with non-cognate peptide-in-MHC showed no expansion.

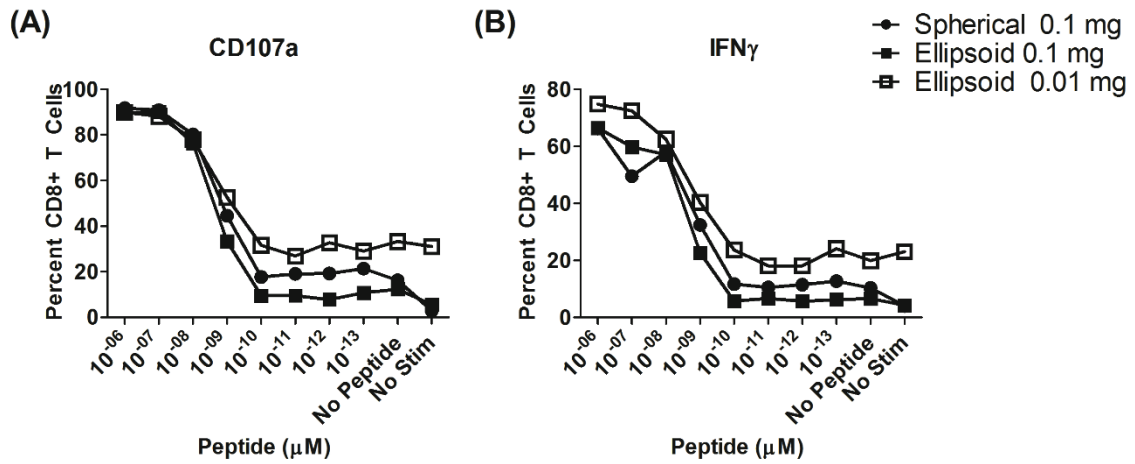

Figure 6.8: **Functional Assessment of T Cells After Expansion**

Intracellular cytokine staining after stimulation of aAPC-activated T cells. CD8+ isolated splenocytes were activated with 0.1 mg spherical aAPC (filled circle), 0.1 mg of ellipsoidal aAPC (filled square), or 0.01 mg of ellipsoidal aAPC (unfilled square). Seven days later, T cells were restimulated with splenocytes from C57BLACK6 mice pulsed with the indicated dose of cognate GP100 peptide. Unpulsed splenocytes (No Peptide) or no splenocytes (No Stim) were used as controls. Cytokine production is reported as percentage of T cells making indicated cytokine.

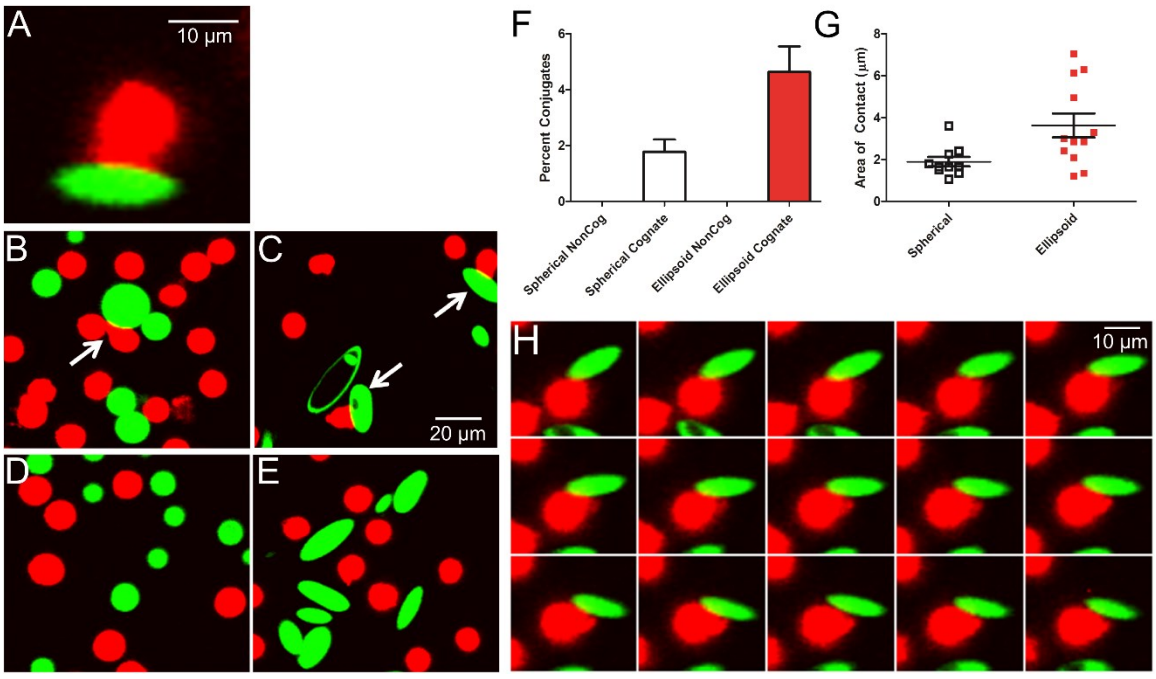

Figure 6.9. **Confocal imaging of aAPC (green) conjugate formation to CD8+ T cells (red).**

(A) Conjugates appear as areas of close membrane apposition between aAPC and cells, with CD8+ T cell morphology rearrangement into a distinctive cap. (B) Spherical and (C) ellipsoidal aAPC form cell-bead conjugates, which are more frequently observed with ellipsoidal aAPC. (D-E) Conjugate formation is not observed with aAPC bearing non-cognate MHC-peptide. (F) 4.6 ± 0.9% of CD8+ T cells incubated with ellipsoidal aAPC (red) compared to 1.8 ± 0.4% with spherical aAPC (unfilled) were observed to have formed conjugates (p=0.01). (G) The area of contact between cells and aAPC was 1.9 ± 0.2 μm for spherical (unfilled) and 3.6 ± 0.6 μm for ellipsoidal (red) cognate aAPC (p = 0.01). (H) Time-lapse image of a single CD8+ T cell interacting with one ellipsoidal cognate aAPC; images acquired 2 s apart.

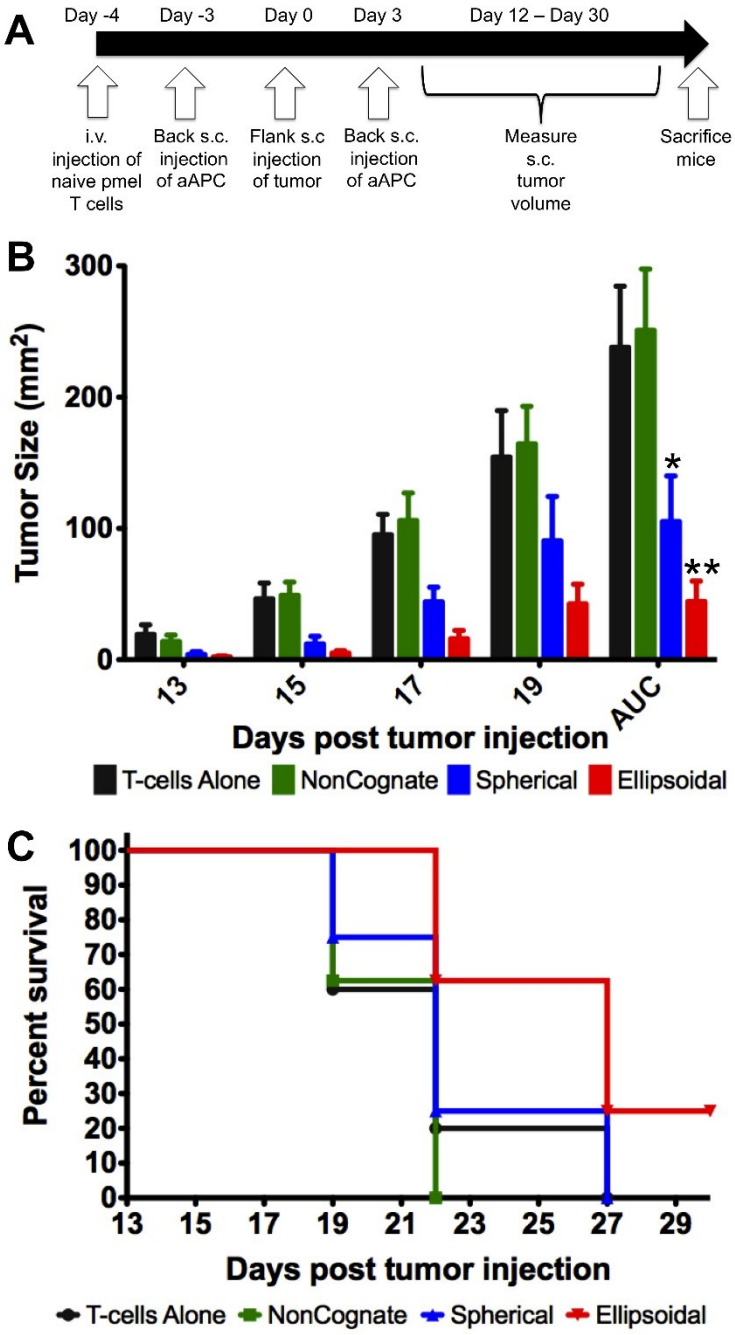

Figure 6.10 In vivo tumor-prevention model.

(A) Experimental protocol and timeline. (B) Tumor size measurements for mice injected with cancer and CD8+ T cells alone or also injected with non-cognate ellipsoidal (NonCognate), cognate spherical (Spherical), and cognate ellipsoidal aAPC (Ellipsoidal). AUC = area under the

curve. * p = 0.02 vs. non-cognate; ** p = 0.0009 vs. non-cognate. For comparison of ellipsoidal cognate and spherical cognate by AUC, p = 0.13. (C) Survival curve – mice were sacrificed and declared "dead" when tumor size reached 200 mm^2. Subcutaneous injection of ellipsoidal aAPC resulted in increased survival vs. spherical non-cognate particles (p=0.05), ellipsoidal non-cognate particles (p=0.004), and CD8+ T cells alone (p=0.05).

Supplemental calculation

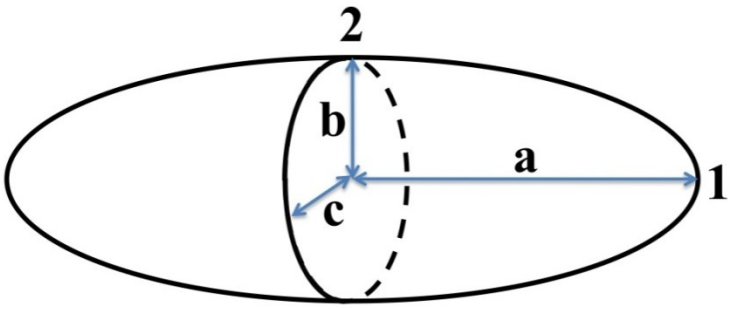

Determining the lengths of a, b, c: For a spheroid that has been elongated in 1 dimension, since total volume is conserved from a sphere, the length of the short axes is related to the length of the long axis by $b = c = \frac{1}{\sqrt{a}}$

Surface area of a prolate spheroid: Since the geometrical shape corresponds to a prolate spheroid (a > b = c), the surface area of the spheroid can be determined by the following formula[1]:

$$S = 2\pi a^2 + 2\pi \frac{ac}{e} \sin^{-1} e \text{ where } e = \sqrt{1 - \frac{b^2}{a^2}}$$

This surface area was then normalized by the surface area of a sphere with radius 1.

Equivalent protein density: Equivalent protein density with total protein content held constant is the inverse of the normalized surface area (density = 1/SA).

Radius of curvature: The radius of curvature is the radius of a circle with the same curvature as the observed curve at that point. Thus, for flatter curves, the radius of curvature increases, as that flatness requires a larger circle to describe it.

An ellipse can be described parametrically by $\begin{matrix} x(t) = a\cos(t) \\ y(t) = b\cos(t) \end{matrix}$.

For any parameterized equation of the form $\begin{matrix} x = x(t) \\ y = y(t) \end{matrix}$,

the radius of curvature can be calculated[2] from:

$R = \frac{(x'^2 + y'^2)^{3/2}}{|x'y'' - y'x''|}$, where $\begin{matrix} x' = dx/dt \\ y' = dy/dt \end{matrix}$ and $\begin{matrix} x'' = d^2x/dt^2 \\ y'' = d^2y/dt^2 \end{matrix}$.

So for an ellipse:

$$R = \frac{(a^2\sin^2(t) + b^2\cos^2(t))^{3/2}}{ab\sin^2(t) + ab\cos^2(t)} = \frac{(a^2\sin^2(t) + b^2\cos^2(t))^{3/2}}{ab}$$

To calculate the radius of curvature at the tip, since t = 0 corresponds to point **1** (**Fig. S5**), R_a can be calculated using *a* and *b* as the two axes of the ellipse. To calculate the radius of curvature at the tip, since t = π/2 corresponds to point **2** (**Fig. S5**), R_b can be calculated using *a* and *b* as the two axes of the ellipse and plugging in t = π/2. Thus,

$$R_a = \frac{b^3}{ab} = \frac{b^2}{a}$$
$$R_b = \frac{a^3}{ab} = \frac{a^2}{b}$$

And since the bc plane at 2 is already described by a circle, $R_c = b = c$.

6.5 References:

1. Fletcher DA, Mullins RD. Cell mechanics and the cytoskeleton. Nature 2010;463(7280):485-492.

2. Dustin ML. T-cell activation through immunological synapses and kinapses. Immunol Rev 2008;221(221):77-89.

3. Dykstra M, Cherukuri A, Sohn HW, Tzeng SJ, Pierce SK. Location is everything: lipid rafts and immune cell signaling. Annu Rev Immunol 2003;21:457-481.

4. Grakoui A, Bromley SK, Sumen C, Davis MM, Shaw AS, Allen PM, et al. The immunological synapse: a molecular machine controlling T cell activation. Science
1999;285(5425):221-227.

5. Lee KH, Holdorf AD, Dustin ML, Chan AC, Allen PM, Shaw AS. T cell receptor signaling precedes immunological synapse formation. Science
2002;295(5559):1539-1542.

6. Monks CR, Freiberg BA, Kupfer H, Sciaky N, Kupfer A. Three-dimensional segregation of supramolecular activation clusters in T cells. Nature
1998;395(6697):82-86.

7. Doh J, Irvine DJ. Immunological synapse arrays: patterned protein surfaces that modulate immunological synapse structure formation in T cells. Proc Natl Acad Sci U S A 2006;103(15):5700-5705.

8. Oelke M, Maus MV, Didiano D, June CH, Mackensen A, Schneck JP. Ex vivo induction and expansion of antigen-specific cytotoxic T cells by HLA-Ig-coated artificial antigen-presenting cells. Nat Med 2003;9(5):619-625.

9. Ugel S, Zoso A, De Santo C, Li Y, Marigo I, Zanovello P, et al. In vivo administration of artificial antigen-presenting cells activates low-avidity T cells for treatment of cancer. Cancer Res 2009;69(24):9376-9384.

10. Mescher MF. Surface contact requirements for activation of cytotoxic T lymphocytes. J Immunol 1992;149(7):2402-2405.

11. Han H, Peng JR, Chen PC, Gong L, Qiao SS, Wang WZ, et al. A novel system of artificial antigen-presenting cells efficiently stimulates Flu peptide-specific cytotoxic T cells in vitro. Biochem Biophys Res Commun 2011;411(3):530-535.

12. Steenblock ER, Fadel T, Labowsky M, Pober JS, Fahmy TM. An artificial antigen-presenting cell with paracrine delivery of IL-2 impacts the magnitude and direction of the T cell response. J Biol Chem 2011;286(40):34883-34892.

13. Steenblock ER, Fahmy TM. A comprehensive platform for ex vivo T-cell expansion based on biodegradable polymeric artificial antigen-presenting cells. Mol Ther 2008;16(4):765-772.
14. Ndhlovu ZM, Oelke M, Schneck JP, Griffin DE. Dynamic regulation of functionally distinct virus-specific T cells. Proc Natl Acad Sci U S A 2010;107(8):3669-3674.
15. Ito F, Carr A, Svensson H, Yu J, Chang AE, Li Q. Antitumor reactivity of antiCD3/antiCD28 bead-activated lymphoid cells: implications for cell therapy in a murine model. J Immunother 2003;26(3):222-233.
16. Lum LG, LeFever AV, Treisman JS, Garlie NK, Hanson JP, Jr. Immune modulation in cancer patients after adoptive transfer of anti-CD3/anti-CD28-costimulated T cells-phase Iclinical trial. J Immunother 2001;24(5):408-419.
17. Taylor PA, Lees CJ, Blazar BR. The infusion of ex vivo activated and expanded CD4(+)CD25(+) immune regulatory cells inhibits graft-versus-host disease lethality. Blood 2002;99(10):3493-3499.
18. Sunshine JC, Green JJ. Nanoengineering approaches to the design of artificial antigen-presenting cells. Nanomedicine 2013;8(7):1173-1189.
19. Balmert SC, Little SR. Biomimetic delivery with micro- and nanoparticles. Adv Mater 2012;24(28):3757-3778.
20. Wang J, Byrne JD, Napier ME, DeSimone JM. More effective nanomedicines through particle design. Small 2011;7(14):1919-1931.
21. Champion JA, Mitragotri S. Role of target geometry in phagocytosis. Proc Natl Acad Sci U S A 2006;103(13):4930-4934.
22. Sharma G, Valenta DT, Altman Y, Harvey S, Xie H, Mitragotri S, et al. Polymer particle shape independently influences binding and internalization by macrophages. J Control Release 2010;147(3):408-412.
23. Champion JA, Katare YK, Mitragotri S. Particle shape: a new design parameter for micro- and nanoscale drug delivery carriers. J Control Release 2007;121(1-2):3-9.
24. Devarajan PV, Jindal AB, Patil RR, Mulla F, Gaikwad RV, Samad A. Particle shape: a new design parameter for passive targeting in splenotropic drug delivery. J Pharm Sci 2010;99(6):2576-2581.
25. Harris BJ, Dalhaimer P. Particle shape effects in vitro and in vivo. Front Biosci (Schol Ed) 2012;4:1344-1353.
26. Barua S, Yoo JW, Kolhar P, Wakankar A, Gokarn YR, Mitragotri S. Particle shape enhances specificity of antibody-displaying nanoparticles. Proc Natl Acad Sci U S A 2013;110(9):3270-3275.
27. Curtsinger J, Deeths MJ, Pease P, Mescher MF. Artificial cell surface constructs for studying receptor-ligand contributions to lymphocyte activation. J Immunol Methods 1997;209(1):47-57.

28. Maus MV, Thomas AK, Leonard DG, Allman D, Addya K, Schlienger K, et al. Ex vivo expansion of polyclonal and antigen-specific cytotoxic T lymphocytes by artificial APCs expressing ligands for the T-cell receptor, CD28 and 4-1BB. Nat Biotechnol 2002;20(2):143-148.
29. Steenblock ER, Wrzesinski SH, Flavell RA, Fahmy TM. Antigen presentation on artificial acellular substrates: modular systems for flexible, adaptable immunotherapy. Expert Opin Biol Ther 2009;9(4):451-464.
30. Suhoski MM, Golovina TN, Aqui NA, Tai VC, Varela-Rohena A, Milone MC, et al. Engineering artificial antigen-presenting cells to express a diverse array of costimulatory molecules. Mol Ther 2007;15(5):981-988.
31. Yoo JW, Mitragotri S. Polymer particles that switch shape in response to a stimulus. Proc Natl Acad Sci U S A 2010;107(25):11205-11210.
32. Schneck JP, Slansky JE, O'Herrin SM, Greten TF. Monitoring antigen-specific T cells using MHC-Ig dimers. In: Coligan JE, editor. Current Protocols in Immunology, 2001.
33. Durai M, Krueger C, Ye Z, Cheng L, Mackensen A, Oelke M, et al. In vivo functional efficacy of tumor-specific T cells expanded using HLA-Ig based artificial antigen presenting cells (aAPC). Cancer Immunol Immunother 2009;58(2):209-220.
34. Rothstein SN, Federspiel WJ, Little SR. A unified mathematical model for the prediction of controlled release from surface and bulk eroding polymer matrices. Biomaterials 2009;30(8):1657-1664.
35. Batycky RP, Hanes J, Langer R, Edwards DA. A theoretical model of erosion and macromolecular drug release from biodegrading microspheres. J Pharm Sci 1997;86(12):1464-1477.
36. von Burkersroda F, Schedl L, Gopferich A. Why degradable polymers undergo surface erosion or bulk erosion. Biomaterials 2002;23(21):4221-4231.
37. Gottschalk RA, Hathorn MM, Beuneu H, Corse E, Dustin ML, Altan-Bonnet G, et al. Distinct influences of peptide-MHC quality and quantity on in vivo T-cell responses. Proc Natl Acad Sci U S A 2012;109(3):881-886.
38. Arens R, Schoenberger SP. Plasticity in programming of effector and memory CD8 T-cell formation. Immunol Rev 2010;235(1):190-205.
39. Bullock TN, Mullins DW, Engelhard VH. Antigen density presented by dendritic cells in vivo differentially affects the number and avidity of primary, memory, and recall CD8+ T cells. J Immunol 2003;170(4):1822-1829.
40. Seder RA, Darrah PA, Roederer M. T-cell quality in memory and protection: implications for vaccine design. Nat Rev Immunol 2008;8(4):247-258.
41. Kroger CJ, Alexander-Miller MA. Cutting edge: CD8+ T cell clones possess the potential to differentiate into both high- and low-avidity effector cells. J Immunol 2007;179(2):748-751.

7 Conclusions

Artificial Antigen Presenting Cells are reductionist systems for inducing T cell activation and proliferation. There are two basic approaches to using aAPC: they can be injected *in vivo* as a direct vaccine, or used to expand T cells *in vitro* for adoptive transfer. I have addressed both approaches in this work. Nano-aAPC were initially envisioned as a platform to improve biocompatibility and trafficking after *in vivo* administration. Ellipsoid micro-aAPC were also administered in this manner. However, in both cases tumor inhibition was not particularly robust, and required the co-administration of tumor-specific transgenic cells and pre-treatment of tumors. This may be due to continuing difficulties with aAPC trafficking. While nano-aAPC had more drainage from subcutaneous injection sites than micro-aAPC, the majority of particles were not found in the lymph node after subcutaneous injection, and were quickly cleared after intravenous administration. Thus, better performance will require techniques to co-localize T cells and aAPC after administration. Even smaller aAPC may have better drainage to lymph nodes and tumors, or chemokines could be delivered from aAPC to attract T cells to the site of injection.

In contrast, adoptive transfer of nano-aAPC activated cells combined with lymphodepletion mediated rejection of established tumors without use of transgenic cells. *In vitro* culture eliminates issues of trafficking and clearance of aAPC. Furthermore, lymphodepletion can remove tumor immune suppression networks. Thus, for the near-term, adoptive transfer appears to be a more effective method for tumor rejection than direct vaccination. However, adoptive transfer is still prohibitively complex and expensive, and further simplifying adoptive transfer and improving direct vaccination aAPC remain valuable goals.

In this work, I develop aAPC of differing size and shape from traditional spherical, cell-sized aAPC. Our efforts are guided by a desire to both re-capitulate and improve biology. Non-spherical aAPC were designed to mimic endogenous T cell-APC interactions, which rely on a large surface area and contact surface that is minimized by spherical aAPC. In contrast, nano-aAPC are decidedly not inspired by typical endogenous interactions, and it remains to be seen whether they can re-capitulate micro-scale interactions such as immune synapses or asymmetric cell division. However, the use of magnetic field induced-clustering led to a nano-aAPC/CD3 aggregate that resembled a T cell "cap" or synapse-like structure, and which was associated with robust activation. Thus, both the paradigm of mimicking and replacing endogenous interactions were valuable in developing our work.

Furthermore, the development of new aAPC platforms required a basic understanding of T cell activation. The T cell membrane is spatially heterogenous on a nano-scale, a characteristic which exerts greater influence on nano-aAPC binding and T cell activation than micro-aAPC. Guided by the concatenation of TCR/CD3 clusters during activation, we developed magnet-induced clustering to manipulate these clusters with an external magnetic field. Thus, the development of new expansion platforms develops in parallel with mechanistic studies of the basis of T cell expansion.

8 Acknowledgments

I want to begin by thanking my family: Sanja, Vjekoslav, Maria, Dijana, and Nada. I would be nowhere without their love, support, teaching, encouragement, and guidance. To Kopal, thank you for being my best friend, for the support and the distractions and for keeping me sane. I love you all.

I was lucky enough to find a laboratory where I had both the freedom to explore and the guidance to learn. I want to thank Jonathan Schneck for his mentorship, for being a role-model, and for allowing me to pursue a unique research path that wouldn't have been possible anywhere else. It was a transformative experience.

To Joanie, thank you for being the realistic ying to my excitable yang, for the cookies and the beer bread, for looking up protocols in your notebooks and keeping me grounded. To Matthias, I appreciate the guidance and always valued your insight tremendously, thank you for helping to shape my work. To Dr. Edidin, thank you for challenging me to be better, and for being a role-model and for teaching me how to think like a scientist. To Dr. Green and Dr. Mao, I greatly valued your feedback and collaboration.

To the original team, Matt Li, Aaron Selya, Jessica Lee, and Yen-Ling Chiu, thank you for being patient with me and teaching me while I was finding my way. To the new team, Carl Haupt, Christian Schuetz, Andy Tu, Leah Sibener, Alyssa Kosmides, Ami Bessler, Kent Aje, and Juan Varela, thank you for putting up with me and bringing fresh energy to the laboratory .

To Drs. Siliciano, Raben, and Shortle, thank you for taking a chance on me and giving me the opportunity to study at this amazing institution. To Sharon, Bern, and Martha, thank you for the help, the support, and for taking care of our MD-PhD family.

9 Curriculum Vitae

Karlo Perica

Contact Information
Johns Hopkins School of Medicine
733 N. Broadway, BRB 639
Baltimore, Maryland 21205
Tel: 410.614.0642

Education
Johns Hopkins University, Baltimore, MD.
Ph.D in Biomedical Engineering, March 2014.
Dissertation: "Nanoscale Artificial Antigen Presenting Cells For Cancer Immunotherapy"
Advisor: Jonathan Schneck, MD PhD

Yale University, New Haven, CT.
B.S. in Biomedical Engineering, May 2007.
Advisor: Tarek Fahmy.

Awards and Honors
1. **Finalist, Excellence in Teaching Award**. 2013. Nominated by undergraduates as one of ten finalists for best teaching assistant in Whiting School of Engineering.
2. **AACR Millenium Scholar-in-Training**. American Association of Cancer Research award to "support young investigators who will be presenting meritorious proffered papers."
3. **1st Place, Pfizer/Carey School of Business Case Competition**. 2012. Delivered winning presentation on social media based strategies for increasing vaccination in developing markets. Competed against 12 teams from business and medical schools across the country. $3000 first place prize.
4. **Immunology Retreat Best Presentation**. 2012. Awarded by Johns Hopkins Immunology Training Program
5. **Johns Hopkins Institute for NanoBioTechnology Cancer Pilot Grant**. 2011. $50,000 research grant.
6. **Cancer Research Institute Pre-Doctoral Fellowship**. 2010 (ongoing). $15,000/year student fellowship.
7. **Chrysalis Scholar** – American Academy of Allergy, Asthma & Immunology award for promising young clinician-scientists.

Publications (* co-first authors)
1. Sunshine JC*, Perica K* et al. Particle Shape Dependance of CD8+ T Cell Activation By Artificial Antigen Presenting Cells. Biomaterials. 2014 Jan;35(1):269-77. PMID: 24099710
2. Perica et al. Nanoscale Artificial Antigen Presenting Cells for T Cell Immunotherapy. Nanomedicine. 2014 Jan;10(1):119-29. PMID: 23891987

3. Perica et al. Modulation of MHC Binding by Lateral Association of TCR and Coreceptor. Biophys J. 2012 Nov 7;103(9):1890-8.
   PMID: 23199917. * Selected for New and Notable
4. Samstein*, Perica* et al. The use of deoxycholic acid to enhance the oral bioavailability of biodegradable nanoparticles. Biomaterials. 2008 Feb;29(6):703-8.
   PMID: 18006053

National and International Conferences

1. [Abstract/Conference]. Perica et al. “Nanoscale Artificial Antigen Presenting Cells for T Cell Immunotherapy.” American Association of Cancer Research Annual Meeting. Washington, DC. April 2013.
2. [Abstract/Conference] Perica et al. “Ellipsoid Rather Than Spherical Microparticles Are More Efficient Platforms for T Cell Expansion.” Cancer Research Institute Symposium. New York, NY. Oct 2012.
3. [Abstract/Conference] Perica et al. "Dynamic Changes in T Cell Membrane Organization Modulate Antigen Binding." American Association of Immunologists Annual Meeting. Boston, MA. May 2012.
4. [Abstract/Conference] Perica et al. “ “Cancer Research Institute Symposium. New York, NY. Oct 2011.
5. [Abstract/Conference] Perica et al. "Persistent Changes in T Cell Receptor Surface Organization Visualized by Quantum Dot Probes with k-Space Image Correlation Spectroscopy.” American Association of Immunologists Annual Meeting. Baltimore, MD. May 2010.
6. [Abstract/Conference] Perica et al. "Persistent Changes in T Cell Receptor Surface Organization Visualized by Quantum Dot Probes with k-Space Image Correlation Spectroscopy.” Days of Molecular Medicine. Stockholm, Sweden. May 2010.
7. [Abstract/Conference] Perica et al. "A Novel Formulation for Oral Drug Delivery Using Bile Salts.” Biomedical Engineering Society Annual Meeting. Chicago, IL. 2006.
8. [Abstract/Conference] Perica et al. Support Vector Machine Training for Adverse Drug Event Detection. Mountain West Biomedical Engineering Conference. Snowbird, UT. Sep. 2005.